2014-07-07

The Cellular Consequences of FUS/TLS Depletion: A Loss of Function Model for Amyotrophic Lateral Sclerosis: A Dissertation

Catherine L. Ward
University of Massachusetts Medical School

THE CELLULAR CONSEQUENCES OF FUS/TLS DEPLETION: A LOSS OF FUNCTION MODEL FOR AMYOTROPHIC LATERAL SCLEROSIS

A Dissertation Presented

By

Catherine Louise Ward

Submitted to the faculty of the
University of Massachusetts Graduate School of Biomedical Sciences, Worcester
in partial fulfillment of the requirement for the degree of

DOCTOR OF PHILOSOPHY

July 7, 2014

BIOCHEMISTRY AND MOLECULAR PHARMACOLOGY

THE CELLULAR CONSEQUENCES OF FUS/TLS DEPLETION: A LOSS OF FUNCTION MODEL FOR AMYOTROPHIC LATERAL SCLEROSIS

A Dissertation Presented
By
Catherine Louise Ward

The signatures of the Dissertation Defense Committee signify completion and approval as to style and content of the Dissertation

_____
Daryl A. Bosco, Ph.D., Thesis Advisor

_____
Melissa J. Moore, Ph.D., Member of Committee

_____
Kendall L. Knight, Ph.D., Member of Committee

_____
Angela Ho, Ph.D., Member of Committee

The signature of the Chair of the Committee signifies that the written dissertation meets the requirements of the Dissertation Committee

_____
Robert H. Brown Jr., D.Phil., MD, Chair of Committee

The signature of the Dean of the Graduate School of Biomedical Sciences signifies that the student has met all graduation requirements of the School

_____
Anthony Carruthers, Ph.D.
Dean of the Graduate School of Biomedical Sciences

Biochemistry and Molecular Pharmacology
July 7, 2014

For my family and friends who
I have neglected over the past six years
but continue to love me anyway

ACKNOWLEDGMENTS

There are many people whom I would like to acknowledge for their assistance and guidance throughout the course of my PhD career. First and foremost, my mentor, Daryl Bosco. Little did I know five and a half years ago how lucky I was to be joining your lab. Your ability to be caring, comforting, stern, and intimidating all at the same time is what kept me going throughout this whole process. The knowledge you have instilled in me over the years goes well beyond experimental technique and scientific insight. Thank you so much for everything.

I would also like to thank my lab family who turned every incubator contamination, ugly western blot, and negative result into a good laugh: Melissa Rotunno, Reddy Sama, Laura Kaushansky, Sivakumar Boopathy, Desiree Baron, Kristin Boggio, Maeve Tischbein, and Kiera Sapp. You make this final stage of the PhD process bittersweet. A big thank-you to my extended lab-family as well: the Brown lab and Landers lab, particularly Peter Sapp and John Landers who have always been at the ready with good conversation and helpful advice.

For their mentoring and guidance throughout the years I would also like to thank the members of my thesis advisory committee: Dr. Robert Brown, Dr. Melissa Moore, and Dr. Ken Knight. Additionally, thank-you to Dr. Zuoshang Xu, Dr. Larry Hayward, Dr. Melissa Moore, and Dr. Jill Zitzewitz for serving on my qualifying exam committee. I would also like to think Dr. Angela Ho for being a

part of my dissertation examination committee. Your time is very much appreciated.

Lastly, many thank-you's to my parents, Wayne and Catherine, and sisters, Christina, Lynn, and Laura. Your love and support throughout the years has been unparalleled and it makes me proud to make you proud. Finally, thank you to my fiancé, Stephen Douthwright for still loving me after every bad day and mood-swing that graduate school has provided me with over the years. I am so lucky to have you to share my life with.

ABSTRACT

Amyotrophic lateral sclerosis (ALS) is a fatal neurodegenerative disease characterized by the death of motor neurons, generally leading to paralysis and death within 3-5 years of onset. Over 50 different mutations in the gene encoding FUS/TLS (or FUS) will result in ALS, accounting for ~4% of all inherited cases. FUS is a multifunctional protein with important functions in DNA/RNA processing and stress response. How these mutations affect the structure or function of FUS protein and ultimately cause ALS is not known. The fact that mutations cause the protein to mislocalize from the nucleus to the cytoplasm of cells suggests that ALS pathogenesis may occur through a loss of nuclear function, gain of toxic cytoplasmic function, or both. Several FUS knockout animal models have been utilized for investigating a loss of function hypothesis and show phenotypes such as early lethality, reduced lifespan, and locomotor defects.

To uncover cellular pathways affected by loss of FUS function, I have characterized the knockdown of FUS in a motor neuron-like cell line, NSC-34. In NSC-34 cells, the depletion of FUS severely impacts cellular proliferation and potentially causes increased levels of DNA damage. A quantitative proteomics analysis performed on cells undergoing various degrees of FUS knockdown revealed protein expression changes for known RNA targets of FUS, consistent with a loss of FUS function with respect to RNA processing. Proteins that changed in expression as a function of FUS knockdown were associated with

multiple processes, some of which influence cell proliferation including cell-cycle regulation, cytoskeletal organization, oxidative stress and energy homeostasis. Importantly, cellular proliferation could be rescued by the re-expression of FUS and by treatment with the small-molecule, rolipram, indicative of potential therapeutic approaches.

Collectively, the work presented in this dissertation demonstrates the importance of FUS for cell health and homeostasis, is suggestive of a role for FUS in DNA damage repair and identifies additional cellular pathways influenced by FUS depletion. Overall, this work provides mechanistic insight into ALS pathogenesis through loss of FUS/TLS function.

TABLE OF CONTENTS

LIST OF TABLES

LIST OF FIGURES

Appendix IV

Appendix V

LIST OF THIRD PARTY COPYRIGHTED MATERIAL

The following material was reproduced from published work:

	Publisher	License number
Appendix II	John Wiley and Sons	3397800087634

The following material was reproduced from published work with no permission required:

	Publisher
Figure I-1	BioMed Central
Figure I-2	SAGE Publications Inc
Figure I-3	SAGE Publications Inc
Figure I-5	SAGE Publications Inc
Appendix III	BioMed Central

LIST OF ABBREVIATIONS

ALS – Amyotrophic lateral sclerosis

EWS – Ewing sarcoma

ET – Essential tremor

fALS – Familial amyotrophic lateral sclerosis

FET – FUS, EWS, TAF15

FTD or FTLD – Frontotemporal lobar degeneration

FUS or FUS/TLS – Fused in sarcoma/Translocated in liposarcoma

G-rich – Glycine-rich

hnRNP – Heterogeneous ribonuclear protein

HR – homologous recombination

NHEJ – non-homologous end-joining

NLS – Nuclear localization signal

NSC-34 – Neuroblastoma x spinal cord hybrid 34

QGSY-rich – Glutamine-glycine-serine-tyrosine-rich

RRM – RNA recognition motif

RGG – Arginine-glycine-glycine

sALS – Sporadic amyotrophic lateral sclerosis

SDS-PAGE – Sodium dodecyl sulfate – Polyacrylamide gel electrophoresis

SOD1 – Cu/Zn superoxide dismutase 1

SYGQ – Serine-tyrosine-glycine-glutamine

TAF15 or TAFII68 – TATA box binding protein associated factor 68 kDa

TARDP or TDP-43 – Transactive response DNA binding protein 43

ZFD – Zinc-finger domain

PREFACE

Parts of this dissertation will appear in:

A loss of FUS/TLS function leads to impaired cellular proliferation. Ward CL, Boggio KJ, Johnson BN, Boyd JB, Douthwright SR, Shaffer SA, Landers JE, Glicksman MA, Bosco DA. (2014)

Parts of this dissertation appeared in:

Sama RR, Ward CL, Kaushansky LJ, Lemay N, Ishigaki S, Urano F, Bosco DA (2013) FUS/TLS assembles into stress granules and is a prosurvival factor during hyperosmolar stress. *J Cell Physiol* 228:2222-2231.

Baron DM, Kaushansky LJ, Ward CL, Sama RR, Chian RJ, Boggio KJ, Quaresma AJ, Nickerson JA, Bosco DA (2013) Amyotrophic lateral sclerosis-linked FUS/TLS alters stress granule assembly and dynamics. *Mol Neurodegeneration* 8:30.

Sama RRK, Ward CL, Bosco DA (2014) Functions of FUS/TLS from DNA repair to stress response: implications for ALS. *ASN Neuro* 6:18

CHAPTER I: INTRODUCTION

Amyotrophic Lateral Sclerosis (ALS)

Amyotrophic lateral sclerosis (ALS), also referred to as Lou Gehrig's disease, is a neurodegenerative disorder characterized by the specific death of upper and lower motor neurons. This neuronal loss results in impairment of motor abilities causing paralysis and eventually death, resulting from respiratory failure. The disease is rapidly progressive, with death occurring usually 3-5 years after symptom onset (NINDS, 2013). Not only is there no cure for this disease, but treatments are very limited as well with only one in existence, Riluzole, that prolongs life by only a few months (Bensimon et al., 1994; Lacomblez et al., 1996). It is estimated that each year 5,000 people in the United States are diagnosed with ALS (NINDS, 2013). Approximately 90-95% of cases are sporadic, occurring without familial inheritance (Renton et al., 2014). That the disease occurs in people mainly between the ages of 50 and 60, in conjunction with its fast progression and the inability to predict its targets, make it especially devastating and an increasingly important area of research. The following sections provide additional information on the nature of this disease and a theory of its pathogenesis.

Clinical symptoms and diagnosis

Early signs of ALS are subtle and depend on the site and type of onset. Limb onset occurs in the arms or legs and is apparent by difficulty in performing simple tasks, such as writing, or an increased frequency of stumbling while walking (Gordon, 2013). Bulbar onset is the second type, accounting for 25% of cases. These individuals first experience difficulty swallowing or speaking, with a tendency to slur their words (Gordon, 2013). Regardless of the type of onset, symptoms quickly progress to other muscle types within the body and become more pronounced over time. Eventually patients are unable to walk or stand, eat without assistance, or even speak. As many of the symptoms of ALS are common in other disease, such as multiple sclerosis, Lyme disease, and spinal muscular atrophy, physicians must proceed with caution when diagnosing ALS. Since there is currently no biomarker of ALS, diagnosis is typically achieved by tracking the progression of symptoms and using specific tests, such as an electromyography (EMG) or a nerve conduction study (NCS), to rule out the diagnosis of other neurological diseases or disorders (NINDS, 2013).

Genetic and cellular contributions

There are two forms of ALS: familial and sporadic. Familial ALS (or fALS) is defined by inheritance of a mutated gene causative for ALS and accounts for ~10% of cases, while sporadic ALS (or sALS) has no evidence of a genetic linkage and comprises the remaining ~90%. The first gene associated with ALS

was Cu, Zn superoxide dismutase-1 (SOD1) in 1993 (Rosen et al., 1993). There are over 160 mutations in SOD1 that cause ALS and mutations in this gene alone account for ~20% of fALS. Over the past two decades many more genes have been identified, bringing the list to over 30 (Sreedharan and Brown, 2013). Within this list is *TDP-43* (TAR-DNA binding protein-43), *FUS/TLS* (fused in sarcoma/translocated in liposarcoma), and the most recently discovered *C9ORF72*, which accounts for approximately 30% of fALS. Together, these four genes are credited with causing 60% of fALS cases (Chen et al., 2013). Also important to note, is that while ALS is predominantly a mid-life disease, several genes have been associated with rare cases of juvenile onset, occurring between the ages of 6 and 26. These genes include *ALSIN* (Hadano et al., 2001), *senataxin* (*SETX*) (Chance et al., 1998), *spatacsin* (*SPG*) (Hentati et al., 1998; Stevanin et al., 2007), *ubiquilin 2* (*UBQLN2*) (Deng et al., 2011), and *FUS/TLS* (Baumer et al., 2010).

While all of these genes are clearly involved in the pathogenesis of ALS, it is still unclear whether their involvement is through a common cellular pathway. Several cellular events have been associated with ALS, including protein aggregation, aberrant RNA processing, oxidative stress, axonal dysfunction, mitochondrial disruption, metabolic disturbance, microglia activation, and aberrant activation of the apoptosis pathway (reviewed in (Chen et al., 2013; Sreedharan and Brown, 2013)). Two of the more prominently studied mechanisms are protein aggregation and aberrant RNA processing (reviewed in

(Sreedharan and Brown, 2013)). Studies of protein aggregation emerged with the very first identified ALS gene: SOD1. Mutant SOD1 obtains a misfolded conformation and accumulates as oligomers, ultimately becoming aggregates. This misfolded protein disrupts normal function of several cellular events, such as protein degradation (Bendotti et al., 2012; Chen et al., 2012) and axonal transport (Morfini et al., 2013). Wild-type SOD1 purified from sporadic ALS tissue also adopts a misfolded conformation and disrupts axonal transport (Bosco et al., 2010b), suggesting involvement of misfolded SOD1 in both familial and sporadic ALS (reviewed in Rotunno and Bosco, 2013). Other ALS-linked proteins that effect protein degradation and axonal function include ubiquilin 2 and valosin-containing protein (reviewed in Robberecht and Philips, 2013) and profilin-1 (Wu et al., 2012), respectively. Similarly, several ALS-genes have overlapping functions in RNA processing. These genes include TDP-43 (Kabashi et al., 2008; Sreedharan et al., 2008), FUS/TLS (Kwiatkowski et al., 2009; Vance et al., 2009), and C9ORF72 (DeJesus-Hernandez et al., 2011; Renton et al., 2011). How RNA processing is affected by mutations in these genes is not fully understood, but evidence suggests misregulation of transcription, splicing, and RNA editing (Polymenidou et al., 2012).

While several ALS-associated proteins can be linked to a common pathogenic mechanism, not one mechanism can account for every reported ALS gene **(Figure I-1)**. This raises the question of whether ALS is a single disease that can be treated with a specific therapy or rather a more complex disorder

caused by separate pathogenic events. That age of onset, clinical phenotypes, and progression of the disease vary greatly between patients suggest the latter. Furthermore, progression and clinical phenotypes can be predicted by genetics. For example, mutations in FUS are associated with early age of onset, bulbar onset, and rapid progression while repeat expansions in C9ORF are associated with shorter survival and cognitive and behavioral changes (reviewed in (Al-Chalabi and Hardiman, 2013)). The end result of motor neuron death is the same regardless of genetic factors, but the therapeutic strategy may need to differ based on the genetic and cellular events involved, such as intercepting the downstream effects of protein aggregation for patients harboring SOD1 mutations or correcting RNA processing defects for patients having FUS or TDP-43 mutations.

Figure I-1. The heterogeneity of ALS pathogenesis. Shown in purple are various ALS-linked genes and the pathogenic mechanisms with which they are associated.

With permission from BioMed Central, this figure was reproduced from: Chen S, Sayana P, Zhang X, Le W (2013) Genetics of amyotrophic lateral sclerosis: an update. Mol Neurodegener 8:28.

Environmental factors and epidemiology studies

Sporadic ALS cases are rarely (~11%) attributed to mutations in the genes causative for fALS (Renton et al., 2014). As ~90% of all ALS cases are sporadic, this equates to ~10% of all ALS cases being accounted for by known genetic mutations. While studying fALS genes and the associated cellular phenotypes provides valuable insight into the cellular pathogenesis of ALS, efforts have been made to determine the environmental causes or risk factors of sporadic ALS. Most epidemiological studies have been performed on European cohorts and have determined sex and age as the most common risk factors (Al-Chalabi and Hardiman, 2013). Men are diagnosed with ALS more frequently by a factor between 1.2 and 1.5, providing a lifetime risk of 1:350 for men and 1:400 for women (Al-Chalabi and Hardiman, 2013). The risk for ALS increases with age, but only up to an age of 75 where it plateaus and may even decline. This plateau affect however, may be due to the decreased likelihood of ALS being identified in older patients who may accept their symptoms as a normal sign of aging (Al-Chalabi and Hardiman, 2013).

Environmental factors have also been evaluated as risk factors for ALS, but these studies are hard to control as variables cannot be isolated and evidence is often circumstantial. The most frequently evaluated factors include exercise level (Scarmeas et al., 2002), participation in soccer (Chio et al., 2005), smoking (Wang et al., 2011a), occupation and participation in the armed services (McGuire et al., 1997), electric shock, and exposure to heavy metals, pesticides

or cyanotoxins (Armon, 2003). Despite this extensive list, no conclusive evidence of an environmental risk factor has been identified (reviewed in (Al-Chalabi and Hardiman, 2013)).

Overlap with Frontotemporal dementia (FTD)

It has become increasingly apparent that ALS is part of a continuum of neurodegenerative diseases, having overlapping features with frontotemporal dementia (FTD, pathologically known as frontotemporal lobar degeneration or FTLD). FTD accounts for 5-15% of dementia and is caused by degeneration of the frontal and temporal lobes. It is characterized clinically by a decline in behavior, personality, and language and molecularly by inclusions of various disease-specific proteins in neurons and glia, such as hyperphosphorylated tau protein, TDP-43 and FUS (reviewed in (Rademakers et al., 2012)). It is estimated that 15% of ALS patients meet the criteria for FTD (Ringholz et al., 2005) and 15% of FTD patients meet the criteria for ALS. In both instances, protein inclusions are a hallmark of the disease. In FTD, 35% of cases show aggregated microtubule-associated protein tau and the majority of cases negative for tau contain inclusions immunoreactive for ubiquitin (reviewed in (Rademakers et al., 2012)), which is also observed in motor neurons of ALS patients. In 2006, TDP-43 was discovered to be the main protein present in these ubiquitinated inclusions of both ALS and FTD patients (Arai et al., 2006; Neumann et al., 2006). Soon after, mutations in TDP-43 were found to be causative for familial

and sporadic ALS (Kabashi et al., 2008; Sreedharan et al., 2008). Additional evidence of an overlap between these diseases came with the discovery of a genetic link between FUS and ALS (Kwiatkowski et al., 2009; Vance et al., 2009) followed by the identification of FUS as a main component of FTLD inclusions negative for tau or TDP-43 (Neumann et al., 2009b). Most recently, a hexanucleotide repeat expansion in *C9ORF72* was found to account for ~25-50% of familial ALS, 10-30% of familial FTD, and also ~80% of cases having features of both FTD and ALS, further solidifying a relationship between these two disorders (DeJesus-Hernandez et al., 2011; Renton et al., 2011).

Disease pathogenesis

When contemplating the development of ALS, a few disease characteristics stand out: onset occurs later in life, the majority of cases are sporadic, and only a very small percentage of cases are attributed to genetic mutations. Clearly genetics is a causative factor, but that genetic mutations can exist since birth and not cause ALS until late adulthood suggests environmental factors are a contributing factor as well. Moreover, the majority of cases are not linked to genetic mutations, which further supports a role for environmental insults in pathogenesis. These facts support the division of ALS development into three scenarios, based on various contributions of cell damage occurring over time, genetics, and environmental factors. These three scenarios, put forth by Drs. Al-Chalabi and Hardiman, are described as monogenic ALS, oligogenic or polygenic

ALS, and gene x environment interaction (Al-Chalabi and Hardiman, 2013). In monogenic ALS, a mutation in a single gene, such as SOD1, accounts for the majority of the risk. To reach a threshold for disease onset, only a small contribution is needed from environmental factors, such as ultraviolet radiation which increases cellular reactive oxygen species (Devasagayam et al., 2004) normally controlled by SOD1. Oligogenic or polygenic ALS, takes into account the 100+ genes identified as risk factors for ALS (Abel et al., 2012). In this scenario, mutations in these genes alone do not cause ALS, but in combination these mutations can put the cell at risk. For instance, several genes associated with protein degradation may be mutated, each slightly affecting the efficiency of this pathway. If these genes are mutated individually the cell can still function normally. In combination however, and in association with environmental factors that contribute to protein aggregation for example, the cell's protein degradation machinery becomes less efficient. Over time, misfolded protein will accumulate until a threshold for cell death occurs and disease onset ensues. In the final scenario, the presence of a specific genetic predisposition in combination with a specific environmental insult is required for the burden to reach the threshold for disease onset. An example may be a mutation in a gene that is required for DNA damage repair followed by exposure to a toxin that damages DNA. The authors further propose that after disease onset occurs, a self-perpetuating process follows, causing a rapid decline in health. In summary, these three scenarios help

explain the relationship between time, environment, and genetic predisposition that collectively contribute to the onset of ALS.

Fused in Sarcoma/Translocated in Liposarcoma (FUS/TLS)

Fused in Sarcoma/Translocated in Liposarcoma (FUS/TLS), or FUS, was first discovered in 1993 as a fusion oncoprotein in myxoid liposarcoma (Crozat et al., 1993; Rabbitts et al., 1993). During the remainder of the 20th century, FUS-related research focused on characterizing its involvement in sarcomas and its nucleic acid associations, with a role in RNA splicing being the dominant interest through the mid 2000's (Lerga et al., 2001; Rapp et al., 2002; Meissner et al., 2003; Delva et al., 2004; Belly et al., 2005). During the 15 years following its discovery in sarcomas, an average of ~2.5 FUS-related publications were produced a year. In February of 2009, mutations in FUS were found to be causative for ALS (Kwiatkowski et al., 2009; Vance et al., 2009) and since then the average number of FUS-associated publications per year has risen to an astounding 50! FUS has proven to be a complex multifunctional protein important for numerous cellular processes fundamental to cell health and homeostasis. The sections below provide a description of the physical properties of FUS, its functions in the nucleus and cytoplasm, and its role in disease with a focus on ALS.

Functional domains and structure

FUS is a 55 kDa protein consisting of 526 amino acids. It is an RNA/DNA binding protein that functions at all stages of gene expression from transcription to protein translation (Sama et al., 2014) and belongs to the FET (formerly TET) family of proteins, also consisting of Ewing's Sarcoma (EWS) and TATA box binding protein associated factor 68 kDa (TAF15) (Tan and Manley, 2009a). Based on sequence determinants, FUS consists of an N-terminal QGSY-rich ("prion-like") domain, glycine-rich region, RNA-recognition motif (RRM), zinc-finger domain, C-terminal arginine-glycine-glycine (RGG)-rich domains, and nuclear export and localization signals **(Figure I-2)**. Biochemical and structural studies have determined that overall FUS is highly unstructured with organization apparent only in the zinc-finger and RRM domains (Iko et al., 2004). The flexible nature of the protein may be important in allowing FUS to interact with nucleic acids and various proteins essential for the host of functions it performs. In fact, every domain of FUS contributes to the protein's myriad of functions performed throughout the cell **(Figure I-2)**.

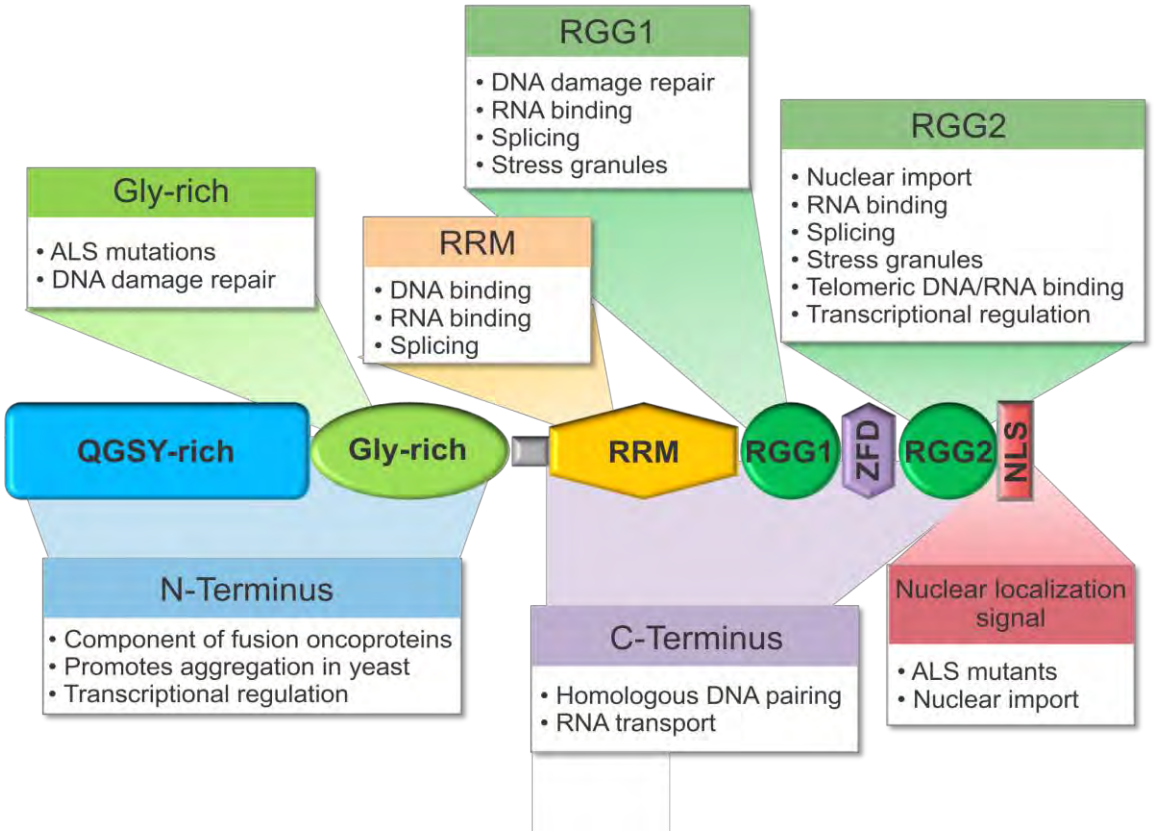

Figure I-2. The functional domains of FUS. FUS binds DNA, RNA and proteins to perform a diverse array of functions. Summarized here are the known functions of FUS annotated onto the domain structure of the protein. (QGSY-rich, glutamine-glycine-serine-tyrosine-rich or “prion-like” domain; Gly-rich, glycine-rich; RGG, arginine-glycine-glycine-rich; RRM, RNA recognition motif; ZFD, zinc-finger domain; NLS, nuclear localization signal).

Nuclear and cytoplasmic functions

FUS is a multifunctional protein involved in a diverse array of cellular processes. As a resident of the nucleus, FUS binds both DNA and RNA. Interactions with DNA form the basis for several putative functions of FUS in the context of DNA processing **(Figure I-3)**. For example, FUS directly binds both single- and double-stranded DNA (Baechtold et al., 1999; Liu et al., 2013), localizes to RNAPII promoters (Tan et al., 2012) and telomeres (Dejardin and Kingston, 2009; Takahama et al., 2009) and is associated with higher order DNA structures, such as G-quadruplexes (Baechtold et al., 1999; Takahama and Oyoshi, 2013; Takahama et al., 2013). These associations underlie the roles of FUS in modulating transcription, telomere length, and DNA damage repair (Takahama et al., 2013) (reviewed in: (Sama et al., 2014)). Additionally, interactions between RNA and FUS coincide with several important functions of FUS in RNA processing. For example, FUS binds long introns (Hoell et al., 2011; Ishigaki et al., 2012; Lagier-Tourenne et al., 2012; Rogelj et al., 2012) consistent with a role for FUS in pre-mRNA splicing (reviewed in (Ling et al., 2013)). FUS binding sites were also identified within the 3'UTR of target genes (Lagier-Tourenne et al., 2012), which may contribute to mRNA export from the nucleus and localization within the cell for local translation (Barrett et al., 2012). In fact, FUS is also known as hnRNP P2 (heterogeneous ribonucleoprotein P2) (Calvio et al., 1995), and collectively hnRNPs are known to function in mRNA splicing, packaging, trafficking/nuclear export, stability, and translation (Han et al., 2010).

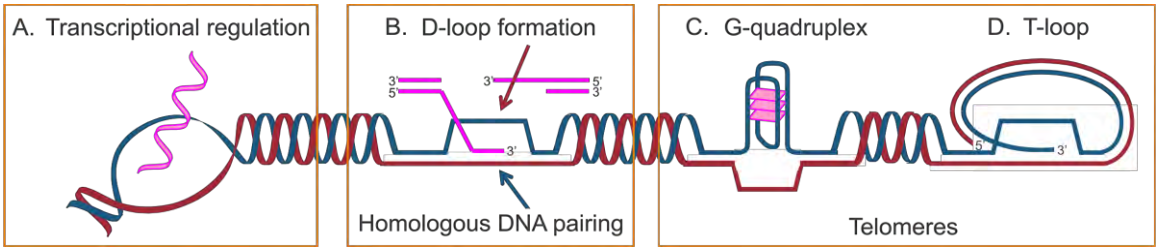

Figure I-3. FUS directly binds DNA. (A) FUS binds the promoters of >1000 genes, indicative of a role in transcriptional regulation. **(B)** FUS binds both single- and double-strand DNA and is important for two critical steps in homologous recombination: D-loop formation and homologous DNA pairing. When a double-strand break occurs in DNA, the 5' end of the break is trimmed back to create a 3' overhang of single-stranded DNA. This 3' single-stranded DNA then binds a complementary sequence within duplex DNA of a homologous chromosome or sister chromatid, a process called strand invasion (reviewed in (Li and Heyer, 2008)). **(C)** FUS binds G-quadruplexes in telomeres. **(D)** Analogous to the role of FUS in D-loop formation, FUS may also be important for T-loop formation at the ends of telomeres. T-loops are formed when a single-strand, G-rich DNA overhang at the end of a chromosome forms a loop and anneals to a complementary 5' C-rich sequence ((Griffith et al., 1999) and reviewed in (Greider, 1999)).

The classification of FUS as an hnRNP highlights its ability to shuttle between the nucleus and cytoplasm (Zinszner et al., 1997; Fujii and Takumi, 2005) and its importance in both compartments. In the cytoplasm in fact, FUS is found in neuronal dendrites (Belly et al., 2005; Fujii et al., 2005; Yoshimura et al., 2006; Aoki et al., 2012) where it translocates with mRNAs important for the development and function of spines (reviewed in (Dormann and Haass, 2013)). FUS is also found in translationally active RNA/protein foci (Yasuda et al., 2013) within the cytoplasm, as well as stress granules formed in response to osmotic stress ((Sama et al., 2013) See also Appendix II), further demonstrating the cytoplasmic importance of FUS.

FUS/TLS in disease

As its name implies, FUS is part of an onco-fusion protein that causes malignant myxoid liposarcoma. The N-terminal transcriptional activation domain of FUS is fused to the transcription factor CHOP (also known as DDIT3), forming FUS-CHOP (Crozat et al., 1993; Rabbitts et al., 1993) which accounts for more than 90% of myxoid liposarcoma cases (Antonescu et al., 2000). In some cases of Ewing's sarcoma family tumors, FUS is fused to the transcription factor ERG (Shing et al., 2003). A similar fusion of FUS and ERG, with inclusion of different exons, has also been found in rare cases of acute myeloid leukemia (Ichikawa et al., 1994; Panagopoulos et al., 1994). Additionally, fusion of FUS with ATF1 and BBF2H7 will cause angiomatoid fibrous histiocytoma (Waters et al., 2000;

Raddaoui et al., 2002) and low-grade fibromyxoid sarcoma (Storlazzi et al., 2003), respectively. Fusion proteins containing FUS, or family members EWS and TAF15, actually participate in nearly half of all sarcomas (Riggi et al., 2007). FUS also has a strong presence in neurological disorders **(Figure I-4)**. In 2009, mutations in FUS were found to be associated with ALS (Kwiatkowski et al., 2009; Vance et al., 2009) with over 40 pathogenic mutations identified to-date (Dormann and Haass, 2013). Additionally, FUS is closely associated with frontotemporal dementia (FTD; pathologically defined as frontotemporal lobar degeneration, FTLD) as a component of pathological protein inclusions (Munoz et al., 2009; Neumann et al., 2009b; Neumann et al., 2009a; Urwin et al., 2010). While all cases of ALS-FUS are associated with genetic mutations, FTLD-FUS is characterized by neuronal FUS inclusions (Rademakers et al., 2012) with only rare cases associated with genetic FUS abnormalities (Van Langenhove et al., 2010). FUS inclusions now define several different subtypes of FTLD (Rademakers et al., 2012), including atypical FTLD-U (Neumann et al., 2009b; Urwin et al., 2010), neuronal intermediate filament inclusion disease (Neumann et al., 2009a), and basophilic inclusion body disease (Munoz et al., 2009); collectively referred to as FTLD-FUS (Mackenzie et al., 2010).

Most recently, several mutations in FUS were linked to essential tremor (ET) (Merner et al., 2012; Rajput et al., 2013; Wu et al., 2013; Zheng et al., 2013), an adult onset movement disorder having clinical overlap with Parkinson's disease (Benito-Leon and Louis, 2006). Historically, ET has been classified as

monosymptomatic, mainly characterized by a kinetic arm tremor, and it is estimated that 30-50% of cases are misdiagnosed as Parkinson's disease or other forms of tremor (Benito-Leon and Louis, 2006). More recently however, it was recognized that cognitive symptoms, such as loss of memory, depression, and deficits in executive function are associated with ET (reviewed in (Bermejo-Pareja and Puertas-Martin, 2013)). Pathologically, this disease is associated with cerebellar degeneration, accumulation of Lewy bodies in the brainstem, and accumulation of neurofilament in Purkinje cell axons (Benito-Leon and Louis, 2006). Until recently however, post-mortem brain examinations were uncommon so an exact pathological description of the disease is still unavailable. Genetically, familial inheritance is a risk factor for ET, but other than several mutations in FUS, no clear genetic links to the disease have been made aside from the identification of a few chromosomal susceptibility loci (Benito-Leon and Louis, 2006). The most commonly ET-associated mutation in FUS is G290X, which results in a truncated transcript (Merner et al., 2012). This truncated transcript appears to be degraded by nonsense-mediated decays, effectively decreasing expression of FUS (Merner et al., 2012), suggestive of loss of FUS function contributing to disease pathogenesis. That several other groups have not identified FUS mutations in their ET cohorts however, may imply FUS mutations are causative for ET only in rare cases (Parmalee et al., 2012; Hedera et al., 2013; Labbe et al., 2013; Ortega-Cubero et al., 2013).

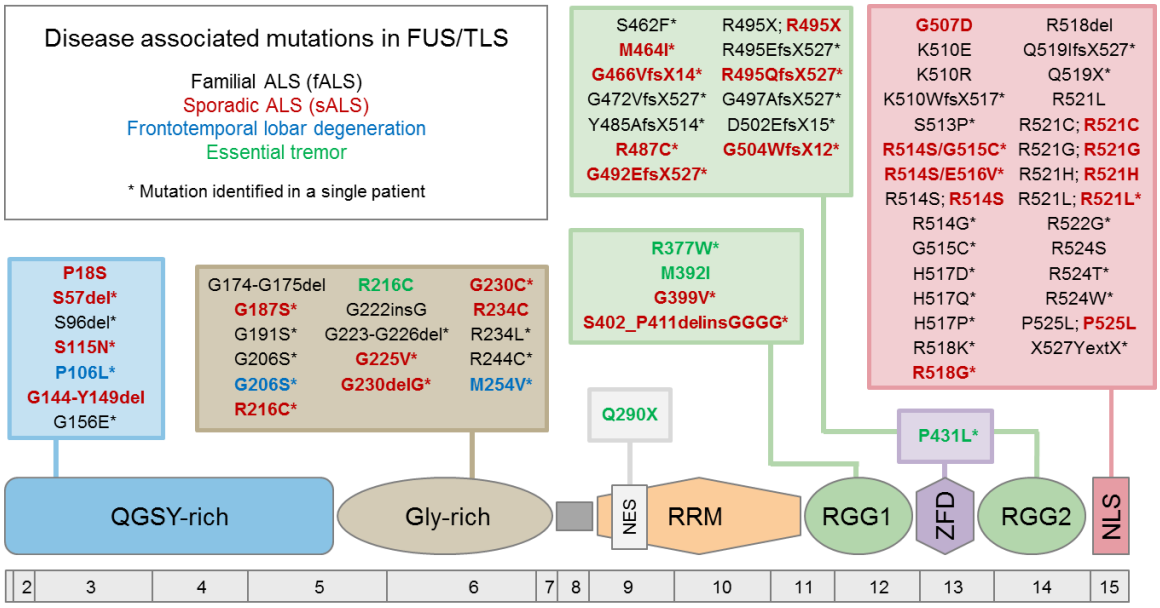

Figure I-4. Disease associated mutations in FUS/TLS. Mutations in FUS are linked to familial and sporadic amyotrophic lateral sclerosis (fALS and sALS), frontotemporal lobar degeneration, and essential tremor. Summarized here are the known mutations associated with each disease, annotated onto the domain structure of the protein. Mutations identified in a single patient are denoted by asterisks. (QGSY-rich, glutamine-glycine-serine-tyrosine-rich; Gly-rich, glycine-rich; NES, nuclear export signal; RRM, RNA recognition motif; RGG, arginine-glycine-glycine-rich; ZFD, zinc-finger domain; NLS, nuclear localization signal).

Information in this figure was compiled from the following sources:

Deng H, Gao K, Jankovic J (2014) The role of FUS gene variants in neurodegenerative diseases. Nat Rev Neurol 10:337-348.

Dormann D, Haass C (2013) Fused in sarcoma (FUS): An oncogene goes awry in neurodegeneration. Mol Cell Neurosci 56:475-486.

Lattante S, Rouleau GA, Kabashi E (2013) TARDBP and FUS mutations associated with amyotrophic lateral sclerosis: summary and update. Hum Mutat 34:812-826.

Mechanism of FUS/TLS in Amyotrophic Lateral Sclerosis

In 2009 two groups simultaneously published the discovery of a genetic linkage between FUS and ALS (Kwiatkowski et al., 2009; Vance et al., 2009). Over the following years, ~25 additional groups published findings of FUS mutations in ALS patients from French, Italian, Belgian, German, Japanese, Dutch, Spanish, Taiwanese and Chinese populations demonstrating the global contribution of mutant FUS to ALS. Currently, over 50 ALS-linked mutations in FUS have been identified, contributing to both sporadic and familial ALS. Overall, FUS mutations account for ~4% of familial ALS, ~1% of sporadic ALS, and is also attributed with being a main contributor of juvenile ALS (Chen et al., 2013). While the mechanism behind FUS pathogenesis in ALS is not known, data is consistent with both a gain of toxic function and a loss of normal function for FUS variants.

Gain of function hypothesis

The fact that mutations in FUS cause the protein to mislocalize to the cytoplasm and the degree of this mislocalization correlates with age of onset (Dormann et al., 2010), makes a gain of toxic function in the cytoplasm an attractive hypothesis. That FUS binds both nucleic acid and proteins could predict aberrant interactions of FUS with various cytoplasmic species, interfering with normal cytoplasmic processes. An aberrant interaction that has drawn considerable attention within the field over the past few years is the assembly of ALS-linked mutant FUS into cytoplasmic puncta called stress granules (reviewed in

(Wolozin, 2012; Bentmann et al., 2013; Li et al., 2013)). Stress granules are stalled translational complexes that form in response to environmental or metabolic stress. The proposed function of stress granules is the triage of mRNAs, dictating their fate for expression, degradation, or suppression in order to express the appropriate repertoire of proteins to re-establish homeostasis (Anderson and Kedersha, 2008; Kedersha et al., 2013). Cytoplasmically localized mutant FUS is consistently detected within stress granules under conditions of protein over-expression, oxidative stress, heat-shock and endoplasmic reticulum (ER)-stress (Bosco et al., 2010a; Dormann et al., 2010; Gal et al., 2011; Kino et al., 2011; Bentmann et al., 2012). The association of FUS with stress granules correlates with its cytoplasmic expression, with variants such as FUS P525L and R495X exhibiting the most robust levels of both cytoplasmic mislocalization and stress granule incorporation (Bosco et al., 2010a; Dormann et al., 2010). Baron et al. demonstrated that the presence of mutant-FUS in stress granules alters several properties that may be important for stress granule function ((Baron et al., 2013) see also Appendix III). Under conditions of sodium arsenite, an inducer of oxidative stress, the expression of mutant FUS delays the assembly and expedites the disassembly of stress granules. Furthermore, the size and abundance of stress granules are enhanced by mutant-FUS, which may be an outcome of the increased protein- and/or mRNA load within these structures caused by mutant FUS-specific interactions (Baron et al., 2013). Intriguingly, stress granule marker proteins have been detected in pathological aggregates of

post-mortem tissues from individuals with ALS and FTLD (Dormann et al., 2010; Liu-Yesucevitz et al., 2010; Bentmann et al., 2013; Kim et al., 2013), suggesting that these granules may accumulate during chronic stress and thus serve as precursors to the end-stage pathological aggregates seen in these disorders (Wolozin, 2012).

Loss of nuclear function hypothesis

That not all ALS-causing mutant FUS proteins mislocalize to the cytoplasm argues against a purely gain of toxic cytoplasmic function mechanism for FUS in ALS. A gain of toxic function could also occur in the nucleus, or alternatively, mutations in FUS could mediate disease through a loss of proper FUS function in the nucleus. Suggestive of the latter is the correlation between disease severity and the degree of nuclear FUS depletion (Dormann et al., 2010). Furthermore, FUS is predominantly a nuclear protein and has numerous nuclear functions important for cellular processes fundamental to cell health and homeostasis, such as the repair of damaged DNA and regulation of transcription and splicing (Sama et al., 2014). Disruption of any of these processes could have a detrimental impact on cellular viability.

In vivo models: To assess the effects of a complete loss of FUS function several groups have established *in vivo* models of FUS depletion through targeted knockdown with RNAi or creating null alleles for complete knockout of the protein

(Table I-1). In *Drosophila* models, knockdown or knockout of *cabeza*, the *Drosophila* homolog of FUS (Stolow and Haynes, 1995), caused temperature dependent pupal lethality, physiological defects such as eye degeneration and wing defects, locomotor defects in both larvae and adult flies, and a shorter adult lifespan (Wang et al., 2011b; Sasayama et al., 2012; Xia et al., 2012). Zebrafish injected with antisense morpholino oligonucleotides targeting FUS showed signs of motor defects in that they lacked a touch-evoked escape response. Additionally, the outgrowth and length of hyperbranched and unbranched axons of motor neurons were reduced with FUS knockdown, supportive of a neurodegenerative phenotype in these animals (Kabashi et al., 2011). To test a loss of function hypothesis, wild-type FUS and mutant FUS variants were expressed in both the *Drosophila* and zebrafish models and assessed for their ability to rescue the phenotypes caused by FUS depletion. While the reintroduction of wild-type FUS rescued pupal lethality, locomotor speed, and adult lifespan in *Drosophila*, expression of FUS variants R522G or P525L was unable to rescue locomotor speed or median lifespan of adult flies (Wang et al., 2011b), demonstrating loss of function of these variants. In the zebrafish model, R521H demonstrated no ability to rescue, R521C only partially rescued, and the S57deletion mutant rescued the phenotypes to a similar degree as the expression of wild-type FUS (Kabashi et al., 2011). The S57deletion mutation is a rare variant identified in only one sporadic ALS case, suggesting it may not be a pathogenic mutant, which could explain its wild-type-like nature in this model.

Variants R521H and R521C however, demonstrated phenotypes consistent with a loss of function model.

Two knockout mouse models of FUS have also previously been studied. Kuroda et al. generated a *FUS-/-* mouse model that lived to adulthood, but were smaller in size, showed sensitivity to ionizing radiation, and demonstrated male sterility and reduced female fertility (Kuroda et al., 2000). An additional *FUS-/-* line, created in an inbred background, was perinatal lethal and defective in B-cell development. Furthermore, these mice showed several signs of chromosomal instability, such as chromosome breakage, aneuploidy, and centromeric fusions (Hicks et al., 2000). These lines were created nine years before the discovery of FUS in ALS and therefore it is unlikely that they were monitored for signs of motor-neuron degeneration. Consistent between both lines however, were signs of genomic instability, suggestive of a role for FUS in maintaining DNA integrity.

System		Publication	Method of FUS depletion	Summary of results
in vivo	Flies	(Machamer et al., 2014)	Caz null; or RNAi in neurons	increased synaptic activity
		(Xia et al., 2012)	Caz null; or RNAi	physiological defects, neuromuscular junction structure defects, reduced locomotion, reduced viability
		(Sasayama et al., 2012)	RNAi in neurons	reduced locomotion, shorter lifespan, shorter axon length
		(Wang et al., 2011b)	Caz null	physiological defects, reduced locomotion, shorter lifespan
	Fish	(Kabashi et al., 2011)	antisense morpholino oligonucleotide	reduced locomotion, shorter hyperbranched and unbranched axons
	Mice	(Hicks et al., 2000)	interrupted gene in exon 12 (inbred background)	perinatal death, reduced number of lymphocytes, defective B-cell development, numerous signs of genomic instability
		(Kuroda et al., 2000)	interrupted gene in exon 8 (outbred background)	male sterility due to defective spermatogenesis, reduced female fertility, sensitivity to ionizing radiation
in vitro	Neuronal cells in culture	(Fujii et al., 2005)	hippocampal neurons from knockout mice (Hicks et al., 2000)	abnormal dendritic branching and spine morphology
		(Ishigaki et al., 2012)	lentiviral transduction of shRNA into E15 cortical neurons (6 days, 80% knockdown)	alterations in mRNA expression and pre-mRNA splicing
		(Nakaya et al., 2013)	siRNA transfection of ES cell-derived neurons (3 days, 44% knockdown)	alterations in mRNA expression and pre-mRNA splicing
		(Orozco et al., 2012)	lentiviral transduction of shRNA into rat hippocampal neurons (7 days)	no overt toxicity; lack of exon 10 splicing in Tau; axons were shorter and had enlarged growth cones
	Non-neuronal cells in culture	(Hoell et al., 2011)	siRNA transfection into HEK cells (3 days)	mRNA expression unchanged
		(Kim et al., 2010)	siRNA transfection into HEK or HeLa cells (2days)	decreased HDAC6 mRNA and protein levels
		(Tan et al., 2012)	siRNA transfection into HEK cells	altered expression of candidate genes
		(van Blitterswijk et al., 2013)	siRNA transfection into HEK cells (2 days)	alterations in mRNA expression and pre-mRNA splicing
		(Yamazaki et al., 2012)	lentiviral transduction of shRNA into HeLa cells	reduction in SMN nuclear bodies
		(Wang et al., 2013)	siRNA transfection into U2OS cells	reduced efficiency of DNA damage repair pathways

Table I-1. Summary of investigations of FUS knockdown/knockout models.

DNA damage models: Recently, the importance of FUS in the DNA damage repair pathway was firmly established after several groups demonstrated a localization of FUS to sites of DNA damage and a deficiency in DNA damage repair in the absence of FUS. Collectively, six fALS-linked mutant FUS proteins were evaluated in these assays. With the exception of one for which there was conflicting results (Rulten et al., 2013), all of the variants localized to sites of DNA damage to a similar degree as wild-type FUS (Mastrocola et al., 2013; Wang et al., 2013). In assessing the ability of mutant FUS to function in DNA damage repair, mutant FUS protein was expressed in cells devoid of FUS. FUS knockdown decreases the efficiency of two common double-strand break repair pathways: homologous recombination (HR) and non-homologous end-joining (NHEJ). All of the FUS variants tested (R244C, R514S, H517Q, R521C) were unable to rescue the defect in HR-mediated DNA repair observed with FUS knockdown (Wang et al., 2013). Efficiency of NHEJ was also not fully rescued by mutant FUS, although the deficit was greater for HR (Wang et al., 2013). This demonstrates a loss of DNA damage repair function by mutant FUS despite proper localization of the protein to sites of DNA damage **(Figure I-5)**. As damaged DNA accumulates normally as a function of age (Gorbunova et al., 2007), inefficient DNA repair due to FUS mutations could have an additive effect over time, leading to neuronal death later in life as a result of unrepaired DNA. FUS in the DNA damage response is discussed further in Chapter II.

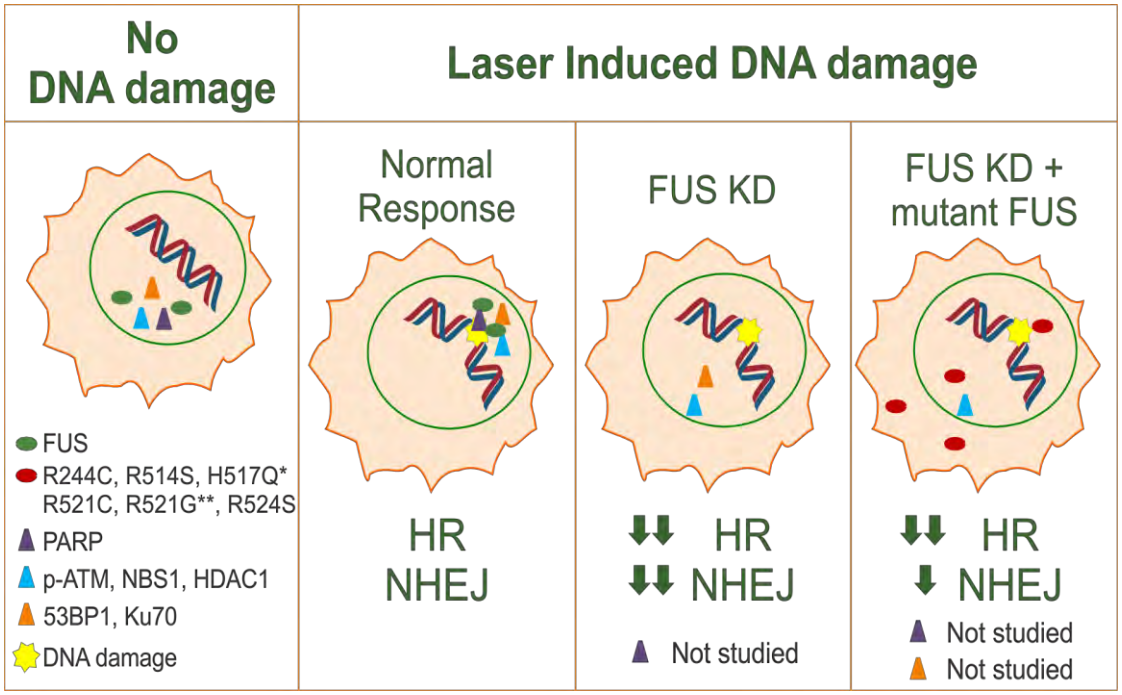

Figure I-5. FUS is recruited to sites of DNA damage and contributes to DNA-damage repair. Under normal conditions FUS (green oval) and common repair proteins (triangles) localize to sites of laser induced DNA damage (yellow star). Under conditions of FUS knock-down (KD), these repair proteins are not recruited to sites of DNA damage and the efficiency of both homologous recombination (HR) and non-homologous end joining (NHEJ) is reduced. Mutant-FUS (red ovals) is still able to localize to sites of damage in the absence of endogenous FUS (**discrepancy in the literature for the degree of localization of variant R521G). Exogenous mutant-FUS does not fully rescue DNA-damage repair when endogenous FUS is knocked-down (*exception, FUS H517Q), although mutant-FUS is able to recover NHEJ to a greater extent than HR (*NHEH is fully recovered by FUS H517Q).

As nuclear functions of FUS also include transcriptional regulation and pre-mRNA splicing, several groups have investigated the effects of FUS depletion on mRNA abundance and splicing events **(Table I-2)**. As a transcriptional co-regulator, FUS interacts with several transcription factors (Hallier et al., 1998; Uranishi et al., 2001; Sato et al., 2005; Kim et al., 2010; Du et al., 2011) as well as RNA Polymerase II (RNAP2) (Immanuel et al., 1995; Bertolotti et al., 1996; Bertolotti et al., 1998; Schwartz et al., 2012) and RNA Polymerase III (RNAP3) (Tan and Manley, 2009b) and regulates the expression of their target genes. The ability of FUS to interact with and regulate the transcriptional activity of RNA polymerases suggests a general role for FUS in cellular transcriptional regulation. In fact, FUS chromatin immunoprecipitation of HeLa lysates followed by promoter microarray analyses revealed that FUS directly binds DNA in promoter regions. This study found that FUS bound to 1,161 promoter regions for genes involved in various cellular processes, including gene expression, cell cycle, and neuronal functions (Tan et al., 2012). Not surprisingly therefore, several groups using genome-wide expression array analyses reported alterations in mRNA abundance upon FUS knockdown in a variety of cell types using different FUS depletion strategies ((Hoell et al., 2011; Ishigaki et al., 2012; Lagier-Tourenne et al., 2012; Rogelj et al., 2012; Nakaya et al., 2013; van Blitterswijk et al., 2013)) and reviewed in (Ling et al., 2013)). Additionally, global effects on alternative splicing has been revealed through genome-wide exon array analyses (reviewed in (Ling et al., 2013)) of FUS depletion in primary

neurons (Ishigaki et al., 2012; Lagier-Tourenne et al., 2012; Rogelj et al., 2012; Nakaya et al., 2013) as well as non-neuronal cells (van Blitterswijk et al., 2013), demonstrating that FUS likely plays a general role in splicing in various cell types. Whether mutant FUS mimics FUS knockdown and exerts the same effects on transcriptional regulation and splicing has yet to be determined.

Summary

Five years after the discovery of FUS mutations in ALS, the question still remains whether these mutations result in a gain of toxic function or a loss of normal function. The work presented in this thesis investigates a loss of function hypothesis, modeled by FUS knockdown in mammalian cells in culture. Chapter II introduces this knockdown system and a reduced cellular proliferation phenotype that results from FUS depletion. As a candidate approach to providing mechanistic insight into this phenotype, DNA damage repair was investigated. Upon FUS knockdown, levels of phosphorylated H2AX, a common marker of DNA damage, are elevated in a FUS dependent manner, demonstrating a correlation between FUS levels and DNA damage accumulation. Chapter III takes a broader approach to providing mechanistic insight and uses quantitative proteomics to identify proteins differentially expressed upon FUS knockdown. Several fundamental cellular pathways were enriched within the functions of differentially expressed proteins, including cell-cycle regulation, cytoskeletal organization, oxidative stress and energy homeostasis. Further, the

work in Chapter III demonstrates therapeutic potential for the treatment of cellular deficiencies associated with loss of FUS function by showing reversal of the phenotype by FUS re-expression or treatment with the small molecule, rolipram. Collectively, the work presented in this dissertation demonstrates the importance of FUS for cell health and homeostasis, supports a role for FUS in DNA damage repair and identifies additional cellular pathways influenced by loss of FUS function as relevant to the pathogenesis of ALS.

		Investigations of FUS in RNA processes				
Publication: General description		**mRNA Expression (method)**	**mRNA Splicing (method)**	**Binding targets (method)**	**RNA binding specificity**	**Key categories identified by Gene Ontology (GO) Term analysis[VI]**
Hoell et al., 2011	Comparison of FET family and mutant FUS RNA targets	FUS knockdown in HEK-293 cells (microarray)	N/A	HA-tagged WT, R521H or R521G in HEK-293 cells (PAR-CLIP[i])	Introns; AU-rich stem loops (15-fold higher affinity than GGU repeat)	RNAs uniquely bound by mutant-FUS: endoplasmic reticulum and ubiquitin-proteasome related
Colombrita et al., 2012	Comparison of FUS and TDP-43 RNA targets	N/A	N/A	Cytoplasmic fraction of NSC-34 (RIP-CHIP[ii])	3'UTR; limited sequence specificity	RNAs bound by FUS: transcriptional regulation, cell cycle, ribonucleoprotein biogenesis, RNA splicing, stress response/ DNA repair, purine ribonucleotide binding and ubiquitin-mediated proteolysis
Ishigaki et al., 2012	RNA binding specificity of FUS; expression and splicing regulation by FUS	FUS knockdown in primary cortical neurons (exon array)	FUS knockdown in primary cortical neurons (exon array)	mouse cerebellum (HITS-CLIP[iii])	Introns and 3'UTR; regions with secondary structure	Changes in mRNA abundance: signaling cascades and metabolic processes Alterna ively spliced mRNA: vesicle transport, neuronal impulse and neuronal projection
Rogelj et al., 2012	Comparison of FUS and TDP-43 RNA targets; expression and splicing regulation by FUS	*FUS -/-* embryonic mouse brain (splice-junction microarray)	*FUS -/-* embryonic mouse brain (splice-junction microarray)	embryonic mouse brain (iCLIP[iv])	Long introns; no preference for stem-loops; limited sequence specificity	Alternatively spliced mRNA: cell adhesion, apoptosis, neuronal development and axonogenesis
Lagier-Tourenne et al., 2012	Species comparison of FUS RNA targets; comparison of targets, expression and splicing regulation between FUS and TDP-43	FUS knockdown in adult mouse brain and spinal cord (RNA-seq)	*FUS -/-* embryonic mouse brain; FUS knockdown in adult mouse brain (splicing-sensitive microarrays)	Naïve mouse brain; non-disease human brain (CLIP-seq[v])	Long introns and 3'UTR; GUGGU is an enriched RNA sequence motif	RNAs bound by FUS: components of the synapse and molecules residing in neuronal projections
Nakaya et al., 2013	Species comparison of FUS RNA targets; expression and splicing regulation by FUS	FUS knockdown in embryonic stem cell (ESC) derived mouse neurons (RNA-seq)	FUS knockdown in ESC derived mouse neurons (RNA-seq)	human temporal lobe cortices; ESC derived mouse neurons (HITS-CLIP[iii])	Introns; limited sequence specificity	RNAs bound by FUS: synapse, cell adhesion, neuronal projection and neuronal recognition processes
van Blitterswijk et al., 2013	Comparison of FUS overexpression, FUS knockdown and expression of mutant-FUS on mRNA expression and splicing	FUS knockdown; overexpression of WT, R521G or R522G in HEK-293 cells (RNA-seq)	FUS knockdown; overexpression of WT, R521G or R522G in HEK-293 cells (RNA-seq)	N/A	N/A	Changes in mRNA abundance: ribosome, spliceosome, mismatch repair and DNA replication

Table I-2. Summary of investigations of FUS involvement in RNA processes.

[i]PAR-CLIP – photoactivatable ribonucleoside-enhanced crosslinking and immunoprecipitation

[ii]RIP-Chip - RNA-binding protein immunopurification, microarray

[iii]HITS-CLIP - High-throughput sequencing of RNA isolated by crosslinking immunoprecipitation

[iv]iCLIP – individual-nucleotide resolution crosslinking and immunoprecipitation

[v]CLIP-seq – crosslinking immunoprecipitation, high-throughput RNA sequencing (RNA-seq)

[VI]gene categories that are highlighted in the original work, see original publication for a full list of GO terms

PREFACE TO CHAPTER II:

The work presented in this chapter was performed by Catherine L. Ward with the exception of the immunofluorescence images in figures 2 and 3 which were acquired by Dr. Desiree Baron.

The work presented in this Chapter intended to uncover a role for FUS in DNA damage repair and investigate the functional capacity of ALS-linked mutant FUS. Despite exhaustive troubleshooting and experimental optimizations, the findings were suggestive, but largely inconclusive and were not pursued for publication. Following the termination of this project, three groups published conclusive evidence of a functional role for FUS in double-strand break repair, which is disrupted when FUS contains ALS-linked mutations. Collectively, investigations of a role for FUS in DNA damage repair are discussed herein.

CHAPTER II: A LOSS OF DNA DAMAGE REPAIR FUNCTION OF FUS/TLS IN AMYOTROPHIC LATERAL SCLEROSIS

Introduction

Over 50 mutations in the gene *Fused in sarcoma/translocated in liposarcoma* (FUS/TLS, or FUS) have been identified as causative for amyotrophic lateral sclerosis, or ALS. FUS is a multifunctional protein involved in a host of cellular processes related to DNA and RNA metabolism and cellular stress response (Sama et al., 2014). Since the discovery of FUS mutations in ALS (Kwiatkowski et al., 2009; Vance et al., 2009) much research has been focused on determining the related pathogenic mechanism(s). An initial observation was the cytoplasmic mislocalization of FUS mutant protein (Kwiatkowski et al., 2009; Vance et al., 2009) which appears to correlate with disease severity (Dormann et al., 2010). This is characteristic of mutations within the nuclear localization signal (NLS) of the protein, which account for nearly half of all mutations **(Figure I-4)**. This observation has led to many researchers investigating a gain of toxic function as a pathogenic mechanism for cytoplasmic variants (Hoell et al., 2011; Huang et al., 2011; Baron et al., 2013). In addition to mutations within the NLS, 25% of mutations are clustered in the glycine-rich region of FUS **(Figure I-4)** and these proteins retain proper nuclear localization (Dormann et al., 2010). This evidence argues against a purely gain of toxic function in the cytoplasm and instead could predict a loss of nuclear function as

the pathogenic mechanism. FUS is predominantly localized to the nucleus and functions in transcriptional regulation, pre-mRNA splicing, and DNA damage repair (Sama et al., 2014). Loss of function in any of these pathways could have detrimental consequences for cell health and homeostasis. In fact, several *in vivo* models have demonstrated lethality upon FUS knockout. In mice, FUS knockout is perinatal lethal (Hicks et al., 2000) and *Drosophila* models exhibit pupal lethality and/or a shortened adult lifespan (Wang et al., 2011b; Sasayama et al., 2012; Xia et al., 2012). To directly assess a loss of function from ALS-linked mutations, Wang et al. expressed mutated FUS in a *Drosophila* null model and found ALS-linked variants R522G and P525L were unable to fully rescue the lifespan of adult flies as compared to the re-expression of wild-type. These variants were also unable to rescue other loss of function phenotypes, such as locomotor speed (Wang et al., 2011b). This study supported a loss of function hypothesis for mutant FUS in ALS pathogenesis.

While several animal models have demonstrated the necessity of FUS for viability, the necessity of FUS at the cellular level has not been fully elucidated. FUS is involved in numerous cellular pathways, but whether these pathways are dependent on FUS function is not known. To study the influence of FUS depletion on cell health and homeostasis at the cellular level, I characterized an inducible FUS knockdown system in NSC-34 cells (neuroblastoma x spinal cord hybrid) and discovered a defect in cellular proliferation upon FUS depletion. Several nuclear functions of FUS could contribute to this response. As a

candidate approach I chose to investigate a defect in DNA damage repair as a causative factor, as FUS knockout mice demonstrated early lethality associated with exposure to ionizing radiation (Kuroda et al., 2000). Finally, to investigate the functional capacity of ALS FUS variants, I developed a system that allowed for the knockdown of endogenous FUS in cultured mammalian cells with simultaneous expression of exogenous wild-type or mutant FUS.

Results

FUS depletion induces a defect in cell proliferation. To determine the effect of FUS depletion in mammalian cells, I utilized NSC-34 cell lines (neuroblastoma x spinal cord hybrid) containing stable inducible shRNA targeted to either the open reading frame of FUS (shFUS) or a scrambled control sequence (shSC) (Sama et al., 2013). After four days of induction, FUS levels were depleted >90% in the shFUS line while remaining at endogenous levels in the shSC line **(Figure II-1A)**. Observation of cell confluency after four days of shRNA induction revealed a striking reduction in cell abundance for the cell line expressing shFUS. Quantification of cell number revealed a 50% decrease in the shFUS line compared to either uninduced cells or cells expressing shSC **(Figure II-1B)**. This finding was supported by an MTT assay of cell viability which showed ~50% reduction in viability in shFUS cells compared to only a ~20% reduction in shSC cells **(Figure III-1C)**. Together with a lack of observable cell death, this data demonstrates a defect in cell proliferation upon the knockdown of FUS.

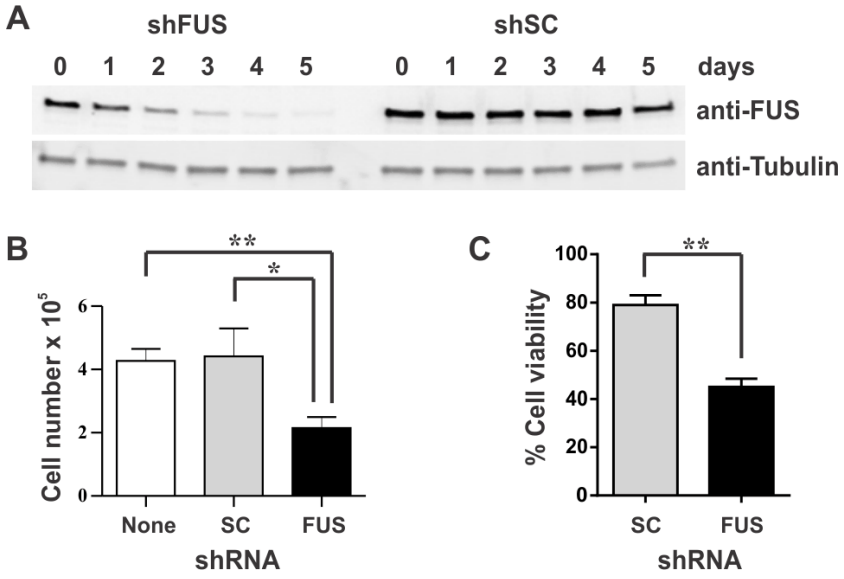

Figure II-1. FUS knockdown causes a decrease in cellular proliferation. NSC-34 cells stably expressing inducible shRNA targeting exon 5 of FUS (shFUS) or a scrambled control sequence (shSC) were used to model the effects of loss of FUS function. **(A)** Representative western blot demonstrating >90% FUS knockdown after induction with 1μg/ml doxycycline in cells expressing shFUS. Tubulin serves as a loading control. **(B-C)** Four days of FUS knockdown by induction of shFUS resulted in ~50% reduction in cell proliferation, compared to uninduced cells or cells expressing shSC, as determined by cell counting **(B)** or MTT assay **(C)**. Data shown are the average of 3 independent experiments ± standard error. Statistical significance was determined by a student's t-test (*P <0.05; **P <0.01).

Assessing the functional capacity of mutant FUS. We next sought to determine whether mutant FUS could rescue the proliferation defect produced by knockdown of endogenous wild-type FUS. To this end, I established NSC-34 cells stably expressing exogenous human wild-type FUS or mutant R495X (Baron et al., 2013). R495X is a clinically severe mutation and has a high degree of cytoplasmic mislocalization (Bosco et al., 2010a), making it an ideal variant for studying loss of nuclear function. To knockdown endogenous FUS while simultaneously expressing exogenous FUS, siRNA targeting the 3' untranslated region (3'UTR) of murine FUS was designed and proved to be more efficient at knocking down endogenous wild-type FUS (endo-WT) than the exogenous human variants (exo-WT or exo-R495X) **(Figure II-2A)**. Four days after siRNA transfection, MTT assays were performed to assess the ability of exogenous wild-type or mutant FUS to inhibit a proliferation defect from occurring during the knockdown of endogenous FUS. In cells expressing exogenous WT- or R495X-FUS, MTT levels were still reduced ~40-50% after knockdown of FUS, compared to transfection of scrambled control siRNA **(Figure II-2B)**.

The lack of rescue by exogenous human wild-type FUS could suggest that the proliferation defect is an off-target effect of siRNA and not truly an effect of FUS depletion. To address this, we knocked-down FUS in two different cell lines using a total of four different siRNA sequences and consistently observed a proliferation defect **(Chapter III: Figure III-1).** Thus, the lack of rescue could be due to either inefficient expression levels of the exogenous protein or the inability

of human FUS to function as murine FUS. Despite the lack of a 3'UTR in the exogenous constructs, there was a significant degree of knockdown of the exogenous protein **(Figure II-2A)**. This is presumably through the production of siRNA during degradation of the murine transcript that can target human FUS. Despite continued attempts to increase exogenous levels of wild-type FUS, we were never able to maintain near-endogenous levels.

To navigate the possibility of human FUS being unable to rescue the knockdown of mouse FUS, we attempted the same rescue experiment in HEK-293T cell lines stably expressing inducible GFP-tagged human wild-type FUS or mutant R495X (Bosco et al., 2010a). Expression of exogenous protein was induced one day prior to the transfection of siRNA and in this system exogenous levels remained high while endogenous levels of FUS were depleted **(Figure II-2C)**. MTT levels however, were not rescued by either the expression of exogenous wild-type or mutant protein **(Figure II-2D)**. While the exogenous protein was expressed at near-endogenous levels and was the same species as the endogenous protein, the addition of a GFP-tag could have potentially conflicted with the proper folding of FUS or altered relevant FUS interactions within the cell. As a final attempt, I developed HEK-293T cells stably expressing HA-tagged exogenous FUS, but was unable to achieve high levels of the exogenous protein. In the end, despite numerous attempts and extensive troubleshooting, I was unable to produce a reliable model system to study the functional capacity of mutant FUS.

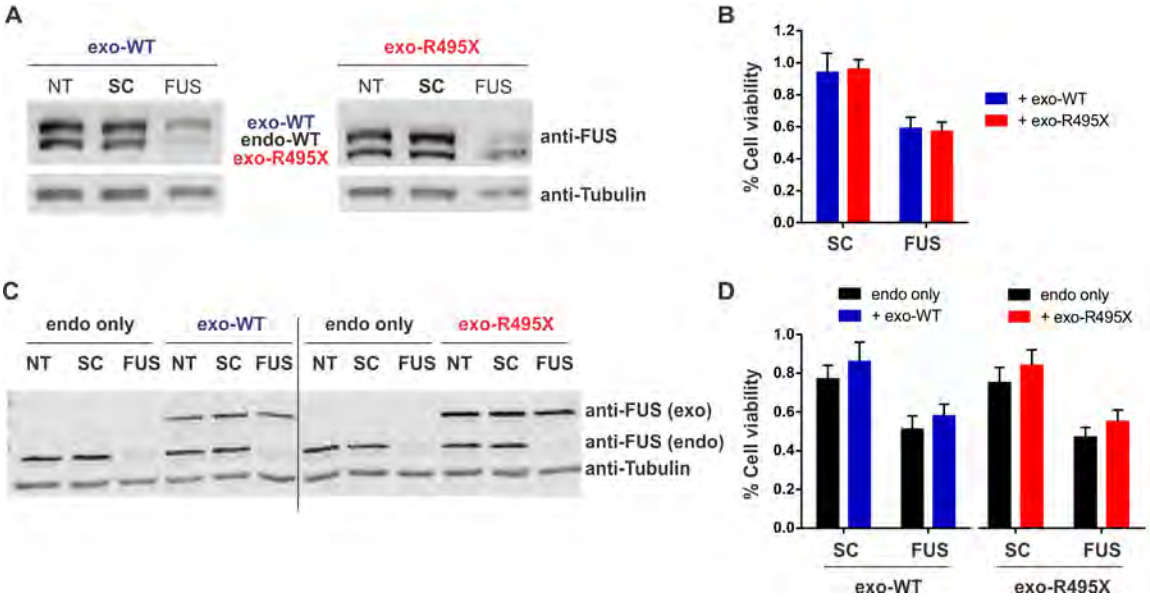

Figure II-2. Testing the functional capacity of ALS-linked mutant FUS. (A) Western blot analysis of the indicated cell lysates. Endogenous wild-type FUS (endo-WT) in NSC-34 cells was knocked-down by the transfection of siRNA targeting the 3'UTR of FUS. Exogenously expressed human wild-type FUS (exo-WT; left) or mutant R495X (exo-R495X; right) is still expressed after the knockdown of endogenous wild-type. **(B)** Expression of exogenous human FUS protein, wild-type or mutant R495X, was unable to rescue the ~50 % proliferation defect caused by knockdown of endogenous mouse FUS. **(C)** Exogenous GFP-tagged FUS, either wild-type (exo-WT; left) or mutant R495X (exo-R495X; right), was expressed in HEK-293T cells. Transient transfection of siRNA targeting the 3'UTR of FUS caused a specific knockdown of endogenous wild-type FUS, while leaving exogenous protein expression unaffected. (**D**) Expression of exogenous protein, either wild-type (left) or mutant R495X (right), was unable to rescue the proliferation defect induced by knockdown of endogenous FUS.

FUS depletion induces elevated levels of phosphorylated H2AX (γH2AX), a marker of DNA damage. In addition to *FUS-/-* mice being sensitive to ionizing radiation (Kuroda et al., 2000), evidence of the importance of FUS in homologous DNA pairing (Akhmedov et al., 1995; Bertrand et al., 1999) and D-loop formation (Baechtold et al., 1999), supports a role for FUS in DNA damage repair, as these are essential steps of homologous recombination. Since cell cycle arrest is a component of the DNA repair process (reviewed in (Zhou and Elledge, 2000)), we investigated whether the FUS knockdown-induced defect in cell proliferation was occurring as a consequence of damaged DNA. To this end, we monitored levels of phosphorylated H2AX (γH2AX), a common marker of DNA damage. Four days after induction of FUS knockdown in NSC-34 cells, γH2AX levels were increased as compared to control cells expressing shSC **(Figure II-3A)**. This finding was recapitulated in HEK-293T cells after transient transfection of siRNA targeting a unique sequence of FUS **(Figure II-3B)**, indicating this result was not an off-target effect or specific to FUS knockdown in NSC-34 cells. Furthermore, γH2AX levels remained elevated over the course of 10 days with continued FUS knockdown, but if FUS levels were allowed to recover by the washout of shRNA induction, γH2AX levels returned to baseline **(Figure II-3C)**. Together, this data demonstrates a direct correlation between FUS levels and γH2AX elevation.

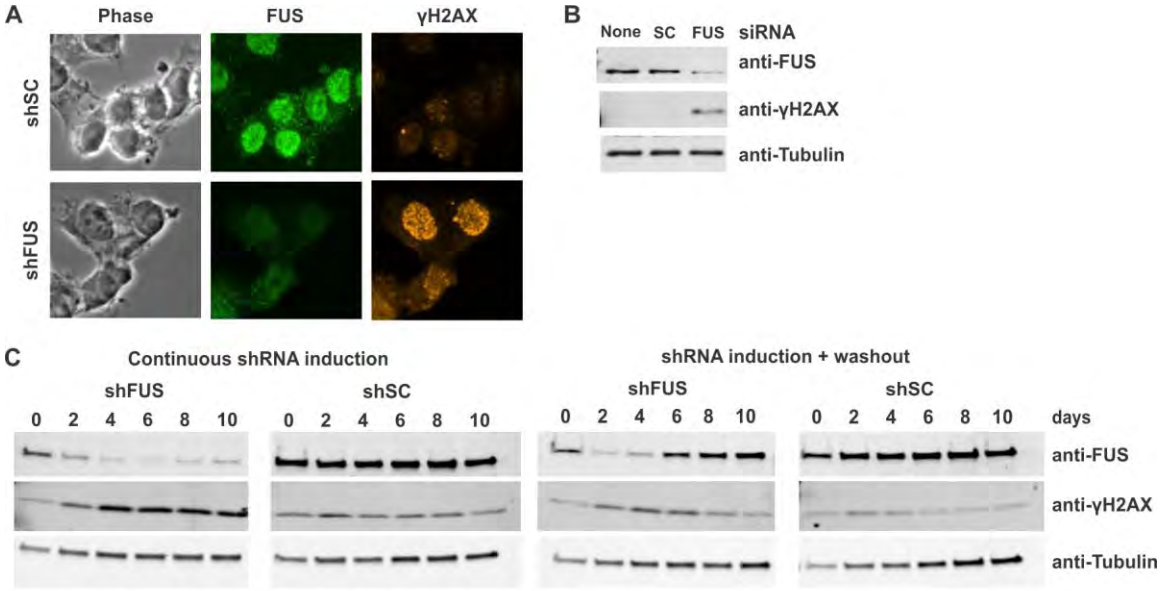

Figure II-3. FUS knockdown causes elevated levels of γH2AX. (A) Representative immunofluorescence images demonstrating increased γH2AX foci in cells with knocked-down FUS expression four days after induction of shFUS. **(B)** Western blot analysis of HEK-293T lysates after four days of the indicated siRNA treatment. Increased expression of γH2AX is present in lysates having knocked-down expression of FUS. Tubulin serves as a loading control. **(C)** NSC-34 cells expressing inducible shRNA were either continuously induced or induced for 24h after which induction was washed-out. Western blot analysis of the indicated lysates demonstrates an increase in γH2AX, correlating with FUS knockdown (left; continuous induction), which is recovered as FUS levels return to baseline (right; induction + washout). Tubulin serves as a loading control.

In addition to being a marker of DNA damage, γH2AX is also elevated as a result of DNA fragmentation in the later stages of apoptosis (Rogakou et al., 2000). To determine whether γH2AX was elevated as a result of apoptosis, we probed for early markers of apoptosis, specifically cleaved caspase-3 and cleaved-PARP, for their temporal relationship to γH2AX. While increased γH2AX was evident as early as 48h by immunofluorescence **(Figure II-4A)** and 60h by western analysis **(Figure II-4B)**, cleaved caspase-3 and cleaved-PARP remained nearly undetectable throughout 96h of FUS knockdown. Furthermore, DNA harvested at 48 and 96h of FUS knockdown had an identical pattern to DNA harvested at 0h of FUS knockdown, differing from that of a positive control demonstrating a typical pattern of fragmented DNA **(Figure II-4C)**. Together, this data suggests γH2AX is elevated upon FUS depletion as a consequence of increased DNA damage, independent of apoptosis.

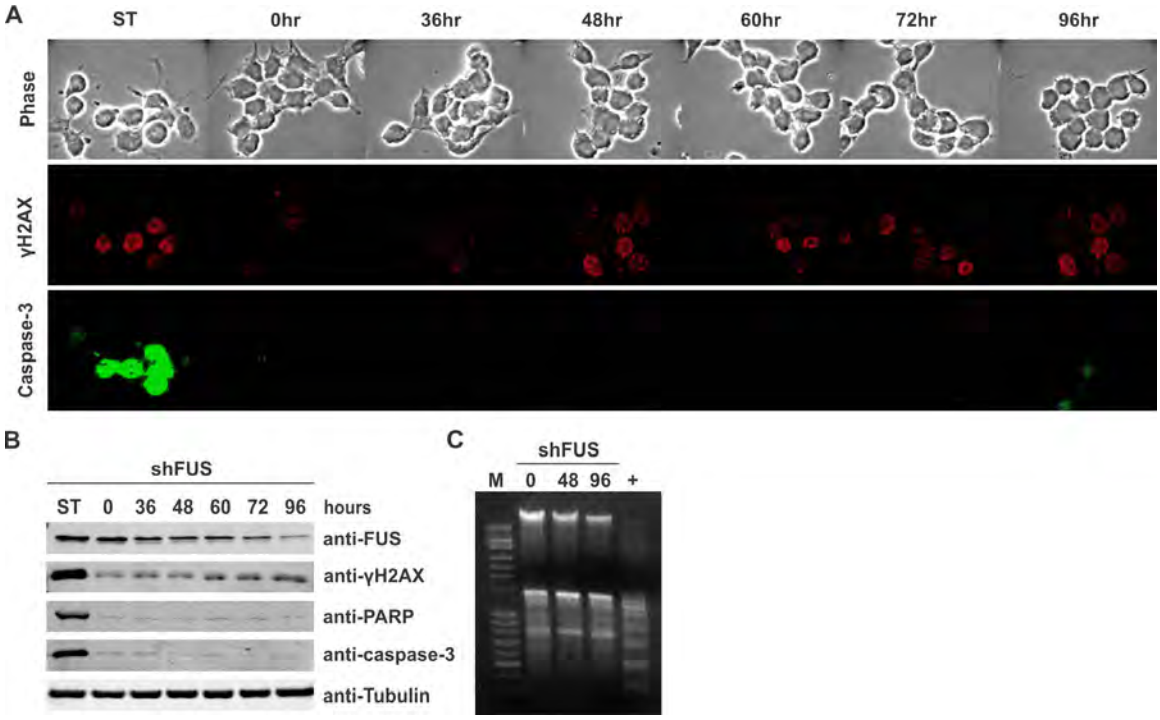

Figure II-4. FUS knockdown-induced γH2AX is independent of apoptosis. NSC-34 cells were induced to express shFUS for the knockdown of FUS expression and monitored over time for the presence of apoptosis markers. **(A)** Representative immunofluorescence images demonstrate increased γH2AX foci by 48h of shFUS induction without evidence of cleaved caspase-3. Cells treated with 1μM staurosporine (ST) for 2h serve as a control for positive cleaved caspase-3 staining. **(B)** Western blot analysis of the indicated lysates reveals increased levels of γH2AX correlating with decreased FUS expression while levels of cleaved-PARP and cleaved caspase-3 remain unchanged. **(C)** DNA harvested from cells after 0, 48, or 96h of shFUS expression was separated by electrophoresis. DNA fragmentation, as demonstrated by a positive control (+), is not present after FUS knockdown (M = DNA size marker).

Next, we sought to determine the mechanism associated with the elevated levels of DNA damage. Was this phenomenon due to a higher rate of DNA damage, a lower rate of DNA repair, or both? In order to assess physical DNA damage and track levels and repair rates over time, we sought to employ the Comet assay, a gel electrophoresis method used to measure the abundance of double strand breaks in the DNA of individual cells. The Comet assay reports baseline DNA damage as well as tracks the repair of damaged DNA after an insult such as ionizing radiation (Olive and Banath, 2006; Wood et al., 2010). While in the process of establishing this method within the lab, inconsistencies arose in the reproducibility of γH2AX elevation following FUS knockdown. In these experiments, γH2AX reports the level of DNA damage that occurs spontaneously during the normal life of cells in culture, without the addition of DNA damaging agents. It would stand to reason then, that the culture condition of the cells had been altered, leading to less exposure to spontaneous DNA damage. Despite troubleshooting numerous variables, such as components of growth media, incubator conditions and the integrity of our cell lines, we were unfortunately unable to resolve this issue and further investigations were not pursued.

Discussion

While several groups have investigated the effects of FUS knockdown in both neuronal (Ishigaki et al., 2012; Orozco et al., 2012; Nakaya et al., 2013) and replicating cells (Kim et al., 2010; Hoell et al., 2011; Tan et al., 2012; Yamazaki et al., 2012; van Blitterswijk et al., 2013), our work is the first to report an effect on cell health or proliferation. Our knockdown system is unique from other studies in that every cell stably expresses an inducible shRNA construct targeting FUS, ensuring a homogeneous FUS knockdown, in contrast to transient transfections which vary based on transfection efficiencies. The homogenous knockdown of FUS in our system allows for any resulting phenotype to be widespread and more evident. Moreover, our studies were carried out for four days while others were assessed after only two or three when an alteration in cell abundance would be less apparent. That a proliferation defect was detected in our hands using four different FUS RNAi sequences in two different cells lines (data shown in Chapter III) supports this finding as a direct cause of FUS depletion and not an off-target effect of the experimental approach.

To investigate the cellular events leading to the FUS knockdown-induced proliferation defect, we took a candidate approach and measured levels of DNA damage, as several lines of evidence implicate FUS in DNA damage repair (Akhmedov et al., 1995; Baechtold et al., 1999; Bertrand et al., 1999; Kuroda et al., 2000). Although our work remains inconclusive due to a lack of reproducibility in our experimental system, our results are suggestive of an

accumulation of unrepaired DNA as a result of FUS depletion. Shortly after this project was halted, a role for FUS in the DNA damage repair process was firmly established when three independent groups reported the localization of FUS to sites of damaged DNA (Mastrocola et al., 2013; Rulten et al., 2013; Wang et al., 2013). Furthermore, in the absence of FUS the efficiency of DNA double-strand break repair pathways, specifically homologous recombination (HR) and non-homologous end-joining (NHEJ), were decreased 30-50%. This reduction is thought to be significant considering a ~50% reduction in these repair processes is observed when the expression of known DNA-repair proteins is reduced (Mastrocola et al., 2013; Wang et al., 2013). In primary mouse cortical neurons, cells that mainly utilize the NHEJ pathway for DNA double strand break repair ((Sharma, 2007) and reviewed in (Rao, 2007)), FUS depletion resulted in a ~65-80% reduction in repair efficiency as well as an increase in levels of damaged DNA, as determined by the Comet assay (Wang et al., 2013). Together, these findings confirmed FUS is important for efficient DNA damage repair in both proliferating cells and in post-mitotic, non-proliferating cells such as neurons.

In addition to confirming the requirement of FUS in DNA damage repair, Wang et al. determined that FUS functions upstream of many common DNA damage repair proteins. For instance, the redistribution of FUS to sites of DNA damage occurred prior to that of other key DNA-repair proteins, including NBS1 (Nijmegen breakage syndrome-1), p-ATM (phosphorylated-ataxia telanogiectasia mutated), γH2AX (phosphorylated histone 2A.X) and Ku70 (Wang et al., 2013).

Additionally, the abundance of γH2AX foci was reduced when FUS expression was knocked-down, despite an increase in DNA damage reported by the Comet assay (Wang et al., 2013). This finding was in contrast to what we had seen in NSC-34 and HEK cells **(Figure II-2)**, as in our hands the knockdown of FUS resulted in an elevation of γH2AX foci. An important difference between these two studies was in the induction of DNA damage. While Wang et al. elicited the DNA damage response through treatment with etoposide, an inducer of double strand breaks, our study lacked experimental induction of DNA damage. Together these studies may indicate that FUS plays various roles in the DNA damage response depending on the level and type of damage that has occurred.

While the capacity of mutant FUS to function in the models presented here was inconclusive due to the lack of a proper system, several other models have addressed a loss of function hypothesis for mutant FUS. In studies of DNA damage repair, Wang, et al. knocked-down the expression of endogenous FUS in U2OS cells and directly examined the ability of several ALS-linked variants to perform either HR- or NHEJ-mediated DNA repair. All of the FUS variants tested (R244C, R514S, H517Q, R521C) were deficient in HR-mediated DNA repair relative to wild-type FUS. Overall, the impaired role of FUS variants in DNA repair was more pronounced in HR than NHEJ, where in the latter pathway nuclear FUS H517Q fully rescued the loss of WT FUS expression (Wang et al., 2013). With the exception of mutant R521G for which there are conflicting results (Rulten et al., 2013), all FUS variants tested (R244C, R514S, H517Q, R521C,

R521G, and R524S) were recruited to sites of DNA damage (Mastrocola et al., 2013; Wang et al., 2013). Therefore, in the context of DNA damage repair mutant FUS displayed proper localization, but was unable to perform its function, demonstrating a loss of function by mutant FUS.

Accumulating evidence makes a strong case for a role of FUS in the DNA damage response and that ALS-linked mutants are deficient in this function makes defective DNA damage repair a plausible mechanism for ALS. Damaged DNA accumulates normally as a function of age, presumably due to a life-time exposure to DNA damaging agents and a decline in quality control pathways (reviewed in (Gorbunova et al., 2007)). Defects in DNA repair due to FUS mutations are therefore expected to manifest in adulthood, which coincides with the mean age of onset (~55 years) for FUS-ALS. Neurons may be particularly susceptible to accumulated DNA damage, as they lack the ability to replicate and self-renew. In support of this, post-mortem brain sections from the motor cortex of ALS patients harboring either FUS R521C or P525L mutations display increased levels of the γH2AX DNA damage marker relative to control brain sections (Wang et al., 2013). However, it should be noted that γH2AX levels also correlate with apoptosis (Rogakou et al., 2000), which is an established cell-death pathway in both ALS and related disorders (Pasinelli and Brown, 2006). Therefore, an alternative interpretation of these data is that there are increased levels of apoptosis in these end-stage diseased tissues, which is to be expected. A recent transgenic mouse however, that expresses FUS R521C and exhibits

severe motor defects and death 4-6 weeks after symptom onset, exhibited elevated levels of several DNA damage markers (e.g., γH2AX, phosphorylated p53, and ATF3) in the central nervous system in the absence of apoptosis markers (Qiu et al., 2014). Comet assays performed on isolated neurons supported this observation, with >50% of neurons from R521C mice demonstrating comet tails compared to the ~20% from non-transgenic control littermates. These neurons lacked cleaved caspase-3 signal and were TUNEL-negative, indicating that damaged DNA and motor neuron death do not result from apoptosis (Qiu et al., 2014).

Conclusion

Together, this evidence supports a disruption of DNA damage repair as a function of mutant-FUS expression. Whether this is causative for ALS is yet to be determined and perhaps investigating additional FUS variants for DNA repair efficiency *in vivo* will offer more conclusive evidence. Loss of other nuclear functions of FUS however, could just as easily be the determining factor in ALS pathogenesis. To investigate the cellular effects of FUS depletion outside of this one candidate pathway, we further characterized the FUS knockdown-induced proliferation defect and using quantitative proteomics, identified several other cellular pathways modified by FUS depletion, as discussed in Chapter III.

Materials and Methods

Tissue culture. All cell lines used herein have been described previously: NSC-34 cell lines expressing inducible shFUS1 of shSC (Sama et al., 2013), NSC-34 cell lines constitutively expressing exogenous human wild-type FUS or mutant R495X (Baron et al., 2013), and HEK-293T cells expressing inducible GFP-tagged human FUS, wild-type or mutant R495X (Bosco et al., 2010a). For the induction of shRNA or GFP-tagged FUS in NSC-34 or HEK-293T cells respectively, cells were treated with 1µg/ml doxycycline (Sigma, D9891) or 0.1 µg/ml tetracycline (Fisher Scientific, BP912-100).

siRNA knockdown of FUS

RNA oligonucleotides for FUS (sequences below) and a scrambled control sequence (guide: 5'-aauucuccgaacgugucacgu-3'; passenger: 5'-gugacacguucggagaaucuu-3') were purchased through Sigma-Aldrich and 10µM annealed stocks were prepared by combining guide and passenger strands in the following buffer: 100mM potassium acetate, 30mM HEPES-KOH pH 7.4, 2mM magnesium acetate. For knockdown in HEK-293T cells, cells were plated in a 24-well plate at 2,000 cells/well and allowed to adhere overnight. Transfection was performed in OPTI-MEM (Invitrogen, 31985070) using 0.4µl Lipofectamine RNAiMax (Invitrogen, 13778030) and 0.2nM siRNA per well (guide: 5'-uugggugaucaggaauuggaa-3'; passenger: 5'-ccaauuccugaucacccacuu-3'). For knockdown in NSC-34 cells, cells were plated in a 24-well plate at

10,000 cells/well. Transfection was performed as above, but with 0.5µl RNAiMax and 10nM siRNA per well (guide: 5'-uaggguagucugacacacaca-3'; passenger: 5'-ugugugucagacuacccucuu-3').

Cell proliferation assays. For cell counting experiments, inducible NSC-34 cells were plated in 6-well plates at 40,000 cells/well and induced with 1µg/ml doxycycline the following morning, or left uninduced. Four days later, cells were resuspended in 3ml phosphate buffered saline (Invitrogen, 10010-049) and counted in triplicate using a hemocytometer. For MTT assays, NSC-34 and HEK cells were plated in technical triplicate in a 24-well plate and induced to express shRNA or transfected with siRNA the following morning, as described above. After four days, the media from each well was removed and replaced with 400µl fresh media and 100µl of 5mg/ml MTT (3-[4,5-dimethylthiazol-2-yl]-2,5-diphenyl tetrazolium bromide; Invitrogen, M-6494). After a 35 min incubation at 37ºC, 300µl lysis buffer (10% SDS in 1:1 *N*,*N*_-dimethylformamide:water/2% acetic acid/2.5% HCl 1M)(Reixach et al., 2004) was added to each well. Plates were covered with a seal and incubated at 37ºC overnight followed by OD quantification at 550nm. Results are expressed as % cell viability relative to untreated controls using the following equation: $100 \times (OD_{RNAi} - OD_{blank})/(OD_{untreated} - OD_{blank})$. The OD_{blank} was determined by wells containing MTT and tissue culture media without cells.

Immunofluorescence. Cells grown on glass coverslips were fixed for 5-10 min with 4% paraformaldehyde and blocked with PBSAT (1X PBS/1% BSA/0.5% Triton-X 100) for 30-60 min at room temperature. Primary antibodies were diluted in PBSAT and added to the coverslips at room temperature for 1 hr. Primary antibody dilutions were as follows: 1:500 for anti-FUS (Bethyl laboratories, A300-293A), 1:500 for γH2AX (Millipore, 05-636), and 1:500 for cleaved caspase-3 (Cell Signaling, 9664). After primary antibody incubation, coverslips were washed with PBSAT and incubated for 45 minutes with Alexa Fluor 488-conjugated donkey anti-rabbit IgG (Jackson ImmunoResearch Labs, 711-545-152) or donkey anti-mouse Cy3 (Jackson ImmunoResearch Labs, 715-165-151), diluted at 1:2000 in PBSAT. Lastly, cells were stained with 34 ng/mL DAPI and coverslips were mounted with ProLong Gold anti-fade reagent (Invitrogen, P36930).

Western blotting. Cells were lysed for 30 min at 4ºC with either 50 mM Tris HCl (pH 7.5) containing 0.5M NaCl, 1% NP-40, 1% deoxycholic acid, 0.1% SDS, and 2mM EDTA or RIPA buffer (Boston BioProducts, BP-115-500), supplemented with protease (Roche, 11836170001) and phosphatase (Roche, 4906837001) inhibitors. Concentration of cell lysates was determined using a *bicinchoninic* acid (BCA) assay (Thermo Scientific Pierce, 23227) and samples were prepared in Laemmli SDS-sample buffer (Boston BioProducts, BP-111R). Standard western blotting procedures were followed, using Tris-glycine SDS-PAGE and electrotransfer onto PVDF membrane at 100V for 1 hour at 4ºC. Membranes

were blocked for 1h at room temperature with Odyssey Blocking Buffer (LiCor, 927–40003) diluted 1:1 with PBS containing 0.1% tween-20 (PBST), followed by overnight incubation at 4ºC with primary antibodies diluted in PBST. Primary antibody dilutions were as follows: 1:500 anti-FUS (Genscript, generated against C-terminal peptide CKFGGPRDQGSRHDSEQDNSD)(Sama et al., 2013), 1:500 anti-tubulin (Sigma, T9026), 1:500 anti-cleaved PARP1 (Cell Signaling, 9544), 1:500 anti-cleaved caspase-3 (Cell Signaling, 9664), and 1:100 anti-γH2AX (Millipore, 05-636). Following primary antibody incubation, membranes were washed with PBST and incubated for 1h with secondary antibody diluted 1:10,000 in 1:1 Odyssey Blocking Buffer:PBST. Secondary antibodies included anti-mouse IRDye 680 (Licor, 926-68072) or IRDye 800 (LiCor, 926-32210) and anti-rabbit IRDye 680 (LiCor, 926-68023) or IRDye 800 (Licor, 926-32211). After washing with PBST, membranes were imaged with an Odyssey Infrared Imager (LiCor, Model 9120) and protein band intensities were quantified with the Odyssey Software (LiCor, V3.0).

For separation of human and mouse FUS protein in NSC-34 cell lysates, ~25µg of total protein lysate was loaded per sample onto a 15% Tris-glycine gel, which was run at 215V at 4ºC for ~5 hours, until the 50kDa ladder band reached the bottom of the gel. Electrotransfer onto PVDF membrane and antibody conditions were performed as described above.

DNA electrophoresis. DNA was purified from NSC-34 cells using an Apoptotic DNA Ladder Kit (Roche, 11835246001). DNA samples (2µg) were loaded onto a 1.0% agarose gel containing SYBR Safe DNA stain (Life Technologies, S33102) and run at 75V in TBE buffer (Tris-borate-EDTA) for 1.5hr, followed by imaging with a UV light source.

PREFACE TO CHAPTER III:

The work and analysis presented in this chapter was performed by Catherine L. Ward with the following exceptions:

Mass spectrometry was performed by Dr. Kristin Boggio (mass spectrometry core facility, UMMS), high-throughput small molecule screen was performed and analyzed by Dr. Bethann Johnson with assistance from Drs. Justin Boyd and Marcie Glicksman (Laboratory for Drug Discovery in Neurodegeneration, Harvard NeuroDiscovery Center), and live-cell imaging was performed by Stephen R. Douthwright (Sluder lab, UMMS).

CHAPTER III: A LOSS OF FUS/TLS FUNCTION LEADS TO IMPAIRED CELLULAR PROLIFERATION

Abstract

Fused in Sarcoma/Translocated in liposarcoma (FUS/TLS or FUS) is a multifunctional RNA/DNA-binding protein that is pathologically associated with cancer and neurodegeneration. To gain insight into the vital functions of FUS and how a loss of FUS function impacts cellular homeostasis, FUS expression was reduced in different cellular models through RNA interference. Our results demonstrate that a loss of FUS expression severely impairs cellular proliferation. A quantitative proteomics analysis performed on cells undergoing various degrees of FUS knockdown revealed protein expression changes for known RNA targets of FUS, consistent with a loss of FUS function with respect to RNA processing. Proteins that changed in expression as a function of FUS knockdown were associated with multiple processes, some of which influence cell proliferation including cell-cycle regulation, cytoskeletal organization, oxidative stress and energy homeostasis. FUS knockdown also correlated with increased expression of the closely related protein EWS (Ewing's sarcoma). We demonstrate that the maladaptive phenotype resulting from FUS knockdown is reversible and can be rescued by re-expression of FUS or partially rescued by the small-molecule rolipram. These results provide insight into the pathways and

processes that are regulated by FUS as well as the cellular consequences for a loss of FUS function.

Introduction

Fused in sarcoma/translocated in liposarcoma, FUS/TLS (or FUS), is a member of the TET family of proteins that also includes Ewing's sarcoma (EWS) and TATA-binding protein-associated factor 15 (TAF15). TET-proteins carry out RNA/DNA processing activities in the context of diverse cellular functions (Tan and Manley, 2009a). FUS is predominately expressed in the nucleus where it plays a role in transcription, splicing and DNA damage repair (Dormann and Haass, 2013) and also shuttles to the cytoplasm, where it has been found in translationally active RNA/protein foci (Yasuda et al., 2013) as well as stress granules formed in response to osmotic stress (Sama et al., 2013).

With such a broad host of cellular functions, it is not surprising that FUS is associated with several human diseases. For example, FUS is part of an onco-fusion protein that causes malignant myxoid liposarcoma. The N-terminal transcriptional activation domain of FUS is fused to the transcription factor CHOP (also known as DDIT3), forming FUS-CHOP (Crozat et al., 1993; Rabbitts et al., 1993) which accounts for more than 90% of myxoid liposarcoma cases (Antonescu et al., 2000). In fact, onco-fusion proteins containing TET-family proteins cause nearly half of all sarcomas (Riggi et al., 2007). FUS also has a strong presence in neurodegenerative disorders such as adult onset

(Kwiatkowski et al., 2009; Vance et al., 2009) and juvenile amyotrophic lateral sclerosis (ALS), (Baumer et al., 2010) different subtypes of frontotemporal lobar degeneration (FTLD) (Rademakers et al., 2012) including atypical FTLD-U, (Neumann et al., 2009b; Urwin et al., 2010) neuronal intermediate filament inclusion disease (Neumann et al., 2009a) and basophilic inclusion body disease (Munoz et al., 2009) (collectively referred to as FTLD-FUS (Mackenzie et al., 2010)), and polyglutamine diseases such as Huntington's disease and spinocerebellar ataxia (Doi et al., 2009; Woulfe et al., 2009). The pathological role of FUS in these disorders has not been elucidated, although the observation that FUS is depleted from the nucleus and/or becomes sequestered into aggregates within neurons and glia during the course of neurodegeneration is consistent with a mechanism involving a loss of FUS function (Mackenzie et al., 2011; Rademakers et al., 2012; Dormann and Haass, 2013). FUS is also associated with essential tremor (ET), an adult-onset movement disorder (Merner et al., 2012; Rajput et al., 2013; Wu et al., 2013; Zheng et al., 2013). A loss of FUS function in the context of ET is proposed based on a non-sense mutation in FUS that causes the mRNA to become degraded through the non-sense mediated decay pathway (Merner et al., 2012).

To study the impact of FUS depletion on cell survival and homeostasis, we developed cellular models of FUS knockdown and discovered FUS to be critical for cellular homeostasis. Knockdown of FUS in both HEK-293T and neuronal NSC-34 cells caused a significant defect in cellular proliferation with moderate

signs of cell death. Importantly, the cell proliferation defect induced by FUS depletion is reversible, as both re-expression of FUS and treatment with rolipram, a phosphodiesterase-4 inhibitor that suppresses oxidative stress, ameliorated this phenotype. A quantitative proteomics analysis revealed 61 proteins that changed as a function of FUS knockdown. Interestingly, several of these proteins correspond to known RNA binding targets of FUS. The proteins and pathways uncovered through this analysis not only define the consequences of FUS depletion from the cell, but also serve as potential therapeutic targets for ameliorating adverse phenotypes arising from a loss of FUS function.

Results

Cell number and viability directly correlate with FUS protein expression. To investigate the cellular consequences of a loss of FUS function, FUS expression was knocked down in both NSC-34 (neuroblastoma x spinal cord)(Cashman et al., 1992) and HEK-293T cells. NSC-34 cell lines stably expressed tetracycline inducible shRNA specific for exon 5 of FUS (shFUS1 and shFUS2; **Figure III-1A**) or a scrambled shRNA control (shSC) (Sama et al., 2013). After shFUS induction for four days, FUS expression was knocked down ~95% **(Figure III-1B)**. In addition, we designed siRNA to target the 3'UTR of either human or mouse FUS **(Figure III-1A)** as well as a scrambled siRNA control. Transient transfection of 3'UTR siRNA (si3'UTR) for four days resulted in ~85% knockdown of FUS in HEK-293T cells **(Figure III-1B)**. Cell viability as determined by the

MTT assay was reduced 40-50% in NSC-34 cells stably expressing shFUS and HEK-293T cells expressing si3'UTR relative to control cells expressing scrambled RNA sequences **(Figure III-1C)**. Transient transfection of siRNA was less efficient in NSC-34 cells **(Figure III-1D)**, resulting in only ~55% FUS knockdown **(Figure III-1B)** and a modest 15% decrease in cell viability compared to scrambled control siRNA **(Figure III-1C)**. A reduction in viability (~20%) was also observed upon expression of scrambled control sequences, likely reflecting the toxicity associated with transient transfection, continuous shRNA production and/or doxycycline exposure (Ahler et al., 2013). Nonetheless, these data demonstrate a reduction in cell viability as a consequence of FUS knockdown, achieved by targeting several unique sequences within FUS in two different cell lines.

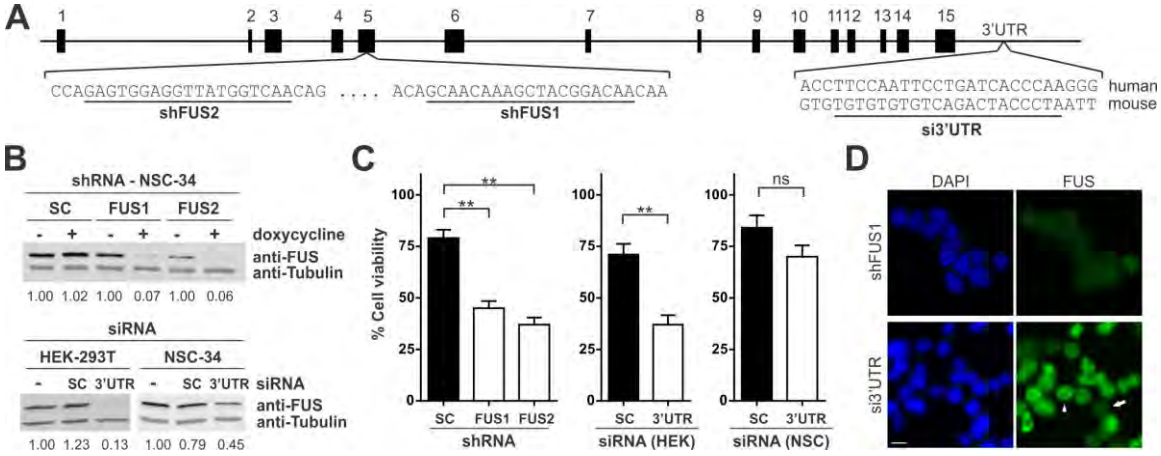

Figure III-1. FUS knockdown causes a reduction in cell viability. (**A**) FUS was targeted for knockdown by doxycycline induction of stably expressed shRNA directed at non-overlapping regions in exon 5 (shFUS1, shFUS2) or by transient transfection of siRNA targeting the 3'UTR of either the human or mouse *FUS* sequence. (**B**) Western blot analyses of the indicated cell lysate derived from FUS knockdown experiments. After four days of shFUS induction in NSC-34 cells (top) or transient transfection of 3'UTR FUS siRNA in HEK-293Tcells (bottom left), FUS expression was reduced by ~95% and ~85%, respectively, compared to controls. A less efficient FUS knockdown of ~55% was observed for NSC-34 cells (bottom right) transiently transfected with 3'UTR FUS siRNA. Numbers below the blots refer to densitometry measurements of the experimental condition (doxycycline-induced or transfected) relative to the untreated control condition for the respective cell line. SC refers to a scrambled (RNA) control sequence. Tubulin serves as a loading control. (**C**) MTT analyses revealed a decrease in cell viability upon FUS knockdown after four days compared to SC expressing cells (left, shRNA in NSC-34 cells; middle, 3'UTR FUS siRNA in HEK-293T cells; right, 3'UTR FUS siRNA in NSC-34 cells). All conditions are reported as percent viability relative to untreated cells. Data shown are the average of 3 independent experiments $\pm$ standard error. Statistical significance was determined by a student's t-test (***P* <0.01). (**D**) Representative immunofluorescence images demonstrating the degree of endogenous FUS (green) knockdown in NSC-34 cells induced to express shFUS1 versus transiently transfected with 3'UTR FUS siRNA for four days. Nuclei are stained with DAPI (blue). Arrow = detectable FUS knockdown, arrowhead = no detectable knockdown. Scale bar = 10 μm.

To further investigate the relationship between FUS expression and cellular homeostasis, we quantified cell number and cellular viability as a function of FUS depletion over time using the inducible shFUS1 NSC-34 cell line (unless otherwise noted, this line was used for all subsequent experiments). With continuous induction of shFUS with tetracycline in NSC-34 cells, FUS protein levels gradually decreased over time relative to uninduced cells and remained low for 10 days **(Figure III-2A)**. Uninduced cells exhibited an exponential growth rate with a 3.5-4 -fold increase in cell number every two days, whereas this growth rate decreased to 2-fold in cells subjected to continuous FUS knockdown **(Figure III-2B)**. Plotting cellular viability by the MTT assay as a function of FUS expression across multiple experiments further demonstrates the direct correlation between FUS expression and cellular homeostasis **(Figure III-2C)**. Tetracycline was removed from shFUS expressing cells after 24h in a 'wash-out' experiment, wherein FUS levels returned to baseline within six days **(Figure III-2A)**. It is noted that FUS expression was not restored when cells were induced with doxycycline due to the longer half-life of doxycycline relative to tetracycline. Interestingly, re-expression of FUS rescued the defect in cellular proliferation; the rate of cell growth was the same in shFUS cells under the wash-out condition as uninduced cells between days 8 and 10 **(Figure III-2B)**. Therefore, the adverse effects of FUS knockdown are reversible.

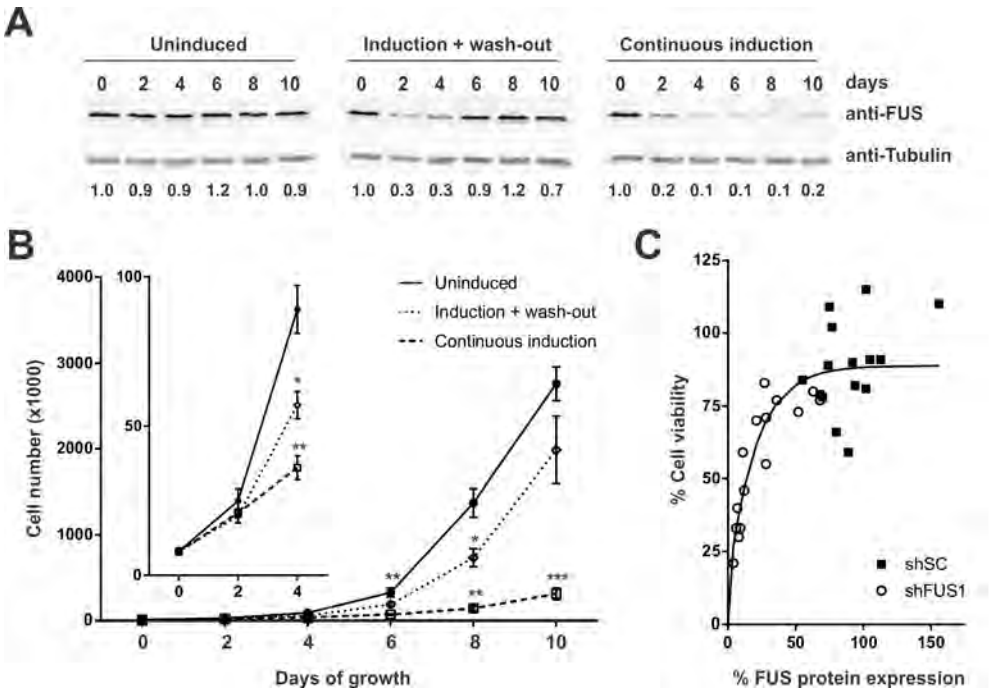

Figure III-2. Decreased cell viability correlates with the degree of FUS knockdown. (**A**) NSC-34 cells expressing shFUS1 were uninduced, induced with tetracycline for 24h after which tetracycline was removed (induction + wash-out) or subjected to continuous induction and FUS knockdown. Western blot analyses of the indicated FUS knockdown experiment reveal FUS expression is restored in the wash-out condition by day six. Numbers below the blots refer to densitometry measurements that were normalized to 'day zero', which represents the starting-point of the experiment. Tubulin serves as a loading control. (**B**) Quantification of cell number as a function of time for the indicated conditions. Cells with continuous FUS knockdown exhibited the slowest growth rate between days 2 and 4 (inset) and throughout the 10-day experiment. Upon re-expression of FUS, the growth rate for cells in the wash-out condition was accelerated and became similar to that of the uninduced condition. Data shown are the average of 3 independent experiments $\pm$ standard error. Statistical significance was determined by a student's t-test (*P <0.05; **P <0.01; ***P <0.001; day 6 significance is for the continuous induction condition). (**C**) Cell viability, as determined by the MTT assay, correlates with the level of FUS protein expression, as determined by western/densitometry analyses. Data are compiled from three independent FUS knockdown experiments, where shSC or shFUS1 was induced in NSC-34 cells for 1-5 days. An exponential fit of this data was created with GraphPad prism.

Apoptosis is not activated during the cellular response to FUS knockdown. Several factors influence the rate of cellular proliferation: the rate of cell division, the percentage of cells undergoing cell division, and cell death (Andreeff M GD, 2000). Overt cell death (i.e., a large percentage of cells detaching from the culture dish) was never observed during FUS knockdown experiments. Western blot analyses confirmed that levels of the apoptosis markers cleaved-PARP1 and cleaved-caspase 3 remained unchanged throughout a 96h FUS knockdown time-course and were markedly lower than cells treated with staurosporine, an initiator of apoptosis **(Figure III-3A)**. To rule-out apoptosis occurring through a caspase-independent pathway, we probed for nuclear translocation of apoptosis inducing factor (AIF) (Joza et al., 2001) at 24h intervals of FUS knockdown. Cells treated with ethacrynic acid (EA) as a positive control exhibited a robust nuclear translocation of AIF, whereas AIF nuclear translocation was not detected at any time point for FUS knockdown cells (shown for FUS knockdown cells after 96h, **Figure III-3B)**.

Time-lapse video microscopy was employed next to track the fate of a single population of cells during FUS knockdown. Imaging was initiated 24h after shRNA induction and continued for the duration of a 4 day induction. A normal frequency of cell division was observed in shSC cells, with cells nearing confluency by the end of the experiment **(Figure III-3C)**. A lack of cell division events was observed in cells expressing shFUS. Quantification of cell number in still frame images revealed a consistent ~1.7-fold increase in cell number every

24h for control cells, whereas the relative change in cell number decreased over time for shFUS cells **(Figure III-3D)**, consistent with a reduction in cell proliferation **(Figure III-2)**. Live-cell imaging also allowed us to address the occurrence of cell death, which was detected when cells lifted from the coverslip. The total number of cells decreased for the shFUS line between days 3 (195 cells) and 4 (165 cells), providing evidence of cell death during FUS depletion. These data demonstrate that a modest level of cell death occurred as a function of FUS knock down, possibly through a necrosis pathway as there was no evidence of apoptosis **(Figure III-3A and III-3B)**. Rather than cell death, our data point to a decrease in the frequency of cell division as the main factor that leads to reduced cell number and viability upon FUS knockdown.

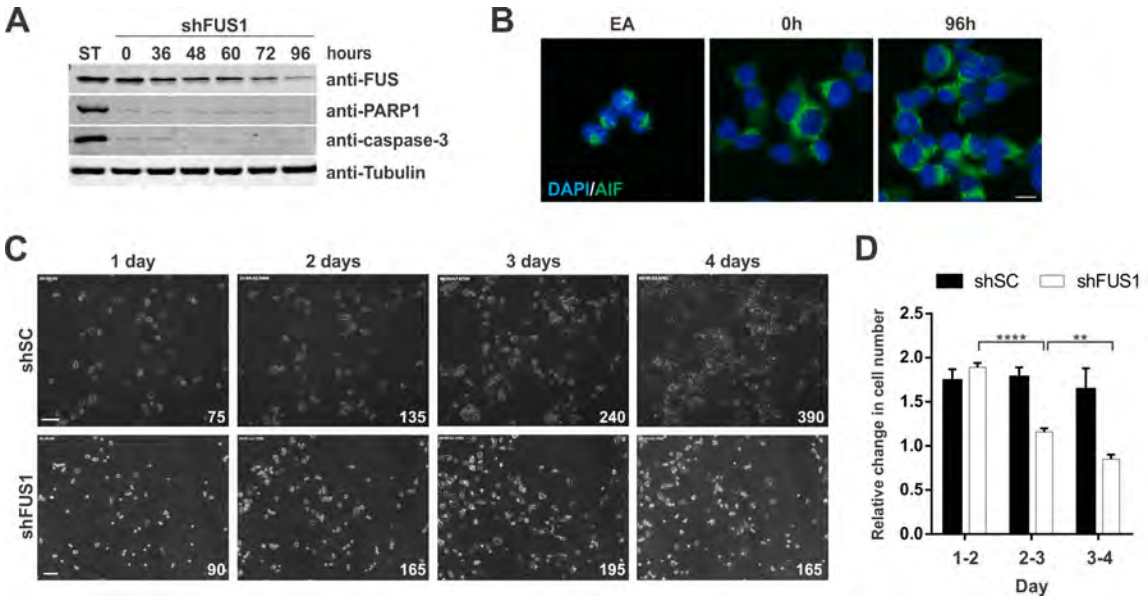

Figure III-3. Apoptosis is not activated during the cellular response to FUS knockdown. (**A**) Levels for apoptosis markers, cleaved-PARP1 and cleaved-caspase-3, do not change with FUS knockdown as determined by western blot analyses of cell lysates derived from the indicated time points. As a positive control for apoptosis, NSC-34 cells were treated with 1μM staurosporine (ST) for 2 hours. Tubulin serves as a loading control (**B**) Representative immunofluorescence images demonstrating localization of apoptosis inducing factor (AIF; green) in NSC-34 cells. AIF translocates to the nucleus in cells treated with 100μM ethacrinic acid (EA) for 8h but not upon shFUS1 induction for 96h. Images are representative of 2 independent experiments. Nuclei are stained with DAPI (blue). Scale bar = 10μm. (**C**) Still frame images from time-lapse video microscopy obtained every 24h. One day after the induction of shSC (top) or shFUS1 (bottom), cells were filmed using time-lapse microscopy for the duration of a 4d knockdown. The average number of cells from three independent counts of each image is indicated at the bottom right. Scale bar = 100μm. (**D**) The change in cell number at 24h time points relative to the previous time point, where ratios >1.0 are indicative of cell growth and ratios <1.0 of cell death. Data shown are the average of three independent counts of the still frame images ± standard deviation. Statistical significance was determined by a student's t-test (***P* <0.01; *****P* <0.0001).

A phosphodiesterase-4 inhibitor, rolipram, partially rescues the cell proliferation defect induced by FUS knockdown. In addition to rescuing the proliferation defect by re-expressing FUS **(Figure III-2)**, we sought to determine whether small molecules could exert a similar protective effect. To test this possibility, a small-molecule screen was performed to identify compounds that prevented the FUS knockdown phenotype. The assay was first converted from a 24-well to a 384-well format and high-content imaging of Hoechst stained nuclei was used to count viable cells (see Methods). Using this platform, the effect of FUS knockdown on cell viability was reduced from ~40% **(Figure III-1C)** to ~25% **(Figure III-4)**, perhaps due to the reduced plate format and cell plating. This small signal window was a challenge for high throughput screening and therefore compounds were screened in triplicate. Nonetheless, we were able to screen a chemical library consisting of 1086 small molecules, 606 of which were drugs approved by the Food and Drug Administration (FDA) and 480 of which were purified natural products. Eight compounds were initially identified (0.74% hit rate) that reversed the FUS knockdown phenotype, and five-point dose-response curves in the range of 0.1 to 30 μM were generated for each. Although seven compounds were not confirmed after retesting by this analysis (data not shown), one compound, rolipram **(Figure III-4A)**, was found to partially restore the 25% decrease in cell number induced by FUS knockdown; rather than a 25% decrease in cell number upon FUS knockdown there was only ~10% decrease with rolipram doses between 0.1 and 10 μM. Therefore, rolipram conferred a

protective effect **(Figure III-4B)**. Rolipram is an inhibitor of cAMP specific phosphodiesterase-4 with antidepressant and anti-inflammatory functions, (Zhu et al., 2001) including suppression of nitric oxide production (Beshay et al., 2001). The protective effect was less pronounced at 30 μM, suggesting rolipram might exert toxicity at higher doses. Rolipram also recovered the slight cell number deficit caused by shSC expression, indicating rolipram may exert a general effect on cell proliferation. However, this effect was modest relative to shFUS1 cells and was not statistically significant **(Figure III-4B)**. A western blot analysis demonstrated that the protective effect of rolipram was not due to re-expression of FUS **(Figure III-4C)**. These data suggest that rolipram or related compounds could be further explored in the context of therapeutics for disorders arising from a loss of FUS function.

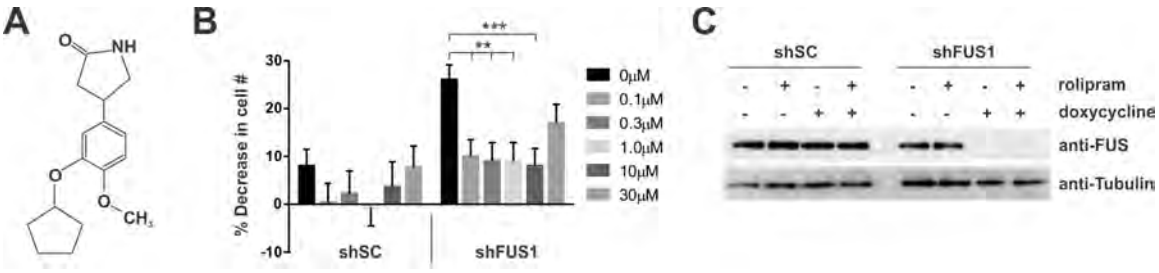

Figure III-4. Rolipram partially rescues the cell proliferation defect induced by FUS knockdown. (**A**) Molecular structure of rolipram. (**B**) NSC-34 cells were induced to express shSC or shFUS1 followed by the addition of rolipram at various concentrations (0 - 30μM). After four days, cell number was quantified relative to uninduced controls by Hoechst staining. In the absence of rolipram, cell number was reduced 25% by shFUS1 induction and 8% by shSC (n = 28 replicate wells from two independent experiments). This defect was significantly reversed at all rolipram concentrations in shFUS1 cells (n = 20 replicate wells from two independent experiments; ***P* <0.01, ***P <0.001). To a lesser extent, rolipram also recovered the deficit in shSC cells (n = 20 replicate wells from two independent experiments). Error bars represent ± standard error. Statistical significance was determined by comparing cells (shSC or shFUS1) treated with rolipram to the untreated (0 □M rolipram) condition using the Student's t-test. (**C**) Western blot analysis of cell lysates corresponding to the indicated conditions. FUS was knocked down only in cells induced with doxycycline to express shFUS1 and remained knocked down in the presence of 1μM rolipram. Tubulin serves as a loading control.

Proteomic changes resulting from FUS knockdown. Next we sought to better understand the pathways involved in the reduced cellular proliferation phenotype observed upon FUS depletion. To this end, we performed quantitative proteomics using tandem mass tags (TMT) and mass spectrometry to assess changes in the proteome at both an early (24h) and late stage (96h) of FUS knockdown (Thompson et al., 2003; Dayon et al., 2008). This approach labels peptides from each cell lysate condition with unique isobaric tags. The samples are then combined and processed simultaneously allowing for an accurate comparison of protein levels between conditions **(Figure III-5A)**. The 24h time point is expected to reveal initial cellular changes occurring relatively early in response to FUS knockdown, when FUS protein expression was reduced by only ~55% **(Figure III-5B)** and cell viability by only ~25% **(Figure III-2C)**. The 96h time point was expected to reveal more robust changes, in part because the FUS knockdown phenotype is more severe **(Figure III-5B and Figure III-1C)** and also because this later time point allows for an accumulation of protein expression changes, which depend on the timescale of both protein translation and turnover. Although it is standard to only compare cells with a specific gene knocked down to cells expressing a scrambled RNA sequence, we also included the uninduced condition in the quantitative proteomics pipeline **(Figure III-5A)** to ascertain whether a particular protein changed in expression solely as a consequence of FUS knockdown, or whether the process of shRNA induction also influenced the expression of that protein.

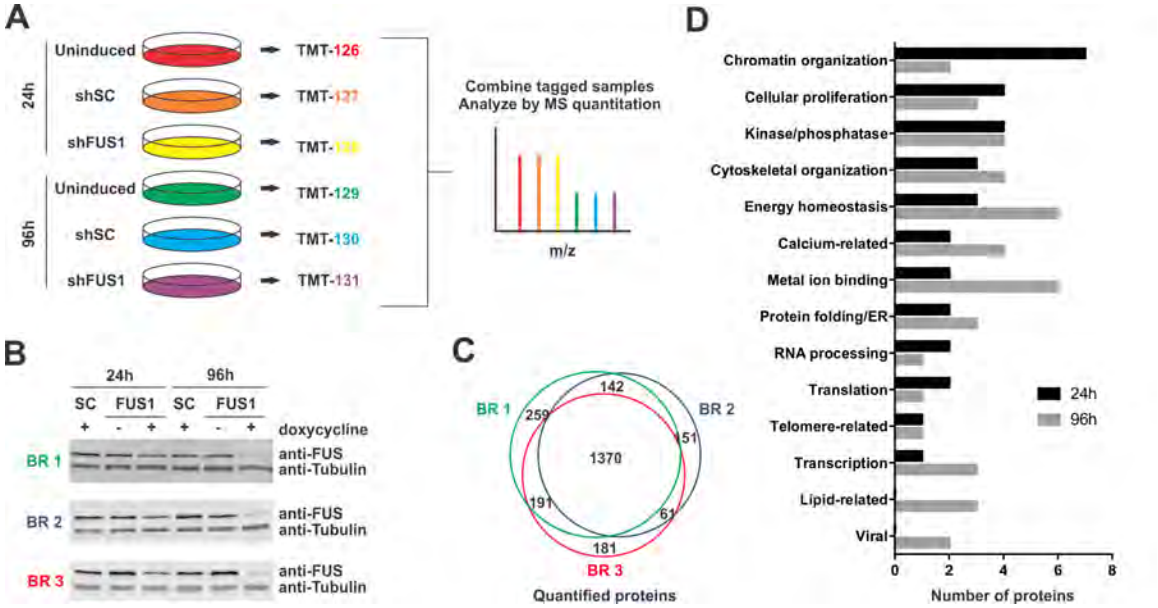

Figure III-5. Quantification of the cellular proteome after FUS depletion. (**A**) Schematic of mass spectrometry pipeline. Briefly, NSC-34 cells were induced with doxycycline for 24 or 96h to express either scrambled control shRNA (shSC) or shRNA targeting FUS (shFUS1). Uninduced cells were included as an additional control. Denatured lysates were digested and the resulting peptides were labeled with unique isobaric mass tags (tandem mass tags: TMTs 126-131) and combined for mass spectrometry (MS) analysis. (**B**) Western blot analysis confirmed FUS knockdown in lysates used for proteomics. Three biological replicates (BR 1, green; BR 2, blue; BR 3, red) were included. Tubulin serves as a loading control. (**C**) A total of 2,355 proteins were quantified by mass spectrometry over three biological replicates (BR 1-3). (**D**) Proteins differentially expressed between the shSC and shFUS1 samples by a fold change of at least $\pm$0.25 in two of three replicates were grouped into functional categories based on the literature (Table 1).

First, changes in the proteome arising from a loss of FUS were assessed by comparing shFUS and shSC samples, as shSC cells control for expression changes resulting from shRNA expression and doxycycline exposure. A total of 2,355 proteins were quantified, with ~60% (1,370 proteins) overlap between the three biological replicates **(Figure III-5C)**. Only those proteins differentially expressed between the shFUS and shSC samples by a fold change of at least $\pm$ 0.25 in two of three replicates with a p-value < 0.05 were included in our final analysis. Sixty-one proteins, in addition to FUS, met this criterion at either 24 or 96h **(Table III-1)**. Interestingly, 16 of these hits were previously identified as RNA binding targets of FUS, raising the possibility that these expression changes stem from a loss of FUS function and/or interaction with the corresponding transcripts **(Table III-1, asterisks)**.(Hoell et al., 2011; Colombrita et al., 2012; Nakaya et al., 2013) Of the 61 hits, 31 were various histone variants which we grouped into five main histone clusters (H1, H2A, H2B, H3 and H4) due to the redundancy of the peptides used to identify each protein. Similarly, KAP0 and KAP1, the regulatory subunits of protein kinase A, were counted as a single hit due to a lack of unique peptides identified for each protein. With this condensed list of only 34 proteins, DAVID analysis (Database for Annotation, Visualization, and Integrated Discovery) could not identify significant enrichment of GO terms or functional categories. Thus, hits were assigned categories manually based on information provided by UniProtKB, the National Center for Biotechnology Information (NCBI) and GeneCards **(Figure III-5D and Table III-1)**. Chromatin

organization represented the most common category for proteins differentially expressed between shFUS and shSC cells at 24h. Categories for which there were at least four differentially expressed proteins at either 24 or 96h included cellular proliferation, kinases/phosphatases, cytoskeletal organization, energy homeostasis, calcium-related and metal ion binding. Of these, energy homeostasis, calcium-related and metal ion binding were more prominent at 96 than 24h, suggesting changes in these proteins and/or pathways are triggered by FUS knockdown and become more pronounced during the cellular response to FUS depletion.

	ID	Protein Name	24h			96h			Calcium-associated	Cell proliferation	Cytoskeleton	Energy homeostasis	Chromatin organization	Kinase/phosphatase	Lipid-related	Metal ion binding	Protein folding/ER	RNA processing	Transcription	Translation	Telomere-related	Viral associated
			1	2	3	1	2	3														
	MT2	Metallothionein-2		++	+	++	++	+++								X						
*	MARCS	Myristoylated alanine-rich C-kinase substrate		+	++			++	X	X	X											
	REEP2	Receptor expression-enhancing protein 2		+	++			+														
	ADT4	ADP/ATP translocase 4		+	+							X										
*	EWS	RNA-binding protein EWS		+		+	+	+	X							X			X			
*	U5S1	116 kDa U5 small nuclear ribonucleoprotein component		+	+													X				
	TBAL3	Tubulin alpha chain-like 3		+	+			+			X											
*	TOPK	Lymphokine-activated killer T-cell-originated protein kinase		+	+									X								
	FPPS	Farnesyl pyrophosphate synthase		+			+	+				X			X							
	CHSP1	Calcium-regulated heat stable protein 1					+	++	X									X				
	KAD1	Adenylate kinase isoenzyme 1					+	+				X		X								
*	SYAC	Alanine--tRNA ligase, cytoplasmic					+	+									X			X		
*	IDHC	Isocitrate dehydrogenase [NADP] cytoplasmic					+	+				X				X						
	FKB10	Peptidyl-prolyl cis-trans isomerase FKBP10					+	+	X							X	X					
	ENV2	Retrovirus-related Env polyprotein from Fv-4 locus				+	+															X
*	OSBP1	Oxysterol-binding protein 1	+				+	+							X							
	ENV1	MLV-related proviral Env polyprotein				+	+															X
*	COX5A	Cytochrome c oxidase subunit 5A, mitochondrial				+	+					X				X						
	TYB10	Thymosin beta-10			+	+		+			X											
*	RAP1A	Ras-related protein Rap-1A				+		+		X	X											
	RL29	60S ribosomal protein L29		+	+	+														X		
*	TEBP	Prostaglandin E synthase 3			+	+	+								X		X		X		X	
*	RBBP7	Histone-binding protein RBBP7	+		+	+		+		X			X						X			
*	ROA3	Heterogeneous nuclear ribonucleoprotein A3		+	++													X			X	
*	KAP0 / KAP1	cAMP-dependent protein kinase type I regulatory subunits alpha and beta	+		+	++	+	+				X		X								
	PPBT	Alkaline phosphatase, tissue-nonspecific isozyme		+	+	++	+							X								
*	NPM	Nucleophosmin		+	++			+		X			X				X			X		
	S100A6	Protein S100-A6	+	+		++	++	+	X	X	X					X						
*	RRBP1	Ribosome-binding protein 1		+	++												X					
	H2A1	Histone H2A (H2A.J; type 1,1-F,H,K; 2-A,C; 3)		+	++	+							X									
	H14	Histone H1 (1.1-1.5; 1t)		++	++								X									
	H2B1B	Histone H2B (type 1-A,B,C/E/G, F/J/L,H,K,M,P; 2-B,E; 3-A,B)		+	+++		+						X									
	H3C	Histone H3 (3.1-3.3, 3.3C)		+	+++								X									
	H4	Histone H4		+	+++								X									
	FUS	RNA-binding protein FUS	++	++	+++	+++	++	++										X	X		X	

Fold-change	-1.50	-1.25	-1.0	-0.75	-0.50	-0.25	0	0.25	0.50	0.75	1.0	1.25	1.50

Table III-1. Fold change and functional categories of proteins differentially expressed after 24 or 96 hours of FUS knockdown in at least 2 of 3 biological replicates. Due to a lack of unique peptides identified between histone variants, these hits were combined into the five major histone families (H1, H2A, H2B, H3, and H4). Similarly, KAP0 and KAP1 were grouped due to a lack of unique peptides identified for each protein. Asterisks denote transcripts previously determined to be bound by FUS; FC = fold change

+ denotes FC between $|0.25|$ and $|0.50|$

++ denotes FC between $|0.50|$ and $|1.0|$

+++ denotes FC between $>|1.0|$

Next we sought to validate protein-hits that exhibited the largest changes in expression upon FUS knockdown. The 96h time point revealed the most robust expression changes, and therefore we focused first on proteins with the largest expression changes at 96h. S100A6, also known as calcyclin due to roles in both calcium binding and the cell cycle,(Lesniak et al., 2009) exhibited a relatively large decrease in expression in shFUS cells compared to shSC cells at 96h **(Table III-1)**. By comparing both lines to the uninduced condition, it became apparent that this difference is due in part to an increase in expression of S100A6 in shSC cells **(Table III-2)**. Differential expression of S100A6 was validated by both western blot **(Figure III-6A)** and qPCR analyses at 96h **(Figure III-6B)** and qPCR at 24h **(Figure III-6C)**. Metallothionein-2 (MT2), a multifunctional protein involved in zinc homeostasis and antioxidation,(Vasak and Meloni, 2011) exhibited a large increase in expression in shFUS cells relative to shSC cells at 96h **(Table III-1)**. The differential expression of MT2 in shFUS and shSC cells was validated by qPCR at 96h **(Figure III-6B)** and 24h **(Figure III-6C)**, however we were unable to quantify the expression of this protein by western blot analysis, presumably due to the relatively small size of this protein (6kDa). The RNA-binding protein EWS, which like FUS is a member of the TET-family of proteins, also increased in expression in shFUS cells **(Table III-1, Figure III-6B and Figure III-6D)** as well as in HEK-293T cells transiently transfected with si3'UTR for FUS knockdown **(Figure III-6D)**. This appears to be a specific relationship between FUS and EWS expression as FUS knockdown

did not influence the expression of other related RNA binding proteins such as TDP43 and hnRNPA1, or the other TET-family member TAF15 (data not shown). Similar to EWS, thymosin beta-10 (TYB10), a monomeric-actin binding protein that inhibits actin polymerization,(Sribenja et al., 2009) also increased in expression upon FUS knockdown **(Table III-1 and Figure III-6B)**, but could not be validated by western blot presumably due to the small size of the protein (5kDa).

Lastly we validated the differential expression of histones, which decreased in expression by 20-65% after 24h of FUS but appeared to recover by 96h. This difference arises from an increase in expression of histones in shSC cells relative to both shFUS and uninduced cells **(Table III-2)**, which was validated by western blot analysis for histones H2B and H3 **(Figure III-6E)**. Histones H2A and H4, which were investigated based on availability of PCR primers, were not significantly different between lines by qPCR analysis **(Figure III-6C)** suggesting that the change in histone expression may predominately occur at the protein rather than mRNA level.

	24h	Protein Name	shFUS/shSC			shSC/uninduced			shFUS/uninduced		
*	MARCS	Myristoylated alanine-rich C-kinase substrate	0.32		0.51	-0.07		-0.30	0 25		0.21
	REEP2	Receptor expression-enhancing protein 2	0.34		0.62	-0.14		-0.25	0.19		0.37
	ADT4	ADP/ATP translocase 4	0.36		0.43	-0.24		-0.16	0.13		0.27
*	U5S1	116 kDa U5 small nuclear ribonucleoprotein component	0.33		0.35	-0.12		-0.17	0 21		0.18
	TBAL3	Tubulin alpha chain-like 3	0.31		0.34	-0.19		-0.20	0.12		0.13
*	TOPK	Lymphokine-activated killer T-cell-originated protein kinase	0.29		0.25	-0.11		-0.09	0.18		0.15
	RL29	60S ribosomal protein L29	-0.25		-0.36	-0.04		0.17	-0.30		-0.19
*	RBBP7	Histone-binding protein RBBP7	-0.31		-0.36	0.10		0.07	-0.21		-0.30
*	ROA3	Heterogeneous nuclear ribonucleoprotein A3	-0.32		-0.56	0.07		0.42	-0.25		-0.14
*	KAP0 / KAP1	cAMP-dependent protein kinase type I regulatory subunits	-0.26		-0.42	0.12		0.14	-0.15		-0.28
	PPBT	Alkaline phosphatase, tissue-nonspecific isozyme	-0.32		-0.39	-0.01		-0.09	-0.33		-0.30
*	NPM	Nucleophosmin	-0.25		-0.64	0.17		0.50	-0.08		-0.14
*	RRBP1	Ribosome-binding protein 1	-0.42		-0.56	0.04		0.30	-0.38		-0.27
	FUS	RNA-binding protein FUS	-0.61	-0.56	-1.09	0.04	0.43	0.75	-0.57	-0.13	-0 35
	MT2	Metallothionein-2	0.55		0.42	-0.25		-0.39	0 30		0.03
	S100A6	Protein S100-A6	-0.47		-0.30	0.42		0.26	-0.05		-0.04
	H1	Histone H1 (t; 1.1-1.5)	-0.59		-0.98	0.50		1.02	-0.09		0.05
	H2A	Histone H2A (type 1; 1-F,H,K; 2-A,C; 3; J)	-0.29		-0.94	0.56		1.08	0 27		0.14
	H2B	Histone H2B (type 1-A,B,C/E/G,F/J/L,H,K,M,P; 2-B,E; 3-A,B)	-0.47		-1.15	0.45		1.00	-0.02		-0.15
	H3	Histone H3 (C; 3.1-3.3)	-0.26		-1.50	0.33		1.34	0 07		-0.16
	H4	Histone H4	-0.34		-1.43	0.38		1.22	0 04		-0.22
	96h	Protein Name	shFUS/shSC			shSC/uninduced			shFUS/uninduced		
	MT2	Metallothionein-2	0.52	0.73	1.43	-0 33	-0.26	-0.94	0.19	0.47	0.49
*	EWS	RNA-binding protein EWS	0.32	0.35	0.33	-0.12	-0.21	-0.22	0.19	0.14	0.12
	CHSP1	Calcium-regulated heat stable protein 1	0.32		0.56	-0.14		-0 28	0.17		0.29
	TYB10	Thymosin beta-10	0.27		0.47	0.19		-0 07	0.46		0.40
*	SYAC	Alanine--tRNA ligase, cytoplasmic	0.26		0.37	-0.13		-0.18	0.13		0.19
*	OSBP1	Oxysterol-binding protein 1	0.39		0.26	-0.66		-0.18	-0.26		0.08
*	RAP1A	Ras-related protein Rap-1A	-0.27		-0.29	0.26		0.12	-0.01		-0.17
	ENV2	Retrovirus-related Env polyprotein from Fv-4 locus	-0.25		-0.28	0.02		0 07	-0.23		-0.20
	H2B1A	Histone H2B type 1-A	-0.25		-0.30	0.34		-0 09	0.09		-0.39
	ENV1	MLV-related proviral Env polyprotein	-0.27		-0.30	0.04		0 09	-0.23		-0.21
*	RBBP7	Histone-binding protein RBBP7	-0.28		-0.25	0.15		0 08	-0.13		-0.17
*	TEBP	Prostaglandin E synthase 3	-0.31		-0.28	0.21		0.13	-0.10		-0.15
*	COX5A	Cytochrome c oxidase subunit 5A, mitochondrial	-0.27		-0.32	0.34		0 02	0.07		-0.31
	PPBT	Alkaline phosphatase, tissue-nonspecific isozyme	-0.61		-0.29	0.09		0 04	-0.52		-0.25
*	KAP0 / KAP1	cAMP-dependent protein kinase type I regulatory subunits	-0.53	-0.35	-0.48	0.31	-0.07	0.27	-0 22	-0.42	-0 22
	S100A6	Protein S100-A6	-0.83	-0.62	-0.49	0.65	0.14	0.34	-0.18	-0.48	-0.15
	FUS	RNA-binding protein FUS	-1.39	-0.86	-0.93	0.53	0.53	0.13	-0 86	-0.34	-0 81
	FPPS	Farnesyl pyrophosphate synthase	0.42		0.41	-0.74		-0 50	-0.32		-0.08
*	IDHC	Isocitrate dehydrogenase [NADP] cytoplasmic	0.28		0.49	-0.48		-0 50	-0.19		-0.02
	FKB10	Peptidyl-prolyl cis-trans isomerase FKBP10	0.26		0.46	-0.26		-0 34	-0.01		0.11
	KAD1	Adenylate kinase isoenzyme 1	0.33		0.46	-0.46		-0 29	-0.13		0.17

Table III-2. Relative protein fold-changes. Three comparisons were made: cells expressing shFUS1 compared to cells expressing shSC, cells expressing shSC to uninduced cells, and cells expressing shFUS1 to uninduced cells. Values highlighted in red and green show a positive or negative fold change of at least 0.25, respectively, between shFUS1 and shSC cells. Proteomic analysis was performed on three biological replicates however, only those replicates having a significant expression change between shFUS and shSC are shown for clarification (for full heatmap see Table III-1). Differential expression for those proteins below the double line at 24h and 96h is due to a change in the shSC cells that is lacking in shFUS1 cells. Transcripts bound by FUS are denoted by an asterisk. Due to a lack of unique peptides identified between histone variants, these hits were combined into the five major histone families (H1, H2A, H2B, H3, and H4). Similarly, KAP0 and KAP1 were grouped due to a lack of unique peptides identified for each protein.

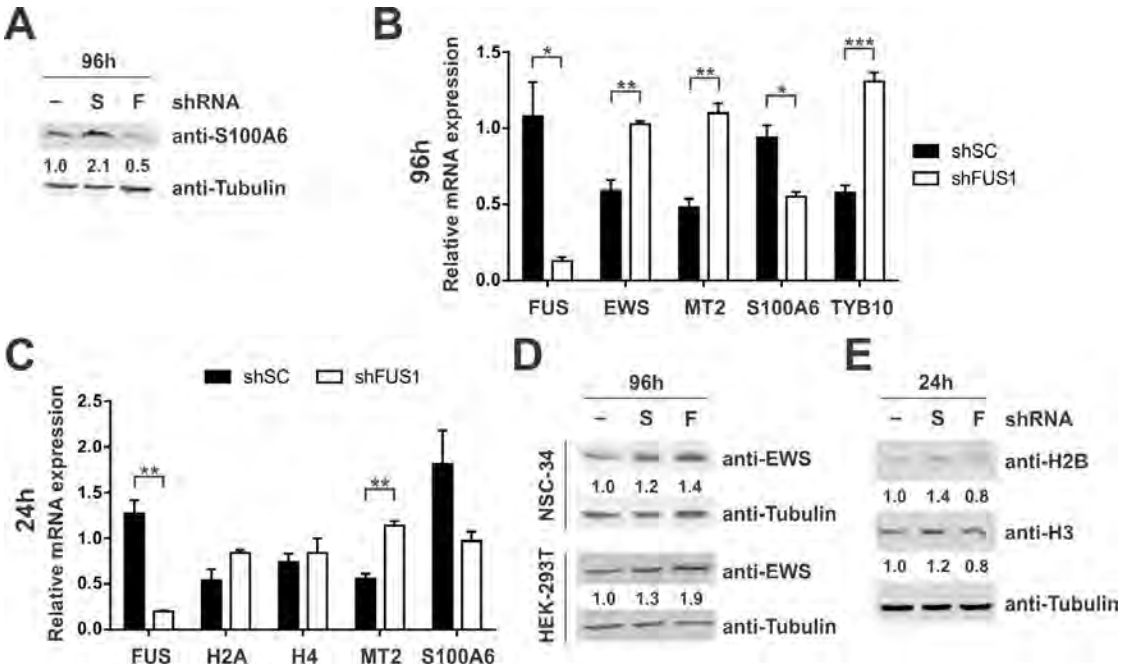

Figure III-6. Western and qRT-PCR validation of proteins differentially expressed upon FUS depletion. (**A**) Western blot analysis of lysates from uninduced NSC-34 cells (-) and cells induced to express scrambled control shRNA (S) or shRNA targeting FUS (F) for 96h. Numbers below the blots refer to densitometry measurements relative to uninduced cells and demonstrate increased expression of S100A6 in shSC cells with a concomitant decrease in shFUS1 cells. Tubulin serves as a loading control. (**B-C**) Quantitative RT-PCR analysis after 96h (**B**) or 24h (**C**) of shRNA induction. mRNA expression relative to uninduced cells was determined for the indicated genes after shSC or shFUS1 induction in NSC-34 cells. Data shown are the average of 3 independent experiments $\pm$ standard error. Statistical significance was determined by a Student's t-test (*P <0.05; **P <0.01; ***P <0.001). (**D**) Representative western blot analysis of lysates from NSC-34 cells or HEK-293T cells after 96h demonstrating increased expression of EWS with FUS knockdown relative to controls. (**E**) Representative western blot analysis of lysates from NSC-34 cells induced to express shRNA for 24h demonstrating increased histone expression in shSC cells with a concomitant decrease in shFUS1 cells.

Discussion

Elucidating the vital functions of FUS is a complex but important objective. Genetic alterations in FUS cause human diseases such as cancer and neurodegeneration. A loss of FUS function has been suggested to cause the neurodegenerative diseases ALS, FTLD and ET, however the multifunctional nature of FUS has made it difficult to discern which functions of FUS are relevant to these disorders (Dormann and Haass, 2013). The effect of FUS knockdown or knockout *in vivo* has produced conflicting results, as some reports describe animal lethality (Hicks et al., 2000; Huang et al., 2011; Sasayama et al., 2012; Xia et al., 2012) whereas others report no effect of FUS knockdown on survival.(Kuroda et al., 2000; Kabashi et al., 2011; Lagier-Tourenne et al., 2012) Consistent with the latter, signs of apoptosis or gross cellular death were not observed here upon knockdown of FUS in cultured mammalian cells **(Figure III-3)**. Rather, we demonstrate for the first time that a reduction in FUS expression impairs cell proliferation **(Figure III-1,2,3)**. To gain insight into the mechanism for FUS-mediated inhibition of cell proliferation, quantitative proteomics was performed on cells undergoing various degrees of FUS knockdown, as no other study to date has performed a comprehensive analysis of protein expression changes as a function of FUS knockdown or knockout.

As one might expect, proteins associated with cell proliferation changed in expression upon FUS knockdown at 24 and 96h **(Figure III-5D, Table III-1)**. One of these proteins, S100A6, exhibited reduced expression in shFUS lines after

96h **(Table III-1, Figure III-6)**. This finding is consistent with previous observations of S100A6 knockdown correlating with reduced cell-proliferation in other cell types.(Ohuchida et al., 2005; Lesniak et al., 2009) (Ohuchida et al., 2005) (Lesniak et al., 2009) Moreover, FUS binds the promoter of S100B,(Tan et al., 2012) a family member of S100A6, raising the possibility that S100A6 expression is directly modulated by FUS. FUS also binds the *CCND1* promoter and inhibits expression of the cell-cycle protein cyclin D1 in response to DNA damage signals (Wang et al., 2008). A general role for FUS in cell-cycle regulation is also suggested by RNA binding targets of FUS identified through RIP/CHIP experiments (Colombrita et al., 2012). However, we did not detect expression changes for these targets or any other classical cell-cycle related proteins through our proteomics analysis, suggesting that additional factors contribute to the observed cell proliferation defect.

Cytoskeletal dynamics is another factor that is fundamentally important for cell proliferation (Provenzano and Keely, 2011). Proteins belonging to the cytoskeletal organization category changed in expression upon FUS knockdown at 24 and 96h **(Figure III-5D)**, including RAP1A and the actin binding proteins MARCS and TYB10 **(Table III-1)**. TYB10 binds and sequesters actin monomers thereby inhibiting actin polymerization and has been implicated in neurite formation (Sribenja et al., 2009). Altered expression of these cytoskeletal proteins upon FUS knockdown could therefore contribute to the cell proliferation defect observed here, and is also consistent with impaired neurite outgrowth

upon FUS depletion reported by others (Kabashi et al., 2011; Orozco et al., 2012).

MT2 exhibited one of the largest changes in expression between shFUS and shSC cells **(Table III-1)**. MT2 plays a protective role against metal toxicity, oxidative stress and ionizing radiation. Accordingly, levels of this protein were shown to increase in response to these stressors (Aschner et al., 2006; Vasak and Meloni, 2011). That expression of MT2 was higher in shFUS cells relative to shSC cells at 24h, a difference that became more pronounced at 96h **(Figure III-6, Table III-1)**, implicates a role for one of the aforementioned stressors in the FUS knockdown-induced proliferation defect. We speculate that oxidative stress may be the relevant stressor, as FUS regulates the transcription of oxidative-stress protection genes and a loss of this function leads to elevated ROS (Sanchez-Ramos et al., 2011). In support of this notion, rolipram partially rescued the proliferation defect upon FUS knockdown through a mechanism that did not involve increased expression of FUS **(Figure III-4)**. Rolipram has been shown to boost expression of antioxidizing enzymes, (Gorur et al., 2008) suppress nitric oxide levels (Beshay et al., 2001; Gorur et al., 2008) and exert a protective effect in animal models of spinal cord injury (Nikulina et al., 2004) and neurodegeneration (Gong et al., 2004; Yang et al., 2008; Smith et al., 2009). While the impact of rolipram on cellular proliferation was strongest for shFUS cells, we note an increase in cell number for the control line in response to certain doses of rolipram that may signify a general effect of rolipram on cell

proliferation. (Nakagawa et al., 2002; Xiao et al., 2011) Therefore, rolipram would need to be further assessed in additional *in vitro* and appropriate *in vivo* models of loss of FUS function.

We also detected an increase in EWS expression upon FUS knockdown **(Table III-1, Figure III-6)**. EWS and FUS are both members of the TET family of proteins and exhibit overlapping functions (Tan and Manley, 2009a), raising the intriguing possibility that increased EWS expression serves as a compensatory mechanism for the loss of FUS function in cells. It follows that exogenous expression of this protein could ameliorate the proliferation defect observed upon FUS knockdown, analogous to the re-expression of FUS **(Figure III-2)**. An alternative, though not mutually exclusive, explanation for elevated levels of EWS is that regulation of EWS at the RNA level is directly impacted by FUS knockdown, as discussed below.

In agreement with previous studies, our proteomics analysis revealed protein expression changes induced by doxycycline and/or shRNA expression (i.e., proteins that changed in shSC cells relative to uninduced cells; **Table III-2**) (Khan et al., 2009; Jackson and Linsley, 2010; Ahler et al., 2013). In fact, a recent study reported that expression of genes involved in glycolysis and cellular metabolism were altered upon doxycycline treatment.(Ahler et al., 2013) We also detected differential expression for proteins associated with energy homeostasis (FPPS, IDHC, and KAD1) upon shSC induction at 96h. Intriguingly, these same changes were not detected in shFUS cells **(Table III-2)**. Thus,

doxycycline exposure and/or shRNA expression elicited changes in gene expression, possibly in response to a stress associated with these stimuli (Grimm et al., 2006; Jackson and Linsley, 2010; Ahler et al., 2013), but under conditions of FUS knockdown this response was impaired. In other words, cells lacking FUS failed to respond as expected. These results underscore the importance of including an untreated control condition to assess the direction of change for the experimental condition, shFUS in this case. For example, without the untreated condition we would have reported a decrease in histones for shFUS cells at 24h, when in fact there was an increase in shSC and no response in shFUS cells **(Table III-2).** The reason histones are increased in shSC cells at 24h is unclear, however the association of FUS with different histone-related processes may explain the lack of response in shFUS cells (Wang et al., 2008; Kim et al., 2010; Colombrita et al., 2012; Takahama et al., 2013).

Which protein expression changes are directly triggered by a loss of FUS, and which reflect downstream consequences to these initial triggers? Of the sixty-one proteins identified here, none have been reported to have differential mRNA expression upon FUS knockdown. (Hoell et al., 2011; Ishigaki et al., 2012; Lagier-Tourenne et al., 2012; Rogelj et al., 2012; Nakaya et al., 2013) Sixteen, however, correspond to reported RNA binding targets of FUS **(Table III-1, asterisks)**. (Hoell et al., 2011; Colombrita et al., 2012; Nakaya et al., 2013) We posit that the protein expression changes for these targets are a direct consequence of a loss of FUS function with respect to RNA processing. For

example, FUS binds RNA corresponding to several differentially expressed proteins discussed above including EWS, cytoskeletal-related proteins (RAP1A and MARCS) and energy homeostasis-related proteins (IDHC, Kap0, Kap1 and Cox5A) (Hoell et al., 2011).

The results of our study have important implications for disease, particularly neurodegenerative disorders that may be mediated through a loss of FUS function. Although mature neurons are post-mitotic and do not proliferate, the loss of FUS function may adversely impact neurodevelopment during a stage when cellular proliferation is critical. Moreover, the processes and proteins that are altered here upon FUS knockdown, particularly those relating to cytoskeletal organization, oxidative stress and calcium handling, are relevant to the homeostasis of mature neurons (Mattson and Magnus, 2006). We also note that glia cells, which do proliferate, play both neuroprotective and pathogenic roles in neurodegeneration (Aguzzi et al., 2013). That FUS is aggregated and depleted from the nucleus of glia cells in some neurodegenerative disorders(Mackenzie et al., 2011; Suzuki et al., 2012) raises the possibility that glial proliferation and function may also be impaired. Importantly, our data demonstrate it is possible to reverse the adverse effects of FUS depletion by replacing the FUS protein or by small-molecule intervention. Proteins that exhibit differential expression upon FUS knockdown **(Table III-1)** may also serve as therapeutic targets for ameliorating the loss of FUS function in disease.

Acknowledgements

We thank Dr. Zuoshang Xu for critical review of the manuscript. We thank Dr. Shinsuke Ishigaki (Nagoya University) for the inducible shRNA NSC-34 cell lines and many helpful discussions; Dr. Desiree Baron (University of Massachusetts Medical School; UMMS), Dr. Miguel Sena-Esteves (UMMS) and Kiera Sapp (UMMS) for their assistance with experiments; Dr. Jennifer Broderick (UMMS) for assistance in designing siRNA constructs; Dr. Greenfield Sluder (UMMS) for use of live-cell imaging equipment, Dr. Craig Peterson (UMMS) for use of histone antibodies, and the Proteomics and Mass Spectrometry Facility (UMMS) for assistance with the proteomics analyses. We acknowledge financial support from the ALS Therapy Alliance-CVS Pharmacy (DAB, MAG), ALS Association (DAB), the US National Institutes of Health/ National Institute on Neurological Disorders and Stroke (R01NS078145 and R01NS067206 DAB; R01NS079836 DAB and MAG), the Harvard NeuroDiscovery Center (MAG), and General Medicine (R01GM30758 to Dr. Greenfield Sluder).

Materials and Methods

Tissue culture. The creation of and culture conditions for NSC-34 cell lines expressing shFUS1 or shSC have been described previously. (Sama et al., 2013) The tetracycline-inducible shFUS2 line was created and cultured in the same manner (shFUS2: 5'-GAGTGGAGGTTATGGTCAA-3'). For the expression of shRNA, cells were treated with 1µg/ml doxycycline (Sigma, D9891) or 0.1

μg/ml tetracycline (Fisher Scientific, BP912-100). Naïve NSC-34 cells (a kind gift from Dr. Neil Cashman) were cultured in Dulbecco's modified Eagle's medium with sodium pyruvate (Invitrogen, 10313) supplemented with 10% fetal bovine serum (Sigma-Aldrich, F4135), 2mM L-glutamine (Invitrogen, 25030081) and 1% penicillin and streptomycin solution (Invitrogen, 15140122). HEK-293T cells were maintained in Minimum Essential Media (Invitrogen, 10370) supplemented with 10% fetal bovine serum (Sigma-Aldrich, F4135) and 1% penicillin and streptomycin solution (Invitrogen, 15140122).

siRNA knockdown of FUS. RNA oligonucleotides for FUS (sequences below) and a scrambled control sequence (guide: 5'-aauucuccgaacgugucacgu-3'; passenger: 5'-gugacacguucggagaaucuu-3') were purchased through Sigma-Aldrich and 10μM annealed stocks were prepared by combining guide and passenger strands in the following buffer: 100mM potassium acetate, 30mM HEPES-KOH pH 7.4, 2mM magnesium acetate. For knockdown in HEK-293T cells, cells were plated in a 24-well plate at 2,000 cells/well and allowed to adhere overnight. Transfection was performed in OPTI-MEM (Invitrogen, 31985070) using 0.4μl Lipofectamine RNAiMax (Invitrogen, 13778030) and 0.2nM siRNA per well (guide: 5'-uugggugaucaggaauuggaa-3'; passenger: 5'-ccaauuccugaucacccacuu-3'). For knockdown in naïve NSC-34 cells, cells were plated in a 24-well plate at 10,000 cells/well. Transfection was performed as

above, but with 0.5µl RNAiMax and 10nM siRNA per well (guide: 5'-uaggguagucugacacacaca-3'; passenger: 5'-ugugugucagacuacccucuu-3').

MTT viability assay. Cells were plated in technical triplicate in a 24-well plate and induced to express shRNA or transfected with siRNA to initiate FUS knockdown. After the desired duration of knockdown, the media from each well was removed and replaced with 400µl fresh media and 100µl of 5mg/ml MTT (3-[4,5-dimethylthiazol-2-yl]-2,5-diphenyl tetrazolium bromide; Invitrogen, M-6494). After a 35 min incubation at 37ºC, 300µl lysis buffer (10% SDS in 1:1 *N*,*N*_-dimethylformamide:water/2% acetic acid/2.5% HCl 1M)(Reixach et al., 2004) was added to each well. Plates were covered with a seal and incubated at 37ºC overnight followed by OD quantification at 550nm. Results are expressed as % cell viability relative to untreated controls using the following equation: 100 x $(OD_{RNAi} - OD_{blank})/(OD_{untreated} - OD_{blank})$. The OD_{blank} was determined by wells containing MTT and tissue culture media without cells.

Immunofluorescence. Cells grown on glass coverslips were fixed for 5-10 min with 4% paraformaldehyde and blocked with PBSAT (1X PBS/1% BSA/0.5% Triton-X 100) for 30-60 min at room temperature. Primary antibodies were diluted in PBSAT and added to the coverslips at room temperature for 1 hr. Primary antibody dilutions were as follows: 1:500 for anti-FUS (Bethyl laboratories, A300-293A) and 1:100 for anti-Apoptosis Inducing Factor (Cell Signaling, 4642). After

primary antibody incubation, coverslips were washed with PBSAT and incubated for 45 minutes with Alexa Fluor 488-conjugated donkey anti-rabbit IgG (Jackson ImmunoResearch Labs, 711-545-152), diluted at 1:2000 in PBSAT. Lastly, cells were stained with 34 ng/mL DAPI and coverslips were mounted with ProLong Gold anti-fade reagent (Invitrogen, P36930).

Western blotting. Cells were lysed for 30 min at 4ºC with either 50 mM Tris HCl (pH 7.5) containing 0.5M NaCl, 1% NP-40, 1% deoxycholic acid, 0.1% SDS, and 2mM EDTA or RIPA buffer (Boston BioProducts, BP-115-500), supplemented with protease (Roche, 11836170001) and phosphatase (Roche, 4906837001) inhibitors. Concentration of cell lysates was determined using a *bicinchoninic* acid (BCA) assay (Thermo Scientific Pierce, 23227) and samples were prepared in Laemmli SDS-sample buffer (Boston BioProducts, BP-111R). Standard western blotting procedures were followed, using Tris-glycine SDS-PAGE and electrotransfer onto PVDF membrane at 100V for 1 hour at 4ºC. For detection of S100A6, Tris-tricine SDS-PAGE was used (BioRad, 456-3066) followed by electrotransfer onto 0.22 µm nitrocellulose at 100V for 30 min at 4ºC. Membranes were blocked for 1h at room temperature with Odyssey Blocking Buffer (LiCor, 927–40003) diluted 1:1 with PBS containing 0.1% tween-20 (PBST), followed by overnight incubation at 4ºC with primary antibodies diluted in PBST. Primary antibody dilutions were as follows: 1:500 anti-FUS (Genscript, generated against C-terminal peptide CKFGGPRDQGSRHDSEQDNSD)(Sama et al., 2013), 1:500

anti-tubulin (Sigma, T9026), 1:500 anti-cleaved PARP1 (Cell Signaling, 9544), 1:500 anti-cleaved caspase-3 (Cell Signaling, 9664), 1:500 anti-EWS (Santa Cruz, sc-28327), 1:1000 anti-H2B (Active motif), 1:1000 anti-H3 (Abcam, 1791), and 1:200 anti-S100A6 (Cell Signaling, 13162). Following primary antibody incubation, membranes were washed with PBST and incubated for 1h with secondary antibody diluted 1:10,000 in 1:1 Odyssey Blocking Buffer:PBST. Secondary antibodies included anti-mouse IRDye 680 (Licor, 926-68072) or IRDye 800 (LiCor, 926-32210) and anti-rabbit IRDye 680 (LiCor, 926-68023) or IRDye 800 (Licor, 926-32211). After washing with PBST, membranes were imaged with an Odyssey Infrared Imager (LiCor, Model 9120) and protein band intensities were quantified with the Odyssey Software (LiCor, V3.0).

Time-lapse video microscopy. Stable NSC-34 cells were plated on glass coverslips and induced to express either shSC or shFUS1. Twenty-four hours later, coverslips were assembled into chambers as previously described (Uetake Y, 2012) and imaged at 37ºC with BH2 (Olympus) microscopes equipped with phase-contrast optics using 10X objectives/ 0.3–0.32 NA. Image sequences were gathered using Retiga EX (Qimaging, Corp.) or Retiga EXi Fast (Qimaging, Corp.) cameras. Images were acquired every 3 min with C-imaging software (Hamamatsu Photonics) and were exported as QuickTime videos using CinePak compression (Apple).

Small-molecule high-content screen. shFUS1 NSC-34 cells were plated onto 384-well plates (Corning 3712) at 500 cells/well in 40 µL of culture media (described above) using a Multidrop automated liquid handler (Thermo Fisher Scientific). Gas-permeable seals were used to reduce any uneven evaporation effects. After overnight incubation, 5 µl doxycycline was transferred using a Biomek NX robotic liquid handler (Beckman Coulter) into each experimental well to attain a final concentration of 1 µg/ml. An equal volume of doxycycline solvent (dd H_2O) was added to control wells. Four hours after doxycycline addition, 5 µl of compounds from the LDDN library (described below) were transferred using the robotic liquid handler into experimental wells to attain a final concentration of 1 µM and 0.1% DMSO. An equal volume of DMSO in media was added to control wells. Plates were incubated for 96h. Screening of compounds was performed in triplicate due to the small activity window (25%) as determined during assay development using this format.

A subset of the Laboratory for Drug Discovery in Neurodegeneration (LDDN) chemical library was used, consisting of 606 compounds approved by the Food and Drug Administration (Prestwick) and 480 purified natural products. Compounds for high-throughput screening were stored as DMSO stocks at -20°C and assay-ready 384-well plates with 1.67 mM compound concentration in 100% DMSO were diluted in media to attain a final concentration of 1 µM in 0.1% DMSO just before use.

After 96h, cells were fixed with 4% paraformaldehyde for 20 min and washed three times with phosphate-buffered saline (ELx405 plate washer, BioTek). The cells were labeled with 1 μg/ml Hoechst stain to visualize nuclei. Images were captured on the IN Cell Analyzer 2000 (GE Healthcare). The entire well was imaged in 4 fields at 25 ms exposure time using excitation filter D360/40 and emissions filter HQ460/40 in combination with a 10X/.45 NA objective. Image stacks were batched and analyzed using IN Cell Workstation software (GE Healthcare). For the feature extraction protocol, cells were segmented using the multi-target analysis algorithm and nuclei were segmented as defined with a minimum area of 50 μm^2 with a sensitivity setting of 70. Total nuclei per well was used as a measure of cell count.

A compound was considered a “hit” and selected for confirmation if it rescued the shFUS1 knockdown-induced decrease in cell number by >3 standard deviations (SD) from the mean of the shFUS1 knockdown control wells (shFUS1 +doxycycline) on each of the three replicate plates. Hits were confirmed via a 5-point dose-response curve (0.1 to 30 μM) using compounds that were re-ordered from the commercial suppliers. For confirmation studies, compounds were added to both shSC and shFUS1 expressing cells in the presence of doxycycline. Western blot analysis of FUS expression after 96h of 1 μM compound incubation was performed using a similar protocol to that described above.

Quantitative Proteomics. NSC-34 cells were either uninduced, or induced to express shSC or shFUS1 for 24 or 96h (for a total of 6 samples), followed by lysis with RIPA buffer (Boston Bio Products) supplemented with protease inhibitors (Roche). Protein content was measured using a standard BCA Assay (Thermo Scientific) and lysates were treated according to manufacturers' instructions, with slight method alteration in the detergent removal step. Briefly, 100 µg of lysate was diluted to a final concentration of 1 µg/µL with 100 mM triethyl ammonium bicarbonate (TEAB). Disulfide bonds were reduced with 0.5 M tris(2-carboxyethyl)phosphine (TCEP) for 1 hour at 55°C and cysteine residues were alkylated with 375 mM iodoacetimide (IAA) for 30 minutes at ambient temperature, protected from light. Lysates were then treated for detergent clean up using Detergent Removal Spin Columns (Thermo Scientific) according to manufacturers' instructions and digested overnight at 37°C with Trypsin (Promega, sequencing grade) in a 1:25 enzyme:protein digest ratio. Amine reactive TMT reagents (Thermo Scientific, 6-plex kit) were dissolved in acetonitrile and allowed to react with peptides for 1 hour at ambient temperature. After 1 hour, the reaction was quenched upon addition of 5% hydroxylamine hydrochloride and a 15 minute incubation at room temperature. Following labeling, the samples were combined in an equi-volume ratio (1:1:1:1:1:1) and dried down prior to reconstitution in 5% acetonitrile, 0.1% trifluoroacetic acid (TFA) for mass spectrometric analysis. The assignment of TMT tag (126 to 131) to each sample was random (www.random.org) to guard against bias.

Assignments were made such that no sample had the same tag identity between three independent experiments.

Three independent experiments were tested, with each experiment analyzed in technical triplicate. LC-MS/MS experiments were performed on a QExactive hybrid mass spectrometer (Thermo Scientific) equipped with a nanoAcquity UPLC (Waters). Run conditions match those of the “sensitive” conditions previously recommended(Kelstrup et al., 2012). Briefly, approximately 1 µg of labeled peptides were loaded on a 100 µm i.d. fused-silica precolumn packed with 2 cm of Magic C18AQ resin (5 µm, 200Å, Michrom Bioresources) at a flow rate of 4.0 µL/min for 4 min in 5% acetonitrile, 0.1% formic acid (FA) and eluted using a gradient at 300 nL/min onto a 75 µm i.d. analytical column packed with 25 cm of Magic C18AQ resin (3 µm, 100 Å, Michrom Bioresources) to a gravity-pulled tip. Separation was achieved by applying a 5%-35% acetonitrile gradient in 0.1% FA over 180 minutes at 300 nL/min. In detail, the time program was: 0−180 min, 5−35% B; 180−181 min, 35-90% B; 181-191 min, 90% B; 191-192 min, 90-5% B; 192-210 min, 5% B; 210 min, stop. Solvent A was water with 0.1% FA and solvent B was acetonitrile with 0.1% FA. Electrospray ionization was enabled via liquid junction into a QExactive hybrid mass spectrometer (Thermo Scientific). Mass spectra were acquired over m/z 300-1750 at 70,000 resolution (m/z 200) and data-dependent acquisition selected the top 12 most abundant precursor ions for tandem mass spectrometry by HCD fragmentation

using an isolation width of 1.2 m/z, collision energy of 30, and a resolution of 35,000.

Mass spectra were submitted to MASCOT (Matrix Science, v2.4.1) and searched against the Mouse SwissProt database (16627 entries). Search specifications included: allow up to two missed cleavage sites, enzyme specified as trypsin, MS tolerance – 10 ppm, and MS/MS tolerance – 0.05 Da. Specified fixed modifications include Carbamidomethyl and TMT6plex. Specified variable modifications include Gln→pyro-Glu, Oxidation, and N-term Acetyl.

ProteoIQ (Premier Biosoft, v2.6.03) was used to quantify reporter ion signals. Search specifications included: reporter ion tolerance – 0.05 Da; minimum peptide length – 6 amino acids; minimum # of spectra – 2; minimum # of peptides – 2; minimum peptide probability – 0.05; minimum protein probability – 0.5; maximum p-value – 0.05; minimum fold change - |0.25|; 3 external replicates; data centroided. Reporter ions were normalized by total labeling of each species and relative expression was weighted by species intensity.

Quantitative real-time PCR (qRT-PCR). RNA was harvested from cells (BioRad, 732-6820) and converted to cDNA (BioRad, 170-8841), according to the manufacturer's instructions. Quantitative real-time PCR was performed in technical triplicate using PrimePCR primer assays (BioRad, 100-25636) and SYBR Green Supermix (BioRad, 172-5121) according to manufacturer's guidelines and using the following PCR program in a CFX384 Touch Real-Time

PCR Detection System (BioRad): 95ºC for 2 min, 40 cycles of 95ºC for 5 sec and 60ºC for 30 sec, and a melt-curve of 65-95ºC (0.5ºC increments/5 sec). Quantification of differential mRNA expression was calculated by the comparative Ct method using Bio-Rad CFX Manger 3.1 software. Briefly, threshold cycle (Ct) values were normalized to the B2M reference gene Ct value to obtain ΔCt values. The ΔCt value for the control condition was subtracted from the ΔCt of the experimental condition to calculate a ΔΔCt. Fold change relative to the control samples was then calculated by $2^{-(\Delta\Delta Ct)}$.

CHAPTER IV: DISCUSSION AND FUTURE DIRECTIONS

ALS is a devastating neurodegenerative disease that results in death for 2 out of every 100,000 people a year. Disease onset is nearly unpredictable, treatments are limited and ineffective, and a cure is nonexistent. After onset, the disease progresses very quickly with survival typically only 3-5 years, during which time the affected individual loses all motor function until they are unable to speak, eat, move, or even breathe on their own. While statistics report "ALS affects about 1-2 individuals per 100,000 per year" (Robberecht and Philips, 2013), this number is far greater when considering the impact ALS has on friends and families of an ALS patient. As the patient's motor abilities quickly decline their need for assistance quickly increases and it is estimated that for every year a person lives with ALS, an average of $63,000 is required for their care (study by the Muscular Dystrophy Association, 2013). So while ALS is a 'rare' disease with only 30,000 people living with ALS in the United States, the impact ALS has on the human population far exceeds this number.

Despite the urgent need for a treatment and the large amount of research being conducted, little is known about the definitive causes of ALS. This can be attributed to the sporadic nature of the disease. Only 5-10% of cases can be tracked by familial inheritance and of these only ~60% have been linked to specific genetic mutations (Sreedharan and Brown, 2013; Renton et al., 2014). Studying genes associated with familial ALS, however, has provided valuable

insight into the cellular mechanisms of this disease. The discovery of FUS mutations for example, has led to several important advances in the field, particularly adding support for defective RNA processing as a pathogenic mechanism and strengthening the link between ALS and FTD.

Here, I have investigated a loss of function hypothesis for mutant FUS in ALS pathogenesis. To this end, I developed several FUS knockdown mammalian cell culture models and assessed the cellular effects of FUS depletion. The models displayed a defect in cell abundance and suggested a link between FUS function and DNA damage repair (Chapter II). This link has been supported by several recent reports demonstrating inefficient DNA damage repair in the absence of FUS (Mastrocola et al., 2013; Wang et al., 2013). Upon further characterization, the model revealed a FUS knockdown-induced reduction in cell proliferation, highlighting that FUS is essential for cell health and homeostasis (Chapter III). This defect in proliferation was accompanied by expression changes of proteins associated with multiple processes, such as cell-cycle regulation, cytoskeletal organization, oxidative stress and energy homeostasis. Together, this work demonstrates that an array of cellular pathways respond to, or are influenced by, a loss of FUS function. The way in which a loss of FUS function in these pathways may be important for ALS pathogenesis is discussed below.

Cell cycle regulation and ALS

As investigated in both Chapters II and III, depletion of FUS results in decreased cellular proliferation. This response may be indirect, occurring as a result of other cellular events, such as increased DNA damage (Chapter II), oxidative stress, cytoskeletal disorganization, or energy homeostasis (discussed in Chapter III). Several reports however, demonstrate a direct role for FUS in cell cycle regulation. For example, RIP/CHIP experiments (RNA-binding protein immunoprecipitation-microarray) identified an enrichment of cell cycle-related RNA binding targets of FUS (Colombrita et al., 2012). FUS also binds the *CCND1* promoter and inhibits expression of the cell-cycle protein cyclin D1 in response to DNA damage signals (Wang et al., 2008). Additionally, in prostate cancer cells FUS mediates cell proliferation stimulated by androgen (Brooke et al., 2010; Haile et al., 2011), seemingly through transcriptional regulation of several important cell cycle proteins (Brooke et al., 2010).

These findings seem to suggest an important role for FUS in regulating the cell cycle in proliferating cell types. Motor neurons however, are post-mitotic and are a non-proliferating cell type. Thus, how could regulation of cell proliferation by FUS be important for ALS pathogenesis? Accumulating evidence suggests that inappropriate cell cycle re-entry in neurons induces apoptosis and may therefore be a relevant mechanism in neurodegeneration (Herrup and Yang, 2007; Bonda et al., 2010b). For instance, the cyclin D/CDK4,6 complex is responsible for reinitiating the cell cycle in non-proliferating cells (Sherr, 1994)

and interestingly, increased expression of cyclin D and cdk4 is evident in motor neurons of ALS mice and patient tissue (Nguyen et al., 2003; Ranganathan and Bowser, 2003). Furthermore, FUS has been shown to regulate cyclin D expression (Wang et al., 2008). Thus, one could speculate that loss of FUS function from ALS-mutations leads to re-expression of cyclin D1 and re-initiation of the cell cycle, causing neuronal cell death. In support of this, ALS mutations cause nuclear FUS depletion or alternatively, are located in a domain of FUS responsible for transcriptional activity **(Figure I-2)**, either of which could disrupt FUS-mediated repression of cell cycle-related transcription.

To date, the regulation of cyclin D1 expression by FUS has only been demonstrated in macrophage (Wang et al., 2008) and prostate cancer cells (Brooke et al., 2010; Haile et al., 2011). Preliminary steps towards investigating this function in neurons are discussed in Appendix I, but this work was not pursued as part of this dissertation. Briefly in sum, I recapitulated the effect of FUS knockdown on cyclin D1 expression in macrophage cells, but did not detect increased cyclin D1 immunofluorescence in cortical neurons after FUS depletion. My investigations however, were only preliminary and were not performed in a rigorous manner. Therefore, a role for FUS in neuronal cell cycle control remains to be fully investigated. Additionally, the effect of mutant FUS expression on cell cycle regulation has not been addressed, in either neurons or mitotic cells.

While re-expression of cell cycle proteins in neurons seems to correlate with apoptosis, it is still unclear whether this is an upstream event in ALS

pathogenesis, or just a misregulation that occurs at the final stages of the cell's life. Thus, investigations of this phenomenon may advance our understanding of *how* motor neurons die, but may not answer the question of *why* motor neurons die and therefore provide little therapeutic insight.

DNA damage and ALS

Accumulating evidence within the literature firmly establishes the importance of FUS in DNA damage repair. FUS binds both single- and double-stranded DNA (Baechtold et al., 1999; Liu et al., 2013), is important for homologous DNA pairing (Akhmedov et al., 1995; Bertrand et al., 1999) and D-loop formation (Baechtold et al., 1999), localizes to sites of DNA damage (Mastrocola et al., 2013; Rulten et al., 2013; Wang et al., 2013), and is required for efficient DNA damage repair (Mastrocola et al., 2013; Wang et al., 2013). Furthermore, evidence shown here (Chapter II) suggests an accumulation of DNA damage in cells depleted of FUS. As a normal result of aging, DNA damage accumulates in neurons, presumably due to a decline in quality control pathways (reviewed in (Gorbunova et al., 2007)). That mutations in FUS cause inefficient DNA damage repair in neurons (Wang et al., 2013), could worsen this problem, resulting in a faster accumulation of damaged DNA and neuronal apoptosis. In support of this, post-mortem brain sections from the motor cortex of ALS patients harboring either FUS R521C or P525L mutations display increased levels of the γH2AX DNA damage marker relative to control brain sections (Wang et al., 2013).

Furthermore, a transgenic mouse expressing FUS R521C also exhibits elevated levels of DNA damage markers (e.g., γH2AX, phosphorylated p53, and ATF3) in the central nervous system (Qiu et al., 2014). Together, this evidence points towards inefficient DNA damage repair as a relevant model for FUS-mediated ALS.

While no other ALS-linked proteins have been directly linked to DNA damage repair, more general evidence of DNA damage as a pathogenic mechanism in ALS exists. Post-mortem patient tissue of ALS show elevated levels of DNA damage, including 8-hydroxy-2'-deoxy-guanosine (8-oxo-G), and decreased activity of DNA repair enzymes (Coppede, 2011). 8-oxo-G results from oxidation of nucleic acids and is one of the most common DNA lesions in neurons (reviewed in (Coppede, 2011)). That oxidative stress is a pathological hallmark of ALS suggests that DNA damage arising from reactive oxygen species (ROS) may represent a general mechanism of ALS pathogenesis. FUS appears to also play a role in controlling ROS levels as a co-transcriptional regulator of oxidative stress protection genes, as knockdown of FUS resulted in decreased transcription of these genes with a concomitant increase in ROS levels (Sanchez-Ramos et al., 2011). Therefore, FUS appears to function both upstream and downstream of DNA damage, as a transcriptional regulator stimulating expression of oxidative stress protection genes and as a member of the DNA damage repair pathway. As FUS animal models continue to be investigated and additional neuronal models are created, I predict an important

link between mutant-FUS and DNA damage repair will come to light and prove to be important for understanding ALS pathogenesis.

Insights from gene expression studies

FUS is a multifunctional protein with roles in numerous fundamental processes **(Figure I-2)**. A challenge is to determine which of these functions is affected by ALS-linked mutations. As an hnRNP protein (heterogeneous ribonucleoprotein) and part of the FET family, it is well established that FUS is involved in mRNA splicing and transcriptional regulation. In fact, several large gene expression studies have been performed **(Table I-1)** and collectively show that FUS binds thousands of mRNA targets and depletion of FUS alters transcriptional regulation and alternative splicing (reviewed in (Ling et al., 2013)). Similarly, overexpression of mutant FUS affects these same processes. Mutant FUS lacked an interaction with ~3,000 targets shown to bind wild-type FUS and gained ~900 unique interactions (Hoell et al., 2011). Furthermore, mutant-FUS preferentially bound the 3'UTR of its targets while wild-type FUS preferred intronic regions (Hoell et al., 2011). The implications of these observations are that thousands of transcripts could be irregularly spliced in disease or have altered stability, affecting numerous cellular pathways.

While these studies clearly demonstrate that both FUS depletion and expression of mutant FUS affect mRNA processing, none of these studies addressed whether similar alterations occurred at the protein level or whether

these alterations had any effect on cell health. To this end, my work demonstrated a decline in cell health and homeostasis upon FUS depletion and investigated changes in the proteome (Chapter III). Differentially expressed proteins were grouped into functional categories, revealing enrichment for proteins involved in chromatin organization, cytoskeletal organization, energy homeostasis, calcium and metal ion binding, and cellular proliferation **(Table III-1)**. Consistent with oxidative stress being a hallmark of ALS, metallothionein-2 (MT2), a multifunctional protein involved in zinc homeostasis and antioxidation (Vasak and Meloni, 2011), was increased 85% after FUS knockdown. That levels of MT2 are known to increase in response to metal toxicity, oxidative stress, and ionizing radiation (Aschner et al., 2006; Vasak and Meloni, 2011), suggests one of these stressors is induced by FUS knockdown. Likely, this stressor is oxidative stress, as FUS depletion has previously been shown to increase reactive oxygen species (Sanchez-Ramos et al., 2011). Also changing significantly with FUS depletion was protein S100A6, which decreased by 36%. This protein is a calcium binding protein whose levels correlate with cellular proliferation status and is suggested to function in cytoskeletal organization (Lesniak et al., 2009). While the exact functions of this protein have not been fully elucidated, evidence from ALS SOD G93A mice suggests it is up-regulated specifically in mutant SOD1 animals as a calcium buffering protein (Hoyaux et al., 2000). That FUS binds the promoter of S100B (Tan et al., 2012), a family member of S100A6, raises the possibility that FUS may directly regulate

expression of S100A6. Loss of FUS function mutations in ALS therefore may affect the expression of S100A6, as shown here for FUS depletion, thereby limiting the calcium buffering ability of the cell and causing excitotoxicity and neuronal death.

While providing valuable insight into potential ALS-related FUS functional pathways, the large gene expression studies discussed above and proteomics analysis presented here in Chapter III, do little to confirm which altered FUS functions or affected pathways are actually leading to neuronal death. Moving forward more studies need to be performed in neuronal models with relevant levels of mutant protein as opposed to overexpression. Additionally, a complete loss of FUS function in ALS is unlikely, although several *in vivo* studies suggest mutant FUS may affect the levels and/or activity of wild-type (Machamer et al., 2014; Qiu et al., 2014). With the recent development of human induced pluripotent stem cells (iPSC) it is now possible to study motor neurons derived from patient cells expressing disease relevant copies of these ALS-linked proteins. Utilizing iPS cells will undoubtedly provide important insight into the question of whether a loss of function or gain of function mechanism is contributing to FUS-mediated ALS pathogenesis.

G-quadruplexes: a common link between FUS functions?

As FUS is a multifunctional protein with links to numerous cellular pathways, it is difficult to determine which functions are most relevant to study in terms of ALS

pathogenesis. That ALS-linked mutations affect several FUS functions, such as DNA damage repair, transcription, and splicing, makes this task even more difficult and suggests disruption of any FUS-associated process is detrimental. For this reason, finding a common link between how FUS performs these specific functions could be of great value.

One noteworthy property of FUS that spans several functions is the binding of FUS to G-quadruplex nucleic acid structures. In a study that determined RNA polymerase II promoters bound by FUS, it was noted that many FUS-bound promoters are predicted to contain G-quadruplex structures (Tan et al., 2012). Furthermore, the complementary strand of the consensus motif most strongly bound by FUS is expected to form a G-quadruplex (Tan et al., 2012), suggesting a correlation between G-quadruplexes and the function of FUS in RNA polymerase II-mediated transcription. In addition to transcription start sites, G-quadruplexed DNA is common within telomeres. Recently, FUS overexpression was found to affect telomere histone methylation and telomere length and interestingly, the localization of FUS to telomeres required binding to G-quadruplexed DNA (Takahama et al., 2013). FUS also binds telomeric RNA (termed TERRA), specifically through a G-quadruplex dependent interaction (Takahama et al., 2013). The importance of telomeres in genome stability and cellular aging is well known. That FUS appears to play a role in regulating telomere length establishes an interesting area of research for FUS in cell aging with potential importance to neurodegeneration.

More well-studied than transcriptional regulation and genomic maintenance is the role of FUS in RNA processing. Several genome-wide studies have been conducted to determine the RNA targets of FUS and whether they can be predicted through sequence motifs. While early studies suggested a GGUG motif preference for FUS binding (Lerga et al., 2001) which is generally accepted and has been confirmed by a subsequent study (Lagier-Tourenne et al., 2012), others propose that FUS is more selective for a conformational motif (Hoell et al., 2011; Colombrita et al., 2012; Ishigaki et al., 2012; Nakaya et al., 2013; Takahama and Oyoshi, 2013). As demonstrated for telomeric RNA, this secondary structure could potentially be a G-quadruplex, however this possibility was not investigated in these studies.

Binding to both telomeric DNA- and RNA- G-quadruplexes requires the arginine-glycine-glycine (RGG) domain at the C-terminus of FUS **(Figure I-2)** (Takahama and Oyoshi, 2013; Takahama et al., 2013). Similarly, the FUS-related protein EWS has also been reported to bind G-quadruplexed DNA and RNA (Takahama et al., 2011b) via a similar RGG domain (Takahama et al., 2011a), suggesting this binding specificity may be important for functions common between these two proteins. The effect of mutating residues in the RGG domain on binding affinity has not been determined, but several ALS-linked mutations in FUS are present in this domain **(Figure I-4)** which could conceivably affect binding.

Recently an abnormal hexanucleotide GGGGCC repeat expansion in C9ORF72 was determined to be the most common cause of familial and sporadic ALS (DeJesus-Hernandez et al., 2011; Renton et al., 2011). One theory as to how this leads to disease is that this repeat expansion sequesters RNA binding proteins, thereby inhibiting them from performing their normal functions (Taylor, 2014). There have been several attempts to determine the RNA-binding proteins associated with this repeat expansion and numerous hits have been identified *in vitro* that co-localize with C9ORF72 RNA-foci in diseased patient cells (Donnelly et al., 2013; Lee et al., 2013; Mori et al., 2013; Sareen et al., 2013; Xu et al., 2013). That both the DNA and RNA of this repeat expansion form G-quadruplexes (Fratta et al., 2012; Reddy et al., 2013; Haeusler et al., 2014) predicts an association of FUS with this expanded repeat which may come to light as more comprehensive analyses are performed.

A Model for ALS Pathogenesis

Understanding the normal functions of FUS and how these functions are altered by ALS-linked mutations is important for understanding the pathogenesis of FUS-mediated ALS. An equally important and even more challenging question to consider is how mutations in so many diverse genes can cause the same disease. There are over 100 genes associated with ALS with several having a relatively high incidence, such as SOD1, TDP-43, FUS, and C9ORF72, with firm genetic support of their involvement in ALS pathogenesis. How does

one make sense of disease pathogenesis with so many seemingly diverse players involved? To this end, much research has been focused on identifying functional overlap between ALS-associated proteins. Presented below is a discussion of two related cellular processes in which several ALS-associated proteins function, followed by a description of a potential pathogenic mechanism involving these fundamental processes.

Protein misfolding

A main suspect in ALS pathogenesis is misfolded protein. This stems from investigations of mutant superoxide dismutase-1 (SOD1), the first genetic link to ALS (Rosen et al., 1993). Mutant SOD1 misfolds and oligomerizes, leading to the induction of several cellular stresses, including proteasomal disruption and endoplasmic reticulum (ER) stress (Sreedharan and Brown, 2013). Wild-type SOD1 can also obtain a misfolded conformation which has been identified in cases of sporadic ALS, further implicating this misfolded species in disease pathogenesis (Rotunno and Bosco, 2013). Other ALS-associated proteins that adopt a misfolded or less stable conformation include TDP-43 (Mackness et al., 2014), FUS/TLS, and Pfn-1 (Bosco lab, unpublished).

When a cell detects misfolded protein it initiates the unfolded protein response (UPR). The UPR is a three pronged approach to dealing with the stress of protein misfolding: 1) translation of new protein is halted, 2) production of molecular chaperones is increased, and 3) proteins that cannot be refolded

are degraded by the proteasome or autophagosome. Evidence of UPR activation has been seen in ALS human samples as well as ALS mouse models, implicating stress from misfolded proteins in ALS (Matus et al., 2013). That several ALS-associated proteins have known functions in protein degradation pathways may help provide a link between protein homeostasis and ALS pathogenesis. These proteins include ubiquilin-2 (UBQLN2), optineurin (OPTN), p62/sequestosome 1 (p62/SQSTM1), valosin-containing protein (VCP), chromatin modifying protein 2B (CHMP2B), factor induced gene 4 (FIG4), Alsin, vesicle associated membrane protein associated protein B (VAPB), and C9ORF72. VAPB associates with the endoplasmic reticulum and is thought to be important for activation of the UPR (Kanekura et al., 2006). The remaining proteins assist in protein degradation by fulfilling important functions in the proteasome pathway (UBQLN2, VCP, p62/SQSTM1) or autophagy (UBQLN2, VCP, p62/SQSTM1, CHMP2B, OPTN, FIG4, Alsin, C9ORF72) (Farg et al., 2014) reviewed in (Chen et al., 2013; Ling et al., 2013; Robberecht and Philips, 2013).

Stress response in ALS

Misfolded proteins and ALS-linked mutant proteins, such as SOD1 (Nishitoh et al., 2008), TDP-43 (Walker et al., 2013), and FUS (Farg et al., 2012), initiate the UPR by causing ER-stress, which is a cellular response strongly associated with the pathogenesis of ALS (Matus et al., 2013). As such, investigations of potential biomarkers and therapeutic strategies have been

centered on key features of the ER-stress response (Matus et al., 2013). One effect of ER-stress is the formation of stress granules, which are protein/RNA structures that are thought to occur as a means of halting translation of proteins unnecessary to overcome the stress at hand (Kedersha and Anderson, 2007; Anderson and Kedersha, 2008; Kedersha et al., 2013). One response of ER-stress is the inhibition of protein translation through phosphorylation of eukaryotic translation initiation factor 2α (eIF2α) (Hetz, 2012), a key event in stress granule formation (Kedersha et al., 1999).

In addition to being a product of ER-stress, the relevance of stress granules in ALS pathogenesis came to light with the discovery that ALS-linked mutant FUS associates with stress granules (Bosco et al., 2010a). Furthermore, wild-type FUS incorporates into stress granules under conditions of hyperosmolar stress (Sama et al., 2013), as does TDP-43 (Dewey et al., 2010), which has also been seen in stress granules formed from various other stressors (Colombrita et al., 2009; Liu-Yesucevitz et al., 2010; Aulas et al., 2012), including ER-stress (Walker et al., 2013). The effects of mutant FUS and TDP-43 on stress granule function are in the early stages of investigation, but have so far been determined to affect several characteristics of stress granules, such as size, number, and assembly rate (Dewey et al., 2010; Baron et al., 2013). FUS and TDP-43 are two RNA-binding proteins that are genetically linked to ALS and share similar domain structures, are both components of inclusions in ALS and

FTLD, and share many functions, such as transcription, RNA splicing, and transport of mRNA.

Recently, a third ALS-linked protein, profilin-1, was found to associate with stress granules and mutations in this protein may also affect stress granule dynamics (Figley et al., 2014). Profilin-1 is an important protein in the regulation of actin polymerization making this finding intriguing as cytoskeletal organization is key for stress granule formation and disassembly (Bartoli et al., 2011). It has yet to be determined whether actin assembly is altered by ALS-linked profilin-1 mutations, however one could speculate that if this were the case, stress granule function would be disturbed as a result. Several other ALS-linked proteins are also associated with stress granules: hnRNPA1, hnRNPA2, and ataxin-2. Mutations in these proteins do not account for very many ALS cases, however, they are implicated as risk factors for the disease.

While it is significant that six different ALS-associated proteins are all components of stress granules, it has also been proposed that stress granules could be precursors to the pathological aggregates found in ALS patient tissue (Dewey et al., 2012). Several stress granule nucleating factors, such as T cell intracellular antigen 1 (TIA 1), nucleolysin, TIAR and eukaryotic translation initiation factor 3 subunit (eIF3), are present in TDP-43 containing aggregates in patient ALS tissue (Liu-Yesucevitz et al., 2010). The implications of this observation are that stress granules, containing TDP-43, formed in response to a cellular stress and persisted long enough to further incorporate TDP-43 to the

point of forming an aggregate. Persistent stress granules could be the result of a heightened state of cell stress that does not get resolved. Alternatively, the incorporation of ALS-linked mutant protein, such as FUS or TDP-43, may impair the function of stress granules such that homeostasis is not re-established, resulting in a vicious cycle in which the system put in place to deal with stress actually causes more stress, worsening over time.

Tipping the balance of proteostasis in ALS

That numerous ALS-associated proteins are involved in stress granules and protein degradation pathways suggests that these processes contribute to ALS pathogenesis through a common cellular event, such as the maintenance of protein homeostasis, also known as proteostasis (Ong and Kelly, 2011). To maintain proteostasis, the cell responds to misfolded protein and ER-stress by eliciting a stress signal that induces stress granule formation and the stalling of translation while also utilizing protein degradation machinery to rid the cell of protein that cannot be refolded **(Figure IV-1 top)**. As the efficiency of the proteasome and autophagy systems normally decline with age , mutations in proteins involved in these pathways may exacerbate this effect, causing the system to surpass a threshold for which it can handle defects in proteostasis. This in turn may cause an accumulation of misfolded proteins which leads to a heightened level of cell stress, persistent stress granules, and eventually protein aggregates. In support of this theory, many disease-associated aggregates are

ubiquitinated (Blokhuis et al., 2013), indicating activation of the UPR. Furthermore, inhibition of the proteasome has been shown to induce stress granule formation (Mazroui et al., 2007), demonstrating a link between these two cellular processes. Whether **(Figure IV – 1 bottom)**. As stress granule function and protein degradation are intimately linked, disruption of either would be detrimental, leading to cell death and neurodegeneration, as supported by the fact that many ALS-linked proteins are associated with these processes.

Neuronal vulnerability

All cells maintain protein homeostasis using these fundamental processes and mutant ALS-associated proteins are expressed ubiquitously in all cell types. Why then are neurons susceptible to disturbances in these processes while other cell types appear to be impervious? The difference is the post-mitotic status of neurons. Neurons do not replicate and once a neuron is differentiated and established within an organism, it will remain there for the duration of the organism's life. Mitotic cells however, are turned-over as new cells are continuously being produced. This is necessary as mitotic cells have a limit to the number of times they can divide before they are destined for apoptosis. That disease onset for ALS occurs later in life implies there is a temporal factor involved in the development of the disease. If protein homeostasis is compromised in a neuron, the level of misfolded proteins and cellular stress will accumulate over time. Eventually, a threshold is reached at which the cell can no

longer survive. It could take decades to reach this threshold, which for a neuron is within its lifetime while mitotic cells reach the end of their life long before enough stress is accumulated to create a problem. In this way, neurons become more susceptible over time to stress, eventually leading to neurodegeneration.

Conclusion

The multifunctional nature of FUS makes its role in ALS pathogenesis difficult to ascertain. Investigating ALS-linked FUS mutant protein has revealed disruptions in the DNA damage repair, transcriptional regulation, and RNA splicing functions of FUS. Additionally, mutant protein mislocalizes to the cytoplasm and causes abnormal stress granule formation and dissolution, having implications of an altered cellular stress response. Which of these abnormal properties of mutant FUS protein is most relevant to ALS pathogenesis? Is association with G-quadruplexes an important connection between FUS function and C9ORF72-mediated ALS? Since the discovery of FUS in ALS in 2009, over 250 studies of FUS have been published. With this expansive interest and the development of animal and induced pluripotent patient stem cell models, determining the role of FUS in ALS pathogenesis will surely come to fruition.

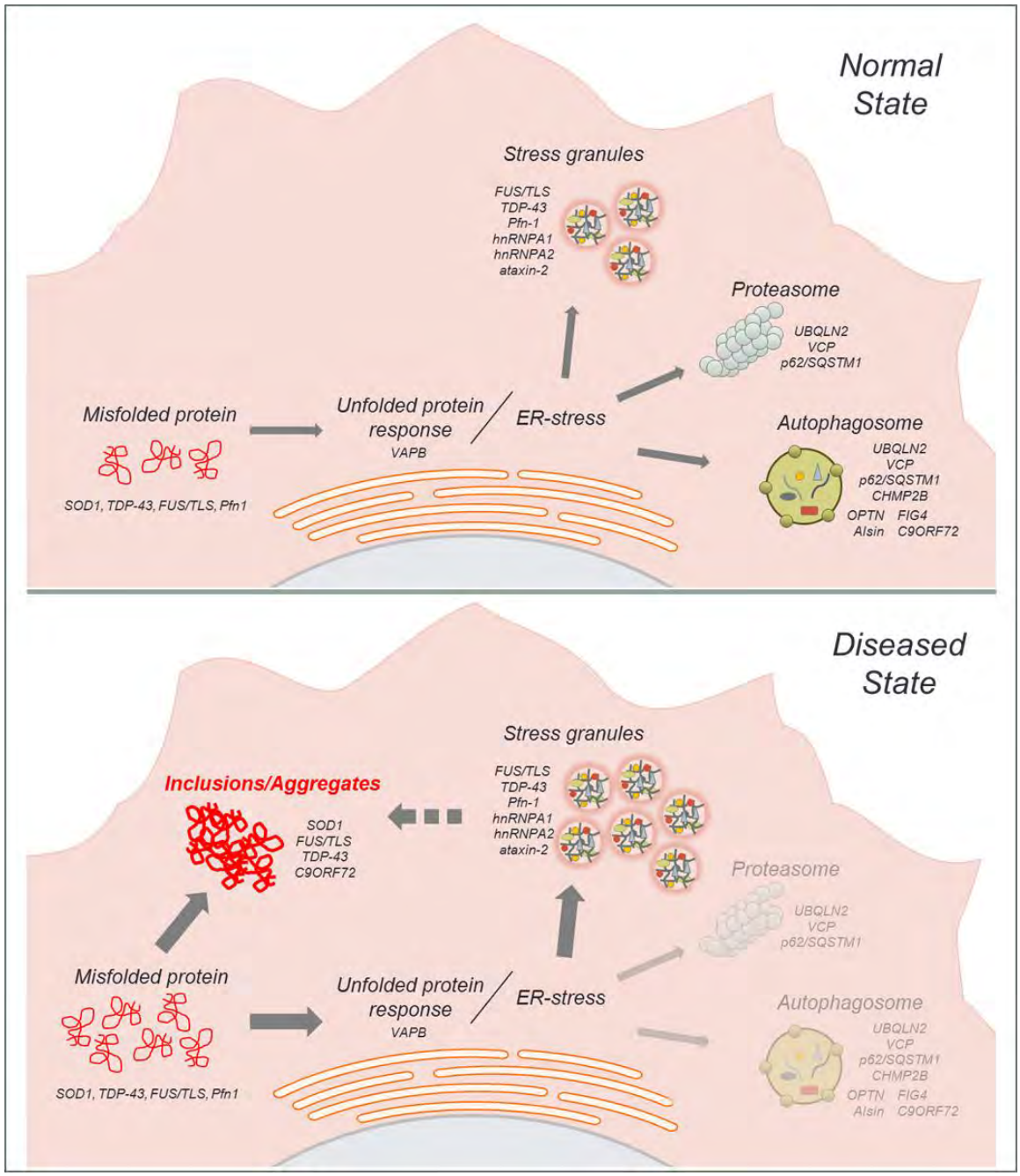
Normal State
Stress granules
FUS/TLS
TDP-43
Pfn-1
hnRNPA1
hnRNPA2
ataxin-2
Proteasome
UBQLN2
VCP
p62/SQSTM1
Misfolded protein
SOD1, TDP-43, FUS/TLS, Pfn1
Unfolded protein response
VAPB
ER-stress
Autophagosome
UBQLN2
VCP
p62/SQSTM1
CHMP2B
OPTN FIG4
Alsin C9ORF72
Diseased State
Stress granules
FUS/TLS
TDP-43
Pfn-1
hnRNPA1
hnRNPA2
ataxin-2
Inclusions/Aggregates
SOD1
FUS/TLS
TDP-43
C9ORF72
Proteasome
UBQLN2
VCP
p62/SQSTM1
Misfolded protein
SOD1, TDP-43, FUS/TLS, Pfn1
Unfolded protein response
VAPB
ER-stress
Autophagosome
UBQLN2
VCP
p62/SQSTM1
CHMP2B
OPTN FIG4
Alsin C9ORF72

Figure IV-1. A model of ALS pathogenesis. The normal cellular response to naturally occurring protein misfolding is the initiation of the unfolded protein response, resulting in the formation of stress granules for translation inhibition, and the upregulation of protein degradation machinery, such as the proteasome and autophagosome (*top*). In a diseased state, the balance between these systems may be altered. Mutations in various proteins could lead to higher levels of misfolded protein and aggregates, increased levels of ER-stress, accumulation and improper function of stress granules, and inefficient protein degradation by autophagy and the proteasome, which are already known to be less efficient with age. Over time the cell reaches a threshold of stress at which it can no longer survive, culminating in neuronal loss and disease onset.

PREFACE TO APPENDIX I:

All of the work presented in this appendix was performed by Catherine L. Ward.

APPENDIX I: INVESTIGATING A ROLE FOR FUS/TLS IN SUPPRESSION OF NEURONAL CELL CYCLE REINITIATION

The Cell Cycle

The cell cycle is a vital process that is fundamental to all life. It is crucial during development and for the replenishment of cells that have undergone apoptosis. The cell cycle is composed of two main stages: interphase and mitosis. Interphase is broken up into three phases, Growth1 (G1), S-phase, and Growth 2 (G2) which each play specific roles in preparing the cell for mitosis. During G1, the cell grows in size and produces the proteins and nucleic acids necessary for undergoing DNA replication, which occurs during S-phase. After S-phase is complete and the cell contains two copies of DNA, the cell enters G2 where it rapidly grows in size and increases protein synthesis. After G2, the cell undergoes mitosis and it divides into two daughter cells, with each containing one copy of DNA (reviewed in (Vermeulen et al., 2003)).

Cell cycle progression. Progression through each stage of the cell cycle is regulated by the interactions of several specific proteins: cyclins and cyclin-dependent kinases. As their name implies, levels of cyclins fluctuate, correlating with specific phases of the cell cycle. Cyclin E for example, increases throughout G1, is highest during the G1-S transition and decreases throughout S phase. Cyclin A, on the other hand, increases during S-phase and reaches its peak

during G2. Regulating the levels of cyclins is important as these proteins are required during specific cellular stages for the function of cyclin-dependent kinases (CDKs). Cyclin D1 for example, starts being expressed in G1 and forms a complex with cyclin-dependent kinases 4 (CDK4), which is turn phosphorylates retinoblastoma, allowing for the transcription of genes required for S-phase. As a complex, cyclins are the regulatory subunits while CDKs are the catalytic subunits, inactive until bound to their corresponding cyclin.

In addition to cyclins and cyclin-dependent kinases which promote cell cycle progression, there are additional proteins that inhibit cell cycle progression. There are two families of inhibitory proteins: the cip/kip (CDK interacting protein/kinase inhibitory protein) and the INK4a/ARF (inhibitor of kinase 4/alternative reading frame) families. As their name implies, the INK4a/ARF family inhibits the activity of CDK4, arresting the cell cycle in G1. The cip/kip family on the other hand, is active throughout the entire cell cycle, inhibiting the activity of numerous cyclin/CDK complexes (reviewed in (Vermeulen et al., 2003)).

Checkpoints: maintaining DNA integrity. Throughout the cell cycle, several quality control checkpoints exist to ensure DNA integrity is maintained before the cell progresses to the next phase. Before leaving S-phase, DNA is assessed to ensure complete replication and in mitosis there is a checkpoint to ensure spindles are formed properly before the two sets of DNA are separated. The

two growth phases, G1 and G2, each contain a checkpoint to determine whether any DNA damage has occurred prior to allowing the cell entry into S-phase or mitosis, respectively, where the integrity of DNA is crucial. If any abnormalities are discovered during these checkpoints, the cell cycle will arrest until the error has been corrected. Cell cycle arrest is achieved by the rapid induction of inhibitors and signaling cascades which ultimately shut down expression of proteins required for cell cycle progression (reviewed in (Vermeulen et al., 2003)).

FUS and cell cycle regulation. Several pieces of literature exist demonstrating a role for FUS in cell cycle regulation. Presented here in Chapter III, in response to FUS knockdown, proliferation of NSC-34 cells was reduced and could be recovered with FUS re-expression, demonstrating a direct correlation between FUS levels and cell proliferation status. The expression of several proteins associated with cellular proliferation was also altered upon FUS knockdown. That a previous study demonstrated an enriched binding of FUS to mRNAs encoding for cell cycle related proteins (Colombrita et al., 2012) suggests FUS affects cellular proliferation through its role in RNA processing. In support of this, a study in RAW264.7 macrophage cells showed that FUS is recruited to the promoter of cyclin D1 in response to ionizing radiation and inhibits its expression (Wang et al., 2008). This finding is an example of how FUS may be important for cell cycle arrest after the induction of DNA damage. This study further

demonstrated that knockdown of FUS in RAW264.7 cells resulted in an increase in cyclin D1 mRNA expression (Wang et al., 2008); a finding which was reproduced in our lab at both the mRNA **(Figure AI-1A)** and protein level **(Figure AI-1B,C)**. While appropriate experiments were not performed to test this, this increase in cyclin D1 expression would suggest active cell proliferation in the absence of FUS, whereas in NSC-34 cells, knockdown of FUS caused a defect in cell proliferation (Chapter III). This could be suggestive of FUS having a bi-directional role in cell cycle regulation; normally FUS promotes cell cycle progression whereas under conditions of cell stress, FUS promotes cell cycle arrest.

Two other studies have suggested a role for FUS in cell cycle regulation, specifically in terms of androgen stimulated proliferation of prostate cancer cells. In a study by Haile et al., a four day knockdown of FUS in prostate cancer cells reduced cellular proliferation stimulated by androgen (Haile et al., 2011). In contrast however, Brooke et al. show that a three day knockdown of FUS increased androgen-dependent cell cycle progression (Brooke et al., 2010). Moreover, they show FUS promotes cell cycle arrest by reducing levels of CDK6 and cyclin D1 and by increasing inhibitors of proliferation, such as the CDK inhibitor, p27 (Haile et al., 2011). The discrepancy between these two studies has not been explained. Together however, in addition to the study by Wang et al. and the work presented in Chapter III, it is evident that FUS may have important functions in controlling proper activity of the cell cycle.

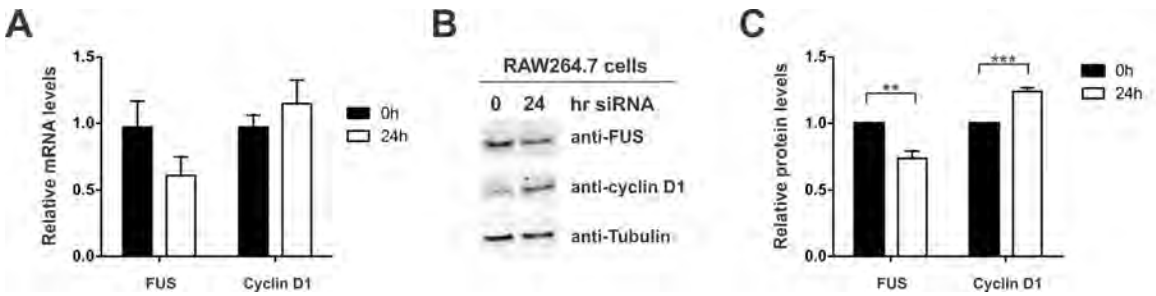

Figure AI-1. Knockdown of FUS causes an increase in cyclin D1 expression in RAW264.7 macrophage cells. RAW264.7 macrophage cells were transfected with 20pmol of siRNA specific for FUS. (**A)** Twenty-four hours post-transfection, RNA was harvested and levels of FUS and cyclin D1 mRNA were measured by qRT-PCR. Data shown is the average of two independent experiments run in technical quadruplicate ± standard error. (**B**) Representative western blot of the indicated cell lysates demonstrating increased expression of cyclin D1 after knockdown of FUS. Tubulin serves as a loading control. (**C**) Western blot densitometry analysis demonstrating a decrease in FUS expression at 24h of siRNA transfection with a concomitant increase in cyclin D1. Data shown is the average of four independent experiments ± standard error. Statistical significance was determined by a student's t-test (***P* <0.01; ****P* <0.001).

The post-mitotic neuron

Neurons are specialized cell types that differ from non-neuronal cells in a number of ways. One characteristic that sets them apart is their post-mitotic status. During development and neuronal differentiation, neurons exit the cell cycle and enter a phase called G_0 (Herrup and Yang, 2007). Very little is known about how neurons exit the cell cycle after development, but accumulating evidence suggests keeping the cell cycle suppressed is essential for neuronal health and viability.

Cell cycle re-initiation and neurodegeneration. It is widely established that neurons do not proceed through the cell cycle once the developmental process is complete and neurons are considered matured. Cell cycle proteins are almost undetectable in adult neurons and machinery for DNA replication is non-existent. However, accumulating evidence demonstrates that neuronal tissue from various neurodegenerative disease cases have elevated levels of numerous cell cycle proteins (Herrup and Yang, 2007). This is suggestive of loss of neuronal cell cycle control in late onset neurodegeneration. For instance, in patient tissue from Alzheimer's disease (AD), re-expression of several cell cycle proteins has been observed including, cyclin A, B, D, and E, as well as CDKs, CKD inhibitors, and the proliferating cell nuclear antigen protein (PCNA) indicative of S-phase (reviewed in (Herrup and Yang, 2007)). Furthermore, these proteins were only expressed in neuron types susceptible in AD and were present before any signs

of classic AD pathology, such as amyloid β deposition (reviewed in (Bonda et al., 2010a; Herrup, 2012)). There have also been reports of cell cycle protein re-expression in other neurological conditions including, ataxia telangiectasia, Parkinson's disease, stroke, and ALS (Herrup and Yang, 2007). In ALS mice and patient tissue, evidence of increased cyclin D and CDK4 expression has been noted in motor neurons, the cell type susceptible in ALS (Nguyen et al., 2003; Ranganathan and Bowser, 2003). That the cyclin D/CDK4 complex is responsible for reinitiating the cell cycle in cells maintaining a resting G_0 state (Sherr, 1994) it follows that cell cycle reinitiation could be occurring in ALS motor neurons. Interestingly, experimental expression of cell cycle proteins in neurons initiates apoptosis, further supporting a link between these two events.

Conclusion

While cell cycle reinitiation is an interesting model for neurodegeneration-associated neuronal death, the hypothesis is still in its early stages and is not currently a widely accepted model. Furthermore, it is not certain whether this reinitiation is an upstream event, or a downstream event occurring as an early stage of apoptosis. As several reports have demonstrated a role for FUS in maintaining cyclin D1 levels and regulating cellular proliferation, one could speculate that FUS may also play a role in suppressing the cell cycle in neurons. Thus, the nuclear depletion of FUS by ALS-linked mutations, could potentially lead to expression of cyclin D1 and an aberrant cell cycle reinitiation. To date,

the regulation of *CCND1* by FUS has only been demonstrated in macrophage cells (Wang et al., 2008) and prostate cancer cells (Brooke et al., 2010; Haile et al., 2011), and remains to be investigated in neurons. Further studies of the role of FUS in neuronal gene expression are necessary for concluding whether FUS plays a role in cell cycle-related neuronal death.

PREFACE TO APPENDIX II:

The following chapter is a manuscript published in the Journal of Cellular Physiology (Publisher: John Wiley and Sons; License #3397800087634).

My contributions to this manuscript included intellectual input, experimental design strategies, and the establishment of the cell viability protocol (MTT assay) used herein. Additionally, I performed preliminary MTT assays and aided in the analysis of MTT assay results and provided reagents and consulting for the culture of NSC-34 cells stably expressing inducible shRNA.

ORIGINAL RESEARCH ARTICLE

2222

Journal of Cellular Physiology

FUS/TLS Assembles Into Stress Granules and Is a Prosurvival Factor During Hyperosmolar Stress

REDDY RANJITH K. SAMA,[1] CATHERINE L. WARD,[1] LAURA J. KAUSHANSKY,[1] NATHAN LEMAY,[1] SHINSUKE ISHIGAKI,[2] FUMIHIKO URANO,[3] AND DARYL A. BOSCO[1,4]*

[1]*Department of Neurology, University of Massachusetts Medical School, Worcester, Massachusetts*

[2]*Department of Neurology, Center for Neurological Diseases and Cancer, Nagoya University Graduate School of Medicine, Nagoya, Japan*

[3]*Division of Endocrinology, Metabolism and Lipid Research, Department of Medicine and Department of Pathology and Immunology, Washington University School of Medicine, St. Louis, Missouri*

[4]*Department of Biochemistry and Molecular Pharmacology, University of Massachusetts Medical School, Worcester, Massachusetts*

FUsed in Sarcoma/Translocated in LipoSarcoma (FUS/TLS or FUS) has been linked to several biological processes involving DNA and RNA processing, and has been associated with multiple diseases, including myxoid liposarcoma and amyotrophic lateral sclerosis (ALS). ALS-associated mutations cause FUS to associate with stalled translational complexes called stress granules under conditions of stress. However, little is known regarding the normal role of endogenous (non-disease linked) FUS in cellular stress response. Here, we demonstrate that endogenous FUS exerts a robust response to hyperosmolar stress induced by sorbitol. Hyperosmolar stress causes an immediate re-distribution of nuclear FUS to the cytoplasm, where it incorporates into stress granules. The redistribution of FUS to the cytoplasm is modulated by methyltransferase activity, whereas the inhibition of methyltransferase activity does not affect the incorporation of FUS into stress granules. The response to hyperosmolar stress is specific, since endogenous FUS does not redistribute to the cytoplasm in response to sodium arsenite, hydrogen peroxide, thapsigargin, or heat shock, all of which induce stress granule assembly. Intriguingly, cells with reduced expression of FUS exhibit a loss of cell viability in response to sorbitol, indicating a prosurvival role for endogenous FUS in the cellular response to hyperosmolar stress.

J. Cell. Physiol. 228: 2222–2231, 2013.

Fused in sarcoma/translocated in liposarcoma (FUS/TLS or FUS) is an RNA/DNA-binding protein that is implicated in a diverse array of cellular processes. FUS, also known as heterogeneous ribonuclear protein hnRNP P2 (Calvio et al., 1995), is a member of the TET family of proteins that also includes EWS (Ewing's sarcoma) and TAF15 (TATA-binding protein-associated factor 15) (Tan and Manley, 2009). FUS was originally discovered in the context of a fusion oncoprotein in myxoid liposarcoma cells (Crozat et al., 1993). Since then, this multifunctional protein has been linked to various aspects of RNA and DNA-processing, including mRNA splicing (Ishigaki et al., 2012), transcription (Wang et al., 2008), and DNA repair (Kuroda et al., 2000). Recently, mutations in FUS have been linked to the fatal neurodegenerative disease amyotrophic lateral sclerosis (ALS; Kwiatkowski et al., 2009; Vance et al., 2009).

FUS is predominately expressed in the nucleus of most cells (Andersson et al., 2008), although it shuttles between the nucleus and cytoplasm during mRNA transport (Zinszner et al., 1997; Fujii and Takumi, 2005). Several reports have shown that ALS-linked FUS mutants associate with cytoplasmic stress granules under conditions of oxidative stress and heat shock (Bosco et al., 2010; Dormann et al., 2010; Gal et al., 2010). Stress granules are stalled translational complexes comprised of mRNA, ribosomes, and RNA-binding proteins that form in response to induced stress, such as hyperosmolar stress, oxidative stress, heat shock, ultraviolet irradiation and viral infection (Anderson and Kedersha, 2009). These dynamic complexes are thought to play a role in sorting mRNAs for expression, storage or degradation (Kedersha and Anderson, 2002). More recently, stress granules have also been shown to directly regulate protein activity in the context of

Author contributions: R.R.K.S., C.L.W., L.J.K., and D.A.B. designed the experiments and analyzed the data; R.R.K.S., C.L.W., L.J.K., and N.L. performed the experiments. S.I. and F.U. constructed the inducible FUS knock-down NSC-34 cells; R.R.K.S. and D.A.B. wrote the manuscript. All authors approved the manuscript.

Contract grant sponsor: Worcester Foundation (DAB).
Contract grant sponsor: US National Institutes of Health/National Institute on Neurological Disorders and Stroke;
Contract grant number: R01NS078145-01.

*Correspondence to: Daryl Bosco, Department of Neurology, Albert Sherman Center, AS6-1057, 368 Plantation Dr., Worcester, MA 01605. E-mail: daryl.bosco@umassmed.edu

Manuscript Received 13 April 2013
Manuscript Accepted 17 April 2013

Accepted manuscript online in Wiley Online Library (wileyonlinelibrary.com): 27 April 2013.
DOI: 10.1002/jcp.24395

cellular signaling (Wippich et al., 2013). In contrast to the aforementioned mutant FUS, much less is known about the association of endogenous FUS with stress granules and the role of endogenous FUS in stress response.

Herein, we sought to examine the response of endogenous FUS to various cellular stressors. We found that inducers of stress granule assembly shown to direct mutant-FUS to stress granules, such as sodium arsenite, thapsigargin, hydrogen peroxide, and heat shock, had no effect on the subcellular distribution of endogenous FUS. In striking contrast, endogenous FUS exhibited a robust redistribution from the nucleus to the cytoplasm and assembled into stress granules under conditions of hyperosmolar stress induced by sorbitol and sucrose. Not only was the response of FUS stress-specific, it was also regulated by methyltransferase activity. Cells with reduced FUS expression were more susceptible to sorbitol-induced toxicity, suggesting that FUS plays protective role with regard to cellular homeostasis. These data establish a novel role for the multifunctional FUS protein in cellular stress response.

Materials and Methods

Cell culture and induced stress

HeLa cells and HEK293 cells were cultured in minimal essential medium (MEM, Gibco, Grand Island, NY) supplemented with 10% fetal bovine serum (FBS, Sigma, St. Louis, MO) and 1% penicillin and streptomycin (P/S, Gibco) under standard culture conditions (37°C, 5% CO_2/95% air). NSC-34 cells and mouse embryonic fibroblasts (MEFs) were cultured in Dulbecco's MEM (DMEM, Gibco) supplemented with 10% FBS and 1% P/S under standard culture conditions. FlpIn HEK293 cells with stably integrated GFP-FUS G515X were cultured as described previously (Bosco et al., 2010). Sorbitol (Sigma) was dissolved directly into the media to obtain a concentration of 0.4 M and added to the cells (Kedersha and Anderson, 2007). Sucrose (Electron Microscopy Sciences, Fort Washington, PA) was dissolved into media to obtain a final concentration of 600 osmol/L and added to the cells (Bevilacqua et al., 2010). Stock solutions of 100 mM sodium arsenite (Sigma) in DMSO (Sigma), 10 mM thapsigargin (Sigma) in DMSO, 1 M hydrogen peroxide (Sigma) in media, 30 mM emetine (Sigma) in water and 20 mM Adenosine-2′,3′-dialdehyde (AdOx, Sigma) in water were prepared and added to the media to obtain the final concentrations of 0.5 mM, 50 μM, 1.5 mM, 50 μg/ml, and 50 μM, respectively. Doxycycline (Sigma) was used at a final concentration of 1 μg/ml from a stock of 50 mg/ml prepared in water. Cells were exposed to heat shock by adding media, pre-warmed to 43°C, followed by immediate transfer to an incubator set to 43°C. ON-TARGETplus SMARTpool (Dharmacon, Waltham, MA) consisting of a pool of siRNAs against FUS (Cat # L-009497-00-0005) and ON-TARGETplus non-targeting pool siRNA (Cat # D-001810-10-05) as control were transfected using Lipofectamine-2000 (Invitrogen, Grand Island, NY) according to the manufacturer's instructions.

NSC-34 cell lines were a kind gift from Dr. Neil Cashman (University of British Columbia). Stable NSC-34 cell lines expressing short hairpin (sh) RNA against mouse FUS (shFUS) or non-targeting scrambled RNA (shSC) were prepared by first transducing with the Tet repressor. A single clone that demonstrated good induction without any leaky expression was then selected. NSC34-TetR cells were then transduced with inducible lentivirus-Tet-on/shFUS or Tet-on/shSC (Ishigaki et al., 2012). Cells were treated with 1 μg/ml doxycycline to induce the expression of the shRNAs.

Immunofluorescence

Immunofluorescence was performed as described in (Bosco et al., 2010). Primary antibody incubation conditions were as follows: 1:500–1,000 rabbit anti-FUS (A300-293A, Bethyl Labs, Montgomery, TX); 1:2,500 mouse anti-TIAR (610352, BD Transduction Labs, San Jose, CA); 1:1,500 rabbit ant-ASYM24 (07-414, Millipore, Billerica, MA); 1:2,500 mouse anti-G3BP (611126, BD Transduction Labs) for 1 h at room temperature; and 1:250 mouse anti-GE-1/hedls/p70 S6 kinase (sc-8418, Santa Cruz Biotechnology, Santa Cruz, CA) for 12 h at 4°C. Secondary anti-mouse IgG antibody conjugated to Dylight 549 (715-505-151, Jackson ImmunoResearch Labs, West Grove, PA) was used at 1:1,500–1:3,000. Secondary anti-rabbit IgG antibody conjugated to Dylight 488 (711-485-152, Jackson ImmunoResearch Labs) and secondary anti-rabbit IgG antibody conjugated to Cy5 (711-175-152, Jackson ImmunoResearch Labs) were used at 1:1,500–1:3,000. GFP signal was enhanced using 1:2,000 Alexa Fluor 488-conjugated rabbit anti-GFP (A21311, Invitrogen). Nuclei were stained with 50 nM 4′,6′-diamidine-2-phenylindole dihydrochloride (DAPI; D1306, Invitrogen) for 5 min at room temperature. Coverslips were mounted with ProLong Gold Antifade Reagent (P36930, Invitrogen).

Image acquisition and quantification

Fixed cell images were acquired using a Solamere Technology Group CSU10B (Salt Lake City, UT) spinning disk confocal system as described (Bosco et al., 2010) or using a Leica DMI6000B microscope (Leica Microsystems, Buffalo grove, IL). For images acquired with the Leica microscope, a 100× objective was used with LAS AF One Software (Leica Microsystems) and the Leica DFC365FX camera. Maximum projection images were created from acquired image stacks ($z = 0.2$–0.25 μm, $n = 6$–44 planes) and analyzed using NIH Image J software.

For quantifying the percentage (%) of nuclear FUS, image stacks ($z = 0.2$ μm, $n = 13$ planes) of 60 cells were collected from $n = 3$ experiments with the spinning disk confocal system above. Images were analyzed using MetaMorph software (Molecular Devices, Sunnyvale, CA). Sum projections of each image stack were created after subtracting the background signal as described (Bosco et al., 2010). The integrated morphometry analysis tool was used to calculate the percent (%) nuclear FUS. Statistical significance between conditions was determined by an ANOVA and Tukey's post hoc pairwise test.

Western blots

Western blots were performed essentially as described in (Bosco et al., 2010). Briefly, blots were incubated at 4°C with shaking overnight in the presence of primary antibodies as per the following dilutions: 1:500 anti-tubulin (Sigma), 1:500 anti-FUS (in house antibody created against 264–284 peptide sequence of FUS, Genscript, Piscataway, NJ), 1:500 anti-FUS (47711, Santacruz, Santa Cruz, CA) and 1:1,000 anti-ASYM24 (07–414, Millipore). Densitometry was performed using the Odyssey infrared imaging systems software (Licor Biosciences, Lincoln, NE).

Immunoprecipitation

Cells resuspended in 50 mM Tris–HCl (pH 7.5) supplemented with 1% NP-40, 150 mM NaCl, 5 mM EDTA, 10% glycerol and complete protease inhibitor (lysis buffer) were briefly sonicated and incubated at 4°C with shaking for 30 min. The lysates were centrifuged for 15 min at 13,000 rpm and 4°C. Pre-clearing of the supernatants was achieved by incubation with 100 μl of Biomag Protein G beads (Invitrogen) at 4°C with shaking for 2 h. The beads were removed with a magnet and the protein concentration of the supernatant was determined using a bicinchoninic assay (ThermoScientific, Billerica, MA). Anti-FUS (Genscript) or anti-GFP antibody (ab290, Abcam, Cambridge, MA) was bound to fresh beads with shaking for 2 h at 4°C. A total of 1 mg of the pre-cleared supernatant was then added to 100 μl of antibody-bound beads

and incubated overnight with shaking at 4°C. The lysate was removed and beads were washed three times with lysis buffer. Proteins bound to the beads were eluted with 1X SDS sample buffer at 95°C for 5 min, and probed by western as described above.

Cell toxicity assays

NSC-34 cell lines shSC and shFUS were plated in 24 well dishes. 48 h after induction with doxycyline, cells were treated with 0.4 M sorbitol or 0.25 mM sodium arsenite for 8 h. For the MTT (3-[4,5-dimethylthiazol-2-yl]-2,5-diphenyl tetrazolium bromide) assay 100 μl of 5 mg/ml MTT (Invitrogen) was added to the wells for 35 min followed by cell lysis overnight with 300 μl lysis buffer (10% SDS in 1:1 *N,N*-dimethylformamide:water/2% acetic acid/2.5% HCl 1 M) and absorbance measurement at 550 nm using the VICTOR V plate reader (Perkin Elmer, Waltham, MA). Cell viability for each sample was calculated using the formula: % viability = $100 \times (OD_{sample} - OD_{blank})/(OD_{untreated} - OD_{blank})$. Lactate dehyrodenase (LDH) assay was performed as per manufacturer's protocol (CytoTox 96 Non-radioactive Cytotoxicity Assay, Promega, Madison, WI). After the 8 h treatment, 50 μl of media from each well was transferred to wells of 96 well plate. 50 μl of substrate mix was then added to each well and the plates were covered and incubated at ambient temperature, protected from light for 30 min. After the incubation, 50 μl stop solution was added to each well and absorbance was recorded at 490 nm using the above plate reader. Percentage (%) cytotoxicity was determined for each experimental condition (Expt) using the formula: % cytotoxicity = $100 \times (OD_{expt} - OD_{untreated})/(OD_{max} - OD_{untreated})$, where OD_{max} represents the absorbance of the media from a well with complete lysis of cells releasing maximum LDH. All assays were performed at least three independent times. Statistical significance was determined by a two-tailed Student's *t*-test.

Results

Endogenous FUS redistributes to the cytoplasm and assembles into stress granules in response to hyperosmolar stress

In order to investigate the role of FUS in stress response, we examined the nucleo-cytoplasmic distribution of FUS in response to various cellular stressors. Hyperosmolar stress induced by the administration of 0.4 M sorbitol to HeLa cells for 1 h resulted in a striking redistribution of FUS from the nucleus to the cytoplasm, where FUS assembled into numerous puncta. A majority of FUS-positive puncta co-localized with the stress granule marker proteins, G3BP (Fig. 1A; supplementary material Movie M1) and TIAR (Fig. 1B; supplementary material Movie M2; Kedersha and Anderson, 2007). The redistribution and incorporation of FUS into stress granules in response to sorbitol is reminiscent of other nuclear hnRNPs, such as hnRNP A1 (Guil et al., 2006) and TDP-43 (Dewey et al., 2011). However, not all hnRNP proteins redistribute to stress granules in response to sorbitol (van der Houven van Oordt et al., 2000), suggesting a functional role in stress response for those hnRNPs that do localize to these structures. In addition to sorbitol, hyperosmolar stress induced by sucrose also caused FUS to redistribute to the cytoplasm and incorporate into stress granules (supplementary Fig. S1).

Since stress granules are functionally related to processing bodies (P-bodies), which are cellular sites of mRNA degradation (Moore, 2005), we also probed for the co-localization of endogenous FUS with GE-1/hedls, a constituent of P-bodies but not stress granules (Kedersha and Anderson, 2007). The majority of P-bodies did not co-localize with FUS-positive granules. However, some P-bodies appeared to associate with and/or dock onto FUS-positive granules (Fig. 1C; supplementary material Movie M3), consistent with the physical association between P-bodies and stress granules that has been previously described (Kedersha et al., 2005; Bosco et al., 2010).

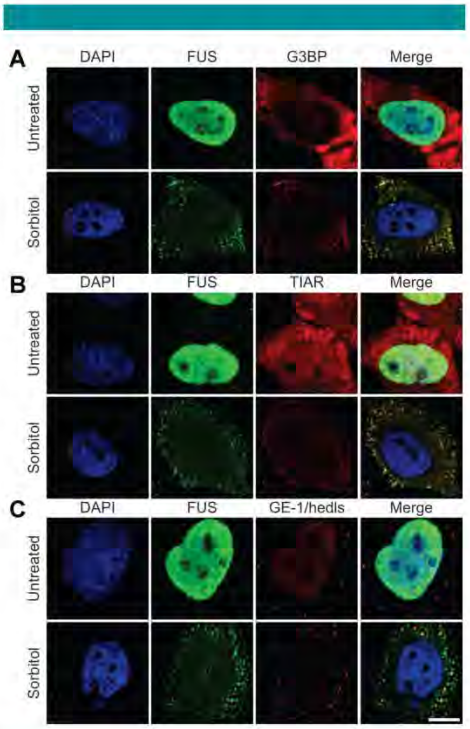

Fig. 1. Endogenous FUS redistributes to the cytoplasm and localizes to cytoplasmic stress granules in response to sorbitol. Confocal images of untreated HeLa cells (top row in each panel) as compared to cells treated with 0.4 M sorbitol for 1 h (bottom row in each panel; A–C) are shown. Cells probed with an anti-FUS antibody (green) and either the stress granule marker anti-G3BP (A) or anti-TIAR (B) revealed that FUS co-localizes with stress granules in response to sorbitol (see also supplementary material Movies M1 and M2). C: P-bodies were detected by anti-GE-1/hedls antibody in both untreated and treated conditions; however, the majority of P-bodies did not exhibit co-localization with FUS (see also supplementary material Movie M3). Cells were counter stained with the nuclear marker DAPI (blue; A–C). Images are representative of at least n = 3 experiments. Scale bar represents 10 μm.

Next, we investigated the effect of sorbitol in other cell lines. Administration of sorbitol to HEK (human embryonic kidney)-293T, MEFs, and NSC-34 (neuroblastoma × spinal cord hybrid; Cashman et al., 1992) cell lines recapitulated the results from HeLa cells; FUS redistributed from the nucleus to the cytoplasm, where it assembled into G3BP- and TIAR-positive stress granules (supplementary material Fig. S2). Therefore, the response of FUS to hyperosmolar stress is not a cell type-specific phenomenon, but rather is detected in several different mammalian cell lines.

In contrast to sorbitol and sucrose, FUS did not redistribute to the cytoplasm when HeLa cells were exposed to inducers of oxidative stress (e.g., sodium arsenite and hydrogen peroxide), endoplasmic reticulum (ER) stress (e.g., thapsigargin) or heat shock, all of which induce the formation of stress granules in a majority of cells (Fig. 2; Kedersha and Anderson, 2007; Emara et al., 2012). Endogenous FUS was not detected in any of the G3BP-positive stress granules that formed under these conditions; we did not detect any cells with elevated cytoplasmic FUS or FUS-positive stress granules under these conditions. Similarly, exogenously expressed wild-type FUS did not redistribute nor assemble into stress granules under the aforementioned conditions (Bosco et al., 2010; Dormann et al., 2010; Bentmann et al., 2012; Daigle et al., 2013), although the effect of sorbitol on endogenous or exogenous FUS has not been reported. Thus our results demonstrate that the formation of stress granules by various stressors is not sufficient to cause a redistribution of FUS to the cytoplasm, indicating that there are specific factors associated with hyperosmolar stress that elicit this response for endogenous FUS.

The assembly of FUS into stress granules is rapid and reversible

The formation of stress granules represents a fast, almost immediate, response of cells to induced stress. To determine the time frame in which FUS responds to sorbitol, we monitored the cellular redistribution of FUS by immunofluorescence microscopy over a 1 h time course of sorbitol exposure. G3BP is an effector of stress granule assembly (Tourriere et al., 2003; Aulas et al., 2012) and was therefore used as a marker to monitor the assembly process. The cytoplasmic redistribution of FUS was detected within 10 min of sorbitol treatment, a time point that preceded the appearance of discreet G3BP-positive cytoplasmic foci, demonstrating that FUS starts to accumulate in the cytoplasm before stress granules are fully formed (Fig. 3A). Within 20 min of sorbitol treatment, discreet G3BP-positive stress granules containing FUS were detected. Therefore FUS appears to incorporate into stress granules on the same time scale that

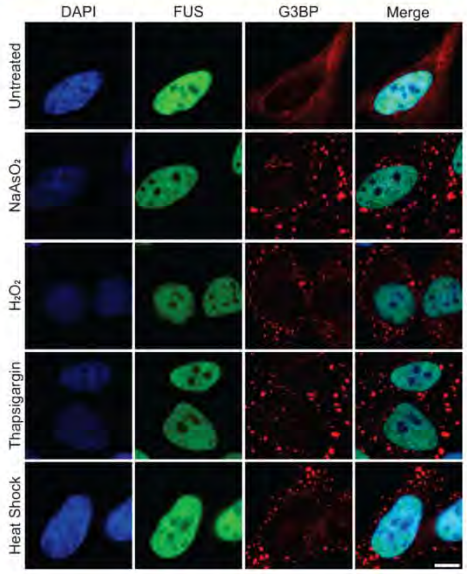

Fig. 2. The recruitment of FUS to cytoplasmic stress granules is stress-specific. HeLa cells were treated with either 0.5 mM sodium arsenite ($NaAsO_2$) for 1 h, 1.5 mM hydrogen peroxide (H_2O_2) for 2 h, 50 μM thapsigargin for 30 min, or heat shock at 43° C for 30 min. Immunofluorescence revealed that G3BP-positive stress granules (red) formed under all stress conditions. FUS (green) remained nuclear and absent from stress granules under these stress conditions, similar to the unstressed condition (top part). Nuclei were stained with DAPI (blue). All images are representative of n = 3 independent experiments. Scale bar represents 10 μm.

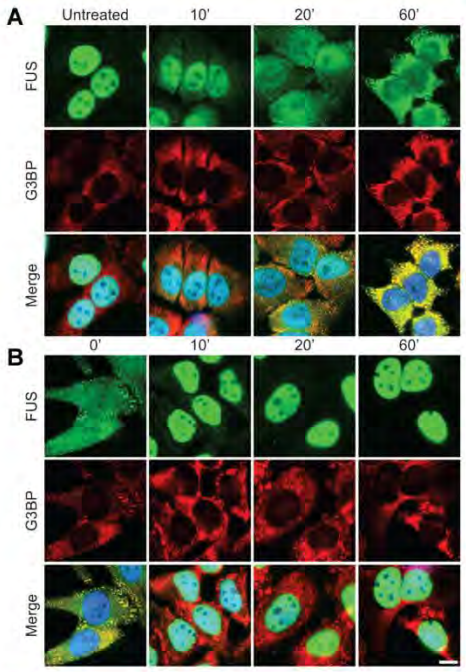

Fig. 3. The response of FUS to sorbitol is rapid and reversible. A: A representative time-course for the cytoplasmic redistribution of FUS into stress granules upon exposure to hyperosmolar stress. HeLa cells were treated with 0.4 M sorbitol for the indicated time points, fixed, and assessed by immunofluorescence with anti-FUS (green) and anti-G3BP (red) antibodies, and the nuclear marker DAPI (blue). Elevated levels of cytoplasmic FUS were detected as early as 10 min. FUS accumulated into discreet stress granules by 20 min. The nucleo-cytoplasmic distribution of FUS continued to shift towards the cytoplasm over the remaining time course. B: A representative time-course for the return of FUS to the nucleus and the concomitant disassembly of stress granules upon withdrawal of sorbitol. HeLa cells were treated with 0.4 M sorbitol for 1 h, after which the sorbitol was replaced with fresh media and the cells were processed as described in (A). A majority of FUS re-localized to the nucleus within 10 min. Some G3BP positive stress granules persisted for up to 1 h. Images are representative of at least n = 3 experiments. Scale bar represents 10 μm.

these foci are being formed. G3BP- and FUS-positive stress granules appear fully formed by 60 min, at which time a substantial fraction of FUS was redistributed to the cytoplasm.

The formation of stress granules is a reversible process (Anderson and Kedersha, 2008). After the induced stress is removed, stress granules disassemble as the cell re-establishes homeostasis. We monitored the disassembly of stress granules in HeLa cells pre-treated with sorbitol to determine the subcellular fate of FUS as cells re-established homeostasis. The disassembly of stress granules was initiated by replacing media containing sorbitol with fresh media lacking sorbitol, and cells were monitored for 60 min by immunofluorescence microscopy as described above. Within 10 min of removing sorbitol from the media, FUS dissociated from stress granules and redistributed to the nucleus in virtually all (~90%) cells. However, G3BP-positive, FUS-negative foci persisted in approximately one third of cells at this time point (Fig. 3B). For the remainder of the time course, FUS was localized to the nucleus while G3BP-positive stress granules gradually continued to disassemble until the 60 min time point, when ~20% of cells contained G3BP-positive stress granules. These data show that FUS exhibits a rapid response not only to the administration of sorbitol (Fig. 3A), but also to the removal of this stressor (Fig. 3B).

Stress granule assembly is required for robust cytoplasmic redistribution of FUS

FUS is a nucleo-cytoplasmic shuttling protein. Therefore, the accumulation of FUS in the cytoplasm can result from increased export of the protein from the nucleus and/or decreased import to the nucleus from the cytoplasm. The nucleo-cytoplasmic equilibrium of FUS may be shifted towards the cytoplasm through FUS binding interactions. For example, injection of anti-FUS antibodies into cells trapped the majority of FUS in the cytoplasm within 2 h (Zinszner et al., 1997). Since the timescale of FUS redistribution from the nucleus to the cytoplasm under conditions of hyperosmolar stress (1 h, Fig. 3) is similar to that in aforementioned antibody study (2 h, Zinszner et al., 1997), we asked whether or not stress granules serve as a "cytoplasmic sink" that effectively traps FUS in the cytoplasm through mass action. Stress granule assembly was inhibited by the addition of 50 μg/ml emetine, which stabilizes polysomes and blocks translation elongation (Kedersha et al., 2000), for 1 h prior to the administration of hyperosmolar stress. As expected, only diffuse G3BP signal (i.e., no G3BP-positive stress granules) was observed under these conditions (Fig. 4A). Interestingly, emetine treatment also markedly attenuated the cytoplasmic redistribution of FUS

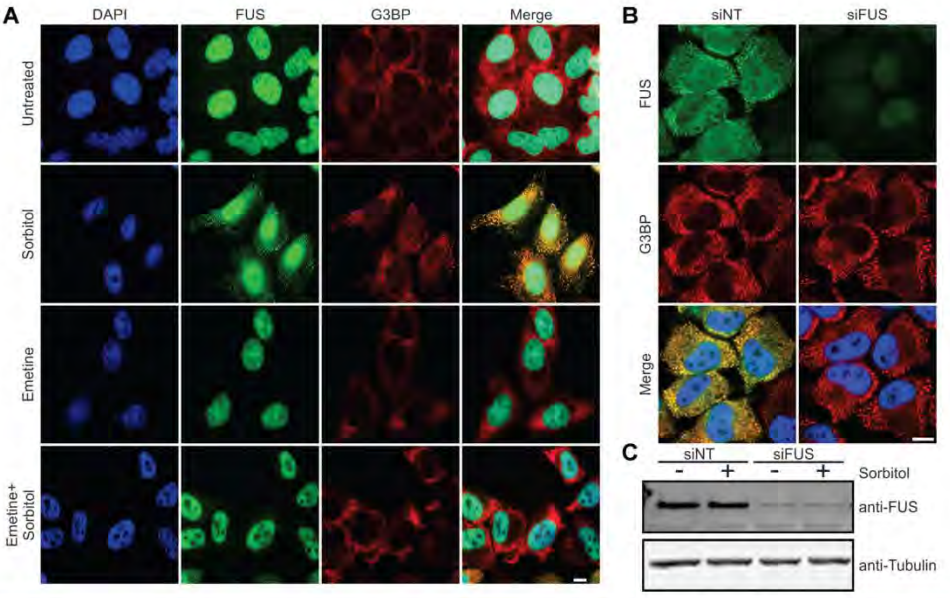

Fig. 4. An inhibitor of stress granule assembly prevents the cytoplasmic redistribution of FUS, though stress granules still assemble in the absence of FUS. A: HeLa cells were treated with 0.4 M sorbitol for 1 h, 50 μg/ml emetine for 1 h or pre-treated with emetine followed by sorbitol treatment. Cells were then fixed and probed by immunofluorescence for DAPI (blue), FUS (green), and G3BP (red). Emetine pre-treatment inhibited both stress granule assembly, as evidenced by the diffuse G3BP signal, and the cytoplasmic redistribution of FUS in the presence of sorbitol. B: HeLa cells were transfected with non-targeting siRNA (siNT) or siRNA against FUS (siFUS) for 48 h, subsequently treated with 0.4 M sorbitol for 1 h, and then processed for immunofluorescence as described above. Cells treated with either siFUS or siNT exhibited normal stress granule formation (B, red) in response to sorbitol, despite a significant reduction in FUS protein levels in siFUS treated cells as evidenced by immunofluorescence (green; B) and Western blot (C). All images are representative of at least n = 3 independent experiments. Scale bar represents 10 μm.

(Fig. 4A) in the presence of sorbitol. These data implicate stress granule formation as a requisite for the cytoplasmic redistribution of FUS, and suggest that the full response of FUS to hyperosmolar stress includes its assembly into stress granules.

Next we investigated the role of FUS in stress granule assembly under conditions of hyperosmolar stress. HeLa cells were first treated with either siRNA specific for FUS or non-targeting siRNA as a control for 48 h, and were then exposed to 0.4 M sorbitol for 30 min to induce the formation of stress granules (Fig. 4B). Although cells treated with FUS siRNA exhibited a ~90% reduction in FUS protein levels (Fig. 4C), these cells produced G3BP-positive stress granules in response to sorbitol that were indistinguishable from control cells (Fig. 4B). While the physical response of FUS to hyperosmolar stress depends on the stress granule assembly pathway (Fig. 4A), FUS does not appear to dictate the ability of stress granules to form.

Methylation regulates the nucleo-cytoplasmic distribution of FUS under hyperosmolar stress

Next we investigated the mechanisms by which FUS relocalizes to the cytoplasm and incorporates into stress granules in response to hyperosmolar stress. Methylation of arginine residues is a post-translational modification that modulates the nucleo-cytoplasmic distribution of hnRNP proteins, such as the cold-inducible RNA-binding protein (CIRP; De Leeuw et al., 2007). Some reports implicate a link between the arginine methylation status of ALS-linked FUS and its subcellular localization (Tradewell et al., 2012; Yamaguchi and Kitajo, 2012). In fact, mass spectrometry analyses demonstrate that up to 20 arginine residues are asymmetrically dimethylated in FUS (Rappsilber et al., 2003). That protein arginine *N*-methyltransferase-1 (PRMT1), which accounts for ~85% of arginine methylation in the cell (Bedford and Clarke, 2009), and FUS interact suggests that the methylation of FUS is catalyzed by PRMT1 (Du et al., 2011; Tradewell et al., 2012; Yamaguchi and Kitajo, 2012). Interestingly, stress granules contain arginine methylated hnRNP proteins, raising the possibility that this post-translational modification influences stress granule dynamics (Xie and Denman, 2011). This notion is supported by an attenuation of fragile X mental retardation protein (FMRP) in stress granules upon exposure to adenosine-2′, 3′-dialdehyde (AdOx) (Dolzhanskaya et al., 2006), a general inhibitor of methyltransferases (O'Dea et al., 1987).

To determine whether or not the methylation status of FUS regulates its subcellular localization under conditions of hyperosmolar stress, we examined the nucleo-cytoplasmic distribution of FUS after treatment of HeLa cells with AdOx. FUS remained predominately nuclear in the presence of AdOx alone (data not shown). However, when cells were pre-treated with AdOx prior to sorbitol exposure, there was a significant effect on the nucleo-cytoplasmic partitioning of FUS compared to cells treated with sorbitol alone (Fig. 5A,B). While sorbitol treatment resulted in a ~50% reduction of nuclear FUS compared to control cells, pre-treatment with AdOx restored ~30% of FUS to the nucleus (Fig. 5B). To quantify the methylation status of the FUS protein itself, FUS was immunoprecipitated from untreated cells or from cells treated with AdOx in combination with sorbitol and probed for asymmetrically dimethylated arginine residues with the ASYM24 antibody (Tradewell et al., 2012). Arginine methylation of FUS in untreated cells was detected by ASYM24 (Fig. 5C), which is expected since FUS is reportedly arginine methylated under homeostatic conditions (Rappsilber et al., 2003). The level of methylated FUS was not significantly altered by the addition of sorbitol (data not shown). However, the arginine methylation status of FUS decreased by more than 50% in cells pre-treated with AdOx (data not shown) or AdOx in combination with sorbitol (Fig. 5C,D). Since AdOx is a general methyltransferase inhibitor, we cannot exclude the possibility that other methylation events influence the subcellular distribution of FUS in these experiments. Nonetheless, these data suggest that the methylation status of FUS must be maintained in order for it to redistribute to the cytoplasm under conditions of hyperosmolar stress, and are consistent with the notion that hypomethylated forms of FUS fail to shuttle out of the nucleus (Tradewell et al., 2012; Yamaguchi and Kitajo, 2012).

Next, we sought to determine if hypomethylated FUS could still assemble into stress granules. Since the assembly of FUS into stress granules occurs concomitantly with cytoplasmic accumulation (Fig. 3), it was necessary to first dissect these two processes. To this end, we transiently transfected HeLa cells with the GFP-tagged FUS 515X truncation construct, which lacks the nuclear localization signal (NLS) and is therefore retained in the cytoplasm under homeostatic conditions (Bosco et al., 2010). GFP-FUS 515X assembled into stress granules in response to 0.4 M sorbitol, and the extent of this association was the same whether cells were pre-treated with AdOx or not (Fig. 6A,B). The same outcome was observed in HEK-293 cells stably expressing GFP-FUS 515X (data not shown). In contrast to the GFP-FUS signal, there was a dramatic decrease in the ASYM24 signal in cells pre-treated with AdOx (Fig. 6A,B), indicating that pre-treatment with AdOx effectively inhibited methyltransferase activity within these cells. Immunoprecipitation with anti-GFP followed by western blot analysis with the ASYM24 antibody confirmed that GFP-FUS 515X was indeed hypomethylated due to AdOx pre-treatment (Fig. 6C). Thus, despite a large reduction in the methylation status of FUS in AdOx pre-treated cells (Figs. 5 and 6), FUS still robustly associated with stress granules. We note that a small fraction of FUS remained dimethylated in the AdOx condition (Fig. 6C), presumably FUS protein that was methylated prior to AdOx exposure but had not turned over during the course of the experiment (Xie and Denman, 2011). In the absence of commercially available antibodies that are specific for dimethylated FUS, we cannot exclude the possibility that stress granules contain some dimethylated FUS in these experiments. However, the dramatic decrease in ASYM24 signal is consistent with a reduced load of methylated proteins within stress granules, and therefore it is unlikely that all of the residual methylated FUS is sequestered into these structures. Together, these studies argue against a role for arginine methylation in regulating the incorporation of FUS in stress granules.

Cells are susceptible to sorbitol toxicity and death when FUS expression is reduced

Given that the full response of FUS to hyperosmolar stress includes its assembly into stress granules (Fig. 4), and that the role of stress granules is to overcome stress and re-establish cellular homeostasis, we investigated whether the expression of FUS is important for cellular viability under conditions of hyperosmolar stress. The normal cellular response to hyperosmolar stress includes cell cycle arrest, during which time cells may adapt to stress and resume proliferation (Burg et al., 2007). However, severe hyperosmolar stress induces apoptosis and cell death (Burg et al., 2007; Bevilacqua et al., 2010). To address the susceptibility of cells to hyperosmolar toxicity in the absence of FUS, we employed inducible NSC-34 cell lines that stably express either shRNA specific for FUS (shFUS) or a scrambled control shRNA (shSC) sequence. These cell lines are advantageous for cell viability measurements since cell death resulting from chemical transfection protocols is eliminated. NSC-34 cells were induced with doxycycline for 48 h, resulting in ~70% knock

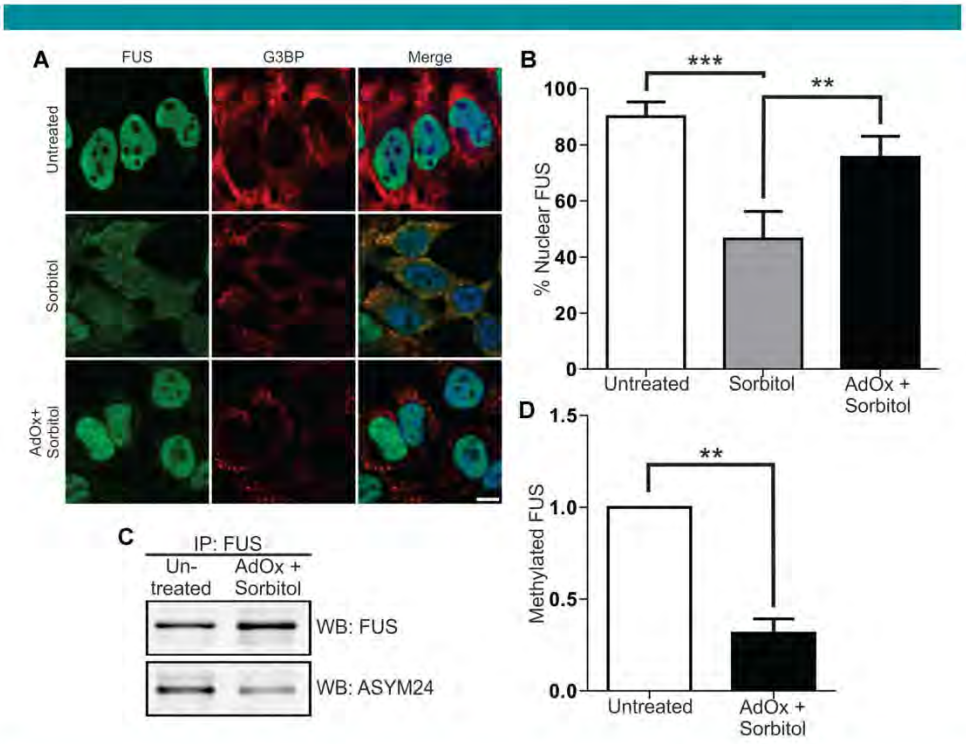

Fig. 5. Methylation regulates the nucleo-cytoplasmic distribution of FUS. A,B: HeLa cells were treated with 0.4 M sorbitol for 1 h, or pre-treated with 50 μM AdOx for 24 h prior to sorbitol treatment (AdOx + sorbitol) and subjected to confocal immunofluorescence imaging with anti-FUS (green) and anti-G3BP (red) antibodies. Sorbitol decreased the percentage of cellular FUS in the nucleus from 90 ± 5.1% in untreated cells to 46.5 ± 9.8%. Pre-treatment of cells with AdOx prior to sorbitol increased the percentage of cellular FUS in the nucleus to 75.6 ± 7.4%. Data shown are the average of three independent experiments ± standard deviation. Statistical significance was determined by ANOVA and Tukey's post hoc pairwise test ($P < 0.005$, ***$P < 0.0005$). No other comparisons were statistically significant. Scale bar represents 10 μm. C: FUS was immunoprecipitated from untreated HeLa cells or from AdOx + sorbitol cells and probed with the ASYM24 antibody by Western blot. FUS was used as a loading control. D: Densitometry analysis of (C) revealed a 68.6 ± 7.8% decrease in the amount of FUS that is arginine dimethylated when cells were pre-treated with AdOx compared to untreated cells. Data shown are the average of three independent experiments ± standard deviation. Statistical significance was determined by Student's t-test (**$P < 0.005$).**

down of FUS in the shFUS line (Fig. 7A) but not a loss of cell viability in either shFUS or shSC cells (data not shown). Cells were then treated for 8 h with either 0.4 M sorbitol or 0.25 mM sodium arsenite as a negative control. Sodium arsenite induces stress granule assembly, however endogenous FUS does not associate with stress granules under this condition (Fig. 2). Moreover, others have reported that mammalian cells with knocked-down FUS expression are not susceptible to sodium arsenite (Aulas et al., 2012). In agreement with this report, we did not detect a difference in percentage cell viability (Fig. 7B) or cell death (Fig. 7C) between shFUS and shSC cells in response to sodium arsenite using the MTT and LDH assays, respectively. In contrast, the percentage of viable cells was approximately twofold lower in the shFUS cells compared to shSC cells after sorbitol treatment (Fig. 7B). That shFUS cells are more susceptible to sorbitol-induced toxicity was confirmed by the LDH cell death assay, which revealed threefold greater cell death in shFUS cells treated with sorbitol compared to shSC cells under the same conditions. Therefore, while the expression of FUS is not required for the assembly of stress granules (Fig. 4B), cellular homeostasis and survival during hyperosmolar stress is mediated by the expression of FUS.

Discussion

Although FUS is predominately expressed in the nucleus of most cell types (Andersson et al., 2008), it can shuttle between the nucleus and the cytoplasm during mRNA transport (Zinszner et al., 1997; Fujii and Takumi, 2005). The equilibrium of FUS expression can be shifted towards the cytoplasm using inhibitors against RNA polymerase II (Pol II; Zinszner et al., 1994) or against the nuclear import receptor Transportin-1 (Trp), also known as Karyopherin β2 (Dormann et al., 2010). Genetic perturbations of its NLS also increase the cytoplasmic expression of FUS in the neurodegenerative disease ALS (Kwiatkowski et al., 2009; Vance et al., 2009). Herein we demonstrate a novel and

robust response of endogenous FUS to hyperosmolar stress, whereby FUS redistributes from the nucleus to the cytoplasm within minutes of exposure to sorbitol (Figs. 1–3) or sucrose (Fig. S1).

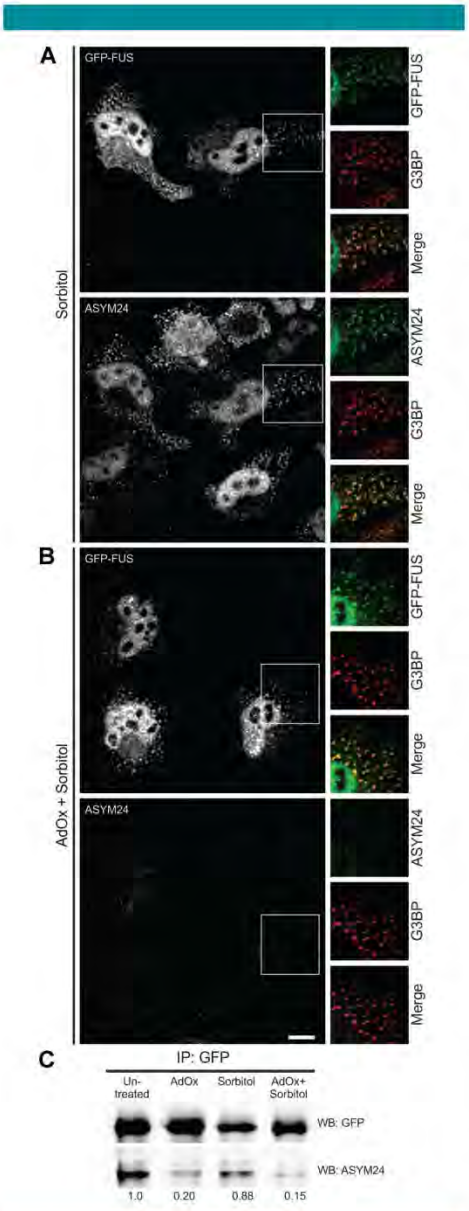

A role for FUS in hyperosmolar stress response is further supported by its association with stress granules under this condition. Stress granules are stalled translational complexes; as such, they are thought to regulate mRNAs processing during stress (Anderson and Kedersha, 2008). Recently, the activity of mTORC1 was shown to correlate with its sequestration inside stress granules, suggesting that these complexes can also regulate cell signaling at the protein level (Wippich et al., 2013). Importantly, no other chemical or environmental stressor has been shown to cause endogenous FUS to redistribute from the nucleus into the cytoplasm and enter into stress granules. While different stressors, such as oxidative stress and heat shock, have been shown to influence the association of ALS-linked mutant forms of FUS with stress granules, the nature of the NLS mutations causes FUS to accumulate in the cytoplasm a priori of stress (Bosco et al., 2010; Dormann et al., 2010). In contrast, hyperosmolar stress triggers both the cytoplasmic redistribution of FUS and its assembly into stress granules. Therefore, the response of endogenous FUS to hyperosmolar stress represents an altogether different mechanism compared to the previously described mutant forms of FUS. Further, our data support a normal and important role for endogenous FUS in stress response (discussed further below), whereas the association of ALS-linked FUS with stress granules is thought to represent a pathogenic mechanism in disease (Wolozin, 2012).

In order to dissect the processes governing the cytoplasmic redistribution of FUS from its incorporation into stress granules, we employed the GFP-FUS G515X construct, which lacks the nuclear localization domain. This allowed us to investigate the role of methylation as a post-translational modification in both events. Inhibition of methyltransferases with AdOx significantly reduced the cytoplasmic redistribution of FUS during hyperosmolar stress (Fig. 5). Moreover, analysis with the ASYM24 antibody revealed that FUS is asymmetrically dimethylated at arginine residues under homeostatic conditions but is hypomethylated in the presence of AdOx (Figs. 5 and 6). These observations, together with a mass spectrometry study demonstrating that ~20 arginine residues within FUS are asymmetrically dimethylated (Rappsilber et al., 2003), supports the possibility that methylation of the FUS protein itself dictates its subcellular localization during hyperosmolar stress. Conversely, the methylation status of FUS, or other cellular factors for that matter, does not appear to regulate the association of FUS with stress granules (Fig. 6). A remaining possibility is that

Fig. 6. Methylation does not regulate the incorporation of FUS into stress granules. HeLa cells were transiently transfected to express GFP-FUS G515X. Cells were exposed to 0.4 M sorbitol for 1 h either (A) in the absence of AdOx or (B) after cells had been pre-treated with 25 μM AdOx for 8 h. A: Confocal imaging showed that GFP-FUS G515X (green) assembles into G3BP-positive stress granules (red) upon sorbitol treatment (top panel). Co-staining with the ASYM24 antibody (a far-red fluorescence probe was employed; green is used in the images for clarity) revealed that these same stress granules contained asymmetrically dimethylated proteins (bottom panel). B: While the ASYM24 signal is dramatically decreased within stress granules and cells pre-treated with AdOx (bottom panel), there is still a robust association of GFP-FUS with stress granules under the same conditions (top panel). Scale bar represents 10 μm. C: Immunoprecipitation of GFP-FUS G515X with an anti-GFP antibody and a subsequent Western blot analysis with ASYM24 revealed that FUS is hypomethylated due to AdOx pretreatment. The ratio of the ASYM24 signal intensity to that of GFP was determined by densitometry and normalized to the untreated condition. Ratios are shown below the blot for each condition. All data are representative of n = 3 independent experiments.

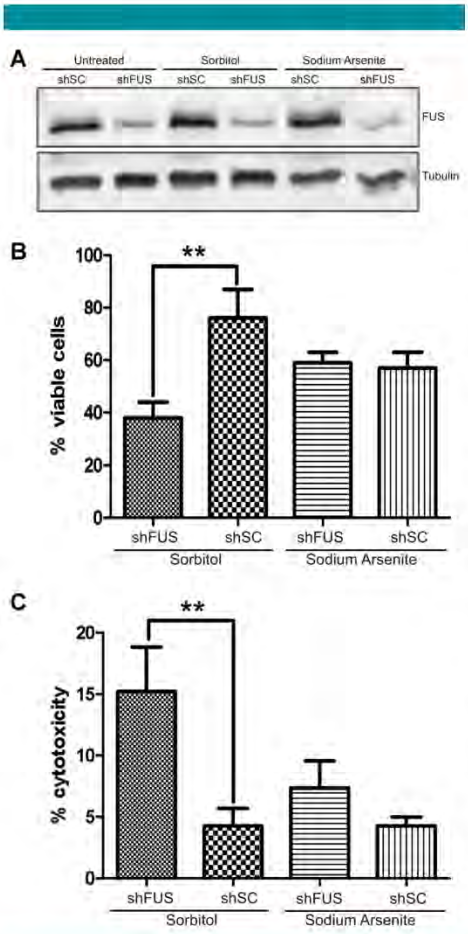

Fig. 7. Reduced FUS expression causes cells to become susceptible to sorbitol induced toxicity. A: Expression of either a non-targeting scrambled shRNA (shSC) or shRNA against FUS (shFUS) was induced by doxycycline for 48 h in NSC-34 cell lines, resulting in ~70% knock-down of the FUS protein as determined by Western blot. Tubulin was used as a loading control. Cells were then treated with 0.4 M sorbitol or 0.25 mM sodium arsenite for 8 h and subjected to the (B) MTT cell viability assay or (C) LDH cell toxicity assay. B: A significant decrease in cell viability was detected in shFUS cells (38 ± 6%) compared to shSC cells (76 ± 11%) when treated with sorbitol, whereas shFUS cells did not exhibit an analogous susceptibility to sodium arsenite (59 ± 4% for shFUS vs. 57 ± 6% for shSC). C: A higher percentage of cell death was detected in shFUS cells (15.2 ± 3.6%) compared to shSC cells (4.2 ± 1.4%) in response to sorbitol, whereas no difference in cell death was detected when these lines were stressed with sodium arsenite (7.4 ± 2.2% for shFUS vs. 4.3 ± 0.7% for shSC). B,C: Data shown are an average from n = 3 independent experiments ± standard deviation. Statistical significance was determined by Student's t-test ($P < 0.005$).**

other post-translational modifications of FUS influence its association with stress granules.

What are the biological implications of FUS in hyperosmolar stress response? Hyperosmolar stress is implicated in a myriad of disease conditions in humans, including renal failure, diabetes, neurodegeneration and inflammation, as well as disorders of the eye, heart, and liver (Brocker et al., 2012). Moreover, the cell shrinkage caused by hyperosmolar stress triggers many adverse subcellular events, such as mitochondrial depolarization, inhibition of DNA replication and transcription, damage to DNA and proteins, and cell cycle arrest, all of which can ultimately lead to cell death (Alfieri and Petronini, 2007; Burg et al., 2007; Brocker et al., 2012).

Our results are consistent with a prosurvival mechanism for endogenous FUS in human conditions that involve hyperosmolar stress. First, the response to hyperosmolar stress is specific, since alternative stressors that induce stress granule assembly such as oxidative stress and heat shock fail to elicit a similar response from endogenous FUS (Figs. 1–3). This data suggests a potentially distinct cellular response to hyperosmolar conditions compared to other stressors. Second, cells are more susceptible to hyperosmolar toxicity when FUS expression is reduced (Fig. 7), supporting a prosurvival role for FUS in this type of stress response.

Other nuclear hnRNPs, such as hnRNP A1, also respond to hyperosmolar stress by redistributing to the cytoplasm and assembling into stress granules. When localized to stress granules, hnRNP A1 is thought to specifically suppress the translation of anti-apoptotic factors and in turn initiate apoptosis under conditions of severe hyperosmolar stress (Bevilacqua et al., 2010). An intriguing possibility is that FUS sequesters specific mRNAs and proteins into stress granules, thereby altering their expression and/or function in response to the hyperosmolar stress. Indeed, recent PAR-CLIP (Hoell et al., 2011) and RIP-Chip (Colombrita et al., 2012) analyses have identified thousands and hundreds, respectively, of mRNA transcripts that are bound by FUS in the cell under homeostatic conditions. Interestingly, FUS binds mRNAs that encode genes involved in DNA damage repair and cell cycle regulation (Colombrita et al., 2012), two pathways that are altered during hyperosmolar stress (Burg et al., 2007).

In summary, our results support a prosurvival function for endogenous FUS during hyperosmolar stress. These findings have implications for human disorders with an etiology that involves hyperosmolar stress. Identifying the factors that regulate the response of FUS to hyperosmolar stress, as well as the pathways affected by FUS under this stress condition, will be critical to further our understanding of this prosurvival role of FUS.

Acknowledgments

We acknowledge the assistance from Dr. Paul Furcinitti of the UMass Medical School Core Digital Imaging Facility. We would like to thank Maeve Tischbein for her assistance with the immunofluorescence experiments, and Dr. Neil Cashman from University of British Columbia for naïve NSC-34 cell lines. We acknowledge financial support from the Worcester Foundation (D.A.B.) and the US National Institutes of Health/ National Institute of Neurological Disorders and Stroke (R01NS078145-01 to D.A.B.) for this work.

Literature Cited

Alfieri RR, Petronini PG. 2007. Hyperosmotic stress response: Comparison with other cellular stresses. Pflugers Arch 454:173–185.
Anderson P, Kedersha N. 2008. Stress granules: The Tao of RNA triage. Trends Biochem Sci 33:141–150.
Anderson P, Kedersha N. 2009. Stress granules. Curr Biol 19:R397–R398.

Andersson MK, Stahlberg A, Arvidsson Y, Olofsson A, Semb H, Stenman G, Nilsson O, Aman P. 2008. The multifunctional FUS, EWS and TAF15 proto-oncoproteins show cell type-specific expression patterns and involvement in cell spreading and stress response. BMC Cell Biol 9:37.
Aulas A, Stabile S, Vande Velde C. 2012. Endogenous TDP-43, but not FUS, contributes to stress granule assembly via G3BP. Mol Neurodegener 7:54.
Bedford MT, Clarke SG. 2009. Protein arginine methylation in mammals: Who, what, and why. Mol Cell 33:1–13.
Bentmann E, Neumann M, Tahirovic S, Rodde R, Dormann D, Haass C. 2012. Requirements for stress granule recruitment of fused in sarcoma (FUS) and TAR DNA-binding protein of 43 kDa (TDP-43). J Biol Chem 287:23079–23094.
Bevilacqua E, Wang X, Majumder M, Gaccioli F, Yuan CL, Wang C, Zhu X, Jordan LE, Scheuner D, Kaufman RJ, Koromilas AE, Snider MD, Hatzoglou M. 2010. eIF2alpha phosphorylation tips the balance to apoptosis during osmotic stress. J Biol Chem 285:17098–17111.
Bosco DA, Lemay N, Ko HK, Zhou H, Burke C, Kwiatkowski TJ, Jr., Sapp P, McKenna-Yasek D, Brown RH, Jr., Hayward LJ. 2010. Mutant FUS proteins that cause amyotrophic lateral sclerosis incorporate into stress granules. Hum Mol Genet 19:4160–4175.
Brocker C, Thompson DC, Vasiliou V. 2012. The role of hyperosmotic stress in inflammation and disease. Biomol Concepts 3:345–364.
Burg MB, Ferraris JD, Dmitrieva NI. 2007. Cellular response to hyperosmotic stresses. Physiol Rev 87:1441–1474.
Calvio C, Neubauer G, Mann M, Lamond AI. 1995. Identification of hnRNP P2 as TLS/FUS using electrospray mass spectrometry. RNA 1:724–733.
Cashman NR, Durham HD, Blusztajn JK, Oda K, Tabira T, Shaw IT, Dahrouge S, Antel JP. 1992. Neuroblastoma x spinal cord (NSC) hybrid cell lines resemble developing motor neurons. Dev Dyn 194:209–221.
Colombrita C, Onesto E, Megiorni F, Pizzuti A, Baralle FE, Buratti E, Silani V, Ratti A. 2012. TDP-43 and FUS RNA-binding proteins bind distinct sets of cytoplasmic messenger RNAs and differently regulate their post-transcriptional fate in motoneuron-like cells. J Biol Chem 287:15635–15647.
Crozat A, Aman P, Mandahl N, Ron D. 1993. Fusion of CHOP to a novel RNA-binding protein in human myxoid liposarcoma. Nature 363:640–644.
Daigle JG, Lanson NA, Jr., Smith RB, Casci I, Maltare A, Monaghan J, Nichols CD, Kryndushkin D, Shewmaker F, Pandey UB. 2013. RNA-binding ability of FUS regulates neurodegeneration, cytoplasmic mislocalization and incorporation into stress granules associated with FUS carrying ALS-linked mutations. Hum Mol Genet 22:1193–1205.
De Leeuw F, Zhang T, Wauquier C, Huez G, Kruys V, Gueydan C. 2007. The cold-inducible RNA-binding protein migrates from the nucleus to cytoplasmic stress granules by a methylation-dependent mechanism and acts as a translational repressor. Exp Cell Res 313:4130–4144.
Dewey CM, Cenik B, Sephton CF, Dries DR, Mayer P, III, Good SK, Johnson BA, Herz J, Yu G. 2011. TDP-43 is directed to stress granules by sorbitol, a novel physiological osmotic and oxidative stressor. Mol Cell Biol 31:1098–1108.
Dolzhanskaya N, Merz G, Aletta JM, Denman RB. 2006. Methylation regulates the intracellular protein-protein and protein-RNA interactions of FMRP. J Cell Sci 119:1933–1946.
Dormann D, Rodde R, Edbauer D, Bentmann E, Fischer I, Hruscha A, Than ME, Mackenzie IR, Capell A, Schmid B, Neumann M, Haass C. 2010. ALS-associated fused in sarcoma (FUS) mutations disrupt Transportin-mediated nuclear import. Embo J 29:2841–2857.
Du K, Arai S, Kawamura T, Matsushita A, Kurokawa R. 2011. TLS and PRMT1 synergistically coactivate transcription at the survivin promoter through TLS arginine methylation. Biochem Biophys Res Commun 404:991–996.
Emara MM, Fujimura K, Sciaranghella D, Ivanova V, Ivanov P, Anderson P. 2012. Hydrogen peroxide induces stress granule formation independent of eIF2alpha phosphorylation. Biochem Biophys Res Commun 423:763–769.
Fujii R, Takumi T. 2005. TLS facilitates transport of mRNA encoding an actin-stabilizing protein to dendritic spines. J Cell Sci 118:5755–5765.
Gal J, Zhang J, Kwinter DM, Zhai J, Jia H, Jia J, Zhu H. 2011. Nuclear localization sequence of FUS and induction of stress granules by ALS mutants. Neurobiol Aging 32:2323.e27–2323.e40.
Guil S, Long JC, Caceres JF. 2006. hnRNP A1 relocalization to the stress granules reflects a role in the stress response. Mol Cell Biol 26:5744–5758.
Hoell JI, Larsson E, Runge S, Nusbaum JD, Duggimpudi S, Farazi TA, Hafner M, Borkhardt A, Sander C, Tuschl T. 2011. RNA targets of wild-type and mutant FET family proteins. Nat Struct Mol Biol 18:1428–1431.
Ishigaki S, Masuda A, Fujioka Y, Iguchi Y, Katsuno M, Shibata A, Urano F, Sobue G, Ohno K. 2012. Position-dependent FUS-RNA interactions regulate alternative splicing events and transcriptions. Sci Rep 2:529.
Kedersha N, Anderson P. 2002. Stress granules: Sites of mRNA triage that regulate mRNA stability and translatability. Biochem Soc Trans 30:963–969.
Kedersha N, Anderson P. 2007. Mammalian stress granules and processing bodies. Methods Enzymol 431:61–81.
Kedersha N, Cho MR, Li W, Yacono PW, Chen S, Gilks N, Golan DE, Anderson P. 2000. Dynamic shuttling of TIA-1 accompanies the recruitment of mRNA to mammalian stress granules. J Cell Biol 151:1257–1268.
Kedersha N, Stoecklin G, Ayodele M, Yacono P, Lykke-Andersen J, Fritzler MJ, Scheuner D, Kaufman RJ, Golan DE, Anderson P. 2005. Stress granules and processing bodies are dynamically linked sites of mRNP remodeling. J Cell Biol 169:871–884.
Kuroda M, Sok J, Webb L, Baechtold H, Urano F, Yin Y, Chung P, de Rooij DG, Akhmedov A, Ashley T, Ron D. 2000. Male sterility and enhanced radiation sensitivity in TLS(−/−) mice. Embo J 19:453–462.
Kwiatkowski TJ, Jr., Bosco DA, Leclerc AL, Tamrazian E, Vanderburg CR, Russ C, Davis A, Gilchrist J, Kasarskis EJ, Munsat T, Valdmanis P, Rouleau GA, Hosler BA, Cortelli P, de Jong PJ, Yoshinaga Y, Haines JL, Pericak-Vance MA, Yan J, Ticozzi N, Siddique T, McKenna-Yasek D, Sapp PC, Horvitz HR, Landers JE, Brown RH, Jr. 2009. Mutations in the FUS/TLS gene on chromosome 16 cause familial amyotrophic lateral sclerosis. Science 323:1205–1208.
Moore MJ. 2005. From birth to death: The complex lives of eukaryotic mRNAs. Science 309:1514–1518.
O'Dea RF, Mirkin BL, Hogenkamp HP, Barton DM. 1987. Effect of adenosine analogues on protein carboxylmethyltransferase, S-adenosylhomocysteine hydrolase, and ribonucleotide reductase activity in murine neuroblastoma cells. Cancer Res 47:3656–3661.
Rappsilber J, Friesen WJ, Paushkin S, Dreyfuss G, Mann M. 2003. Detection of arginine dimethylated peptides by parallel precursor ion scanning mass spectrometry in positive ion mode. Anal Chem 75:3107–3114.
Tan AY, Manley JL. 2009. The TET family of proteins: Functions and roles in disease. J Mol Cell Biol 1:82–92.
Tourriere H, Chebli K, Zekri L, Courselaud B, Blanchard JM, Bertrand E, Tazi J. 2003. The RasGAP-associated endoribonuclease G3BP assembles stress granules. J Cell Biol 160:823–831.
Tradewell ML, Yu Z, Tibshirani M, Boulanger MC, Durham HD, Richard S. 2012. Arginine methylation by PRMT1 regulates nuclear-cytoplasmic localization and toxicity of FUS/TLS harbouring ALS-linked mutations. Hum Mol Genet 21:136–149.
van der Houven van Oordt W, Diaz-Meco MT, Lozano J, Krainer AR, Moscat J, Caceres JF. 2000. The MKK(3/6)-p38-signaling cascade alters the subcellular distribution of hnRNP A1 and modulates alternative splicing regulation. J Cell Biol 149:307–316.
Vance C, Rogelj B, Hortobagyi T, De Vos KJ, Nishimura AL, Sreedharan J, Hu X, Smith B, Ruddy D, Wright P, Ganesalingam J, Williams KL, Tripathi V, Al-Saraj S, Al-Chalabi A, Leigh PN, Blair IP, Nicholson G, de Belleroche J, Gallo JM, Miller CC, Shaw CE. 2009. Mutations in FUS, an RNA processing protein, cause familial amyotrophic lateral sclerosis type 6. Science 323:1208–1211.
Wang X, Arai S, Song X, Reichart D, Du K, Pascual G, Tempst P, Rosenfeld MG, Glass CK, Kurokawa R. 2008. Induced ncRNAs allosterically modify RNA-binding proteins in cis to inhibit transcription. Nature 454:126–130.
Wippich F, Bodenmiller B, Trajkovska MG, Wanka S, Aebersold R, Pelkmans L. 2013. Dual specificity kinase DYRK3 couples stress granule condensation/dissolution to mTORC1 signaling. Cell 152:791–805.
Wolozin B. 2012. Regulated protein aggregation: Stress granules and neurodegeneration. Mol Neurodegener 7:56.
Xie W, Denman RB. 2011. Protein methylation and stress granules: Post-translational remodeler or innocent bystander? Mol Biol Int 2011:137459.
Yamaguchi A, Kitagi K. 2012. The effect of PRMT1-mediated arginine methylation on the subcellular localization, stress granules, and detergent-insoluble aggregates of FUS/TLS. PLoS ONE 7:e49267.
Zinszner H, Albalat R, Ron D. 1994. A novel effector domain from the RNA-binding protein TLS or EWS is required for oncogenic transformation by CHOP. Genes Dev 8:2513–2526.
Zinszner H, Sok J, Immanuel D, Yin Y, Ron D. 1997. TLS (FUS) binds RNA in vivo and engages in nucleo-cytoplasmic shuttling. J Cell Sci 110:1741–1750.

Supporting Information

Additional supporting information may be found in the online version of this article at the publisher's web-site.

Fig. S1. FUS redistributes to the cytoplasm and localizes to cytoplasmic stress granules in response to sucrose. HeLa cells untreated (top row) or treated with 300 mM sucrose for 1 h (bottom row) were fixed and imaged. Cells probed with the anti-FUS (green) and anti-G3BP antibodies revealed that FUS co-localized with stress granules in response to sucrose. Cells were counter stained with the nuclear marker DAPI (blue). Images are representative of at least n = 3 experiments. Scale bar represents 10 μm.

Fig. S2. The response of FUS to sorbitol is recapitulated in several mammalian cell lines. HEK-293 (A), MEF (B), and NSC-34 (C) cells were either untreated (top row in each part) or treated (bottom row in each part) with 0.4 M sorbitol for 1 h. Immunofluorescence with the anti-FUS (green) and anti-G3BP (A) or anti-TIAR (B,C) antibodies showed that FUS localized to stress granules in response to sorbitol in all three cell lines. Cells were counter-stained with the nuclear marker DAPI (blue; A–C). All images are representative of n = 3 independent experiments. Scale bar represents 10 μm.

PREFACE TO APPENDIX III:

The following chapter is a manuscript published in Molecular Neurodegeneration. (Publisher: BioMed Central; no permission or license required for reproduction)

My contributions to this manuscript included intellectual input, experimental design strategies, and the creation and establishment of NSC-34 stable cell lines expressing exogenous human wild-type or R495X FUS used in figure 2. Additionally, I was responsible for the maintenance and culturing of these cells for experimental use and performed the western blot analysis shown in figure 2A.

Baron et al. Molecular Neurodegeneration 2013, 8:30
http://www.molecularneurodegeneration.com/content/8/1/30

MOLECULAR NEURODEGENERATION

RESEARCH ARTICLE Open Access

Amyotrophic lateral sclerosis-linked FUS/TLS alters stress granule assembly and dynamics

Desiree M Baron[1], Laura J Kaushansky[1], Catherine L Ward[1], Reddy Ranjith K Sama[1], Ru-Ju Chian[1], Kristin J Boggio[1], Alexandre J C Quaresma[2], Jeffrey A Nickerson[2] and Daryl A Bosco[1,3*]

Abstract

Background: Amyotrophic lateral sclerosis (ALS)-linked fused in sarcoma/translocated in liposarcoma (FUS/TLS or FUS) is concentrated within cytoplasmic stress granules under conditions of induced stress. Since only the mutants, but not the endogenous wild-type FUS, are associated with stress granules under most of the stress conditions reported to date, the relationship between FUS and stress granules represents a mutant-specific phenotype and thus may be of significance in mutant-induced pathogenesis. While the association of mutant-FUS with stress granules is well established, the effect of the mutant protein on stress granules has not been examined. Here we investigated the effect of mutant-FUS on stress granule formation and dynamics under conditions of oxidative stress.

Results: We found that expression of mutant-FUS delays the assembly of stress granules. However, once stress granules containing mutant-FUS are formed, they are more dynamic, larger and more abundant compared to stress granules lacking FUS. Once stress is removed, stress granules disassemble more rapidly in cells expressing mutant-FUS. These effects directly correlate with the degree of mutant-FUS cytoplasmic localization, which is induced by mutations in the nuclear localization signal of the protein. We also determine that the RGG domains within FUS play a key role in its association to stress granules. While there has been speculation that arginine methylation within these RGG domains modulates the incorporation of FUS into stress granules, our results demonstrate that this post-translational modification is not involved.

Conclusions: Our results indicate that mutant-FUS alters the dynamic properties of stress granules, which is consistent with a gain-of-toxic mechanism for mutant-FUS in stress granule assembly and cellular stress response.

Keywords: Stress granule, Amyotrophic lateral sclerosis, Frontotemporal lobar degeneration, FUS/TLS, Oxidative stress

Background

Mutations in the gene encoding fused in sarcoma/translocated in liposarcoma (FUS/TLS or FUS), also known as the heterogeneous nuclear ribonucleoprotein (hnRNP) P2 [1], are linked to inherited cases of amyotrophic lateral sclerosis (ALS) [2,3]. ALS is a fatal neurodegenerative disease characterized by motor neuron loss, progressive muscle weakening and paralysis [4]. Most ALS-linked FUS mutations are located within the C-terminal nuclear localization signal (NLS) that binds transportin, the nuclear importer that translocates FUS from the cytoplasm into the nucleus [5,6]. Although FUS is predominately localized to the nucleus in most cell types [7], it has nucleo-cytoplasmic shuttling capabilities that may be important for mRNA transport [8]. In fact, FUS is thought to play a role in local translation at the dendrites of neuronal cells [9-11]. Disruption of the FUS/transportin interaction leads to nuclear depletion with concomitant cytoplasmic accumulation of FUS in cultured mammalian cells [6]. The potential relevance of this interaction is underscored by the cytoplasmic accumulation of FUS in both ALS [2,3] and frontotemporal lobar degeneration (FTLD) [12] post-mortem central nervous system (CNS) tissues.

The extent to which FUS mutants redistribute to the cytoplasm correlates with ALS disease severity [6,13].

* Correspondence: Daryl.Bosco@umassmed.edu
[1]Department of Neurology, University of Massachusetts Medical School, Worcester, MA, USA
[3]Department of Biochemistry and Molecular Pharmacology, University of Massachusetts Medical School, Worcester, MA, USA
Full list of author information is available at the end of the article

For example, individuals with the FUS R495X mutation, which leads to truncation of the NLS and significant cytoplasmic retention of FUS, exhibit early disease onset and a relatively severe disease course [13]. Nuclear depletion of FUS may impair putative nuclear functions involving mRNA [14,15] and DNA [16,17] processing. An alternative, though not mutually exclusive, possibility is that mutant-FUS exerts a gain-of-toxic function in the cytoplasm [18].

Recently, a two-hit model has been proposed to account for cytoplasmic FUS toxicity in ALS and FTLD [19]. Cytoplasmic mislocalization of FUS, either through genetic mutations or other unidentified factors, represents the first hit. The first hit alone may not be sufficient to cause disease. However, a second hit stemming from cellular stress directs cytoplasmic FUS into stress granules. Stress granules are stalled translational complexes that form as a normal response to induced stressors such as oxidation, heat-shock, viral infection or hypoxia [20]. The function of stress granules is thought to be in the triage of mRNAs that are destined for expression, storage or degradation, which in turn restores cellular homeostasis [21]. Stress granule function may not be limited to mRNA processing, as the activity of certain proteins can also be controlled by their sequestration into stress granules [22]. It follows that the association of mutant-FUS with stress granules may impair stress response and ultimately cause disease [23]. This notion is supported by evidence of stress granule marker proteins within the pathological aggregates of neurodegenerative disease tissues [6,24,25].

While we and others have firmly established a mutant-specific phenotype with respect to FUS in stress granules [5,6,13,26-30], there is little evidence that mutant-FUS actually alters the properties of stress granules. Although there is no functional assay per se for stress granules, the properties of stress granules that are thought to be relevant to their function include assembly kinetics, dynamics, morphology and abundance [21,31]. Under conditions of oxidative stress, we show that mutant-FUS delays stress granule formation in mammalian cell culture. Once sodium arsenite-induced stress granules are formed, however, those containing mutant-FUS are more dynamic, larger and more abundant compared to stress granules lacking FUS. Upon removal of stress, stress granules disassemble more rapidly in cells expressing cytoplasmic mutant-FUS. Further, we identified the RGG domains within FUS as playing a key role in the assembly of mutant-FUS into stress granules, although the methylation of arginine residues within these RGG domains does not play a significant role. The evidence presented here supports the hypothesis that the association of mutant-FUS with stress granules represents a gain-of-toxic interaction in ALS pathogenesis.

Results

The expression of cytoplasmic mutant FUS influences stress granule assembly and disassembly

We and others previously demonstrated that ALS-linked FUS mutants assemble into stress granules to an extent that directly correlates with their cytoplasmic mislocalization [6,13]. These experiments were performed under conditions of acute stress such that stress granules assembled rapidly and did not address whether mutant-FUS affects the processes of stress granule assembly and disassembly. First, we employed our previously characterized, doxycycline-inducible HEK-293 cell lines expressing GFP-tagged wild-type FUS and ALS-linked FUS mutants (R495X and H517Q) [13] to examine the effect of mutant-FUS on stress granule assembly under conditions of oxidative stress. The R495X mutation truncates the nuclear localization signal (NLS), causing FUS to significantly redistribute from the nucleus to the cytoplasm (Figure 1A and [13]). On the opposite end of the mislocalization spectrum is H517Q, an autosomal recessive mutation in the NLS that induces a mild mislocalization phenotype (Figure 1A and [2,13]).

Stress granule assembly was initiated in GFP-FUS (WT, R495X, and H517Q) cell lines with 0.25 mM sodium arsenite, an inducer of oxidative stress [32] and an environmental toxicant that can cause neural defects [33,34]. Sodium arsenite has been shown to induce the incorporation of cytoplasmic FUS-mutants into stress granules, but does not influence endogenous FUS or exogenously expressed GFP-FUS WT proteins [13,35]. In fact there is no difference in cellular response to sodium arsenite with respect to stress granule formation or cell viability when FUS expression is reduced [31,35]. Therefore, sodium arsenite induces a mutant-specific phenotype with respect to FUS localization to stress granules. The concentration of sodium arsenite employed here was reduced from the 0.5 mM concentration that is typically used [13,36] in order to lengthen the timescale of stress granule assembly and resolve differences in this process between cell lines. Ras GTPase-activating protein-binding protein 1 (G3BP), a stress granule specific marker [36], was used to probe for stress granules by immunofluorescence (IF) over a 90 min time course of sodium arsenite exposure. At 0 min, there were no stress granules; G3BP remained diffusely cytoplasmic and no cytoplasmic GFP-FUS puncta were detected in any cell line (Figure 1A). By 90 min, all cell lines contained stress granules in virtually every cell. As expected, GFP-FUS R495X co-localized with G3BP in stress granules, as did GFP-FUS H517Q albeit to a far lesser degree. In contrast, GFP-FUS WT remained entirely nuclear and was not detected within these structures (Figure 1A and Additional file 1). Strikingly, fewer GFP-FUS R495X expressing cells contained G3BP-positive stress granules compared to GFP-FUS (WT

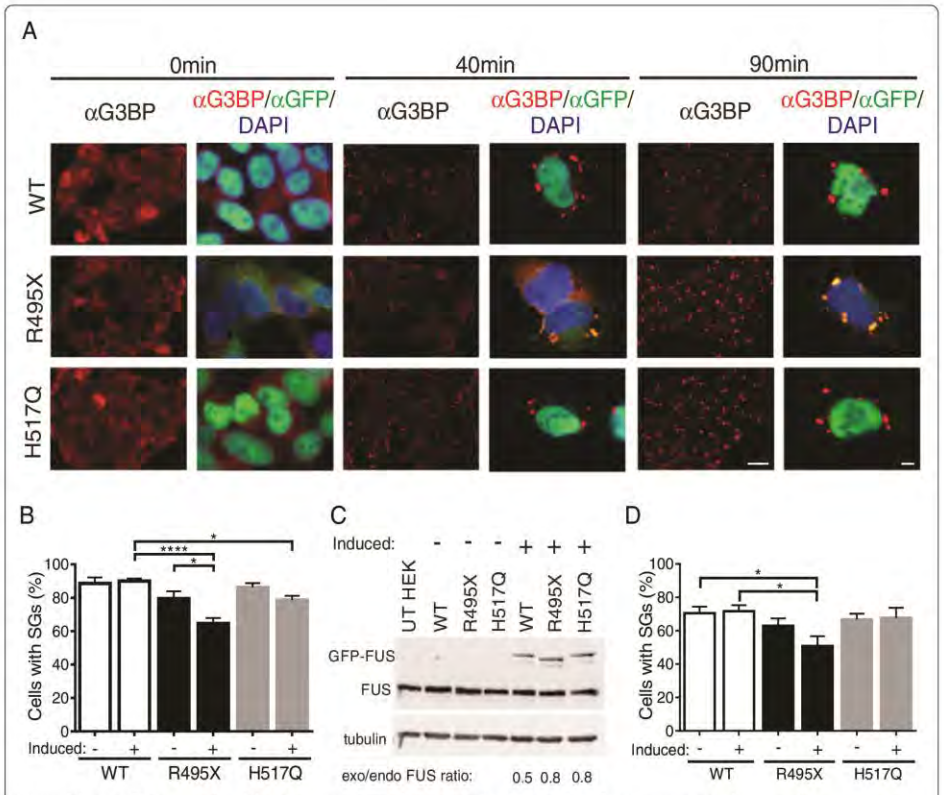

Figure 1 Mutant-FUS expression delays the assembly and expedites the disassembly of stress granules in human cells. **(A)** Representative fluorescence images of HEK-293 cells expressing GFP-FUS (WT, R495X or H517Q) upon treatment with 0.25 mM sodium arsenite for 0, 40 and 90 min. The extent of stress granule formation in each line is illustrated with low magnification (40x) images using the anti-G3BP (red) stress granule marker (columns 1, 3 and 5). The localization of GFP-FUS (green) with respect to the nuclei (DAPI; blue) and stress granules is demonstrated within high magnification (100x) images (columns 2, 4 and 6). Scale bar = 20 and 5 μm, respectively, in low and high magnification images. **(B)** Quantification of the percentage of cells with stress granules at 40 min for the lines in (A) that are either induced (+) or not induced (–) to express GFP-FUS reveal that expression of GFP-FUS R495X causes a significant decrease in the number of cells with stress granules compared to controls. All error bars represent SEMs. Statistically significant differences were determined by one-way ANOVA and Tukey's post-hoc test (****$P < 0.0001$, *$P < 0.05$). Additional significant comparisons include, but are not shown for clarity: uninduced GFP-FUS WT versus induced GFP-FUS R495X ($P < 0.001$), uninduced GFP-FUS H517Q versus induced GFP-FUS R495X ($P < 0.001$), and induced GFP-FUS H517Q versus induced GFP-FUS R495X ($P < 0.01$). **(C)** Western blot and densitometry analyses of cell lines in **(B)** and naive HEK-293 cells (UT) reveal that exogenous (exo) GFP-FUS proteins are expressed at levels similar to each other and within 2-fold of endogenous (endo) FUS (exo/endo FUS ratio). **(D)** Stress granule disassembly was assessed as described in **(B)** for GFP-FUS WT, R495X and H517Q lines after stress was removed for 90 min. Significantly fewer GFP-FUS R495X expressing cells contain stress granules.

and H517Q) lines after approximately 40 min of sodium arsenite exposure (Figure 1A).

Quantification of these results revealed that the greatest difference in cells containing stress granules occurred between the GFP-FUS R495X (65 ± 3.3%) and GFP-FUS WT (90 ± 1.5%) lines after 40 min of sodium arsenite exposure (Figure 1B). Stress granules were also assembled in GFP-FUS H517Q cells (79 ± 2.5%), though to a lesser extent than WT cells. Therefore, the expression of mutant-FUS is not sufficient to cause a delay in stress granule assembly, but rather, the delay in assembly depends on the extent that FUS is redistributed to the cytoplasm (WT<H517Q<R495X). Artifacts from FUS over-expression are not expected to influence these results since the expression levels of all exogenous GFP-FUS proteins were similar to each other and within two-

fold of endogenous FUS (Figure 1C). To rule out an inherent difference between cell lines irrespective of GFP-FUS expression, identical experiments were performed in uninduced cells (i.e., without doxycycline). Uninduced GFP-FUS (WT and H517Q) lines did not express detectable GFP-FUS and behaved similarly to induced GFP-FUS WT cells, confirming that GFP-FUS WT expression has no effect on stress granule assembly. There was a small yet insignificant difference between uninduced GFP-FUS (WT and R495X) lines (Figure 1B). We suspect this may be due to low levels, below the limit of detection via western analysis (Figure 1C), of GFP-FUS R495X expression in the absence of doxycycline. Nonetheless, induced expression of GFP-FUS R495X in these cells significantly attenuated the assembly of stress granules compared to the uninduced condition in the same line (Figure 1B).

The reversible nature of stress granules is an important functional feature of these structures; upon removal of stress, stress granules disassemble as the cell re-establishes homeostasis. Since mutant-FUS delays the assembly of stress granules, we sought to determine whether mutant FUS also influences the reverse process of disassembly. Cells were treated with 0.25 mM sodium arsenite for 1 h, at which point ~100% of cells in all cell lines contained stress granules. The disassembly process was initiated by replacing sodium arsenite with fresh media, and the percentage of cells with stress granules was quantified after 90 min. At this time point, fewer GFP-FUS R495X expressing cells (51 ± 6.0%) contained stress granules compared to GFP-FUS WT (72 ± 3.7%) and GFP-FUS H517Q (68 ± 6.0%). Therefore, expression of GFP-FUS (WT and H517Q) had virtually no effect, while expression of the cytoplasmic GFP-FUS R495X exerted the most pronounced effect on the kinetics of stress granule disassembly (Figure 1D). Interestingly, a similar effect on stress granule assembly and disassembly was observed upon depletion of endogenous TAR DNA-binding protein 43 (TDP-43) [37], which, unlike FUS, is thought to play a normal role in arsenite-induced stress response [31]. Thus, both a loss of TDP-43 function and a potential toxic gain of mutant-FUS function manifests in delayed stress granule assembly and more rapid stress granule disassembly under conditions of oxidative stress.

While HEK-293 GFP-FUS lines are ideal for microscopic measurements of stress granule properties, owing to the GFP tag on FUS and the relatively flat nature of these cells, we wanted to both confirm these stress granule assembly trends in neuronal cells and rule out a potential "tag effect" from GFP. To this end, motor neuron-like NSC-34 [38] cell lines were engineered to constitutively express untagged human FUS WT or FUS R495X using a lentiviral transduction expression system. FUS protein expression in these cells was accomplished with an IRES-containing bicistronic vector (CSCW2-IRES-GFP), which allowed for the simultaneous expression of both FUS and GFP separately (i.e., not as a fusion protein) but from the same RNA transcript. Therefore, GFP served as a reporter for cells transduced to express either untagged FUS WT or R495X. The expression levels of FUS (WT and R495X) proteins were similar to each other and within two-fold of endogenous FUS (Figure 2A and Additional file 2). In the absence of stress, elevated levels of cytoplasmic FUS were observed in NSC-34 cells expressing FUS R495X, and diffuse cytoplasmic G3BP signal was observed in both FUS R495X and WT cells. Upon exposure to 0.25 mM sodium arsenite for 1 hr, FUS was detected within G3BP-positive stress granules only in cells expressing FUS R495X. Although sodium arsenite exposure lead to fewer NSC-34 cells with stress granules overall compared to HEK-293 cells, the same phenotype was observed in that fewer cells formed stress granules in FUS R495X expressing cells compared to those expressing FUS WT (Figure 2B). Quantification of this phenotype revealed a 2.4-fold lower percentage of stress granule-containing NSC-34 cells for FUS R495X (23 ± 1.6%) compared to FUS WT (55 ± 2.8%) lines (Figure 2C). To assess whether the expression of exogenous human FUS proteins had any effect on stress response in these cells, the percentage of cells with stress granules was also quantified in the parent, or non-transduced, NSC-34 cell line after 1 h of sodium arsenite exposure. While FUS WT and R495X lines exhibited the most significant difference, there were also more FUS WT cells with stress granules relative to the parent (37 ± 3.6%) line (Figure 2C). Possible explanations for why an effect of exogenous FUS WT is observed in NSC-34 but not HEK-293 (Figure 1B) cells is that the expression of exogenous human FUS WT exerts an additional stress due to i) higher relative protein levels (compare exogenous to endogenous FUS in Figures 1C and 2A), and/or ii) different species of cells (expression of human FUS in mouse versus human cells), either of which could heighten the stress response of these cells to sodium arsenite. In fact, expression of FUS WT is sufficient to induce stress and toxicity in different model organisms [39-41]. Nonetheless, the efficiency of stress granule assembly in the parent NSC-34 line is more similar to that of FUS WT than FUS R495X (Figure 2C). Moreover, one would expect FUS R495X to also impose an additional stress, and yet stress granule assembly is attenuated in these cells, providing further evidence that expression of mutant-FUS interferes with the assembly of stress granules under conditions of stress.

Unlike HEK-293 cells (Figure 1), the percentage of NSC-34 cells containing stress granules never reached 100% in any line, and the FUS WT line always contained double the percentage of cells with stress granules compared to FUS R495X. This behavior precluded our ability to perform a similar disassembly analysis as described

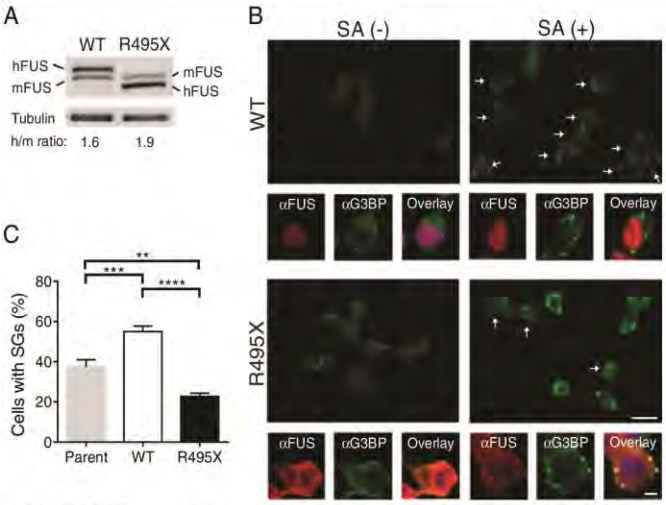

Figure 2 Expression of the FUS R495X mutant interferes with stress granule assembly in neuronal cells. (A) Exogenous human (h) FUS proteins are similar to each other and within 2-fold of endogenous mouse (m) FUS as determined by western blot and densitometry analyses. The ratio of hFUS/mFUS proteins is indicated for each cell line. **(B)** Immunofluorescence images of NSC-34 cells expressing untagged FUS (WT and R495X) either in the absence (–) or presence (+) of 0.25 mM sodium arsenite (SA) for 1 hr. Low magnification (40x) images of SA (+) treated cells using the anti-G3BP stress granule marker (green) show a greater number of stress granule-positive cells (denoted by arrows) in the FUS WT line compared to the FUS R495X line. High magnification (100X) images showing a single cell reveal the localization of FUS (red) and G3BP (note: the far red channel was used for detection of G3BP and the images are shown in green for clarity) under all conditions. DAPI (nuclei) is included in the overlay images. Note that in cells with stress granules, cytoplasmic R495X co-localizes to these structures as expected (see overlay image in bottom right). Scale bar = 20 and 5 μm, respectively, in low and high magnification images. **(C)** Quantitative analysis (as described in Figure 1B) of the percentage of NSC-34 cells with stress granules after 1 hr of sodium arsenite treatment revealed that expression of FUS R495X inhibited stress granule assembly compared to cells expressing FUS WT and the parent line. All error bars represent SEMs. Statistically significant differences were determined by one-way ANOVA and Tukey's post-hoc test (****$P < 0.0001$, ***$P < 0.001$, **$P < 0.01$).

above for HEK-293 cells (Figure 1D), which compared the absolute percentage of cells with stress granules at different time points.

The expression of cytoplasmic mutant-FUS alters the dynamic binding properties of stress granule-associated proteins

Stress granules are highly dynamic structures [32,42,43]. Proteins and mRNA continuously shuttle in and out of stress granules, reversibly binding to other stress granule components in a manner that is thought to regulate both protein signaling activity [22] and mRNA fates towards translational arrest, expression or decay [20]. To study the effect of stress granule-associated mutant-FUS on the dynamic properties of stress granules, we employed fluorescence recovery after photobleaching (FRAP). FRAP measures the relative kinetics and affinities of protein binding within complexes, such as stress granules, over the time course of the experiment [44,45]. Because FRAP reports on binding events in live cells, fluorescently tagged-proteins were employed for these experiments [32,42,43,46]. We transiently expressed monomeric RFP (mRFP)-tagged proteins T-cell-restricted intracellular antigen-1 (TIA-1) or G3BP, two established stress granule-associated proteins, to mark stress granules for FRAP within HEK-293 GFP-FUS (WT and R495X) cells. Overexpression of G3BP is sufficient to form inclusions that resemble stress granules in the absence of stress [31,47]. Since it is not clear whether these G3BP overexpression-induced stress granules have different properties than sodium arsenite-induced stress granules, conditions were optimized for transfection of mRFP-G3BP that minimized the formation of G3BP-positive inclusions *a priori* of sodium arsenite treatment (Figure 3A; see Materials and methods).

During a FRAP experiment on stress granules, the fluorescence from a tagged species (GFP-FUS R495X, mRFP-TIA-1 or mRFP-G3BP in our case) is bleached. The fluorescence signal recovers as bleached molecules unbind from sites in the stress granules, un-bleached fluorescent molecules exchange back into the photobleached area and then bind. The fluorescence recovery time is limited by

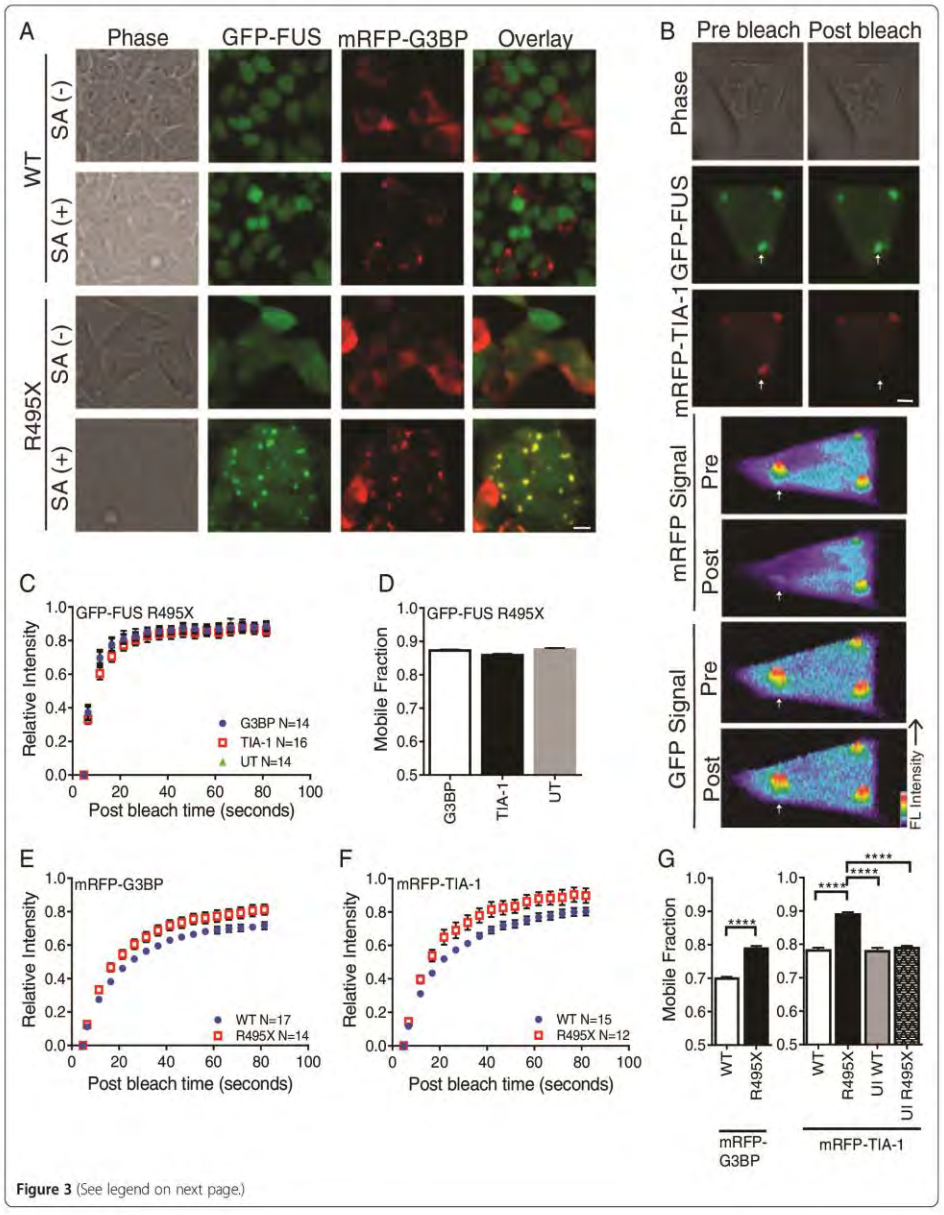

Figure 3 (See legend on next page.)

(See figure on previous page.)

Figure 3 GFP-FUS R495X is weakly bound to stress granules and alters binding of stress granule-associated proteins. (A) Live cell images of GFP-FUS (WT and R495X) expressing HEK-293 cells transfected with mRFP-G3BP. Images are shown before (–) and after (+) treatment with 0.2 mM sodium arsenite (SA) for 1 hr. Scale bar = 10 μm. **(B)** Top three panels: exemplar GFP and mRFP images of a SA treated cell for a mRFP-TIA-1 FRAP experiment before and after photobleaching. The mRFP signal, but not GFP signal, is lost from the stress granule (indicated by arrow). Scale bar = 5 μm. Bottom four panels: fluorescence intensity profiles corresponding to the above panels (rotated 90° clockwise). **(C)** The recovery curve for GFP-FUS R495X in untransfected (UT; green triangle) cells are indicative of fast fluorescence recovery. The GFP-FUS R495X profile does not change upon transfection with either mRFP-G3BP (blue circle) or mRFP-TIA-1 (red square). **(D)** Nearly identical mobile fractions support the conclusions in **(C)**. **(E & F)** Recovery curves for mRFP-G3BP **(E)** and mRFP-TIA-1 **(F)** differ for GFP-FUS WT (blue circle) and R495X (red square) expressing cells. **(G)** Mobile fractions for the curves in **(E & F)** are significantly higher for GFP-FUS R495X (black bars) relative to GFP-FUS WT (white bars) cells. Mobile fractions for mRFP-TIA-1 are the same for the following control experiments: GFP-FUS WT expressing cells (white bars), uninduced (UI) GFP-FUS WT cells (grey bar) and uninduced GFP-FUS R495X cells (hatched bar). Asterisks indicate statistically significant differences between cell lines as determined by two-way ANOVA and Tukey's post-hoc test (****$P < 0.0001$) on data from at least n=2 independent experiments. All error bars represent SEMs. The total number (N) of stress granule analyzed is indicated on the recovery panels.

either diffusion, which is faster than the rates we report here, or by binding kinetics; thus, proteins that are tightly bound to other proteins or cellular structures exhibit relatively long half times of fluorescence recovery ($t_{1/2}$) [44]. The population of fluorescent molecules that exchange with their bleached counterparts over the time course of the experiment comprise the "mobile fraction" [44]. The "immobile fraction" is the population that is tightly bound and does not exchange over the time course of the experiment. Here, each experiment was carried out such that the photobleaching occurred in only a single channel and fluorescence was diminished evenly over the entire stress granule (Figure 3B). Initially, the dynamics of GFP-FUS R495X within stress granules were investigated since the dynamic binding properties of this protein under stress conditions have not been reported. GFP-FUS R495X cells alone or transfected with either mRFP-G3BP (Figure 3A) or mRFP-TIA-1 (Figure 3B) were exposed to 0.20 mM sodium arsenite for 1 hr, at which point the majority of cells contained fully formed stress granules. The fast recovery ($t_{1/2}$ of 3.6 ± 2.1s; Figure 3C) of GFP-FUS R495X by FRAP shows that this protein re-binds within stress granules relatively quickly compared to other stress granule-associated proteins (see below). Moreover, ~87% of GFP-FUS R495X molecules constituted the mobile fraction, indicating that GFP-FUS R495X is weakly bound within stress granules (Figure 3D). Neither the $t_{1/2}$ nor the mobile fraction of GFP-FUS R495X changed significantly upon transient transfection of either mRFP-G3BP or mRFP-TIA-1 (Figure 3C and D). Therefore, neither the process of transient transfection itself, nor the over-expression of stress-granule associated proteins, influenced the dynamic properties of mutant-FUS.

Next we performed FRAP on mRFP-G3BP or mRFP-TIA-1 to determine the effect of mutant-FUS on the dynamic properties of proteins within stress granules. Fluorescence recovery for mRFP-G3BP ($t_{1/2}$ 12 ± 4.4s; 70 ± 2% mobile) and mRFP-TIA-1 ($t_{1/2}$ 12 ± 3.9s; 78 ± 2% mobile) within GFP-FUS WT expressing cells was observed (Figure 3E and F). Our measurements of mRFP-TIA-1 in control HEK-293 cells were similar to those reported for GFP-TIA-1 COS7 cells [32]. In cells expressing GFP-FUS R495X, the fluorescence recovery half times were nearly the same for mRFP-G3BP ($t_{1/2}$ 11 ± 2.8s) and mRFP-TIA-1 ($t_{1/2}$ 10 ± 2.8s). However, the mobile fraction for both mRFP-G3BP and mRFP-TIA-1 increased significantly in GFP-FUS R495X cells to 79 ± 3% and 89 ± 4%, respectively, compared to GFP-FUS WT cells (Figure 3E-G). Control experiments in GFP-FUS WT (induced and uninduced) and GFP-FUS R495X (uninduced) cells confirmed that an increase in mRFP-TIA-1 mobile fraction required the expression of mutant-FUS (Figure 3G). The increased mobile fraction for mRFP-G3BP and mRFP-TIA-1 indicates that these proteins bind more weakly to factors within GFP-FUS R495X positive stress granules compared to stress granules lacking mutant-FUS. As a result, there is increased exchange of mRFP-G3BP and mRFP-TIA-1 between the area that is photobleached and the area that is not photobleached, resulting in fluorescence recovery. Together, these data demonstrate that the incorporation of mutant-FUS into sodium arsenite-induced stress granules decreases the binding of other stress granule-associated proteins within these structures.

Because we and others observed that stress granules form as a result of G3BP overexpression [31,47], we examined whether their dynamic properties were different compared to those stress granules induced by sodium arsenite. mRFP-G3BP exhibited significantly weaker binding (i.e., larger mobile fraction, $P < 0.05$) within stress granules in GFP-FUS WT cells under conditions of G3BP over-expression compared to sodium arsenite stress, indicating that the dynamic properties of these stress granules are inherently different (Additional file 3). The most striking difference was the effect of mutant-FUS: GFP-FUS R495X significantly *increased* mRFP-G3BP binding within stress granules (i.e., smaller mobile fraction) under conditions of G3BP over-expression compared to all other conditions, which is the opposite trend in sodium arsenite-induced stress granules (Figure 3). Therefore, the effect of GFP-FUS R495X on the dynamic properties of stress granules

depends on the stressor and is consistent with observations that the source of stress influences the constituents within stress granules [48]. Irrespective of the stress, our results show that the incorporation of GFP-FUS R495X into stress granules alters the dynamic binding interactions of other well-characterized stress granule-associated proteins within in these structures.

Expression of mutant-FUS increases the size and abundance of stress granules

In addition to dynamics, stress granule size and abundance could also be altered by the presence of mutant-FUS. As such, both stress granule size and abundance were quantified in HEK-293 cell lines expressing either GFP-FUS (WT or R495X) after exposure to 0.5 mM sodium arsenite for 1 hr, at which point stress granules were fully formed (>95% of cells contain stress granules). In contrast to previous methods that measure the area of stress granules, which does not take into account the three-dimensional aspect of these structures, we developed a method to quantify the volume of stress granules based on fluorescence intensity measurements (see Materials and methods). Briefly, fixed cells were labeled with an anti-G3BP antibody and then optically sectioned by confocal microscopy. Three-dimensional reconstruction of these sections allowed us to quantify the volume of selected stress granules (Figure 4A). This analysis revealed that GFP-FUS R495X expressing cells produced significantly larger stress granules (3.8 ± 0.1 μm^3) compared to GFP-FUS WT cells (2.7 ± 0.2 μm^3; Figure 4B and C). This trend is consistent with ALS-linked TDP-43 mutants, which also show an increased stress granule size under conditions of hyperosmolar stress [49], suggesting that this may be a common disease-related characteristic.

Our quantitative analysis also revealed that mutant-FUS expressing cells contained 27% more stress granules per cell (8.8 ± 0.3) compared to WT-FUS (6.9 ± 0.4; Figure 4B and D). This result is consistent with a recent report demonstrating a greater abundance of stress granules within patient FUS (R521C and R514G) fibroblast lines under conditions of sodium arsenite relative to control lines [30]. Moreover, cells expressing ALS-linked TDP-43 also produce more stress granules compared to control cells under stress [25]. Therefore, disease-causing FUS and TDP-43 proteins appear to alter stress granules morphology by increasing their size and abundance.

The RGG domains play a key role in modulating the association of mutant-FUS with stress granules

In order to understand the factors modulating the incorporation of mutant FUS into stress granules, we engineered GFP-tagged FUS constructs lacking the functional domains of FUS and tested their ability to incorporate into stress granules. The functional domains of FUS are as follows: the prion-like QGSY-rich region (QGSY), a glycine-rich region (GLY), an RNA recognition motif (RRM), and two arginine-glycine-glycine-rich domains (RGG1 and RGG2) separated by a C2-C2 zinc finger motif (ZF) (Figure 5A). All of these domains have been shown to play a role in modulating the incorporation of other RNA binding proteins into stress granules [26,50-52] and thus each have the potential to influence the association of mutant-FUS with stress granules. The extent with which FUS mutants localize to arsenite-induced SGs correlates with their level of cytoplasmic expression (Figures 1, 2 and [13]). However, since transient transfection of highly cytoplasmic FUS mutants (e.g., R495X) has the potential to produce cytoplasmic protein aggregates that could confound our stress granule analysis [13], domain deletion constructs were engineered within the background of the less aggregation-prone R521G mutant.

Transient transfection of GFP-FUS R521G deletion constructs in HeLa cells resulted in varying degrees of GFP-FUS cytoplasmic expression: FL, ΔQGSY, ΔRGG1, ΔGLY and ΔRRM were predominately expressed in the nucleus, whereas relatively high cytoplasmic expression was observed for ΔRGG2, which lacks part of the signal used for nuclear import of FUS [5] (Figure 5B). Deletion of the zinc finger motif resulted in a construct that failed to express in mammalian cells (data not shown), possibly because this construct is unstable and/or structurally altered [53]. Although GFP-FUS R521G exhibits cytoplasmic expression upon transient transfection [2], the levels here were not sufficient for an accurate stress granule analysis. It was therefore necessary to increase the cytoplasmic expression of FUS-deletion constructs by co-transfection with maltose binding protein (MBP)-tagged M9M. M9M is a transportin/Kapβ2-specific nuclear import inhibitor that blocks the nuclear import of FUS [6,54]. Co-transfection with MBP-M9M increased cytoplasmic retention of GFP-FUS for all constructs, ensuring that each construct had equal potential to assemble into stress granules (Figure 5B).

Administration of 0.5 mM sodium arsenite for 1 hr induced stress granule formation (Figure 5B) in ~75% of cells for all constructs. A ratio of the GFP signal within stress granules relative to the diffuse GFP-FUS signal in the cytoplasm (stress granule/diffuse FUS signal) was used to quantify the incorporation of each construct within stress granules. Full length GFP-FUS R521G exhibited a robust localization to stress granules with a stress granule/diffuse FUS ratio of 4.75 +/− 0.97 (Figure 5B and C). As expected for a protein that does not associate with stress granules, analysis with free GFP as a negative control produced the lowest ratio of 1.13 +/− 0.11. GFP-FUS R521G ΔQGSY, ΔGLY, and ΔRRM were not significantly different from FL GFP-FUS R521G. In contrast, deletion of the RGG1

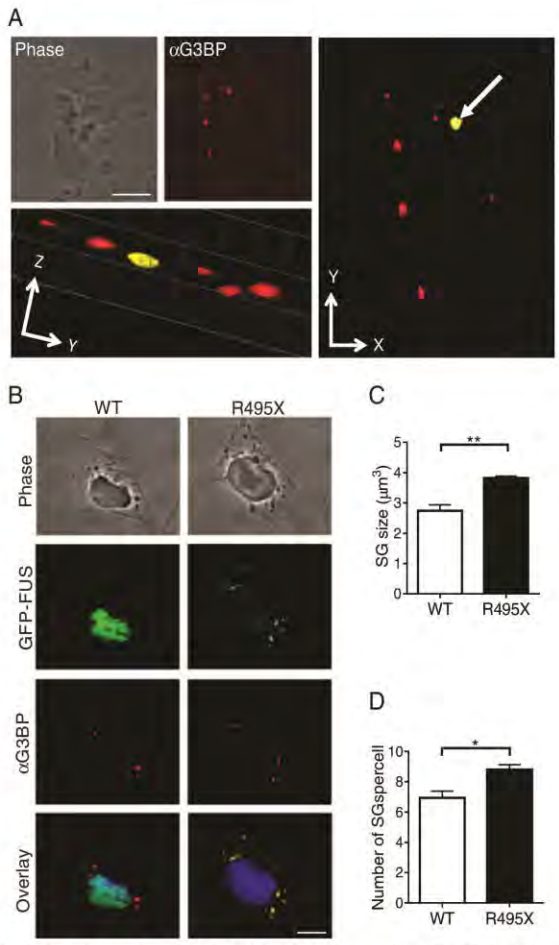

Figure 4 Stress granule size and number are increased in GFP-FUS R495X expressing cells. (A) Clockwise order: representative single-plane phase (top left) and anti-G3BP (stress granule marker; red) immunofluorescence (top middle) confocal images of an HEK-293 cell expressing GFP-FUS WT treated with 0.5 mM sodium arsenite for 1 hr. Three-dimensional (3D) reconstruction was used to quantify stress granule volume (see Materials and methods, and C within this figure). The *xy* (right) and *yz* (bottom; view along arrow in xy image) planes for this 3D reconstructed image are shown; the stress granule highlighted in yellow is marked for volume analysis. Scale bar = 10 μm. **(B)** Representative maximum projection confocal images of GFP-FUS WT and GFP-FUS R495X expressing cells treated as in **(A)** exemplify the size and number of stress granules for each line. Scale bar = 10 μm. **(C and D)** GFP-FUS R495X expressing cells contain stress granules with larger volume **(C)** and in greater abundance **(D)** relative to cells expressing GFP-FUS WT. Asterisks indicate statistically significant differences between cell lines as determined by the Student's t-test (**P < 0.01, *P < 0.05) on data from n=3 independent experiments. All error bars represent SEMs.

domain (ΔRGG1) significantly impaired the localization of FUS into stress granules (1.72 +/− 0.22), and deletion of the RGG2 domain (ΔRGG2) exhibited a similar impairment trend (2.23 +/− 0.48). We note that while distinct FUS-positive stress granules are observed for ΔRGG2, a comparatively high level of GFP-FUS signal remains diffuse, yielding a low stress granule/diffuse FUS ratio. All constructs were expressed at comparable levels (Figure 5D)

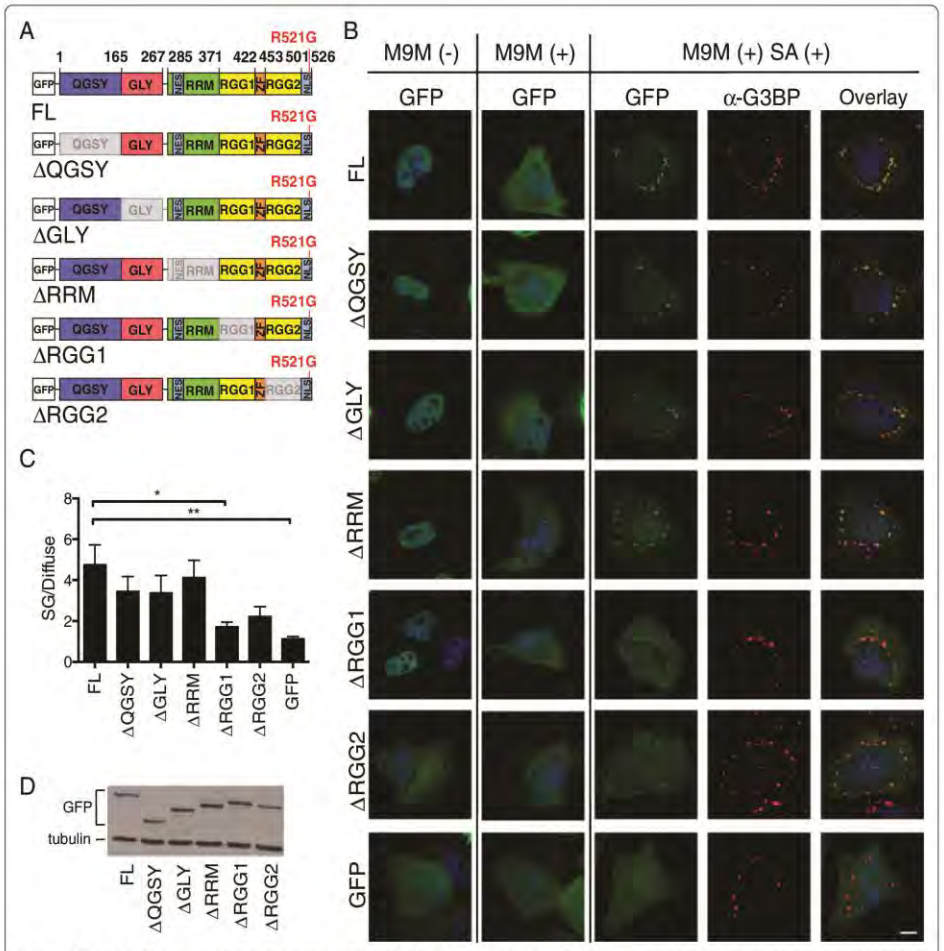

Figure 5 The RGG domains modulate the incorporation of FUS into arsenite-induced stress granules. (A) Illustration of full length (FL) GFP-FUS R521G and constructs lacking the following sequences: Gln-Gly-Ser-Tyr-rich (ΔQGSY), Gly-rich (ΔGLY), RNA recognition motif (ΔRRM), and Arg-Gly-Gly-rich (RGG) regions (ΔRGG1 and ΔRGG2). **(B)** Confocal images of HeLa cells transfected with GFP-FUS R521G constructs (green) alone (–) or co-transfected (+) with MBP-M9M, the transportin-1 inhibitor. Note the increased levels of cytoplasmic GFP-FUS in co-transfected cells (compare columns 1 and 2). Confocal fluorescence images of co-transfected cells treated with 0.5 mM sodium arsenite for 1 hr were used to assess the ability of GFP-FUS R521G constructs (green; column 3) to associate with stress granules (G3BP; red; column 4). The greatest degree of GFP and G3BP co-localization was observed in cells expressing FL GFP-FUS R521G, whereas there was minimal co-localization in control cells expressing free GFP (compare panels in column 5). **(C)** Quantitative analysis (see Materials and methods) of **(B)** reveals that constructs lacking RGG domains (ΔRGG1 and ΔRGG2) exhibit impaired localization to stress granules. Statistically significant comparisons include FL and ΔRGG1 (*$P < 0.05$), FL and GFP (**$P < 0.01$), and ΔQGSY and GFP (*$P < 0.05$; not shown on graph for clarity) by one-way ANOVA followed by a Dunnett's post-hoc test on n=3 independent experiments. All error bars represent SEMs. **(D)** Western blot analysis of HeLa cells in **(B)** demonstrates equivalent expression levels for all GFP-FUS R521G constructs.

and a threshold was applied (see Materials and methods) such that all cells included in this analysis expressed similar levels of FUS. Together, these data demonstrate that the RGG domains in FUS are the most important for mutant-FUS localization to stress granules.

Methylation of mutant-FUS is not required for its assembly into stress

In light of the 20 dimethylated arginine residues within the RGG domains of FUS [55], and the fact that arginine dimethylation dictates protein and RNA interactions as

well as protein subcellular localization [56], we explored the possibility that arginine dimethylation of mutant-FUS regulates its association with stress granules. While methylated FUS has been detected within stress granules in cell culture and pathological CNS inclusions from individuals harboring FUS mutations [5], it is not clear whether methylation is actually required for FUS incorporation into these structures. To investigate this question, HeLa cells were pre-treated with the global methyltransferase inhibitor adenosine 2,3-dialdehyde (AdOx) [57] prior to expression of the highly cytoplasmic GFP-FUS R495X mutant and sodium arsenite exposure. We note that conditions (see Materials and methods) were used to minimize GFP-FUS R495X aggregation in these experiments. Immunoprecipitation of GFP-FUS R495X using an anti-GFP antibody, followed by western analysis with the dimethyl-specific ASYM24 antibody, confirmed that GFP-FUS R495X is hypomethylated in the presence of AdOx (Figure 6A). Despite the significant degree of hypomethylation, GFP-FUS R495X maintains a robust association with stress granules under these conditions (Figure 6B and C). Conversely, the overall ASYM24 signal, including the signal within stress granules, is significantly attenuated. Similar results were seen in our stable HEK-293 GFP-FUS R495X line (data not shown). While the small population of methylated GFP-FUS R495X that remains after AdOx treatment (Figure 6A) could be sequestered into stress granules, the significant decrease in ASYM24 signal (i.e., the decrease in signal for methylated proteins) with no decrease in GFP-FUS signal argues against this possibility. Therefore, while methylated mutant-FUS can assemble into stress granules, this post-translational modification is not a prerequisite for its incorporation.

Discussion

The association of cytoplasmically mislocalized ALS-linked FUS mutants with stress granules is well established [5,6,13,26-30], but what affect does mutant-FUS have on the properties of stress granules? We sought to examine the effect of mutant-FUS on the physical properties of stress granules that are potentially linked to function. While there is no functional assay per se for stress granules, they are believed to represent sites of mRNA triage, which influences whether particular mRNA transcripts are retained within stress granules, translated on ribosomes or degraded within P-bodies [20]. There is also evidence that the signaling activity of proteins can be controlled by their sequestration and/or release from stress granules during stress [22]. Thus, the cellular response to stress is modulated, at least in part, by stress granules. Since mutant-FUS, but not WT-FUS, is incorporated into stress granules under various induced stressors, the mutant protein has the potential to disturb stress granules and impair cellular stress response in ways that could contribute to ALS pathogenesis [19].

Stress granules assemble in response to induced stress. Our results show that ALS-linked, cytoplasmic FUS R495X delays the assembly of stress granules in both HEK-293 (Figure 1) and neuronal NSC-34 (Figure 2) cells under conditions of acute oxidative stress. The predominantly nuclear FUS H517Q mutant also delays stress granule assembly, but to a lesser degree than FUS R495X (Figure 1). Therefore, the delay in stress granule assembly correlates with cytoplasmic levels of mutant-FUS, probably because the protein is poised to enter stress granules once stress is induced. Since over-expression of some ALS-FUS mutants reportedly induce the spontaneous formation of cytoplasmic inclusions that stain positively for stress granule markers [28,29], one might expect the expression of mutant-FUS to correlate with a faster rate of stress granule assembly. However, the properties of stress granules are influenced by the nature of the induced stressor [48], and we show that stress granules induced by protein over-expression exhibit different dynamic properties than those induced by sodium arsenite (Additional file 3). We also demonstrate that mutant-FUS accelerates the disassembly of stress granules (Figure 1D). Therefore, expression of mutant-FUS appears to disfavor the formation of and/or destabilizes stress granules, possibly by interfering with protein interactions within these structures (Figure 3). The effects of mutant-FUS on stress granule assembly and disassembly are reminiscent of effects seen during TDP-43 knock-down [37]. Considering that stress granule assembly is a regulated process [20], factors that either delay or accelerate stress granule assembly/disassembly may adversely affect cellular homeostasis.

Interestingly, once stress granules are formed, mutant-FUS exerts an effect on both stress granule morphology and abundance that may appear counterintuitive based on the effect of FUS during the processes of assembly and disassembly. While the expression of GFP-FUS R495X both disfavors stress granule assembly and weakens stress granule associated interactions, under conditions of persistent stress the size and abundance of stress granules is augmented by the expression of mutant-FUS (Figure 4). This increased size and abundance of stress granules does not necessarily mean these structures are held together more tightly, but rather is a likely consequence of the additional protein load associated with these structures from the GFP-FUS R495X protein itself. This rationale may also be relevant to the increased size of stress granules in ALS-linked TDP-43 mutants under conditions of hyperosmolar stress [49] and suggests that this phenotype may be part of a common disease pathway. An intriguing, but not mutually exclusive, possibility is that mutant-FUS and TDP-43 recruit additional protein partners and mRNA substrates into stress granules, thereby further increasing their size

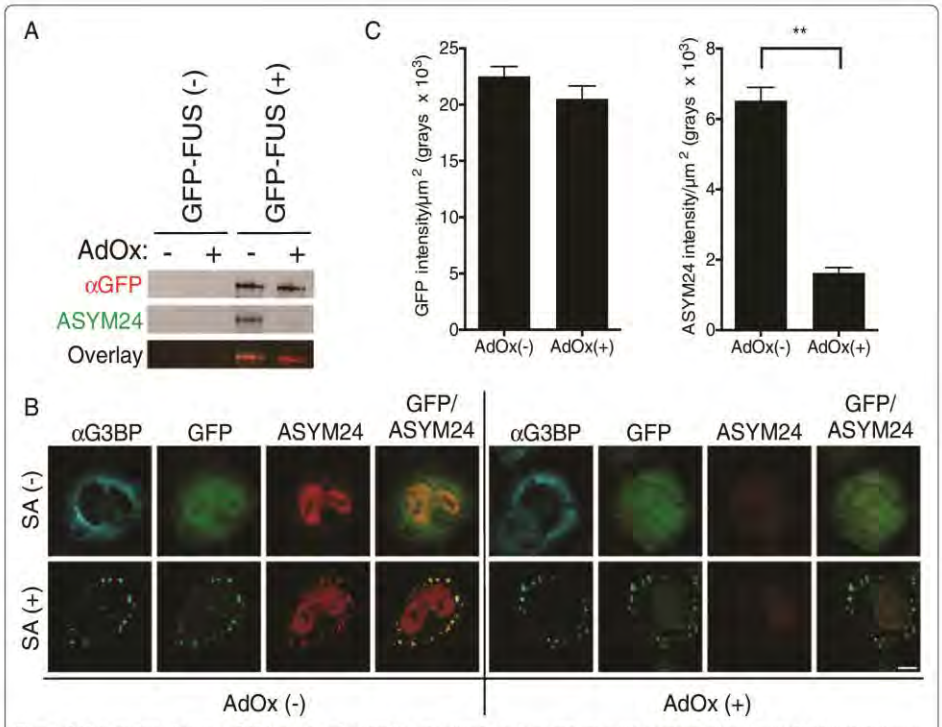

Figure 6 Methylation of mutant-FUS is not required for its assembly into stress granules. HeLa cells transfected with GFP-FUS R495X were pre-treated with the methyltransferase inhibitor adenosine-2,3 dialdehyde (AdOx) and then exposed to sodium arsenite to promote stress granule assembly. **(A)** GFP-FUS R495X was detected by western analysis only for immunoprecipitation (IP) reactions from transfected cells (GFP-FUS (+)). Anti-GFP was used for both IP and western analyses. The ASYM24 antibody revealed that GFP-FUS R495X was hypomethylated on arginine residues when cells were pre-treated with AdOx. **(B)** Confocal fluorescence images revealed a robust association of GFP-FUS R459X with sodium arsenite-induced (SA(+)) stress granules, both in the absence (left panels) and presence (right panels) of AdOx. Conversely, the ASYM24 signal within the same stress granule was dramatically attenuated when cells were pre-treated with AdOx. **(C)** Quantification of n=3 independent experiments from **(B)** further supports the conclusions above. Statistical significance was determined by a Student's t-test (** $P < 0.01$). All error bars represent SEMs.

and abundance (Figure 4 and [25,30]). Indeed, thousands of mRNA transcripts are bound by FUS [58,59] with many distinct mRNAs bound by cytoplasmic mutant-FUS but not WT FUS [59]. Therefore, mutant-FUS may inappropriately process mRNAs and/or facilitate aberrant cytoplasmic protein interactions during stress. The latter possibility is supported by our FRAP analyses, which showed that both mRFP-G3BP and mRFP-T1A-1 exhibit weaker binding and heightened dynamics within sodium arsenite-induced stress granules containing mutant-FUS (Figure 3). In fact, GFP-FUS R495X altered the dynamic properties of stress granules in all of our FRAP experiments, raising the possibility that mutant-FUS interferes with the sorting mechanisms [21,22] associated with these structures under stress.

If the association of mutant-FUS with stress granules does indeed represent a gain of toxic interaction, it will be important to identify factors that modulate this association. Although FUS contains multiple domains that contribute to FUS aggregation [60] and/or are homologous to sequences that direct other proteins into stress granules [26,50-52], our results show that the RGG domains are largely responsible for directing FUS into stress granules (Figure 5). Our results are in general agreement with a recent report by Bentmann et al., which also demonstrated a key role for the RGG domains in assembling FUS into stress granules [26]. However, our results do not support a role for the Gly-rich and RRM domains in this process, whereas the former study did. This discrepancy may be due to the difference in FUS constructs, stressor (sodium

arsenite versus heat shock [26]) and/or the FUS mutation (R521G versus P525L [26]) that were employed in these studies. Whether the RNA-binding ability of FUS is required for its localization to stress granules is not altogether clear [26,27]. Several domains within FUS exhibit RNA-binding capabilities, including the RMM, RGG, and zinc finger domains. Bentmann et al. demonstrated a correlation between cytoplasmic FUS constructs that bound RNA and were incorporated into stress granules, consistent with a role for RNA-binding in the assembly of mutant-FUS into stress granules [26].

That the RGG domains direct mutant-FUS to stress granules raises the possibly that this process is controlled by arginine dimethylation of RGG motifs [61]. Emerging evidence indicates that the RGG motifs within FUS are methylated by protein arginine N-methyltransferase-1 (PRMT1) [55,62,63], and that this post-translational modification can influence the subcellular localization of mutant-FUS [62,63]. While stress granules contain methylated proteins (Figure 6B), and methylated forms of mutant-FUS have been detected in both stress granules and diseased-tissues [5], our data suggests that methylation of FUS is not a prerequisite for its incorporation into stress granules (Figure 6).

How might the incorporation of mutant-FUS into stress granules alter cellular homeostasis under conditions of induced stress, and what are the implications for neurodegenerative disease? We show that mutant-FUS delays stress granule assembly (Figures 1 and 2), decreases the binding of stress granule-associated proteins within stress granules (Figure 3), and increases both size and abundance of stress granules (Figure 4). These physical and dynamic properties of stress granules are thought to be linked to stress granule function, and thus the effects of mutant-FUS may culminate in impaired stress response and, eventually, in neurodegeneration. Although there have been no reports of overt cytotoxicity in mutant-FUS cellular models exposed to sodium arsenite or other stressors, the effects of impaired stress response may appear more distinctly as a function of age, disease progression and/or chronic stress in the human disease [19]. In fact, stress granule marker proteins have been detected within the pathological inclusions of CNS tissues from patients with ALS and FTLD [6,25], supporting the notion that stress response factors are altered during the course of disease. Moreover, these observations raise the possibility that stress granules are precursors to the end-stage aggregates that are characteristic of these diseases [23]. Although our data show that mutant-FUS accelerates stress granule disassembly, under conditions of persistent stress these granules containing mutant-FUS are larger and more numerous and thus have the potential to coalesce into larger aggregates. Extending analyses of stress granules to other models systems, such as human iPS cells from individuals with ALS or ALS rodent models, may allow us to better address whether altered stress granule assembly plays a role in disease onset and/or progression, and whether the association of ALS-linked proteins with stress granules does in fact impact disease.

Conclusions

ALS-linked FUS mutants that mislocalize to the cytoplasm not only incorporate into stress granules under conditions of oxidative stress, but the presence of mutant-FUS in stress granules alters the properties of these structures. Expression of mutant-FUS delays the assembly and expedites the disassembly of stress granules. Furthermore, the morphology and dynamics of these structures is influenced by the presence of mutant-FUS. Therefore, our data are consistent with a gain of toxic function for mutant-FUS with respect to stress granule assembly and dynamics.

Materials and methods

Cell culture and drug treatments

Inducible GFP-FUS expressing FlpIn HEK-293 cells were maintained as described previously [13]. Human cervical carcinoma cells (HeLa) were maintained in Modified Eagle's medium (MEM, Gibco 10370) supplemented with 10% (v/v) heat inactivated fetal bovine serum (Sigma, F4135), 2 mM L-glutamine (Gibco, 25030), and 1% (v/v) penicillin and streptomycin solution (Gibco, 15140). Mouse motor neuron–like hybrid cell lines (NSC-34) [38] constitutively expressing untagged human FUS were maintained in Dulbecco's modified Eagle's medium (Invitrogen, 11965118) supplemented with 10% (v/v) tetracycline-tested fetal bovine serum (Sigma, F6178), and 2 μg/mL puromycin (Invitrogen, A11138-03).

NSC-34 cells constitutively expressing untagged human FUS constructs were generated by lentiviral transduction of the CSCW2-IRES-GFP lentivector (a generous gift from Dr. Miguel Esteves, University of Massachusetts Medical School) containing FUS (WT or mutant R495X). Flow cytometry was used to enrich for expression of the GFP reporter in each line. Cells with equivalent levels of exogenous FUS proteins were employed.

For drug treatments, the following stocks were prepared and stored at freezing temperatures: 50 mg/mL doxycycline (Sigma, D9891) in water (−80°C), 100 mM sodium arsenite (Sigma, 71287) in water (−20°C) and 20 mM adenosine-2,3 dialdehyde ("AdOx"; Sigma, A7154) in water (−20°C). FUS expression in the FlpIn HEK-293 lines was induced with the addition of 1 μg/mL doxycycline for 24 hrs unless otherwise noted. Cells were then exposed to sodium arsenite and/or AdOx as described below.

Plasmids and cloning

The pEmRFP-G3BP and mRFP-TIA-1 plasmids for FRAP analyses were generously provided by Drs. Nancy Kedersha and Paul Anderson (Brigham and Women's Hospital, Harvard Medical School). The mRFP-TIA-1 was subcloned into the low expression lentivirus vector CShPW2 (a gift from Miguel Estevez, UMMS) with NheI and Knp1 restriction sites using BP Clonase II (Invitrogen, 11789–020), thereby creating CShPW2-RFP-TIA-1. MBP-M9M was a kind gift from Dr. Yuh Min Chook (University of Texas Southwestern Medical Center).

GFP-FUS R521G deletion constructs were constructed as follows: PCR amplified full length GFP-FUS R521G, flanked by attB homologous sequences, was cloned into pDONR221 vector (Invitrogen, 12536–017) with BP Clonase II (Invitrogen, 11789–020) to generate the starting plasmid pDONR221:GFP-FUS R521G. To facilitate substitution of the full length gene with deletion/truncation variants, restriction sites for KpnI and XbaI were introduced upstream of the ATG start codon and downstream the TAA stop codon, respectively, using the following primers: **fwd**: GGGGACAAGTTTGTACAAAAAAGCAGGCTGG TACC**ATG**GCCTCAAACGATTATACCC, **rev**: GGGGA CCACTTTGTACAAGAAAGCTGGGTTCTAGA**TTA**AT ACGGCCTCTCCCTGC. To generate deletion constructs, the following primers were designed by joining the upstream and downstream sequences flanking the domain that was deleted: Δ**GLY_fwd**: AGAACCAGTACAACAG CAGCAGTACCATCTTTGTGCAAGGCC; Δ**GLY_rev**: ACTCAATTGTAACATTCTCACCCAGACTGCCAGA CAACAACACCCGGGCAGACTTTAATCGGG; Δ**RR M_rev**: CCACGACCATTGCCACCACCGTTGTTGTC TGAATTATCCTGTTCG; Δ**RGG1_fwd**: CAAGGTCT CATTTGCTACTCGCGCTGGTGACTGGAAGTGTCC; Δ**RGG1_rev**: CATATTCTCACAGGTGGGATTAGGCC GATTAAAGTCTGCCCGGC; Δ**RGG2_fwd**: CCAGTGT AAGGCCCCTAAACCAGATAAGATGGATTCCAGGGG TGAGCAC; Δ**RGG2_rev**: GTGCTCACCCCTGGAATC CATCTTATCTGGTTTAGGGGCCTTACACTGG; Δ**422-526_fwd**: GGGGACAAGTTTGTACAAAAAAGCAGGC TGGTACC**ATG**GCCTCAAACGATTATACCC; Δ**422-526_rev**: GGGGACCACTTTGTACAAGAAAGCTGG GTTCTAGA**TTA**TCGCTGCTGTCCTCCACC. The deletion reactions were performed using the pDONR221: FUS R521G plasmid as template and the QuikChange II Mutagenesis kit (Stratagene; 200523) according to the manufacturer's instructions. For the ΔQGSY truncation construct, PCR was performed using a reverse primer for the full-length R521G gene paired with a forward primer containing the 5'-end sequences of ΔGLY flanked by the restriction enzyme KpnI recognition sequence: Δ**QGSY_fwd**: CAGGCTGGTACCGGTGGTGGAGGTGGAGGT. All constructs were then sub-cloned into the expression vector pDEST-53 (Invitrogen) using Gateway cloning method with LR Clonase II (Invitrogen, 11791–100) according to the manufacturer's instructions.

Immunofluorescence

Standard immunofluorescence protocols were employed as described previously [13]. Briefly, cells were fixed with 4% paraformaldehyde for 10–15 min then blocked with PBSAT (1X PBS/1% BSA/0.5% Triton-X 100) for 30–60 min at ambient temperature. Primary antibodies described in each experiment were diluted in PBSAT and applied to cells at ambient temperature for 1 hr. Primary antibody dilutions were as follows: 1:2000 for mouse anti-G3BP (BD Transduction Labs, 611126), 1:1000 for rabbit anti-G3BP (Proteintech, 130-57-2AP), 1:1500 for rabbit anti-dimethyl arginine ("ASYM24"; Millipore, 07–414) and 1:200 mouse anti-FUS (Santa Cruz, SC-4771). Cells were then incubated with secondary antibodies diluted 1:1000–1:2500 in PBSAT for 45 min at ambient temperature. Secondary antibodies included Dylight 549 conjugated anti-mouse IgG (Jackson ImmunoResearch Labs, 715-505-151), Cy3 conjugated anti-mouse IgG (Jackson ImmunoResearch Labs, 715-165-151), Cy3 conjugated anti-rabbit IgG (Jackson ImmunoResearch Labs, 711-165-152), and Cy5 conjugated anti-mouse IgG (Jackson ImmunoResearch Labs, 715-175-151). GFP signal was enhanced by 1:1000 dilution of Alexa Fluor 488-conjugated rabbit anti-GFP (Invitrogen, A21311). Cells were stained with 34 ng/mL DAPI in dH_2O, and coverslips were mounted with ProLong Gold anti-fade reagent (Invitrogen, P36930).

Western blotting

Standard western blotting protocols were employed as described previously [13]. Primary antibodies described in each experiment were diluted as follows: 1:1000 for mouse anti-GFP (Living Colors; Clontech, 632380), 1:1000 for rabbit anti-dimethyl-arginine ("ASYM24"; Millipore, 07–414), 1:1000 for mouse anti-tubulin (Sigma, T9026), and 1:1000 for rabbit anti-FUS. Rabbit anti-FUS antibodies were generated by GenScript against a C-terminal epitope, using the peptide CKFGGPRDQGSRHDSEQDNSD. Blots were incubated with primary antibodies for 1 hr at ambient temperature or overnight at 4°C. Secondary antibodies, including anti-mouse IRDye 680 (Licor, 926–32220) or IRDye 800 (LiCor, 926–32210) and anti-rabbit IRDye 680 (LiCor, 926–32220) or IRDye 800 (Licor, 926–32211), were diluted 1:10000 and incubated with blots for 1–2 hrs at ambient temperature. Bands were visualized with an Odyssey Infrared Imager (LiCor, Model 9120), and densitometry measurements performed with the Odyssey Software (LiCor, V3.0).

Stress granule assembly and disassembly kinetics

Inducible GFP-FUS (WT, R495X and H517Q) HEK-293 cells were plated on coverslips at a density of 5×10^4

cells/coverslip. The next day, GFP-FUS expression was induced as described above. For stress granule assembly measurements, cells were treated with 0.25 mM sodium arsenite for 40 or 90 min. Coverslips were then fixed and processed for immunofluorescence (IF) with the mouse anti-G3BP and rabbit anti-GFP antibodies listed above. For stress granule disassembly measurements, cells were treated with 0.25 mM sodium arsenite for 60 min, at which time the media containing sodium arsenite was replaced with fresh media. After 90 min in fresh media, cells were processed for IF as described above. The percentage of cells with stress granules was determined as [(the number of cells containing at least one stress granule / total number of cells) × 100]. More than 2000 healthy, interphase, non-crowded cells were counted in multiple (between n=4 and n=11, depending on cell line and condition) independent experiments for both assembly and disassembly conditions. A one-way ANOVA with Tukey's multiple comparisons post-test was used to compare the induced and uninduced groups. Similar parameters were used for assembly kinetics in NSC-34 parent cells and cells expressing untagged human FUS proteins with the following changes: cells were treated with sodium arsenite for 1 hr, and immunofluorescence was performed with the rabbit anti-G3BP and mouse anti-FUS antibodies listed above. More than 2000 cells were counted in at least n=11 independent experiments per condition. Statistical significance was determined by one-way ANOVA with Tukey's multiple comparisons post-test.

Fluorescence recovery after photobleaching

GFP-FUS WT and GFP-FUS R495X HEK-293 cells were plated at a density of 8×10^4 cells/plate in 35 mm glass bottom dishes (MatTek Corp, P35GC-1.5-14-C), allowed to adhere for 48 hrs, then transfected with either CShPW2-RFP-TIA-1 or pEmRFP-G3BP expression plasmids using Lipofectamine 2000 (Invitrogen, 11668–019) according to the manufacturer's instructions with a 1.6 μl Lipo: 3.2 μg DNA ratio. Approximately 23 hr post-transfection, phenol red(−) growth media without (overexpression experiments) or containing 0.2 mM sodium arsenite (stress granule experiments) was applied to the cells for 1 hr prior to FRAP.

FRAP experiments were performed at 37°C as previously described [45]. Multiple cells were analyzed in each experiment over a 30 min period starting at 60 min of sodium arsenite exposure. Experiments were carried out on a Leica SP5 AOBS laser scanning confocal microscope using a 40× 1.3NA water immersion objective or a Leica SP1 system using a 40×, 1.25NA oil immersion objective. No more than two stress granules, from opposite sides of a cell, were individually bleached using a 1-3s laser pulse delivered by a 488 nm or 561 nm laser. A pre-bleach, immediate post-bleach and 16 additional post-bleach images spaced at 5 sec intervals were captured. Leica Confocal Software (Leica Microsystems, Exton, PA) was used to measure fluorescence intensity in the bleached region of interest (ROI), the whole cell, and in a background control area lacking cells at each time point. The data was analyzed and background fluorescence subtracted using Excel. The relative fluorescence intensity (I_{rel}) in the bleached area was calculated as previously shown [45]. Briefly, the following equation was used: $I_{rel,\ t} = (I_t \times (C_0/C_t))-(I_{pbl} \times (C_0/C_{bl}))/(I_0-(I_{pbl} \times (C_0/C_{pbl}))$, where C_0 is the total cellular fluorescence before bleaching, C_{pbl} is the total cellular fluorescence in the post-bleach image, C_t is the total cellular fluorescence at time t, I_0 is the pre-bleach ROI fluorescence intensity, I_t is the ROI fluorescence intensity at time t, and I_{pbl} is the post-bleach ROI fluorescence intensity. The data was normalized using this equation such that the post-bleach ROI fluorescence intensity was set to 0 and the pre-bleach ROI fluorescence intensity to 1. I_t was calculated as the percentage difference between the relative fluorescence asymptote of the recovery curve and a relative recovery of 1, a value that would reflect complete recovery without an immobile fraction. Recovery curves were drawn using Graphpad Prism 6 (Graphpad Software), with individual time points presented as means ± SEMs. Fluorescence recovery half times were calculated from exponential one-phase association curves best fit for the recovery graphs: $F(t) = F_{max}\ (1- e^{-kt})$. Mobile fractions were calculated from the plateau region from each curve, which was identified as the series of data points with < 2% change in slope over time.

At least two independent experiments were performed for all conditions. The total number of stress granules analyzed for each condition is shown in Figure 3. A two-way ANOVA was used to determine statistical significance between the mobile fractions for each of the experiments.

Morphology experiments

Stable GFP-FUS HEK-293 cells were plated and processed for immunofluorescence as described under 'stress granule assembly and disassembly kinetics' above, except that cells were treated with 0.5 mM sodium arsenite for 1 hr. Confocal stacked images (0.2 μm stack step, 4 μm range) were acquired using a Zeiss Axiovert 200 microscope with a PerkinElmer UltraView LAS spinning disc equipped with a 100× phase objective. Imaris analytical software (Bitplane Scientific Software) was used to construct 3D projections of image stacks. Volume measurements were taken of each stress granule with a G3BP fluorescence signal that was at least 2-fold above background. Because P-bodies had an average volume of 0.5 μm^3 (data not shown) by the same analysis, only stress granules with a volume > 0.5 μm^3 were included in the analysis. Data is averaged from three independent experiments per line, using approximately 30 stress granules per condition. Statistical significance was determined using the Student's t-test.

Analysis of FUS deletion constructs in stress granule assembly

HeLa cells were plated on coverslips at a density of 2.5 × 10^4 cells/coverslip and adhered at 37°C for 24 hrs, after which GFP-FUS R521G truncation constructs and MBP-M9M were transiently transfected into cells using Lipofectamine-2000 (Invitrogen, 11668) according to the manufacturer's instructions. Twenty-four hours post transfection, cells were subjected to media containing 0.5 mM sodium arsenite for 1 hr. Cells were processed immunofluorescence with mouse anti-G3BP as described above.

Confocal microscopy was performed using a Solamere Technology Group CSU10B spinning disk confocal system equipped with a Yokogawa CSU10 spinning disk confocal scan head. Image stacks (0.2 μm stack step; 13 stack range) were acquired using a 100× oil objective, a Roper Cool-snap HQ2 camera and MetaMorph V7.6.3 software. Background signal was subtracted by removing fluorescence from a dark-current image (acquired with the laser off) from each raw image. For the GFP images, variations in illumination and detection efficiencies at each pixel were corrected by dividing the dark-adjusted intensities by a normalized flat-field image of a uniformly green fluorescent slide (Chroma Technology, Rockingham, VT, USA) acquired using the same 525/50 nm band-pass filter. Four channels were imaged per cell: FITC for GFP-FUS, Cy3 for G3BP, DAPI for nuclei and phase for cell borders.

The extent of GFP-FUS incorporation into stress granules was analyzed with MetaMorph V7.6.3 software using the Integrated Morphometry Analysis tool. Since cells with a GFP signal brighter than 1.5 × 10^6 grays/μm^2 tended to form cytoplasmic aggregates *a priori* of arsenite treatment (data not shown), only transfected cells with GFP-FUS expression levels < 1.5 × 10^6 grays/μm^2 were selected for analysis. Stress granules were selected using the Cy3 (G3BP) channel as a reference. The slice corresponding to the center of the stress granule was selected from each image stack. Stress granules with an area of at least 0.5 μm^2 were selected. An outline was drawn around each G3BP granule, and this outline was then transferred to the corresponding FITC (GFP-FUS) image, such that the GFP-FUS signal intensity ("stress granules intensity") within that granule could be measured. GFP signal intensity measurements were also acquired in the region proximal to the stress granule, and was referred to as the "Diffuse intensity". The ratio of stress granule intensity (i.e., GFP-FUS inside the stress granule) to diffuse intensity (i.e., GFP-FUS outside the stress granule) was determined for a total of 75–150 stress granules per construct over three independent experiments. Statistical significance was determined by a one-way ANOVA followed by a Dunnett's post hoc test in Graphpad Prism 6 (Graphpad software).

Methyltransferase inhibition studies

HeLa cells were plated at a density of 2.5 × 10^4 cells/coverslip and adhered for 24 hrs, after which GFP-FUS R495X expression constructs were transiently transfected with Lipofectamine-2000 either with or without 25 μM AdOx for 24 hr. Cells were then exposed to 0.5 mM sodium arsenite for 1 hr, and coverslips were processed for immunofluorescence using the mouse anti-G3BP rabbit and ASYM24 antibodies as described above. For quantification, confocal images of 30 cells per condition across three independent experiments were taken, and the intensity of GFP-FUS and ASYM24 signal within stress granules was determined between AdOx-treated and untreated conditions using MetaMorph as described above. Statistical significance was determined using a Student's t-test.

For GFP immunoprecipitation (IP) reactions, cells were lysed for 15 min in IP buffer (400 μL 1% NP-40 (MP Biomedicals, 198596)/50 mM Tris–HCl (Sigma T3253-500G)/5 mM EDTA (Fisher E478-500)/150 mM NaCl and 10% v/v glycerol (Acros 15982–0010) in water; pH 7.5), and centrifuged at 13000 rpm for 15 min at 4°C. The supernatant was pre-cleared with 50 μL Biomag Protein G beads (Qiagen, 311812) for 2 hrs at 4°C. Anti-GFP-coated beads for each sample were prepared by incubating 0.5 μL of anti-GFP (Abcam, ab290) in 400 μL of IP buffer with 50 μL Biomag Protein G beads for 2 hrs at 4°C. IP reactions were performed at 4°C overnight with 100 μg of pre-cleared lysate. Protein elution was accomplished with 50 μL 1X SDS loading buffer (Boston Bioproducts BP11R) for 5 min at 95°C, and 20 μL of sample was subjected to western blot analysis with mouse anti-GFP, mouse anti-tubulin and ASYM24 as described above.

Additional files

Additional file 1: A minor fraction of GFP-FUS H517Q incorporates into stress granules in response to sodium arsenite. Images for the indicated GFP-FUS cell line (top 3 rows) were collected as described in Figure 1A. Antibody markers used for immunofluorescence are indicated on the left. Images overexposed for GFP detection (bottom row) reveal that a minor fraction of GFP-FUS H517Q (green) co-localizes with G3BP-positive stress granules (red). FUS H517Q containing stress granules are denoted by arrows. Conversely, GFP-FUS WT is not detected in stress granule (i.e., there is no GFP-positive signal that co-localized with G3BP), even with high exposure. Scale bar = 5 μm.

Additional file 2: NSC-34 cells expressing untagged human FUS WT and R495X exhibit similar transduction efficiencies. Fluorescent images of the GFP reporter (green) in NSC-34 cells transduced with lentivirus containing untagged human FUS WT or R495X. Transduction efficiencies of approximately 100% were determined for both lines. Cellular nuclei are stained with DAPI (blue). Scale bar = 20 μm.

Additional file 3: Sodium arsenite induced stressed granules display different dynamics compared to those induced by mRFP-G3BP over-expression. (A) Transfection of mRFP-G3BP was sufficient to induce G3BP positive stress granules in a subset of both GFP-FUS WT and GFP-FUS R495X cells as determined by live cell imaging. Scale bar = 20 μm. **(B)** The FRAP recovery curve for mRFP-G3BP inside the stress granule

in (A) was different depending on whether mRFP-G3BP was transfected into GFP-FUS WT (blue circle) or R495X (red square) expressing cells. Note the trend is opposite from sodium arsenite-induced stress granule in Figure 3. **(C)** Quantification of the mobile fraction from the recovery curves in (B) compared to those in Figure 3G revealed that expression of GFP-FUS R495X significantly increased mRFP-G3BP binding (i.e., smaller mobile fraction) to stress granules in the over-expression condition compared to all other conditions. Asterisks indicate statistically significant differences between cell lines as determined by two-way ANOVA (****$P < 0.0001$) on data from n=3 independent experiments. Additional significant comparisons include, but are not shown for clarity: WT in the overexpression versus WT in the sodium arsenite condition ($P < 0.05$); R495X in the overexpression versus R495X in the sodium arsenite condition ($P < 0.0001$); R495X in the overexpression versus WT in the sodium arsenite condition ($P < 0.05$). The total number (N) of stress granules analyzed is indicated. All error bars represent SEMs.

Competing interests
The authors declare that they have no competing interests.

Authors' contributions
DB, LK, and CW planned and performed the majority of experiments; DB, AJQ and JAN planned, performed and analyzed data for FRAP; RJC cloned deletion constructs for structure-function analyses; RRKS and KB contributed to the design and data interpretation for experiments; DB, LK and DAB wrote the paper. All authors read and approved the final manuscript.

Acknowledgements
We thank Dr. Zuoshang Xu for his critical review of the manuscript, Dr. John Landers for helpful discussion, Dr. Paul Furcinitti of the UMass Medical School Core Digital Imaging Facility for his assistance with the confocal microscopy, Dr. Miguel Esteves (University of Massachusetts Medical School) for the CSCW2-IRES-GFP lentivector and production of lentivirus, Drs. Nancy Kedersha and Paul Anderson (Brigham and Women's Hospital, Harvard Medical School) for the pEmRFP-G3BP and mRFP-TIA-1 plasmids, Dr. Yuh Min Chook (University of Texas Southwestern Medical Center) for the MBP-M9M plasmid, Drs. Zuoshang Xu and Stephen Doxsey (University of Massachusetts Medical School) for use of their microscopes, and Nathan Lemay for his assistance with experiments. We acknowledge financial support from the ALS Therapy Alliance-CVS Pharmacy (DAB), ALS Association (DAB), the Worcester Foundation (DAB), and the US National Institutes of Health/National Institute on Neurological Disorders and Stroke (R01NS067206-01 and R01NS078145-01; DAB).

Author details
[1]Department of Neurology, University of Massachusetts Medical School, Worcester, MA, USA. [2]Department of Cell and Developmental Biology, University of Massachusetts Medical School, Worcester, MA, USA. [3]Department of Biochemistry and Molecular Pharmacology, University of Massachusetts Medical School, Worcester, MA, USA.

Received: 16 April 2013 Accepted: 27 August 2013
Published: 31 August 2013

References

1. Calvio C, Neubauer G, Mann M, Lamond AI: **Identification of hnRNP P2 as TLS/FUS using electrospray mass spectrometry.** *RNA* 1995, **1**:724–733.
2. Kwiatkowski TJ Jr, Bosco DA, Leclerc AL, Tamrazian E, Vanderburg CR, Russ C, Davis A, Gilchrist J, Kasarskis EJ, Munsat T, *et al*: **Mutations in the FUS/TLS gene on chromosome 16 cause familial amyotrophic lateral sclerosis.** *Science* 2009, **323**:1205–1208.
3. Vance C, Rogelj B, Hortobagyi T, De Vos KJ, Nishimura AL, Sreedharan J, Hu X, Smith B, Ruddy D, Wright P, *et al*: **Mutations in FUS, an RNA processing protein, cause familial amyotrophic lateral sclerosis type 6.** *Science* 2009, **323**:1208–1211.
4. Bosco DA, Landers JE: **Genetic determinants of amyotrophic lateral sclerosis as therapeutic targets.** *CNS Neurol Disord Drug Targets* 2010, **9**:779–790.
5. Dormann D, Madl T, Valori CF, Bentmann E, Tahirovic S, Abou-Ajram C, Kremmer E, Ansorge O, Mackenzie IR, Neumann M, Haass C: **Arginine methylation next to the PY-NLS modulates Transportin binding and nuclear import of FUS.** *EMBO J* 2012, **31**:4258–4275.
6. Dormann D, Rodde R, Edbauer D, Bentmann E, Fischer I, Hruscha A, Than ME, Mackenzie IR, Capell A, Schmid B, *et al*: **ALS-associated fused in sarcoma (FUS) mutations disrupt Transportin-mediated nuclear import.** *EMBO J* 2010, **29**:2841–2857.
7. Andersson MK, Stahlberg A, Arvidsson Y, Olofsson A, Semb H, Stenman G, Nilsson O, Aman P: **The multifunctional FUS, EWS and TAF15 proto-oncoproteins show cell type-specific expression patterns and involvement in cell spreading and stress response.** *BMC Cell Biol* 2008, **9**:37.
8. Zinszner H, Sok J, Immanuel D, Yin Y, Ron D: **TLS (FUS) binds RNA in vivo and engages in nucleo-cytoplasmic shuttling.** *J Cell Sci* 1997, **110**(Pt 15):1741–1750.
9. Fujii R, Okabe S, Urushido T, Inoue K, Yoshimura A, Tachibana T, Nishikawa T, Hicks GG, Takumi T: **The RNA binding protein TLS is translocated to dendritic spines by mGluR5 activation and regulates spine morphology.** *Curr Biol* 2005, **15**:587–593.
10. Fujii R, Takumi T: **TLS facilitates transport of mRNA encoding an actin-stabilizing protein to dendritic spines.** *J Cell Sci* 2005, **118**:5755–5765.
11. Lagier-Tourenne C, Polymenidou M, Hutt KR, Vu AQ, Baughn M, Huelga SC, Clutario KM, Ling SC, Liang TY, Mazur C, *et al*: **Divergent roles of ALS-linked proteins FUS/TLS and TDP-43 intersect in processing long pre-mRNAs.** *Nature Neurosci* 2012, **15**:1488–1497.
12. Halliday G, Bigio EH, Cairns NJ, Neumann M, Mackenzie IR, Mann DM: **Mechanisms of disease in frontotemporal lobar degeneration: gain of function versus loss of function effects.** *Acta Neuropathol* 2012, **124**:373–382.
13. Bosco DA, Lemay N, Ko HK, Zhou H, Burke C, Kwiatkowski TJ Jr, Sapp P, McKenna-Yasek D, Brown RH Jr, Hayward LJ: **Mutant FUS proteins that cause amyotrophic lateral sclerosis incorporate into stress granules.** *Human Mol Genet* 2010, **19**:4160–4175.
14. Ishigaki S, Masuda A, Fujioka Y, Iguchi Y, Katsuno M, Shibata A, Urano F, Sobue G, Ohno K: **Position-dependent FUS-RNA interactions regulate alternative splicing events and transcriptions.** *Sci Rep* 2012, **2**:529.
15. Rogelj B, Easton LE, Bogu GK, Stanton LW, Rot G, Curk T, Zupan B, Sugimoto Y, Modic M, Haberman N, *et al*: **Widespread binding of FUS along nascent RNA regulates alternative splicing in the brain.** *Sci Rep* 2012, **2**:603.
16. Tan AY, Riley TR, Coady T, Bussemaker HJ, Manley JL: **TLS/FUS (translocated in liposarcoma/fused in sarcoma) regulates target gene transcription via single-stranded DNA response elements.** *Proc Natl Acad Sci U S A* 2012, **109**:6030–6035.
17. Wang X, Arai S, Song X, Reichart D, Du K, Pascual G, Tempst P, Rosenfeld MG, Glass CK, Kurokawa R: **Induced ncRNAs allosterically modify RNA-binding proteins in cis to inhibit transcription.** *Nature* 2008, **454**:126–130.
18. Da Cruz S, Cleveland DW: **Understanding the role of TDP-43 and FUS/TLS in ALS and beyond.** *Curr Opin Neurobiol* 2011, **21**:904–919.
19. Dormann D, Haass C: **TDP-43 and FUS: a nuclear affair.** *Trends Neurosci* 2011, http://www.ncbi.nlm.nih.gov/pubmed/21700347.
20. Anderson P, Kedersha N: **Stress granules: the Tao of RNA triage.** *Trends Biochem Sci* 2008, **33**:141–150.
21. Kedersha N, Anderson P: **Stress granules: sites of mRNA triage that regulate mRNA stability and translatability.** *Biochem Soc Trans* 2002, **30**:963–969.
22. Wippich F, Bodenmiller B, Trajkovska MG, Wanka S, Aebersold R, Pelkmans L: **Dual specificity kinase DYRK3 couples stress granule condensation/dissolution to mTORC1 signaling.** *Cell* 2013, **152**:791–805.
23. Wolozin B: **Regulated protein aggregation: stress granules and neurodegeneration.** *Mol Neurodegener* 2012, **7**:56.
24. Fujita K, Ito H, Nakano S, Kinoshita Y, Wate R, Kusaka H: **Immunohistochemical identification of messenger RNA-related proteins in basophilic inclusions of adult-onset atypical motor neuron disease.** *Acta Neuropathol* 2008, **116**:439–445.
25. Liu-Yesucevitz L, Bilgutay A, Zhang YJ, Vanderwyde T, Citro A, Mehta T, Zaarur N, McKee A, Bowser R, Sherman M, *et al*: **Tar DNA binding protein-43 (TDP-43) associates with stress granules: analysis of cultured cells and pathological brain tissue.** *PloS One* 2010, **5**:e13250.
26. Bentmann E, Neumann M, Tahirovic S, Rodde R, Dormann D, Haass C: **Requirements for stress granule recruitment of fused in sarcoma (FUS) and TAR DNA-binding protein of 43 kDa (TDP-43).** *J Biol Chem* 2012, **287**:23079–23094.

27. Daigle JG, Lanson NA Jr, Smith RB, Casci I, Maltare A, Monaghan J, Nichols CD, Kryndushkin D, Shewmaker F, Pandey UB: **RNA-binding ability of FUS regulates neurodegeneration, cytoplasmic mislocalization and incorporation into stress granules associated with FUS carrying ALS-linked mutations.** *Human Mol Genet* 2013.
28. Gal J, Zhang J, Kwinter DM, Zhai J, Jia H, Jia J, Zhu H: **Nuclear localization sequence of FUS and induction of stress granules by ALS mutants.** *Neurobiol Aging* 2010, **32**:2323.e27-40.
29. Ito D, Seki M, Tsunoda Y, Uchiyama H, Suzuki N: **Nuclear transport impairment of amyotrophic lateral sclerosis-linked mutations in FUS/TLS.** *Ann Neurol* 2011, **69**:152–162.
30. Vance C, Scotter EL, Nishimura AL, Troakes C, Mitchell JC, Kathe C, Urwin H, Manser C, Miller CC, Hortobagyi T, *et al*: **ALS mutant FUS disrupts nuclear localisation and sequesters wild-type FUS within cytoplasmic stress granules.** *Human Mol Genet* 2013, **22**:2676–2688.
31. Aulas A, Stabile S, Vande Velde C: **Endogenous TDP-43, but not FUS, contributes to stress granule assembly via G3BP.** *Mol Neurodegener* 2012, **7**:54.
32. Kedersha N, Cho MR, Li W, Yacono PW, Chen S, Gilks N, Golan DE, Anderson P: **Dynamic shuttling of TIA-1 accompanies the recruitment of mRNA to mammalian stress granules.** *J Cell Biol* 2000, **151**:1257–1268.
33. Rodriguez VM, Carrizales L, Jimenez-Capdeville ME, Dufour L, Giordano M: **The effects of sodium arsenite exposure on behavioral parameters in the rat.** *Brain Res Bull* 2001, **55**:301–308.
34. Tabocova S, Hunter ES 3rd, Gladen BC: **Developmental toxicity of inorganic arsenic in whole embryo: culture oxidation state, dose, time, and gestational age dependence.** *Toxicol Appl Pharmacol* 1996, **138**:298–307.
35. Sama RR, Ward CL, Kaushansky LJ, Lemay N, Ishigaki S, Urano F, Bosco DA: **FUS/TLS assembles into stress granules and is a prosurvival factor during hyperosmolar stress.** *J Cell Physiol* 2013, **228**:2222–2231.
36. Kedersha N, Anderson P: **Mammalian stress granules and processing bodies.** *Methods Enzymol* 2007, **431**:61–81.
37. McDonald KK, Aulas A, Destroismaisons L, Pickles S, Beleac E, Camu W, Rouleau GA, Vande Velde C: **TAR DNA-binding protein 43 (TDP-43) regulates stress granule dynamics via differential regulation of G3BP and TIA-1.** *Human Mol Genet* 2011.
38. Cashman NR, Durham HD, Blusztajn JK, Oda K, Tabira T, Shaw IT, Dahrouge S, Antel JP: **Neuroblastoma x spinal cord (NSC) hybrid cell lines resemble developing motor neurons.** *Dev Dyn* 1992, **194**:209–221.
39. Huang C, Zhou H, Tong J, Chen H, Liu YJ, Wang D, Wei X, Xia XG: **FUS transgenic rats develop the phenotypes of amyotrophic lateral sclerosis and frontotemporal lobar degeneration.** *PLoS Genet* 2011, **7**:e1002011.
40. Ju S, Tardiff DF, Han H, Divya K, Zhong Q, Maquat LE, Bosco DA, Hayward LJ, Brown RH Jr, Lindquist S, *et al*: **A Yeast Model of FUS/TLS-Dependent Cytotoxicity.** *PLoS Biol* 2011, **9**:e1001052.
41. Lanson NA Jr, Maltare A, King H, Smith R, Kim JH, Taylor JP, Lloyd TE, Pandey UB: **A Drosophila model of FUS-related neurodegeneration reveals genetic interaction between FUS and TDP-43.** *Human Mol Genet* 2011, **20**:2510–2523.
42. Guil S, Long JC, Caceres JF: **hnRNP A1 relocalization to the stress granules reflects a role in the stress response.** *Mol Cell Biol* 2006, **26**:5744–5758.
43. Kedersha N, Stoecklin G, Ayodele M, Yacono P, Lykke-Andersen J, Fritzler MJ, Scheuner D, Kaufman RJ, Golan DE, Anderson P: **Stress granules and processing bodies are dynamically linked sites of mRNP remodeling.** *J Cell Biol* 2005, **169**:871–884.
44. Nickerson JA: **The biochemistry of RNA metabolism studied in situ.** *RNA Biol* 2009, **6**:25–30.
45. Quaresma AJ, Sievert R, Nickerson JA: **Regulation of mRNA Export by the PI3 kinase / AKT Signal Transduction Pathway.** *Mol Biol Cell* 2013.
46. Buchan JR, Parker R: **Eukaryotic stress granules: the ins and outs of translation.** *Mol Cell* 2009, **36**:932–941.
47. Tourrière H, Chebli K, Zekri L, Courselaud B, Blanchard JM, Bertrand E, Tazi J: **The RasGAP-associated endoribonuclease G3BP assembles stress granules.** *J Cell Biol* 2003, **160**:823–831.
48. Buchan JR, Yoon JH, Parker R: **Stress-specific composition, assembly and kinetics of stress granules in Saccharomyces cerevisiae.** *J Cell Sci* 2011, **124**:228–239.
49. Dewey CM, Cenik B, Sephton CF, Dries DR, Mayer P, Good SK, Johnson BA, Herz J, Yu G: **TDP-43 is directed to stress granules by sorbitol, a novel physiological osmotic and oxidative stressor.** *Mol Cell Biol* 2010, **31**:1098–1108.
50. De Leeuw F, Zhang T, Wauquier C, Huez G, Kruys V, Gueydan C: **The cold-inducible RNA-binding protein migrates from the nucleus to cytoplasmic stress granules by a methylation-dependent mechanism and acts as a translational repressor.** *Experimental Cell Res* 2007, **313**:4130–4144.
51. Kedersha NL, Gupta M, Li W, Miller I, Anderson P: **RNA-binding proteins TIA-1 and TIAR link the phosphorylation of eIF-2 alpha to the assembly of mammalian stress granules.** *J Cell Biol* 1999, **147**:1431–1442.
52. Rajyaguru P, She M, Parker R: **Scd6 targets eIF4G to repress translation: RGG motif proteins as a class of eIF4G-binding proteins.** *Mol Cell* 2012, **45**:244–254.
53. Iko Y, Kodama TS, Kasai N, Oyama T, Morita EH, Muto T, Okumura M, Fujii R, Takumi T, Tate S, Morikawa K: **Domain architectures and characterization of an RNA-binding protein, TLS.** *J Biol Chem* 2004, **279**:44834–44840.
54. Cansizoglu AE, Lee BJ, Zhang ZC, Fontoura BM, Chook YM: **Structure-based design of a pathway-specific nuclear import inhibitor.** *Nat Struct Mol Biol* 2007, **14**:452–454.
55. Rappsilber J, Friesen WJ, Paushkin S, Dreyfuss G, Mann M: **Detection of arginine dimethylated peptides by parallel precursor ion scanning mass spectrometry in positive ion mode.** *Anal Chem* 2003, **75**:3107–3114.
56. Bedford MT, Clarke SG: **Protein arginine methylation in mammals: who, what, and why.** *Molecular cell* 2009, **33**:1–13.
57. Grant AJ, Lerner LM: **Dialdehydes derived from adenine nucleosides as substrates and inhibitors of adenosine aminohydrolase.** *Biochemistry* 1979, **18**:2838–2842.
58. Colombrita C, Onesto E, Megiorni F, Pizzuti A, Baralle FE, Buratti E, Silani V, Ratti A: **TDP-43 and FUS RNA-binding proteins bind distinct sets of cytoplasmic messenger RNAs and differently regulate their post-transcriptional fate in motoneuron-like cells.** *J Biol Chem* 2012, **287**:15635–15647.
59. Hoell JI, Larsson E, Runge S, Nusbaum JD, Duggimpudi S, Farazi TA, Hafner M, Borkhardt A, Sander C, Tuschl T: **RNA targets of wild-type and mutant FET family proteins.** *Nat Struct Mol Biol* 2011, **18**:1428–1431.
60. Sun Z, Diaz Z, Fang X, Hart MP, Chesi A, Shorter J, Gitler AD: **Molecular Determinants and Genetic Modifiers of Aggregation and Toxicity for the ALS Disease Protein FUS/TLS.** *PLoS Biol* 2011, **9**:e1000614.
61. Rajyaguru P, Parker R: **RGG motif proteins: modulators of mRNA functional states.** *Cell Cycle* 2012, **11**:2594–2599.
62. Tradewell ML, Yu Z, Tibshirani M, Boulanger MC, Durham HD, Richard S: **Arginine methylation by PRMT1 regulates nuclear-cytoplasmic localization and toxicity of FUS/TLS harbouring ALS-linked mutations.** *Human Mol Genet* 2012, **21**:136–149.
63. Yamaguchi A, Kitajo K: **The Effect of PRMT1-Mediated Arginine Methylation on the Subcellular Localization, Stress Granules, and Detergent-Insoluble Aggregates of FUS/TLS.** *PloS One* 2012, **7**:e49267.

doi:10.1186/1750-1326-8-30
Cite this article as: Baron *et al.*: Amyotrophic lateral sclerosis-linked FUS/TLS alters stress granule assembly and dynamics. *Molecular Neurodegeneration* 2013 **8**:30.

PREFACE TO APPENDIX IV:

The work presented in this appendix was performed by Catherine L. Ward with the following exceptions:

Mass spectrometry analysis was performed by either Murat Karabacak (previously of Jeffery Agar's lab, Brandeis University) or John Leszyk (UMMS, mass spectrometry core facility) and p38α activity was determined by Sun Kyong Lee (previously of Gerardo Morfini's lab, University of Illinois at Chicago).

APPENDIX IV: EXPRESSION, PURIFICATION AND CHARACTERIZATION OF ACTIVATED P38 MAPK FROM E-COLI

Abstract

P38α is a ubiquitously expressed mitogen-activated protein kinase (MAPK) involved in a diverse set of physiological and disease-related processes including the control of gene expression, apoptotic cell death, inflammation, tumorigenesis and neurodegeneration. *In vivo*, p38α activation involves dual phosphorylation of a threonine and tyrosine residue within its activation loop by either upstream MAPKs or through autophosphorylation. However, singly phosphorylated p38α or p38α with phosphomimetic mutations also exhibit kinase activity, indicating dual phosphorylation is not an absolute requirement for activity. Here, we report single and double phosphorylation of recombinant p38α expressed in *Escherichia coli*. This result is unexpected, since mammalian recombinant proteins are not typically phosphorylated when expressed in *Escherichia coli*. We describe a simple procedure to produce a relatively large, highly purified source of active p38α. This procedure involves a few simple steps, and does not require ion exchange chromatography or sophisticated protein purification equipment. While commercially available sources of p38α activated by upstream MAPKs *in vitro* are commercially available, an economic source of active p38α that can be produced in most basic science laboratories is expected to benefit many fields of biomedical research.

Introduction

P38 mitogen-activated protein kinase (MAPK) is a member of the MAPK superfamily that also includes extracellular signal-regulated kinases (ERKs) and c-jun N-terminal kinases (JNKs) (Krishna and Narang, 2008). P38 MAPKs and JNKs are also known as stress-activated protein kinases (SAPKs) because they are activated in response to cellular stressors such as oxidative stress, inducers of DNA damage, and proinflammatory cytokines (Krishna and Narang, 2008). Of the four isoforms of p38 that include p38α, p38β, p38γ and p38δ, p38α has been the most extensively studied. Activation of p38α is generally accomplished by upstream kinases called MAPK kinases (MKKs), which phosphorylate both the Thr and Tyr residues within the activation loop sequence Thr-Gly-Tyr. MKKs are in turn phosphorylated and thus activated by MAPK kinase kinases (MKKKs); together the MAPKs, MAPKKs and MAPKKKs comprise a MAPK signaling cascade (Zarubin and Han, 2005). P38α can also become activated by factors outside of this MAPK signaling cascade. For example, TAB-1 (transforming growth factor-b-activated protein kinase 1) binds and induces the autophosphorylation of p38α (Ge et al., 2002). P38α substrates include various transcription factors, kinases and cytoskeletal proteins. A role for active p38α has been reported in several biological processes including gene regulation, inflammation, apoptosis and cell cycle (Krishna and Narang, 2008), as well as in human diseases such as cancer and neurodegeneration (Morfini et al., 2009; Kim and Choi, 2010).

In light of the important roles that p38α plays in various pathways, including our recent finding that p38α may play a role in amyotrophic lateral sclerosis (ALS) pathogenesis (Morfini et al., 2009; Bosco et al., 2010b), we sought to express and purify recombinant p38α for biochemical studies. Unexpectedly, we discovered that p38α is phosphorylated during its expression in *Escherichia coli*, in a manner independent of upstream mammalian MKKs. Thus, p38α might represent a rare example of a mammalian protein that is post-translationally modified by one or more *E. coli* kinase(s). Significantly, phosphorylated p38α isolated from our preparations displays kinase activity, and may therefore substitute commercially available forms of activated p38α that are too costly for many laboratories. To ensure that most basic science labs benefit from this finding, we describe a straightforward protocol to isolate milligram quantities of highly purified, active p38α. Importantly, this protocol does not require a protein purification instrument, such as an FPLC. An economic source of active p38α is expected to benefit laboratories studying the biological functions of this kinase.

Results

Expression and purification of p38α MAPK from E. coli. His-tagged p38α was expressed and purified using a strategy similar to previous methods ((Wang et al., 1997; Bukhtiyarova et al., 2004) and *Materials and Methods*). In agreement with previous reports (Bukhtiyarova et al., 2004), we obtained significantly

greater yields of p38α when expressed in *E. coli* Rosetta (DE3) cells compared to *E. coli* BL21(DE3) cells (data not shown), with an average yield of 10-15 mg of protein per liter of bacterial culture. The cobalt-based TALON resin, as opposed to a more common nickel-based resin, was employed for affinity purification of his-p38α. While TALON resin is advertized to prevent non-specific binding of host proteins, the purity of his-p38α was only ~85% after the first TALON purification step **(Figure AIV-1, lane 2 and 2a)**. Next, we employed the commercially available thrombin protease to cleave the his-tag, and reapplied the thrombin/his-p38α cleavage reaction to the TALON resin. Tag-free p38α was eluted in the flow-through of this chromatography step with a purity of ~95% as assessed by SDS-PAGE and Coomassie Brilliant blue staining **(Figure AIV-1, lane 3)**. Non-specific host proteins and uncleaved p38α were both retained by the TALON resin **(Figure AIV-1, lane 4)**. Residual thrombin was removed by applying the tag-free p38α to a Benzamidine column, which removes serine proteases such as thrombin **(Figure AIV-1, lane 5)**.

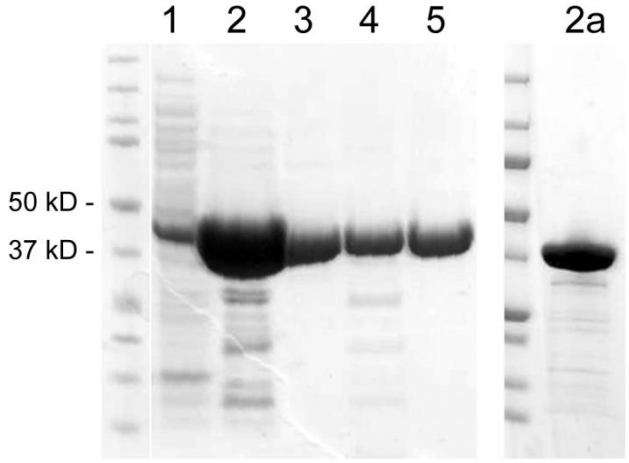

Figure AIV-1. Expression and purification of p38α MAPK from *E. coli*. His-tagged p38α was expressed and purified as described in *Materials and Methods*. Samples from several steps of the purification process were subjected to SDS-PAGE and Coomassie Brilliant blue staining and assessed for purity. Lane 1 shows a sample of the unpurified lysate from *E. coli* induced to express his-tagged p38α. This lysate was applied to a TALON resin column and imidazole-eluted proteins are shown in lane 2, with the most abundant species corresponding to the expected molecular weight (~43,300 kDa) of his-tagged p38α. Eluted proteins were subjected to Thrombin protease treatment to cleave the his-tag from p38α and then reapplied to the TALON column. Tag-free p38α eluted in the flow-through (lane 3), whereas uncleaved his-tagged p38α and non-specific host-proteins were bound to the TALON resin and eluted with imidazole (lane 4). The protein eluting in the flow-through (lane 3) was applied to a Benzamidine column to remove the Thrombin (lane 5). A more diluted sample corresponding to lane 2 is shown in lane 2a such that pure p38α (lane 5) can be directly compared to impure p38α after the first TALON column.

Other purification procedures have been reported for his-p38α and untagged p38α, however these require additional chromatography steps and generally employ an anion exchange column with a salt gradient (Wang et al., 1997; Keesler et al., 1998; Bukhtiyarova et al., 2004; Diskin et al., 2004). We show here that simply removing the his-tag eliminates the non-specific host proteins that bind to the TALON resin. Because our protocol can easily be carried out in batch-mode or with gravity filtration, we expect this protocol to be particularly useful for molecular biology laboratories researching p38α, but that lack protein purification technology such as a fast protein liquid chromatography (FPLC) system. Moreover, a tag-free protein is advantageous for biological and biophysical assays wherein a tag could potentially interfere with the experiment.

Recombinant p38α expressed in E. coli is phosphorylated. We expressed and purified p38α with the intention of performing *in vitro* activation assays. Western blot analysis using an antibody raised against a peptide sequence including phosphorylated Thr180 and Try182 residues of p38α suggested that at least a fraction of p38α from our *E. coli* preparation was dually phosphorylated **(Figure AIV-2A, lane 1)**. Treatment of p38α with lambda protein phosphatase, which removes phosphate groups from serine, threonine and tyrosine residues, abolished this immunoreactivity **(Figure AIV-2A, lane 2)**, further supporting the presence of phosphorylated p38α in our preparations.

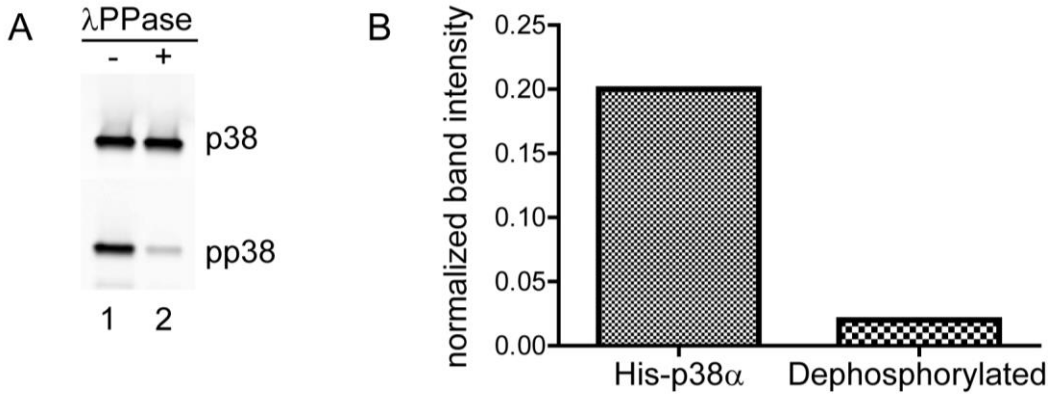

Figure AIV-2. The activation loop of his-p38α isolated from *E. coli* is phosphorylated. Purified his-p38α was dephosphorylated using lambda protein phosphatase as described in *Materials and Methods*. **(A)** Both untreated and dephosphorylated p38α (lanes 1 and 2 respectively), were analyzed by western blotting. Similar p38α loading was confirmed using a phosphorylation-independent anti-p38 antibody from Sigma (p38). In contrast, a phosphorylation-dependent anti-p38 antibody (p-p38) raised against a phosphopeptide containing Thr180 and Tyr182 showed reduced immunoreactivity in lambda phosphatase-treated samples, compared to untreated samples. **(B)** Quantification of the data in **A** is shown. The densitometry of the pp38 bands in lanes 1 and 2 are normalized to the total amount of p38α detected using the phosphorylation-independent anti-p38antibody (p38). A ~100-fold reduction in p-p38 immunoreactivity was seen in lambda phosphatase-treated samples, compared to control, untreated samples.

Fourier-transform mass spectrometry (FT-MS), which provides a high mass-accuracy and high resolution relative to most mass spectrometry techniques (Scigelova et al., 2011), was employed to confirm the phosphorylation status of p38α. The FT-MS spectrum revealed unphosphorylated (m/z 43,319), monophosphorylated (m/z 43,399) and bisphosphorylated (m/z 43,479) p38α peptide species **(Figure AIV-3)**. While it is not possible to quantify the exact ratio of each species based on their relative intensities in the mass spectrum, the unphosphorylated species appears to be present at the highest relative abundance and the bisphosphorylated form at the lowest relative abundance.

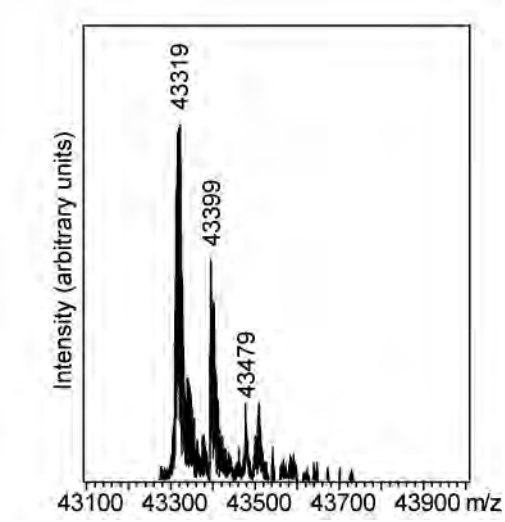

Figure AIV-3. Fourier-transform mass spectrometry confirms that p38α MAPK isolated from *E. coli* is phosphorylated. Shown is the charge deconvoluted FT-MS spectrum that was reconstructed as charge +1 (Data Analysis, Bruker Daltonics). The spectrum reveals the presence of unphosphorylated (average *m/z* 43,319), monophosphorylated (average *m/z* 43,399) and bisphosphorylated (average *m/z* 43,479) p38α species. The monophosphorylated species is present at a higher relative abundance than the bisphosphorylated species.

Next, we designed a mass spectrometry approach to identify phosphorylation sites within our *E. coli* derived p38α. P38α was first excised from an SDS-PAGE/Coomassie Brilliant blue stain gel and proteolytically digested. A titanium dioxide (TiO_2) column was used to enrich for phosphorylated p38α peptides. MALDI-TOF revealed the presence of two phosphopeptides with masses corresponding to 1575.58 and 1591.60 **(Figure AIV-4)**. Based on the results of the Mascot MS/MS database search, peptide 1575.58 corresponds to the p38α peptide monophosphorylated at site Thr180, and peptide 1591.60 corresponds to the oxidized (+16 on Met179) form of this same peptide. The MASCOT scores decrease significantly for both the reduced and oxidized forms of the peptide when the phosphate group is modeled onto Tyr182 **(Table AIV-1)**. Using this approach, we were unable to detect p38α peptides dually phosphorylated at Thr180 and Tyr182. Thus, the monophosphorylated species at relatively high abundance in the FT-MS spectrum likely corresponds to p38α phosphorylated at Thr180.

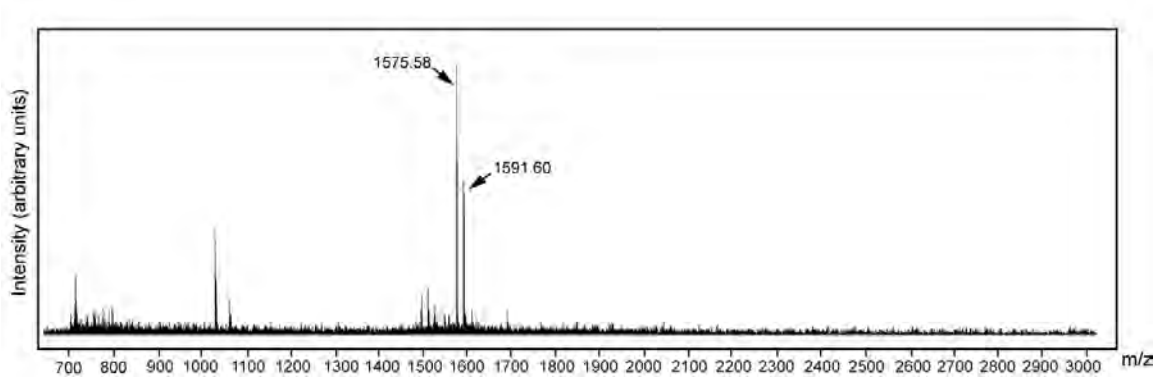

Figure AIV-4. **MALDI-TOF reveals the presence of two phosphorylated p38α MAPK peptides.** P38α was excised from an SDS-PAGE gel stained with Coomassie Brilliant blue and proteolytically digested. Enrichment of phosphorylated p38α peptides was accomplished with a titanium (TiO_2) oxide column. MALDI-TOF revealed the presence of two phosphopeptides with masses corresponding to 1575.58 and 1591.60, representing a peptide monophosphorylated at Thr180 (see Table AIV-1) with and without oxidation, respectively. No other phosphorylated peptides were identified; smaller peaks represent non-specific binding peptides.

Peptide mass (observed)	Peptide sequence[1]	Score[2]
1575.5751	R.HTDDEM**T**GYVATR.W	91.5
	R.HTDDEMTGYVA**T**R.W	58.5
	R.H**T**DDEMTGYVATR.W	42.6
	R.HTDDEMTG**Y**VATR.W	26.2
1591.6010	R.HTDDE**MT**GYVATR.W	64.6
	R.HTDDE**M**TG**Y**VATR.W	32.6

Table AIV-1. Results of MASCOT database search of phosphorylated p38α peptides. [1]The sites of phosphorylation and oxidation are in bold and underlined within the peptide sequence that corresponds to the observed mass in the left column. [2]The highest scoring sequences from the MASCOT search for the 1575.5751 and 1591.6010 peptides are shown. The scores correlate directly with the accuracy of the corresponding phosphorylation and oxidation sites.

Phosphorylated p38α MAPK derived from E. coli exhibits kinase activity. To determine whether recombinant p38α in our preparation exhibits kinase activity, we performed a kinase assay in the presence of recombinant cJun, a well-characterized p38α substrate (Yamagishi et al., 2001). Phosphorimager scanning (^{32}P) revealed that *E. coli*-derived p38α effectively phosphorylates cJun. In contrast, phosphorylation of cJun is not detected in reactions containing dephosphorylated, lambda phosphatase-treated p38α **(Figure AIV-5)**, confirming that the activity of recombinant p38α expressed in *E. coli* depends upon phosphorylation. Collectively, these data demonstrate that recombinant p38α is phosphorylated during expression in *E. coli*, resulting in activation of a fraction of the total p38α expressed.

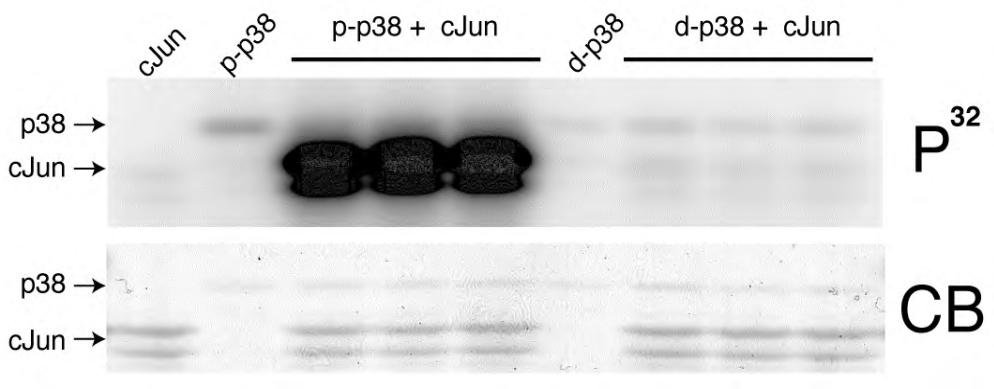

Figure AIV-5. Phosphorylated p38α MAPK expressed in *E. coli* is catalytically active. Recombinant, GST-tagged cJun (cJun), a known substrate of p38α, was incubated in the presence of radiolabelled [γ-^{32}P] ATP with either untreated p38α (p-p38) or p38α treated with lambda protein phosphatase (d-p38). Reactions were separated by SDS-PAGE and processed for autoradiography. Phosphorimager scanning (^{32}P) shows marked phosphorylation of cJun by untreated p38α (p-p38), but not by dephosphorylated p38α (d-p38), indicating that p38α derived from *E. coli* is an active kinase. Coomassie Brilliant blue (CB) staining shows equivalent amounts of recombinant p38α and cJun substrate in all reactions. Control reactions included cJun, p-p38, and d-p38.

Discussion

Despite many reports for recombinant p38α expression and purification in *E. coli*, observations of p38α phosphorylation have not been cited. The bacterial strain and growth conditions described herein are similar to those described by others (Wang et al., 1997; Bukhtiyarova et al., 2004). However, most purification protocols employ at least one anion exchange column (Wang et al., 1997; Keesler et al., 1998; Bukhtiyarova et al., 2004; Diskin et al., 2007), which is known to separate proteins with different phosphorylation states. Our results indicate that phosphorylated p38α represents a subspecies, and suggest that the non-phosphorylated form is present in the highest relative abundance (Figure AIV-3). Thus, it is conceivable that other protocols enriched for the more abundant, unphosphorylated p38α protein at the expense of phosphorylated p38α species.

To our knowledge, there is only one report by Han *et al.* that describes a recombinant form of p38α from *E. coli* that is recognized by an anti-phosphotyrosine antibody and that phosphorylates the myelin basic protein (MBP) substrate. However, these data were not shown, nor were the specific phosphorylation sites identified (Han et al., 1994). Alternative possibilities for why active, phosphorylated forms of p38α from *E. coli* is not generally described are that researchers did not probe for activity, or that the kinase activity was below the limit of detection for the various assays employed.

The p38α protein in our preparation is comprised of heterogeneous species, as defined by their phosphorylation state. Mass spectrometry data unequivocally identified non-phosphorylated and singly-phosphorylated pools of p38α. Western blots using an antibody raised against a peptide dually phosphorylated at Thr180 andTyr182 suggest that our preparation also includes this dually phosphorylated p38α species. Since we did not detect phosphorylated Tyr182 in our MALDI-TOF spectrum, we cannot rule out the possibility that this antibody cross-reacts with singly phosphorylated p38α. An alternative explanation is that the abundance of dually phosphorylated p38α is below the limit of detection for our MALDI-TOF experiment and that the antibody is relatively more sensitive. Should most of the p38α in our preparation be singly-phosphorylated at Thr180, as suggested by our mass spectrometry studies (Figure AIV-4), it would be possible that this protein preparation exhibits less activity than p38α preparations dually phosphorylated *in vitro* at Thr180 and Try182 by upstream MAPKs. However, a recent report showed p38α monophosphorylated at Thr180 displays significant kinase activity that was only 1 order of magnitude lower than bis-phosphorylated p38α (Zhang et al., 2008; Askari et al., 2009). Taken together, these observations suggest that a significant portion of the observed kinase activity in our p38α preparation stems from p38α monophosphorylated at Thr180.

That p38α is phosphorylated and activated in *E. coli* was unexpected, since *E. coli* does not typically modify recombinant mammalian proteins post-

translationally. P38α may be autophosphorylated in *E. coli*, perhaps through a protein-interaction similar to mammalian TAB-1 that induces p38α autophosphorylation (Ge et al., 2002). Accordingly, autophosphorylation has been proposed as the mechanism of phosphorylation for the Lck protein-tyrosine kinase when expressed in *E. coli* (Jullien et al., 1994). An alternative explanation is that recombinant p38α is phosphorylated by bacterial kinases, as suggested for bacterially expressed recombinant p68 RNA helicase (Yang and Liu, 2004). The exact mechanisms underlying phosphorylation of mammalian p38α produced in *E. coli* are unknown.

In sum, we describe a simple method for the production and purification of active p38α from *E. coli* that would be useful to researchers in the MAPK field. In addition, our findings identify p38α as another example of a mammalian protein that is post-translationally modified when expressed in *E. coli*. This observation suggests that careful characterization of post-translational modifications might be needed for other mammalian protein expressed in bacteria.

Materials and Methods

Reagents. [γ-^{32}P] ATP was purchased from MP Biomedicals. Recombinant GST-tagged cJun (1-79) was from Calbiochem. The antibodies employed in this study include anti- phosphorylated p38α (Cell Signaling, 9215) and anti-total p38 (Sigma, M0800). Lambda protein phosphatase was purchased from New England Biolabs (P0753S), Rosetta DE3 cells were from Novagen (EMD

Chemicals, 71400-4), and TALON Metal Affinity Resin from ClonTech (635502). Thrombin protease was purchased from GE/Pharmacia (27-0846-01), and HiTrap Benzamidine Fast Flow column from GE Healthcare. Isopropyl-1-thio-s-D-galactopyranoside (I6758), trypsin (T6567), iodoacetamide (I6125), and lysozyme (L6876) were purchased from Sigma-Aldrich. ProteaseMAX surfactant (V2072) was purchased from Promega, TiO_2 NuTip (NT1TIO.96) from Glygen Corp., and alpha-cyano-4-hydroxycinnamic acid (186002331) from Waters MassPREP.

Expression and purification of His-tagged p38α MAPK. The pET-14b plasmid containing the murine p38α MAPK gene was a generous gift from Dr. Jiahuai Han (The Scripps Research Institute, La Jolla CA). The plasmid encodes full-length murine p38α (Accession Number #NM_011951) with a Histidine (His) tag and a thrombin cleavage site (MGSSHHHHHHSSGLVPRGSH) at the amino terminus. This plasmid was transformed into Rosetta DE3 cells using a standard heat-shock protocol. Transformed colonies from LB/ampicillin plates were grown at 30°C in 5 mls Luria-Bertani (LB) broth, supplemented with 100μg/ml ampicillin (amp) and 34μg/ml chloramphenicol (cam), referred to here as LBAC media. After 8-10 hours these cultures were added to 50 mls of fresh LBAC media and grown overnight at 30°C. Twenty-five to 50 mls of this culture was added to 2L of fresh LBAC media until an OD_{600} between 0.05 and 0.10 was reached. Cells were then allowed to grow at 30°C until an OD_{600} of 0.6-0.7, at which point p38α

expression was induced by the addition of 1mM isopropyl-1-thio-s-D-galactopyranoside (IPTG) for 4 hours. Cells were harvested by centrifugation at 8,000 rpm for 15 minutes. Cell pellets were stored at -80°C or immediately used for his-p38α purification.

Bacterial cells were resuspended in lysis buffer (50mM Tris, 500mM NaCl, 10mM imidazole, and protease inhibitor) (Wang et al., 1997). Lysozyme (1 mg/ml) and NP-40 (0.3%) was added to the lysate, which was then sonicated in a Sonic Dismembrator (Fisher Scientific, Model 500) as follows: once at 10% for 12 sec, three times at 20% for 12 sec, and once at 30% for 12 sec. The lysate was cleared by centrifugation at 15,000 rpm for 30 minutes at 4°C, and then applied to TALON resin equilibrated in Buffer A (50mM sodium phosphate, 300mM NaCl, and 5mM imidazole, pH 7.0) inside a 50 mL conical tube and incubated with gentle rocking at room temperature for 30 minutes. The resin was centrifuged at 2000 rpm for 5 minutes and the supernatant was removed. The resin was washed 3 times with 10 bed volumes of Buffer A before eluting the his-tagged p38α with Buffer B (50 mM sodium phosphate, 300 mM NaCl, and 150mM imidazole, pH 7.0). The protein was then buffer exchanged into phosphate buffered saline (PBS) supplemented with 2mM dithiothreitol (DTT). Yields were typically 10-15mg of ~85% pure protein per liter of LBAC media.

Thrombin cleavage of His-tagged p38α MAPK. For cleavage of the his-tag from p38α, the purified protein was buffer exchanged into Buffer A and treated with 10

units of thrombin protease per mg of fusion protein overnight at 4°C. The protein was then applied to TALON resin a second time to remove the cleaved his-tag and residual un-cleaved p38α. To remove the thrombin protease, the protein was applied to a HiTrap Benzamidine FF column equilibrated with Buffer A. The p38α eluted in the flow-through, and was subsequently buffer exchanged into PBS supplemented with 2mM DTT and stored at -80°C. Protein purity was assessed as ~95% based on SDS-PAGE and Coomassie Brilliant blue staining analysis.

Dephosphorylation of p38α MAPK by lambda phosphatase. His-tagged p38α (1.3 mg) was incubated with 8000 units of lambda protein phosphatase at 30°C overnight, and the reaction was applied to TALON resin as described above. The lambda phosphatase was removed by washing the resin with Buffer A. Dephosphorylated his-tagged p38α was eluted with Buffer B and buffer exchanged into PBS as described above.

In vitro p38α MAPK activity assay. Phosphorylated and dephosphorylated (lambda protein phosphatase treated) forms of his-tagged p38α (500nM each) were incubated with GST-cJun (13.5μM) in kinase buffer (20mM Hepes, pH 7.4, 2mM EGTA, 10mM Magnesium Sulfate, 1mM DTT) at 30°C. Reactions were started by addition of 100μM, γ-^{32}P labeled ATP. After 10 minutes incubation, kinase reactions were stopped by addition of 10μl Laemmli sample buffer.

Reactions were separated by SDS-PAGE and stained with Coomassie Brilliant blue. After destaining, gels were dried and processed for Phosphorimager Typhoon scanning.

Determination of the exact mass of p38α MAPK proteins. The exact masses associated with the his-tagged p38α species in our preparation were determined using Electrospray Ionization Fourier transform ion cyclotron resonance (FT-ICR, FT-MS) mass spectrometer (apex Qe-94, Bruker Daltonics) as described previously (Bosco et al., 2010b). Briefly, purified samples were diluted into either 50% methanol/49.1% water/0.1% formic acid 2 mM ammonium Bicarbonate or 2 mM ammonium bicarbonate in water. Similar phosphorylation patterns were obtained with both solvents, with the acidified solution giving a higher signal/noise ratio.

Mass spectrometry based-identification of phosphorylation sites in recombinant p38α. Phosphorylated and dephosphorylated (lambda protein phosphatase-treated) p38α preparations were processed for tryptic digestion and mass spectrometry analyses as follows. His-tagged p38α proteins were resolved by SDS PAGE analysis and visualized by Coomassie Brilliant blue staining. Bands corresponding to p38α were excised and placed into 1.5ml eppendorf tubes with 1ml of water for 1 hr. The water was removed and 25 μl of 250 mM Ammonium Bicarbonate was added. To reduce the disulfide bond in the proteins, 5 μl of a 45

mM solution of DTT was added and the samples were incubated at 50°C for 30 min. The samples were cooled to room temperature. Alkylation of the cysteines (to prevent disulfide bond formation) was accomplished with the addition of 5 μl of a 100 mM Iodoacetamide solution. After 30 min, the gel slices were washed twice with 1 ml water aliquots. The water was removed and 1ml of 50:50 (50mM Ammonium Bicarbonate: Acetonitrile) was placed in each tube and samples were incubated at room temperature for 1hr. The solution was then removed and 200 μl of Acetonitrile was added to each tube. After the gel slices turned opaque white, the acetonitrile was removed and gel slices were further dried in a Speed Vac. Dried gel slices were rehydrated in 50 μl of 2ng/μl trypsin in 0.01% ProteaseMAX Surfactant: 50mM Ammonium Bicarbonate. Samples were then incubated at 37°C for 21hrs. The supernatant of each sample was then removed and placed in a separate 0.5 ml eppendorf tube. Gel slices were further dehydrated with 60 μl of 80:20 (Acetonitrile: 1% formic acid). The extract was combined with the supernatants of each sample. The samples were then dried down to a 10 μl volume in a Speed Vac.

Aliquots of the extracted peptide digest were then enriched for phosphorylated peptides as follows. Several microliters of the extracted peptide digest was diluted in 10 μl of binding solvent (75:19:6 Acetonitrile: Water: TFA). A 1-10 μl TiO2 NuTip was washed two times with 10 μl aliquots of binding solvent. Phosphopeptides were then bound by repetitive pipetting (20 times) of the 10 μl sample volume. The NuTip was then washed 5 times with binding

solvent and then 5 times with 0.1% TFA. Phosphopeptides were then eluted in a separate tube with a 10 μl volume of 6% NH_4OH after repetitive pipetting (10 times). A 3 μl aliquot of 5% TFA was then added to acidify the sample. The phosphopeptides were further purified prior to MALDI analysis using a micro C18 ZipTip.

Samples containing digested peptides from p38α proteins were deposited onto the MALDI sample target with 1μl of Acetonitrile: 0.1% TFA (80:20) followed by addition of 0.5μl of Matrix solution which consisted of 5 mg/ml of Alpha-Cyano-4-hydroxycinnamic acid in Acetonitrile: 0.1% TFA (50:50). Samples were allowed to air dry prior to insertion into the mass spectrometer. Analyses were performed on a Shimadzu Biotech Axima TOF2 (Shimadzu Instruments) matrix-assisted-laser desorption/ionization Time-of-Flight (MALDI-TOF) mass spectrometer. Peptides were analyzed in positive ion Reflectron mode. The instrument was externally calibrated using a local spot to the sample of interest with Angiotensin II (1046.54), P14R (1533.86) and ACTH (18-39) 2465.20 Da. Collision Induced Dissociation (CID) and/or a Post-Source-Decay (PSD) analysis were performed on the same instrument using a dual timed ion gate for high resolution precursor selection with a laser power about 20% higher than for MS acquisition. CID/PSD fragments were separated in a Curved Field Reflectron (CFR) allowing for a full mass range acquisition of the MS/MS spectrum. All spectra were processed with Mascot Distiller (Matrix Sciences, Ltd.) prior to database searching. Database searches were performed in house with Mascot

(Matrix Sciences, Ltd.). For MS searches the Peptide Mass Fingerprint program was used with a peptide mass tolerance of 100 ppm. For MS/MS searching (CID/PSD spectra) the MS/MS Ion Search program was used with a Precursor tolerance of 100 ppm and a fragment tolerance of 1.5 Da.

PREFACE TO APPENDIX V:

The work presented in this appendix was performed by Catherine L. Ward with the following exceptions:

Mass spectrometry was performed by the mass spectrometry core facility (UMMS) and cross-linking experiments were largely performed by Michelle Dubuke during her lab rotation (UMMS). All figures were prepared by Catherine L. Ward.

APPENDIX V: P38 MAPK PREFERENTIALLY BINDS FALS-LINKED MUTANT AND OXIDIZED WILD-TYPE SOD1 PROTEINS

Abstract

Amyotrophic lateral sclerosis (ALS), also known as Lou Gehrig's disease, is a rapidly progressive and fatal motor neuron disease. The mitogen activated protein kinase, p38, is thought to play a role in the pathogenesis of ALS due to aberrant activity of the kinase and in association with mutant superoxide dismutase-1 (SOD1). Here, we investigate the relationship between SOD1 and p38. Using several familial ALS-linked SOD1 variants and oxidized WT SOD1, as a model for sporadic ALS, we show that p38 MAPK, both alpha and beta isoforms, preferentially bind the mutant and oxidized forms of SOD1, independently of p38 activation.

Introduction

Amyotrophic lateral sclerosis (ALS), is a rapidly progressive and fatal disease characterized by the death of motor neurons. Approximately 10% of ALS cases are familial (fALS), or inherited, with the remaining 90% classified as sporadic cases (sALS). Of the familial cases, ~20% are caused by mutations in the gene superoxide dismutase-1 (SOD1), which was found over two decades ago to be involved in ALS (Rosen et al., 1993). SOD1 is an enzyme which catalyzes the conversion of superoxide anions to hydrogen peroxide. Over 150

mutations in SOD1 have been found to cause ALS, which is thought to occur by a gain of toxic function, as suggested by lack of neurotoxic phenotype in SOD1 knock-out mice (Reaume et al., 1996). This toxic function is thought to be related to the tendency of mutant SOD1 to misfold and aggregate. Wild-type (WT) SOD1 is found to aggregate upon being oxidized (Rakhit et al., 2004; Furukawa et al., 2006) and once oxidized, SOD1 mimics the toxicity and binding interactions of mutant SOD1 (Ezzi et al., 2007). WT SOD1 could therefore be playing a role in sALS pathogenesis through its ability to gain toxic properties similar to those seen with mutated SOD1.

Also shown to be important in the pathogenesis of ALS are the mitogen-activated protein kinases (MAPKs). MAPKs are serine-threonine protein kinases which regulate cellular activities through a signaling cascade initiated by cues from various extracellular or intracellular stimuli. The basic MAPK pathway consists of three components: a MAPK kinase kinase (MAP3K), which phosphorylates a MAPK kinase (MAP2K), which in turns phosphorylates a MAPK (Kim and Choi, 2010). Upon phosphorylation, these kinases become activated allowing for further transmission of the signal cascade. One member of the MAP kinase family associated with ALS is p38. This protein has several isoforms, α, β, γ, δ, and is activated by many cellular stresses, including osmotic shock, cytokines, and oxidative stress. Aberrantly activated p38α can lead to elevated levels of phosphorylated neurofilament heavy chain, which when accumulated, is a pathological feature of ALS (Ackerley et al., 2004). Aberrant activation of p38

also correlates with disease progression in SOD1 G93A mice (Tortarolo et al., 2003) while the p38 inhibitor, SB203580, prevents SOD1 induced apoptosis of motor neurons (Dewil et al., 2007). Additionally, activated p38 was found to be a component of inclusions in human ALS patients and G93A SOD transgenic mice (Bendotti et al., 2005). In light of the associations between p38 MAPK and SOD1 in ALS, we tested the hypothesis that there is a direct binding interaction between modified SOD1 proteins and p38 MAPK. We found that p38 binds SOD1 mutants A4V, G37R, G41D, G85R, and G93A, as well as oxidized WT, while having little affinity for the unmodified WT protein. This binding interaction was direct and independent of p38 activation.

Results

P38 MAPK co-purifies with fALS-linked mutant SOD1, but not WT-SOD. In light of the correlation between p38 and SOD1 in ALS we sought to determine the relationship between these two proteins, starting with probing for a binding interaction. Neuro-2A (N2A) cells stably expressing either WT-SOD1 or a fALS-linked mutant SOD1 (G37R, G41D, or G85R) were lysed and incubated with His-tagged p38α. Using affinity chromatography, the His-tagged p38α was isolated from the reaction. Western analysis of the extracted protein shows that G37R, G41D, and G85R have a 3.7, 4.2, and 5.2 fold increase in affinity for p38α, respectively, as compared to WT SOD1 **(Figure AV-1)**. To account for non-specific binding of the SOD1 proteins to the affinity column, p38α was omitted

from the reactions and the amount of SOD1 eluted from the column **(Figure AV-1; background)** was quantified and subtracted from the experimental values. An equal amount of His-p38α was isolated in each sample, indicating that mutant forms of SOD1 bind p38α to a significantly higher degree than WT-SOD1 **(Figure AV-1)**.

FALS-linked mutant SOD1 proteins bind directly to P38 MAPK. Once a mutant specific binding interaction was established it was next necessary to determine if this binding was a result of a direct interaction. Purified His-tagged p38α was incubated with purified WT SOD1 or the fALS-linked SOD1 mutant A4V. Western analysis following extraction of p38α via affinity chromatography revealed a direct binding interaction of p38α and SOD1 which was exclusive for the mutant protein **(Figure AV-2, lanes 1 and 2)**. Comparison of Western blot band density between WT and mutant A4V revealed a ~23 times greater amount of mutant protein present than WT.

To substantiate the direct binding interaction observed from the affinity pull-downs, crosslinking experiments between fALS-linked mutant SOD1 and p38α were performed. Purified p38α and SOD1 proteins were incubated with the crosslinking agent, dimethyl suberimidate (DMS), which functions to covalently link proteins between the amino groups of lysines at their binding interface. WT-SOD1 and mutants A4V, **(Figure AV-3)** G85R, and G93A, **(Figure AV-4)** were included in the analysis. The crosslinking reactions were analyzed via Western

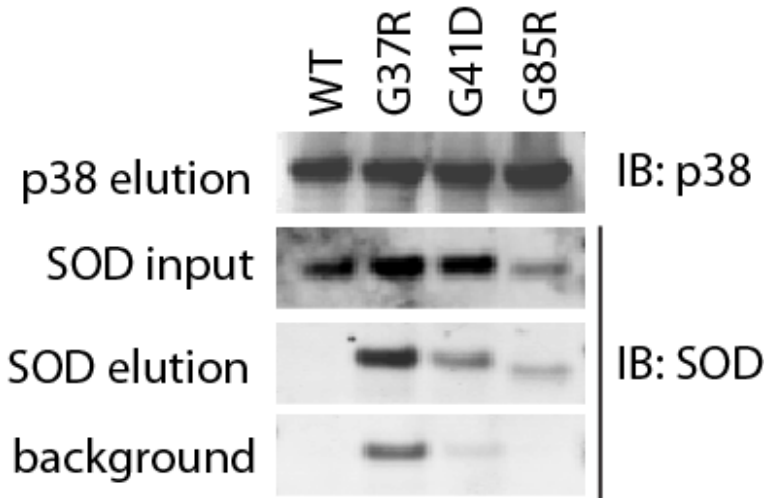

Figure AV-1. Recombinant p38α preferentially binds to fALS-linked mutant SOD1 proteins from N2A cell lysates. Lysates from N2A cells stably expressing fALS-linked SOD1 mutants G85R, G41D, or G37R or SOD1 WT were incubated with the alpha (α) isoform of His-tagged p38 MAPK. The binding reactions were applied to Ni-NTA spin columns and then eluted with imidazole. The elutions were subjected to Western blot analysis using antibodies against p38 and SOD1 as indicated. The Western blots were analyzed and quantified by densitometry. The quantification shows that G37R, G41D, and G85R have a 3.7, 4.2, and 5.2 fold increase in affinity for p38α, respectively, as compared to WT SOD1, demonstrating that p38α preferentially binds fALS-linked mutant SOD1 proteins.

blot using antibodies against p38 and SOD **(Figure AV-3A and AV-4A)**. Several crosslinked species were observed, with molecular weights correlating to a p38α dimer, an SOD1 dimer, and a p38α monomer crosslinked to a SOD1 monomer **(Table AV-1)**. From the density of the Western blot bands probed with anti-p38, the percentage of p38 crosslinked to SOD1 was calculated. 7.62% of WT SOD1 and 11.91% of A4V bound to p38α **(Figure AV-3B)**. Comparison of WT, G85R, and G93A showed 9.85%, 8.99%, and 11.54% of SOD1 protein, respectively, bound to p38α **(Figure AV-4B)** The Western blots were also probed with SOD1 to confirm the crosslinking and to calculate the percentage of SOD1 crosslinked to p38α. Comparison of WT and the A4V mutant showed 1.74% of total WT SOD1 bound to p38α and 17.42% of total A4V **(Figure AV-3C)**. 7.88% of total WT SOD1, 8.85% of total G85R, and 12.69% of total G93A was bound to p38α **(Figure AV-4C)**.

To verify these results, the crosslinking samples were analyzed via SDS-PAGE with silver staining. The protein bands with a molecular weight of 60-65 kD were excised and subjected to mass spectrometry analysis. The analysis of these bands revealed no p38α present in the WT SOD1 crosslinking reaction, indicating that if any p38α was present, it was below the limit of detection **(Table AV-2).** Through these experiments using isolated, purified protein it was established that the binding of p38α and SOD1 was a direct interaction preferential for mutant SOD1.

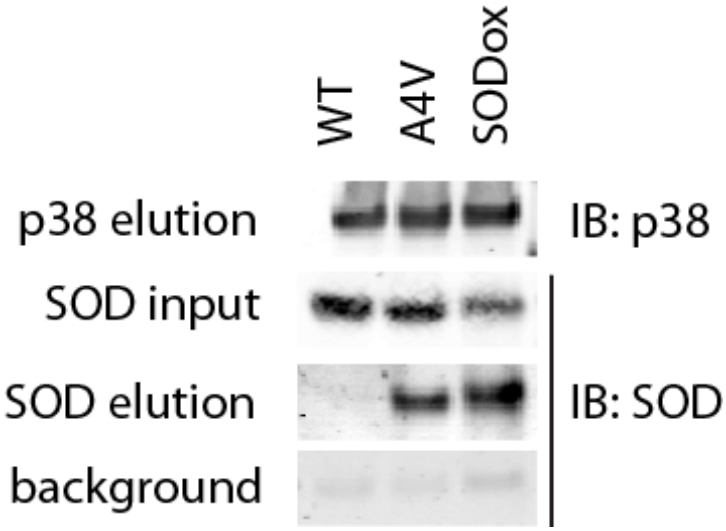

Figure AV-2. Recombinant p38α preferentially binds to recombinant fALS-linked SOD mutant A4V and aberrantly oxidized SOD1 WT (SODox) proteins. Recombinant SOD1 WT, fALS-linked mutant A4V, and SODox (a model protein for sALS) were incubated with the alpha (α) isoform of His-tagged p38. The binding reactions were applied to Ni-NTA spin columns and then eluted with imidazole. The elutions were subjected to Western blot analysis using antibodies against p38 and SOD1 as indicated. The Western blots were analyzed by densitometry and the quantification was corrected for non-specific binding of SOD1 proteins (background). The quantification revealed a ~23 and ~28 times greater affinity of A4V and SODox for p38α, respectively, as compared to WT. Per the Western blot and quantification, it is evident that the mutant and oxidized forms of SOD1 bind p38α to a much higher degree than the unmodified WT protein.

Oxidized WT-SOD1 mimics fALS-linked mutant SOD1 in its ability to bind p38. As a model for sALS, an oxidized form of the wildtype SOD1 protein (referred to here as SODox) was also incubated with p38α and analyzed for a binding interaction via affinity chromatography and Western blot. As with the fALS-linked mutant proteins, the oxidized WT protein had a significantly higher binding affinity for p38α than the unmodified WT protein **(Figure AV-2A, lanes 1 and 3)**. Comparing the Western blot band density between the amount of unmodified WT SOD1 and oxidized WT SOD1 purified with p38α reveals a ~28 times greater amount of oxidized WT protein. Therefore, WT SOD1 when modified by oxidation, mimics the p38α binding capabilities of mutant SOD1 protein.

Mutant SOD1 also binds the beta isoform of p38 MAPK. Being 75% homologous in sequence to the alpha isoform of p38, the binding of the beta isoform to SOD1 was also examined. Recombinant, His-tagged p38β was incubated with a subset of the mutant protein found to bind p38α, including G37R from N2A cells and purified A4V and SODox. After isolating p38β via affinity chromatography, the same binding interactions as observed for p38α were seen **(Figure AV-5)**. Neither purified WT SOD1 nor WT SOD1 from N2A cells bound p38β. Comparison of the Western blot band density reveals that G37R, A4V, and SODox bound p38β 1.6, 1.4, and 0.5 times greater than unmodified WT SOD1, respectively. These results therefore indicate that the binding of oxidized and mutant SOD1 to p38 is not specific for the alpha isoform.

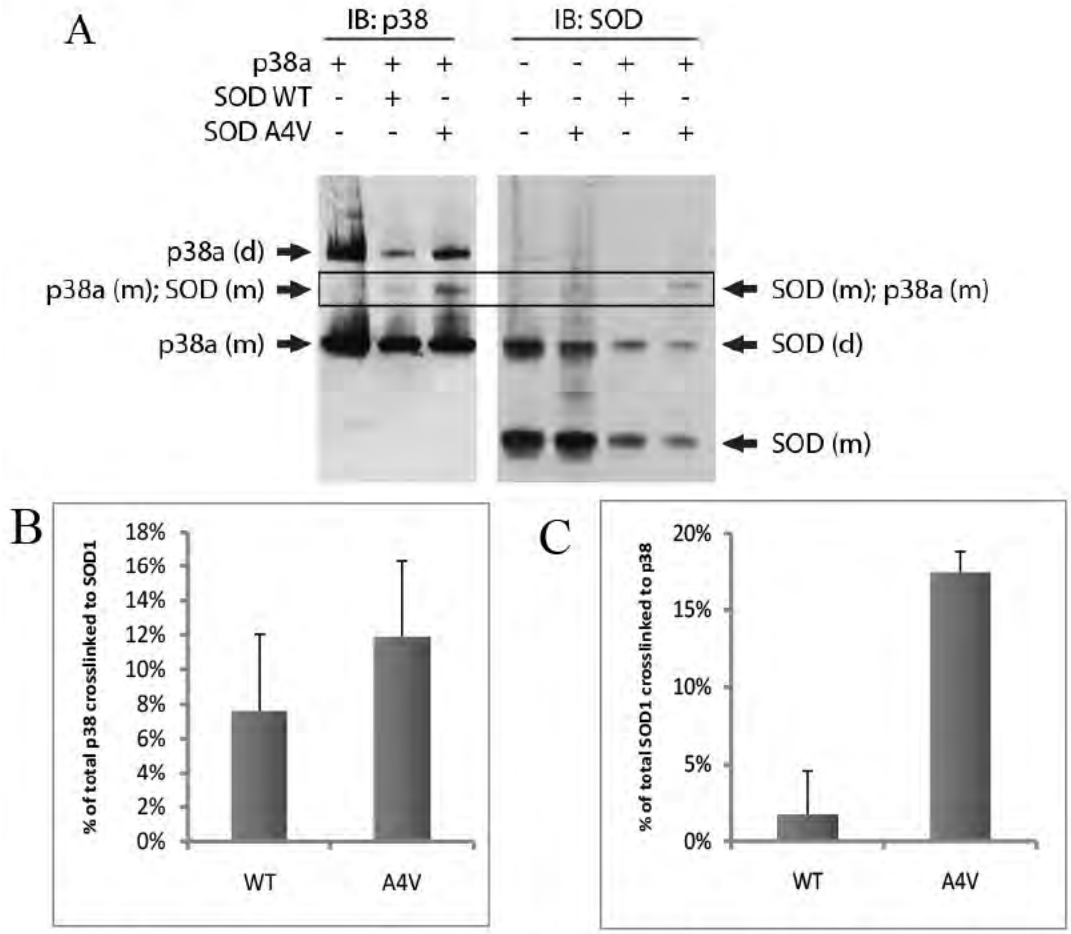

Figure AV-3. Recombinant p38α preferentially binds fALS-linked mutant A4V in crosslinking analyses. Recombinant p38α was combined with either SOD1 WT or fALS-linked SOD1 mutant A4V and treated with the crosslinker dimethyl suberimidate (DMS) for 15 minutes at room temperature. Crosslinking occurred at lysine residues in SOD1 and p38α within 11 Å of each other. The crosslinked species were then identified by Western analysis, probing for SOD1 and p38, and are indicated by the arrows (A). The proposed crosslinked species were determined based on molecular weight (Table AV-1). Monomer (m) and dimer (d) proteins were both detected. Densitometry was performed (n = 2) to determine the percentage of total p38 crosslinked to SOD1 (B) and the percentage of total SOD1 crosslinked to p38 (C).

Discussion

This study has revealed a specific binding interaction between p38 MAPK and oxidized or mutant forms of SOD1, identifying a link between these two proteins relevant to ALS pathogenesis. A series of binding assays utilizing affinity chromatography demonstrated a unique affinity of p38 for SOD1 mutants A4V, G37R, G41D, G85R, and G93A, as well as the oxidized WT protein (SODox), while not binding to the unmodified WT protein. These assays also confirmed that the binding is due to a direct interaction of these proteins and is not mediated by any additional protein interactions.

Important to the link between the familial and sporadic forms of ALS is the binding of p38 to the oxidized wild-type protein. Whereas this protein has no mutations, it mimics the binding capabilities of the mutant protein. This demonstrates that a modification, such as oxidation, to the wild-type protein is enough to cause it to acquire new binding partners that could be significant to the pathogenesis of sporadic ALS.

That p38 interacts with mutant and modified forms of SOD1 is an important observation as a functional interaction between these proteins has also been observed. In a model using giant squid axoplasm, modified SOD1 purified from sporadic ALS patient tissue, as well as recombinantly purified SOD1 mutant protein, inhibited axonal transport in a p38 dependent manner. Additionally, the amount of mutant SOD1 bound to p38 is a very small proportion of the total amount expressed, suggesting that only a subpopulation of the mutant proteins

acquire this potentially toxic binding property. Perhaps when bound to SOD1, p38 acquires new binding partners, altering the transmission of the kinase signaling cascade and activating unintended proteins.

In addition to revealing a unique binding interaction of p38, this work has provided a new tool for studying the kinase activity of the protein. Isolation of a doubly phosphorylated p38 species via *E. coli* expression was accomplished using affinity chromatography followed by purification with an ion exchange column. Being able to purify out these different forms of p38 will enhance the way in which the activity of the kinase is studied.

Studying the relationship between p38 and SOD1 has given us a new tool to enhance the study of p38 as well as an important observation into the activity of these two proteins related to ALS pathogenesis. Further characterizing the nature of this binding interaction unique to mutant and modified WT SOD1 will lead to further insights into their roles in ALS pathogenesis.

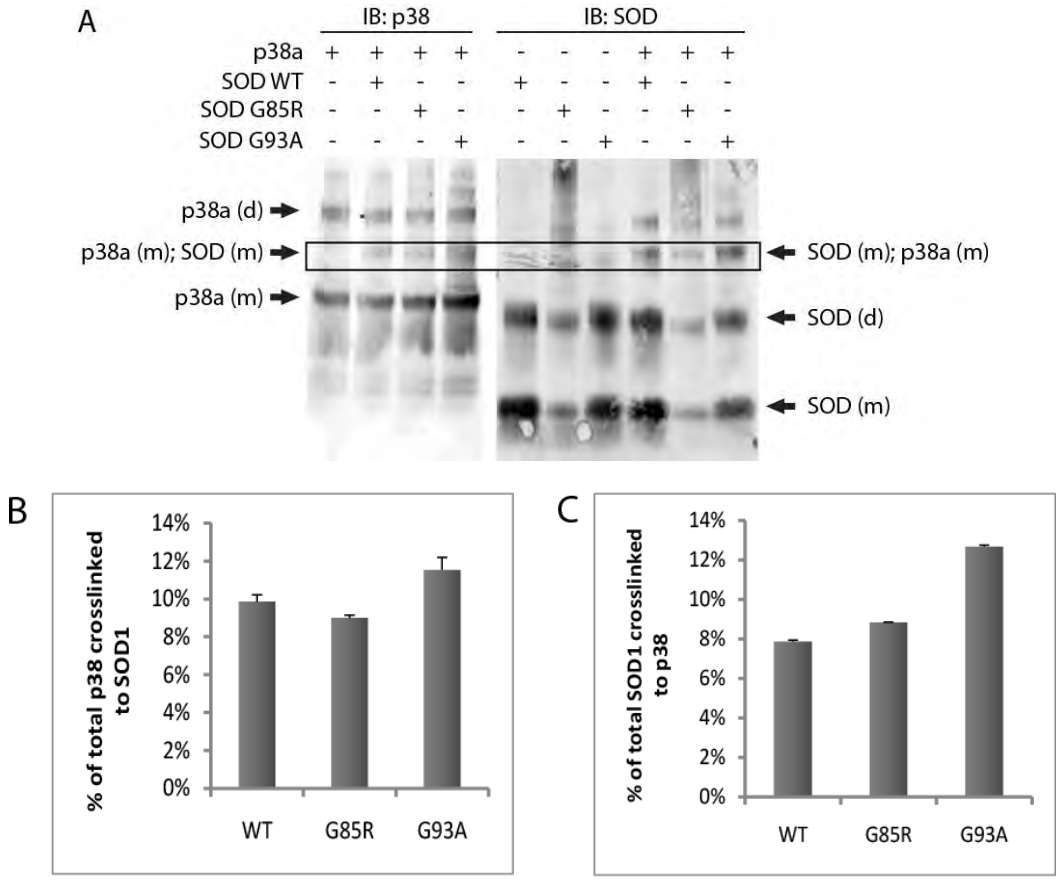

Figure AV-4. Recombinant p38α preferentially binds fALS-linked mutants G85R and G93A in crosslinking analyses. Recombinant p38α was combined with either SOD1 WT or fALS-linked SOD1 mutants G85R and G93A and treated with the crosslinker dimethyl suberimidate (DMS) for 15 minutes at room temperature. Crosslinking occurred at lysine residues in SOD1 and p38α within 11 Å of each other. The crosslinked species were then identified by Western analysis, probing for SOD1 and p38, and are indicated by the arrows (A). The proposed crosslinked species were determined based on molecular weight (Table AV-1). Monomer (m) and dimer (d) proteins were both detected. Densitometry was performed (n = 2) to determine the percentage of total p38 crosslinked to SOD1 (B) and the percentage of total SOD1 crosslinked to p38 (C).

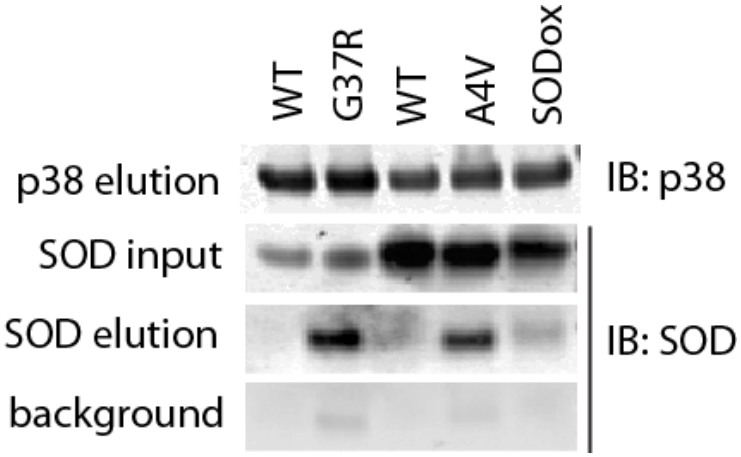

Figure AV-5. The beta isoform of p38 also binds mutant and modified SOD1 proteins. Lysates from N2A cells stably expressing fALS-linked SOD1 mutant G37R or SOD1 WT, as well as recombinant fALS-linked SOD1 mutant A4V and the oxidized form of WT SOD1 (SODox), were incubated with the beta (β) isoform of His-tagged p38 MAPK. The binding reactions were applied to Ni-NTA spin columns and then eluted with imidazole. The elutions were subjected to Western blot analysis using antibodies against p38 and SOD1 as indicated. The Western blots were analyzed by densitometry and the quantification was corrected for non-specific binding of SOD1 proteins (background). The quantification shows that G37R, A4V and SODox have a 1.6, 1.4, and 0.5 fold greater affinity for p38α, respectively, than the WT protein.

Materials and Methods

Cell culture. Flp-in HEK cells (Invitrogen - #R75007) expressing GFP-SOD1 constructs under control of a doxycycline-induced promoter (generous gift from Dr. Larry Hayward, UMMS) were maintained in Dulbecco's Modified Eagle Medium (DMEM) supplemented with 10% TET-tested fetal bovine serum (Atlanta Biologicals,#s10350H), 2mM L-glutamine (Gibco, #25030), 1% penn/strep solution (Gibco, #15140), 15 mg/ml blasticidin (Invitrogen, #R210-01), and 25 ug/ml hygromycin B (Invitrogen, #10687-010). Neuro2A (N2A) cells stably expressing WT or mutant SOD were maintained in 1:1 DMEM and OPTI-MEM media supplemented with 12% fetal bovine serum, 400 µg/ml geneticin (GIBCO, #11811-031), and 1% penicillin/streptomycin/glutamine.

Protein expression and Purification. p38 MAPK plasmid was a gift from Goldsmith and Han labs and myc-tagged SOD1 from Dr. Zuoshang Xu, UMMS. Mutations to the SOD1 WT protein were constructed using mutagenic primers and the QuickChange Site Directed Mutagenesis method (Stratagene).

SOD1 production: Expression of GST-tagged SOD1 in Rosetta DE3 cells (Novagen) was induced by 1mM isopropyl-1-thio-s-D-galactopyranoside (IPTG) for 3 hours at 37^{o}C. Incorporation of metals was achieved by the addition of 200µM $CuCl_2$ and 200µM $ZnCl_2$ prior to the IPTG induction. The bacteria were harvested through centrifugation and lysed with lysis buffer (0.5mM dithiothreitol

Antibody	Molecular weight of bands in each sample (kD)					Species
	WT	A4V		WT	G85R	G93A	
p38	83.9	86.82		82.31	82.31	82.31	p38d
	64.1	64.65		60.19	59.18	59.69	p38m; SODm
	41.8	42.19		38.36	39.07	38.72	p38m
SOD1	69.0	67.1		63.91	66.2	75.36	p38m; SODm
	42.6	42.59		34.02	34.31	37.31	SODd
	20.0	20.19		17.24	17.97	17.24	SODm

Table AV-1. Molecular weight of p38 and SOD1 species resulting from crosslinking analysis. Recombinant p38α was combined with either SOD1 WT or fALS-linked SOD1 mutants A4V, G85R, or G93A. Reactions were treated with the crosslinker dimethyl suberimidate (DMS) for 15 minutes at room temperature. Crosslinking occurred at lysine residues in SOD1 and p38α within 11 Å of each other. Crosslinking reactions were analyzed by Western blot and imaging software (Licor), where each Western blot band was compared to a molecular weight protein ladder. The Western blots were probed with anti-p38 and anti-SOD1 as indicated. The expected protein species was determined based on the molecular weight of the bands.

(DTT), 0.1mM EDTA, protease inhibitor cocktail (Roche, #11873580001), in PBS) and gentle sonication. After centrifuging the lysate, the supernatant was passed through a glutathione Sepharose column, previously washed with PBS. The GST-SOD1 protein was eluted from the column with 10mM glutathione, 50mM Tris (pH 9.5). Cleavage of the GST tag was achieved using six units of Precision Protease (GE/Amersham, 27-0843-01) per milligram of protein. Following cleavage, the protein was dialyzed back into PBS and was run back over the glutathione Sepharose column. The untagged SOD1 protein was further purified using a Q-column in a 10mM Tris buffer at a pH of 8.0. The protein was eluted from the column with a gradient of 10mM Tris, 300mM NaCl pH 8.0 buffer. Purity of the preparation was assessed using SDS-PAGE and mass spectrometry. For the production of SODox, wild-type SOD1 protein was incubated at room temperature with 10mM hydrogen peroxide for 24 hours. The reaction was quenched by buffer exchanging the protein into PBS.

P38 production: Expression of His-tagged p38 in Rosetta DE3 cells (Novagen) was induced by 1mM isopropyl-1-thio-s-D-galactopyranoside (IPTG) for 4 hours at 30^{o}C. The bacteria were harvested by centrifugation and lysed with lysis buffer (50mM Tris pH 7.4, 500mM NaCl, 10mM imidazole, protease inhibitor cocktail) and gentle sonication. Cleared lysate was added to TALON resin (ClonTech) and purification proceeded as per manufacturer's instructions. The his-tag was then cleaved using thrombin protease (GE/ Pharmacia, #27-0846-01)

Sample	Sample Contents	Molecular weight (Da)	PLGS Score	Peptides	Coverage (%)
WT	Trypsin precursor	24393	875.0	12	7.8
	Superoxide dismutase Cu Zn	15794	225.7	3	6.5
A4V	Trypsin precursor	24393	386.4	5	7.8
	Superoxide dismutase Cu Zn	15794	487.0	4	11.1
	Mitogen activated protein kinase	41261	96.6	9	10.3
G85R	Trypsin precursor	24393	1180.1	13	7.8
	Superoxide dismutase Cu Zn	15794	1537.2	11	15.0
	Mitogen activated protein kinase	41261	1094.8	27	22.5
	Glutathione S transferase 26 kDa	25481	185.5	8	14.7
	Keratin type II cytoskeletal 1 Cytokeratin 1 K	65846	62.3	3	2.8
	Keratin type I cytoskeletal 10 Cytokeratin 10	57675	40.6	4	3.3
G93A	Trypsin precursor	24393	1146.1	12	7.8
	Superoxide dismutase Cu Zn	15794	1304.0	12	15.0
	Mitogen activated protein kinase	41261	1609.0	25	19.7

Table AV-2. Mass spectrometry analysis of crosslinked species. The crosslinking reactions shown in Figure AV-3 were subjected to a silver stain (BioRad) following SDS-PAGE. Based on their molecular weights, as shown in Table AV-1, the bands correlating to p38α:SOD crosslinked species were extracted and subjected to mass spectrometry. The analysis shows both p38α and SOD1 present in the crosslinking reactions containing mutant SOD1 proteins A4V, G85R, and G93A, but not in the crosslinking reaction containing SOD1 WT. If p38α and SOD1 WT did bind during the crosslinking reaction, there was not a large enough population of this crosslinked species to be detected.

Binding assays with recombinant p38 MAPK and N2A cell lysates. Total N2A cell lysates were prepared using a lysis buffer composed of 50 mM NaH2PO4, 100 mM imidazole, 300 mM NaCl (pH 8.0), 12 mM deoxycholic acid, 1% NP-40, protease inhibitor cocktail, 50 mM NaF and 10 mM Na2VO3. 700µg of total protein from N2A cell lysates was incubated with 100µg of purified His-tagged p38 for 3 hour at 4°C with rotation. As a control, reactions were also incubated without His-tagged p38. After incubation, the binding reactions were applied to Ni-NTA spin columns (Qiagen), washed with 50 mM NaH2PO4, 20 mM imidazole, 300 mM NaCl (pH 8.0), and eluted with 50 mM NaH2PO4, 500 mM imidazole, 300 mM NaCl (pH 8.0). Speed and duration of spins were as per manufacturer's instructions (Qiagen). The elutions were subjected to SDS-PAGE and probed for p38 and SOD1 using standard Western blot methods with anti-p38 MAP Kinase antibody produced in rabbit (Sigma, M0800) and anti-superoxide dismutase (Cu/Zn Enzyme) produced in sheep (Calbiochem, 574597), respectively.

Recombinant protein binding assays. 10µg of purified SOD1 protein in lysis buffer was incubated with 100µg of purified His-tagged p38 for 3 hour at 4°C with rotation. As a control, reactions were also incubated without His-tagged p38. The binding reactions were applied to Ni-NTA spin columns (Qiagen), washed, and eluted as described above. The elutions were subjected to SDS-PAGE and

probed for p38 and SOD by standard Western blotting techniques with the antibodies described above.

Crosslinking analysis. Proteins were buffer exchanged into 0.2M Triethanolamine (TEA) pH 8.5 and combined such that the final concentration of each protein was 2.5mg/ml. Dimethyl suberimidate · 2HCl (ThermoScientific, #20700) was added in 150M excess and the reaction was allowed to proceed at room temperature for 15 or 30 minutes after which the reaction was quenched by the addition of SDS sample loading buffer and boiling. (as per the manufacturer's instructions) Samples were analyzed via Western blot probing for p38 and SOD1 with the antibodies described above. For verification by mass spectrometry analysis, the samples were first run on an SDS-PAGE gel and subjected to silver stain (Bio-Rad). The bands corresponding to the predicted size of the crosslinked species were then extracted and sent to the Mass Spectrometry Core Facility at UMMS for digestion and analysis.

BIBLIOGRAPHY

Abel O, Powell JF, Andersen PM, Al-Chalabi A (2012) ALSoD: A user-friendly online bioinformatics tool for amyotrophic lateral sclerosis genetics. Hum Mutat 33:1345-1351.

Ackerley S, Grierson AJ, Banner S, Perkinton MS, Brownlees J, Byers HL, Ward M, Thornhill P, Hussain K, Waby JS, Anderton BH, Cooper JD, Dingwall C, Leigh PN, Shaw CE, Miller CC (2004) p38alpha stress-activated protein kinase phosphorylates neurofilaments and is associated with neurofilament pathology in amyotrophic lateral sclerosis. Mol Cell Neurosci 26:354-364.

Aguzzi A, Barres BA, Bennett ML (2013) Microglia: scapegoat, saboteur, or something else? Science 339:156-161.

Ahler E, Sullivan WJ, Cass A, Braas D, York AG, Bensinger SJ, Graeber TG, Christofk HR (2013) Doxycycline alters metabolism and proliferation of human cell lines. PLoS One 8:e64561.

Akhmedov AT, Bertrand P, Corteggiani E, Lopez BS (1995) Characterization of two nuclear mammalian homologous DNA-pairing activities that do not require associated exonuclease activity. Proc Natl Acad Sci U S A 92:1729-1733.

Al-Chalabi A, Hardiman O (2013) The epidemiology of ALS: a conspiracy of genes, environment and time. Nat Rev Neurol 9:617-628.

Anderson P, Kedersha N (2008) Stress granules: the Tao of RNA triage. Trends Biochem Sci 33:141-150.

Andreeff M GD PA (2000) Cell Proliferation, Differentiation, and Apoptosis. In: Holland-Frei Cancer Medicine, 5th Edition (Bast RC Jr KD PR, et al, ed). Hamilton: BC Decker.

Antonescu CR, Elahi A, Humphrey M, Lui MY, Healey JH, Brennan MF, Woodruff JM, Jhanwar SC, Ladanyi M (2000) Specificity of TLS-CHOP rearrangement for classic myxoid/round cell liposarcoma: absence in predominantly myxoid well-differentiated liposarcomas. J Mol Diagn 2:132-138.

Aoki N, Higashi S, Kawakami I, Kobayashi Z, Hosokawa M, Katsuse O, Togo T, Hirayasu Y, Akiyama H (2012) Localization of fused in sarcoma (FUS) protein to the post-synaptic density in the brain. Acta Neuropathol 124:383-394.

Arai T, Hasegawa M, Akiyama H, Ikeda K, Nonaka T, Mori H, Mann D, Tsuchiya K, Yoshida M, Hashizume Y, Oda T (2006) TDP-43 is a component of ubiquitin-positive tau-negative inclusions in frontotemporal lobar degeneration and amyotrophic lateral sclerosis. Biochem Biophys Res Commun 351:602-611.

Armon C (2003) An evidence-based medicine approach to the evaluation of the role of exogenous risk factors in sporadic amyotrophic lateral sclerosis. Neuroepidemiology 22:217-228.

Aschner M, Syversen T, Souza DO, Rocha JB (2006) Metallothioneins: mercury species-specific induction and their potential role in attenuating neurotoxicity. Exp Biol Med (Maywood) 231:1468-1473.

Askari N, Beenstock J, Livnah O, Engelberg D (2009) p38alpha is active in vitro and in vivo when monophosphorylated at threonine 180. Biochemistry 48:2497-2504.

Aulas A, Stabile S, Vande Velde C (2012) Endogenous TDP-43, but not FUS, contributes to stress granule assembly via G3BP. Molecular neurodegeneration 7:54.

Baechtold H, Kuroda M, Sok J, Ron D, Lopez BS, Akhmedov AT (1999) Human 75-kDa DNA-pairing protein is identical to the pro-oncoprotein TLS/FUS and is able to promote D-loop formation. J Biol Chem 274:34337-34342.

Baron DM, Kaushansky LJ, Ward CL, Sama RR, Chian RJ, Boggio KJ, Quaresma AJ, Nickerson JA, Bosco DA (2013) Amyotrophic lateral sclerosis-linked FUS/TLS alters stress granule assembly and dynamics. Mol Neurodegener 8:30.

Barrett LW, Fletcher S, Wilton SD (2012) Regulation of eukaryotic gene expression by the untranslated gene regions and other non-coding elements. Cell Mol Life Sci 69:3613-3634.

Bartoli KM, Bishop DL, Saunders WS (2011) The role of molecular microtubule motors and the microtubule cytoskeleton in stress granule dynamics. Int J Cell Biol 2011:939848.

Baumer D, Hilton D, Paine SM, Turner MR, Lowe J, Talbot K, Ansorge O (2010) Juvenile ALS with basophilic inclusions is a FUS proteinopathy with FUS mutations. Neurology 75:611-618.

Belly A, Moreau-Gachelin F, Sadoul R, Goldberg Y (2005) Delocalization of the multifunctional RNA splicing factor TLS/FUS in hippocampal neurones: exclusion from the nucleus and accumulation in dendritic granules and spine heads. Neurosci Lett 379:152-157.

Bendotti C, Marino M, Cheroni C, Fontana E, Crippa V, Poletti A, De Biasi S (2012) Dysfunction of constitutive and inducible ubiquitin-proteasome system in amyotrophic lateral sclerosis: implication for protein aggregation and immune response. Prog Neurobiol 97:101-126.

Bendotti C, Bao Cutrona M, Cheroni C, Grignaschi G, Lo Coco D, Peviani M, Tortarolo M, Veglianese P, Zennaro E (2005) Inter- and intracellular signaling in amyotrophic lateral sclerosis: role of p38 mitogen-activated protein kinase. Neurodegener Dis 2:128-134.

Benito-Leon J, Louis ED (2006) Essential tremor: emerging views of a common disorder. Nat Clin Pract Neurol 2:666-678; quiz 662p following 691.

Bensimon G, Lacomblez L, Meininger V (1994) A controlled trial of riluzole in amyotrophic lateral sclerosis. ALS/Riluzole Study Group. N Engl J Med 330:585-591.

Bentmann E, Haass C, Dormann D (2013) Stress granules in neurodegeneration--lessons learnt from TAR DNA binding protein of 43 kDa and fused in sarcoma. FEBS J 280:4348-4370.

Bentmann E, Neumann M, Tahirovic S, Rodde R, Dormann D, Haass C (2012) Requirements for stress granule recruitment of fused in sarcoma (FUS) and TAR DNA-binding protein of 43 kDa (TDP-43). The Journal of biological chemistry 287:23079-23094.

Bermejo-Pareja F, Puertas-Martin V (2013) Cognitive features of essential tremor: a review of the clinical aspects and possible mechanistic underpinnings. Tremor Other Hyperkinet Mov (N Y) 2.

Bertolotti A, Lutz Y, Heard DJ, Chambon P, Tora L (1996) hTAF(II)68, a novel RNA/ssDNA-binding protein with homology to the pro-oncoproteins TLS/FUS and EWS is associated with both TFIID and RNA polymerase II. EMBO J 15:5022-5031.

Bertolotti A, Melot T, Acker J, Vigneron M, Delattre O, Tora L (1998) EWS, but not EWS-FLI-1, is associated with both TFIID and RNA polymerase II: interactions between two members of the TET family, EWS and hTAFII68, and subunits of TFIID and RNA polymerase II complexes. Mol Cell Biol 18:1489-1497.

Bertrand P, Akhmedov AT, Delacote F, Durrbach A, Lopez BS (1999) Human POMp75 is identified as the pro-oncoprotein TLS/FUS: both POMp75 and POMp100 DNA homologous pairing activities are associated to cell proliferation. Oncogene 18:4515-4521.

Beshay E, Croze F, Prud'homme GJ (2001) The phosphodiesterase inhibitors pentoxifylline and rolipram suppress macrophage activation and nitric oxide production in vitro and in vivo. Clin Immunol 98:272-279.

Blokhuis AM, Groen EJ, Koppers M, van den Berg LH, Pasterkamp RJ (2013) Protein aggregation in amyotrophic lateral sclerosis. Acta Neuropathol 125:777-794.

Bonda DJ, Lee HP, Kudo W, Zhu X, Smith MA, Lee HG (2010a) Pathological implications of cell cycle re-entry in Alzheimer disease. Expert Rev Mol Med 12:e19.

Bonda DJ, Bajic VP, Spremo-Potparevic B, Casadesus G, Zhu X, Smith MA, Lee HG (2010b) Review: cell cycle aberrations and neurodegeneration. Neuropathol Appl Neurobiol 36:157-163.

Bosco DA, Lemay N, Ko HK, Zhou H, Burke C, Kwiatkowski TJ, Jr., Sapp P, McKenna-Yasek D, Brown RH, Jr., Hayward LJ (2010a) Mutant FUS proteins that cause amyotrophic lateral sclerosis incorporate into stress granules. Human molecular genetics 19:4160-4175.

Bosco DA, Morfini G, Karabacak NM, Song Y, Gros-Louis F, Pasinelli P, Goolsby H, Fontaine BA, Lemay N, McKenna-Yasek D, Frosch MP, Agar JN, Julien JP, Brady ST, Brown RH, Jr. (2010b) Wild-type and mutant SOD1 share an aberrant conformation and a common pathogenic pathway in ALS. Nat Neurosci 13:1396-1403.

Brooke GN, Culley RL, Dart DA, Mann DJ, Gaughan L, McCracken SR, Robson CN, Spencer-Dene B, Gamble SC, Powell SM, Wait R, Waxman J, Walker MM, Bevan CL (2010) FUS/TLS is a novel mediator of androgen-dependent cell-cycle progression and prostate cancer growth. Cancer Res 71:914-924.

Bukhtiyarova M, Northrop K, Chai X, Casper D, Karpusas M, Springman E (2004) Improved expression, purification, and crystallization of p38alpha MAP kinase. Protein Expr Purif 37:154-161.

Calvio C, Neubauer G, Mann M, Lamond AI (1995) Identification of hnRNP P2 as TLS/FUS using electrospray mass spectrometry. RNA 1:724-733.

Cashman NR, Durham HD, Blusztajn JK, Oda K, Tabira T, Shaw IT, Dahrouge S, Antel JP (1992) Neuroblastoma x spinal cord (NSC) hybrid cell lines resemble developing motor neurons. Dev Dyn 194:209-221.

Chance PF, Rabin BA, Ryan SG, Ding Y, Scavina M, Crain B, Griffin JW, Cornblath DR (1998) Linkage of the gene for an autosomal dominant form of juvenile amyotrophic lateral sclerosis to chromosome 9q34. Am J Hum Genet 62:633-640.

Chen S, Zhang X, Song L, Le W (2012) Autophagy dysregulation in amyotrophic lateral sclerosis. Brain Pathol 22:110-116.

Chen S, Sayana P, Zhang X, Le W (2013) Genetics of amyotrophic lateral sclerosis: an update. Mol Neurodegener 8:28.

Chio A, Benzi G, Dossena M, Mutani R, Mora G (2005) Severely increased risk of amyotrophic lateral sclerosis among Italian professional football players. Brain 128:472-476.

Colombrita C, Zennaro E, Fallini C, Weber M, Sommacal A, Buratti E, Silani V, Ratti A (2009) TDP-43 is recruited to stress granules in conditions of oxidative insult. J Neurochem 111:1051-1061.

Colombrita C, Onesto E, Megiorni F, Pizzuti A, Baralle FE, Buratti E, Silani V, Ratti A (2012) TDP-43 and FUS RNA-binding proteins bind distinct sets of cytoplasmic messenger RNAs and differently regulate their post-transcriptional fate in motoneuron-like cells. The Journal of biological chemistry 287:15635-15647.

Coppede F (2011) An overview of DNA repair in amyotrophic lateral sclerosis. TheScientificWorldJournal 11:1679-1691.

Crozat A, Aman P, Mandahl N, Ron D (1993) Fusion of CHOP to a novel RNA-binding protein in human myxoid liposarcoma. Nature 363:640-644.

Dayon L, Hainard A, Licker V, Turck N, Kuhn K, Hochstrasser DF, Burkhard PR, Sanchez JC (2008) Relative quantification of proteins in human cerebrospinal fluids by MS/MS using 6-plex isobaric tags. Anal Chem 80:2921-2931.

Dejardin J, Kingston RE (2009) Purification of proteins associated with specific genomic Loci. Cell 136:175-186.

DeJesus-Hernandez M et al. (2011) Expanded GGGGCC hexanucleotide repeat in noncoding region of C9ORF72 causes chromosome 9p-linked FTD and ALS. Neuron 72:245-256.

Delva L, Gallais I, Guillouf C, Denis N, Orvain C, Moreau-Gachelin F (2004) Multiple functional domains of the oncoproteins Spi-1/PU.1 and TLS are involved in their opposite splicing effects in erythroleukemic cells. Oncogene 23:4389-4399.

Deng HX et al. (2011) Mutations in UBQLN2 cause dominant X-linked juvenile and adult-onset ALS and ALS/dementia. Nature 477:211-215.

Devasagayam TP, Tilak JC, Boloor KK, Sane KS, Ghaskadbi SS, Lele RD (2004) Free radicals and antioxidants in human health: current status and future prospects. J Assoc Physicians India 52:794-804.

Dewey CM, Cenik B, Sephton CF, Johnson BA, Herz J, Yu G (2012) TDP-43 aggregation in neurodegeneration: are stress granules the key? Brain Res 1462:16-25.

Dewey CM, Cenik B, Sephton CF, Dries DR, Mayer P, 3rd, Good SK, Johnson BA, Herz J, Yu G (2010) TDP-43 is directed to stress granules by sorbitol, a novel physiological osmotic and oxidative stressor. Molecular and cellular biology.

Dewil M, dela Cruz VF, Van Den Bosch L, Robberecht W (2007) Inhibition of p38 mitogen activated protein kinase activation and mutant SOD1(G93A)-induced motor neuron death. Neurobiol Dis 26:332-341.

Diskin R, Lebendiker M, Engelberg D, Livnah O (2007) Structures of p38alpha active mutants reveal conformational changes in L16 loop that induce autophosphorylation and activation. J Mol Biol 365:66-76.

Diskin R, Askari N, Capone R, Engelberg D, Livnah O (2004) Active mutants of the human p38alpha mitogen-activated protein kinase. J Biol Chem 279:47040-47049.

Doi H, Koyano S, Suzuki Y, Nukina N, Kuroiwa Y (2009) The RNA-binding protein FUS/TLS is a common aggregate-interacting protein in polyglutamine diseases. Neurosci Res 66:131-133.

Donnelly CJ, Zhang PW, Pham JT, Heusler AR, Mistry NA, Vidensky S, Daley EL, Poth EM, Hoover B, Fines DM, Maragakis N, Tienari PJ, Petrucelli L, Traynor BJ, Wang J, Rigo F, Bennett CF, Blackshaw S, Sattler R, Rothstein JD (2013) RNA toxicity from the ALS/FTD C9ORF72 expansion is mitigated by antisense intervention. Neuron 80:415-428.

Dormann D, Haass C (2013) Fused in sarcoma (FUS): An oncogene goes awry in neurodegeneration. Mol Cell Neurosci 56:475-486.

Dormann D, Rodde R, Edbauer D, Bentmann E, Fischer I, Hruscha A, Than ME, Mackenzie IR, Capell A, Schmid B, Neumann M, Haass C (2010) ALS-associated fused in sarcoma (FUS) mutations disrupt Transportin-mediated nuclear import. The EMBO journal 29:2841-2857.

Du K, Arai S, Kawamura T, Matsushita A, Kurokawa R (2011) TLS and PRMT1 synergistically coactivate transcription at the survivin promoter through

TLS arginine methylation. Biochemical and biophysical research communications 404:991-996.

Ezzi SA, Urushitani M, Julien JP (2007) Wild-type superoxide dismutase acquires binding and toxic properties of ALS-linked mutant forms through oxidation. J Neurochem 102:170-178.

Farg MA, Soo KY, Walker AK, Pham H, Orian J, Horne MK, Warraich ST, Williams KL, Blair IP, Atkin JD (2012) Mutant FUS induces endoplasmic reticulum stress in amyotrophic lateral sclerosis and interacts with protein disulfide-isomerase. Neurobiol Aging 33:2855-2868.

Farg MA, Sundaramoorthy V, Sultana JM, Yang S, Atkinson RA, Levina V, Halloran MA, Gleeson PA, Blair IP, Soo KY, King AE, Atkin JD (2014) C9ORF72, implicated in amytrophic lateral sclerosis and frontotemporal dementia, regulates endosomal trafficking. Hum Mol Genet 23:3579-3595.

Figley MD, Bieri G, Kolaitis RM, Taylor JP, Gitler AD (2014) Profilin 1 Associates with Stress Granules and ALS-Linked Mutations Alter Stress Granule Dynamics. J Neurosci 34:8083-8097.

Fratta P, Mizielinska S, Nicoll AJ, Zloh M, Fisher EM, Parkinson G, Isaacs AM (2012) C9orf72 hexanucleotide repeat associated with amyotrophic lateral sclerosis and frontotemporal dementia forms RNA G-quadruplexes. Sci Rep 2:1016.

Fujii R, Takumi T (2005) TLS facilitates transport of mRNA encoding an actin-stabilizing protein to dendritic spines. Journal of cell science 118:5755-5765.

Fujii R, Okabe S, Urushido T, Inoue K, Yoshimura A, Tachibana T, Nishikawa T, Hicks GG, Takumi T (2005) The RNA binding protein TLS is translocated to dendritic spines by mGluR5 activation and regulates spine morphology. Curr Biol 15:587-593.

Furukawa Y, Fu R, Deng HX, Siddique T, O'Halloran TV (2006) Disulfide cross-linked protein represents a significant fraction of ALS-associated Cu, Zn-superoxide dismutase aggregates in spinal cords of model mice. Proc Natl Acad Sci U S A 103:7148-7153.

Gal J, Zhang J, Kwinter DM, Zhai J, Jia H, Jia J, Zhu H (2011) Nuclear localization sequence of FUS and induction of stress granules by ALS mutants. Neurobiol Aging.

Ge B, Gram H, Di Padova F, Huang B, New L, Ulevitch RJ, Luo Y, Han J (2002) MAPKK-independent activation of p38alpha mediated by TAB1-dependent autophosphorylation of p38alpha. Science 295:1291-1294.

Gong B, Vitolo OV, Trinchese F, Liu S, Shelanski M, Arancio O (2004) Persistent improvement in synaptic and cognitive functions in an Alzheimer mouse model after rolipram treatment. J Clin Invest 114:1624-1634.

Gorbunova V, Seluanov A, Mao Z, Hine C (2007) Changes in DNA repair during aging. Nucleic Acids Res 35:7466-7474.

Gordon PH (2013) Amyotrophic Lateral Sclerosis: An update for 2013 Clinical Features, Pathophysiology, Management and Therapeutic Trials. Aging Dis 4:295-310.

Gorur S, Celik S, Hakverdi S, Aslantas O, Erdogan S, Aydin M, Ocak S, Namik Kiper A (2008) Preventive effect of rolipram, a phosphodiesterase 4 enzyme inhibitor, on oxidative renal injury in acute ascending pyelonephritis model in rats. Urology 72:743-748.

Greider CW (1999) Telomeres do D-loop-T-loop. Cell 97:419-422.

Griffith JD, Comeau L, Rosenfield S, Stansel RM, Bianchi A, Moss H, de Lange T (1999) Mammalian telomeres end in a large duplex loop. Cell 97:503-514.

Grimm D, Streetz KL, Jopling CL, Storm TA, Pandey K, Davis CR, Marion P, Salazar F, Kay MA (2006) Fatality in mice due to oversaturation of cellular microRNA/short hairpin RNA pathways. Nature 441:537-541.

Hadano S et al. (2001) A gene encoding a putative GTPase regulator is mutated in familial amyotrophic lateral sclerosis 2. Nat Genet 29:166-173.

Haeusler AR, Donnelly CJ, Periz G, Simko EA, Shaw PG, Kim MS, Maragakis NJ, Troncoso JC, Pandey A, Sattler R, Rothstein JD, Wang J (2014) C9orf72 nucleotide repeat structures initiate molecular cascades of disease. Nature 507:195-200.

Haile S, Lal A, Myung JK, Sadar MD (2011) FUS/TLS is a co-activator of androgen receptor in prostate cancer cells. PLoS One 6:e24197.

Hallier M, Lerga A, Barnache S, Tavitian A, Moreau-Gachelin F (1998) The transcription factor Spi-1/PU.1 interacts with the potential splicing factor TLS. J Biol Chem 273:4838-4842.

Han J, Lee JD, Bibbs L, Ulevitch RJ (1994) A MAP kinase targeted by endotoxin and hyperosmolarity in mammalian cells. Science 265:808-811.

Han SP, Tang YH, Smith R (2010) Functional diversity of the hnRNPs: past, present and perspectives. Biochem J 430:379-392.

Hedera P, Davis TL, Phibbs FT, Charles PD, Ledoux MS (2013) FUS in familial essential tremor - The search for common causes is still on. Parkinsonism Relat Disord.

Hentati A, Ouahchi K, Pericak-Vance MA, Nijhawan D, Ahmad A, Yang Y, Rimmler J, Hung W, Schlotter B, Ahmed A, Ben Hamida M, Hentati F, Siddique T (1998) Linkage of a commoner form of recessive amyotrophic lateral sclerosis to chromosome 15q15-q22 markers. Neurogenetics 2:55-60.

Herrup K (2012) The contributions of unscheduled neuronal cell cycle events to the death of neurons in Alzheimer's disease. Front Biosci (Elite Ed) 4:2101-2109.

Herrup K, Yang Y (2007) Cell cycle regulation in the postmitotic neuron: oxymoron or new biology? Nat Rev Neurosci 8:368-378.

Hetz C (2012) The unfolded protein response: controlling cell fate decisions under ER stress and beyond. Nature reviews Molecular cell biology 13:89-102.

Hicks GG, Singh N, Nashabi A, Mai S, Bozek G, Klewes L, Arapovic D, White EK, Koury MJ, Oltz EM, Van Kaer L, Ruley HE (2000) Fus deficiency in mice results in defective B-lymphocyte development and activation, high levels of chromosomal instability and perinatal death. Nat Genet 24:175-179.

Hoell JI, Larsson E, Runge S, Nusbaum JD, Duggimpudi S, Farazi TA, Hafner M, Borkhardt A, Sander C, Tuschl T (2011) RNA targets of wild-type and mutant FET family proteins. Nat Struct Mol Biol 18:1428-1431.

Hoyaux D, Alao J, Fuchs J, Kiss R, Keller B, Heizmann CW, Pochet R, Frermann D (2000) S100A6, a calcium- and zinc-binding protein, is overexpressed in SOD1 mutant mice, a model for amyotrophic lateral sclerosis. Biochim Biophys Acta 1498:264-272.

Huang C, Zhou H, Tong J, Chen H, Liu YJ, Wang D, Wei X, Xia XG (2011) FUS transgenic rats develop the phenotypes of amyotrophic lateral sclerosis and frontotemporal lobar degeneration. PLoS Genet 7:e1002011.

Ichikawa H, Shimizu K, Hayashi Y, Ohki M (1994) An RNA-binding protein gene, TLS/FUS, is fused to ERG in human myeloid leukemia with t(16;21) chromosomal translocation. Cancer Res 54:2865-2868.

Iko Y, Kodama TS, Kasai N, Oyama T, Morita EH, Muto T, Okumura M, Fujii R, Takumi T, Tate S, Morikawa K (2004) Domain architectures and characterization of an RNA-binding protein, TLS. J Biol Chem 279:44834-44840.

Immanuel D, Zinszner H, Ron D (1995) Association of SARFH (sarcoma-associated RNA-binding fly homolog) with regions of chromatin transcribed by RNA polymerase II. Mol Cell Biol 15:4562-4571.

Ishigaki S, Masuda A, Fujioka Y, Iguchi Y, Katsuno M, Shibata A, Urano F, Sobue G, Ohno K (2012) Position-dependent FUS-RNA interactions regulate alternative splicing events and transcriptions. Sci Rep 2:529.

Jackson AL, Linsley PS (2010) Recognizing and avoiding siRNA off-target effects for target identification and therapeutic application. Nat Rev Drug Discov 9:57-67.

Joza N, Susin SA, Daugas E, Stanford WL, Cho SK, Li CY, Sasaki T, Elia AJ, Cheng HY, Ravagnan L, Ferri KF, Zamzami N, Wakeham A, Hakem R, Yoshida H, Kong YY, Mak TW, Zuniga-Pflucker JC, Kroemer G, Penninger JM (2001) Essential role of the mitochondrial apoptosis-inducing factor in programmed cell death. Nature 410:549-554.

Jullien P, Bougeret C, Camoin L, Bodeus M, Durand H, Disanto JP, Fischer S, Benarous R (1994) Tyr394 and Tyr505 are autophosphorylated in recombinant Lck protein-tyrosine kinase expressed in Escherichia coli. Eur J Biochem 224:589-596.

Kabashi E, Bercier V, Lissouba A, Liao M, Brustein E, Rouleau GA, Drapeau P (2011) FUS and TARDBP but not SOD1 interact in genetic models of amyotrophic lateral sclerosis. PLoS Genet 7:e1002214.

Kabashi E, Valdmanis PN, Dion P, Spiegelman D, McConkey BJ, Vande Velde C, Bouchard JP, Lacomblez L, Pochigaeva K, Salachas F, Pradat PF, Camu W, Meininger V, Dupre N, Rouleau GA (2008) TARDBP mutations in individuals with sporadic and familial amyotrophic lateral sclerosis. Nat Genet 40:572-574.

Kanekura K, Nishimoto I, Aiso S, Matsuoka M (2006) Characterization of amyotrophic lateral sclerosis-linked P56S mutation of vesicle-associated membrane protein-associated protein B (VAPB/ALS8). J Biol Chem 281:30223-30233.

Kedersha N, Anderson P (2007) Mammalian stress granules and processing bodies. Methods Enzymol 431:61-81.

Kedersha N, Ivanov P, Anderson P (2013) Stress granules and cell signaling: more than just a passing phase? Trends Biochem Sci 38:494-506.

Kedersha NL, Gupta M, Li W, Miller I, Anderson P (1999) RNA-binding proteins TIA-1 and TIAR link the phosphorylation of eIF-2 alpha to the assembly of mammalian stress granules. The Journal of cell biology 147:1431-1442.

Keesler GA, Bray J, Hunt J, Johnson DA, Gleason T, Yao Z, Wang SW, Parker C, Yamane H, Cole C, Lichenstein HS (1998) Purification and activation of recombinant p38 isoforms alpha, beta, gamma, and delta. Protein Expr Purif 14:221-228.

Kelstrup CD, Young C, Lavallee R, Nielsen ML, Olsen JV (2012) Optimized fast and sensitive acquisition methods for shotgun proteomics on a quadrupole orbitrap mass spectrometer. J Proteome Res 11:3487-3497.

Khan AA, Betel D, Miller ML, Sander C, Leslie CS, Marks DS (2009) Transfection of small RNAs globally perturbs gene regulation by endogenous microRNAs. Nat Biotechnol 27:549-555.

Kim EK, Choi EJ (2010) Pathological roles of MAPK signaling pathways in human diseases. Biochim Biophys Acta 1802:396-405.

Kim HJ, Raphael AR, Ladow ES, McGurk L, Weber RA, Trojanowski JQ, Lee VM, Finkbeiner S, Gitler AD, Bonini NM (2013) Therapeutic modulation of eIF2alpha phosphorylation rescues TDP-43 toxicity in amyotrophic lateral sclerosis disease models. Nat Genet.

Kim SH, Shanware NP, Bowler MJ, Tibbetts RS (2010) Amyotrophic lateral sclerosis-associated proteins TDP-43 and FUS/TLS function in a common biochemical complex to co-regulate HDAC6 mRNA. J Biol Chem 285:34097-34105.

Kino Y, Washizu C, Aquilanti E, Okuno M, Kurosawa M, Yamada M, Doi H, Nukina N (2011) Intracellular localization and splicing regulation of FUS/TLS are variably affected by amyotrophic lateral sclerosis-linked mutations. Nucleic Acids Res 39:2781-2798.

Krishna M, Narang H (2008) The complexity of mitogen-activated protein kinases (MAPKs) made simple. Cell Mol Life Sci 65:3525-3544.

Kuroda M, Sok J, Webb L, Baechtold H, Urano F, Yin Y, Chung P, de Rooij DG, Akhmedov A, Ashley T, Ron D (2000) Male sterility and enhanced radiation sensitivity in TLS(-/-) mice. EMBO J 19:453-462.

Kwiatkowski TJ, Jr. et al. (2009) Mutations in the FUS/TLS gene on chromosome 16 cause familial amyotrophic lateral sclerosis. Science 323:1205-1208.

Labbe C, Soto-Ortolaza AI, Rayaprolu S, Harriott AM, Strongosky AJ, Uitti RJ, Van Gerpen JA, Wszolek ZK, Ross OA (2013) Investigating the role of FUS exonic variants in Essential Tremor. Parkinsonism Relat Disord.

Lacomblez L, Bensimon G, Leigh PN, Guillet P, Meininger V (1996) Dose-ranging study of riluzole in amyotrophic lateral sclerosis. Amyotrophic Lateral Sclerosis/Riluzole Study Group II. Lancet 347:1425-1431.

Lagier-Tourenne C et al. (2012) Divergent roles of ALS-linked proteins FUS/TLS and TDP-43 intersect in processing long pre-mRNAs. Nature neuroscience 15:1488-1497.

Lee YB, Chen HJ, Peres JN, Gomez-Deza J, Attig J, Stalekar M, Troakes C, Nishimura AL, Scotter EL, Vance C, Adachi Y, Sardone V, Miller JW, Smith BN, Gallo JM, Ule J, Hirth F, Rogelj B, Houart C, Shaw CE (2013) Hexanucleotide repeats in ALS/FTD form length-dependent RNA foci, sequester RNA binding proteins, and are neurotoxic. Cell Rep 5:1178-1186.

Lerga A, Hallier M, Delva L, Orvain C, Gallais I, Marie J, Moreau-Gachelin F (2001) Identification of an RNA binding specificity for the potential splicing factor TLS. The Journal of biological chemistry 276:6807-6816.

Lesniak W, Slomnicki LP, Filipek A (2009) S100A6 - new facts and features. Biochem Biophys Res Commun 390:1087-1092.

Li X, Heyer WD (2008) Homologous recombination in DNA repair and DNA damage tolerance. Cell Res 18:99-113.

Li YR, King OD, Shorter J, Gitler AD (2013) Stress granules as crucibles of ALS pathogenesis. J Cell Biol 201:361-372.

Ling SC, Polymenidou M, Cleveland DW (2013) Converging mechanisms in ALS and FTD: disrupted RNA and protein homeostasis. Neuron 79:416-438.

Liu-Yesucevitz L, Bilgutay A, Zhang YJ, Vanderwyde T, Citro A, Mehta T, Zaarur N, McKee A, Bowser R, Sherman M, Petrucelli L, Wolozin B (2010) Tar DNA binding protein-43 (TDP-43) associates with stress granules: analysis of cultured cells and pathological brain tissue. PloS one 5:e13250.

Liu X, Niu C, Ren J, Zhang J, Xie X, Zhu H, Feng W, Gong W (2013) The RRM domain of human fused in sarcoma protein reveals a non-canonical nucleic acid binding site. Biochimica et biophysica acta 1832:375-385.

Machamer JB, Collins SE, Lloyd TE (2014) The ALS gene FUS regulates synaptic transmission at the Drosophila neuromuscular junction. Hum Mol Genet.

Mackenzie IR, Ansorge O, Strong M, Bilbao J, Zinman L, Ang LC, Baker M, Stewart H, Eisen A, Rademakers R, Neumann M (2011) Pathological

heterogeneity in amyotrophic lateral sclerosis with FUS mutations: two distinct patterns correlating with disease severity and mutation. Acta Neuropathol 122:87-98.

Mackenzie IR et al. (2010) Nomenclature and nosology for neuropathologic subtypes of frontotemporal lobar degeneration: an update. Acta Neuropathol 119:1-4.

Mackness BC, Tran MT, McClain SP, Matthews CR, Zitzewitz JA (2014) Folding of the RNA recognition motif (RRM) domains of the amyotrophic lateral sclerosis (ALS)-linked protein TDP-43 reveals an intermediate state. J Biol Chem 289:8264-8276.

Mastrocola AS, Kim SH, Trinh AT, Rodenkirch LA, Tibbetts RS (2013) The RNA Binding Protein Fused In Sarcoma (FUS) Functions Downstream of PARP in Response to DNA Damage. J Biol Chem.

Mattson MP, Magnus T (2006) Ageing and neuronal vulnerability. Nat Rev Neurosci 7:278-294.

Matus S, Valenzuela V, Medinas DB, Hetz C (2013) ER Dysfunction and Protein Folding Stress in ALS. Int J Cell Biol 2013:674751.

Mazroui R, Di Marco S, Kaufman RJ, Gallouzi IE (2007) Inhibition of the ubiquitin-proteasome system induces stress granule formation. Molecular biology of the cell 18:2603-2618.

McGuire V, Longstreth WT, Jr., Nelson LM, Koepsell TD, Checkoway H, Morgan MS, van Belle G (1997) Occupational exposures and amyotrophic lateral sclerosis. A population-based case-control study. Am J Epidemiol 145:1076-1088.

Meissner M, Lopato S, Gotzmann J, Sauermann G, Barta A (2003) Proto-oncoprotein TLS/FUS is associated to the nuclear matrix and complexed with splicing factors PTB, SRm160, and SR proteins. Experimental cell research 283:184-195.

Merner ND et al. (2012) Exome sequencing identifies FUS mutations as a cause of essential tremor. Am J Hum Genet 91:313-319.

Morfini GA, Burns M, Binder LI, Kanaan NM, LaPointe N, Bosco DA, Brown RH, Jr., Brown H, Tiwari A, Hayward L, Edgar J, Nave KA, Garberrn J, Atagi Y, Song Y, Pigino G, Brady ST (2009) Axonal transport defects in neurodegenerative diseases. J Neurosci 29:12776-12786.

Morfini GA, Bosco DA, Brown H, Gatto R, Kaminska A, Song Y, Molla L, Baker L, Marangoni MN, Berth S, Tavassoli E, Bagnato C, Tiwari A, Hayward LJ, Pigino GF, Watterson DM, Huang CF, Banker G, Brown RH, Jr., Brady ST (2013) Inhibition of fast axonal transport by pathogenic SOD1 involves activation of p38 MAP kinase. PLoS One 8:e65235.

Mori K, Lammich S, Mackenzie IR, Forne I, Zilow S, Kretzschmar H, Edbauer D, Janssens J, Kleinberger G, Cruts M, Herms J, Neumann M, Van Broeckhoven C, Arzberger T, Haass C (2013) hnRNP A3 binds to GGGGCC repeats and is a constituent of p62-positive/TDP43-negative

inclusions in the hippocampus of patients with C9orf72 mutations. Acta Neuropathol 125:413-423.

Munoz DG, Neumann M, Kusaka H, Yokota O, Ishihara K, Terada S, Kuroda S, Mackenzie IR (2009) FUS pathology in basophilic inclusion body disease. Acta neuropathologica.

Nakagawa S, Kim JE, Lee R, Malberg JE, Chen J, Steffen C, Zhang YJ, Nestler EJ, Duman RS (2002) Regulation of neurogenesis in adult mouse hippocampus by cAMP and the cAMP response element-binding protein. J Neurosci 22:3673-3682.

Nakaya T, Alexiou P, Maragkakis M, Chang A, Mourelatos Z (2013) FUS regulates genes coding for RNA-binding proteins in neurons by binding to their highly conserved introns. RNA 19:498-509.

Neumann M, Roeber S, Kretzschmar HA, Rademakers R, Baker M, Mackenzie IR (2009a) Abundant FUS-immunoreactive pathology in neuronal intermediate filament inclusion disease. Acta neuropathologica.

Neumann M, Rademakers R, Roeber S, Baker M, Kretzschmar HA, Mackenzie IR (2009b) A new subtype of frontotemporal lobar degeneration with FUS pathology. Brain.

Neumann M, Sampathu DM, Kwong LK, Truax AC, Micsenyi MC, Chou TT, Bruce J, Schuck T, Grossman M, Clark CM, McCluskey LF, Miller BL, Masliah E, Mackenzie IR, Feldman H, Feiden W, Kretzschmar HA, Trojanowski JQ, Lee VM (2006) Ubiquitinated TDP-43 in frontotemporal lobar degeneration and amyotrophic lateral sclerosis. Science 314:130-133.

Nguyen MD, Boudreau M, Kriz J, Couillard-Despres S, Kaplan DR, Julien JP (2003) Cell cycle regulators in the neuronal death pathway of amyotrophic lateral sclerosis caused by mutant superoxide dismutase 1. J Neurosci 23:2131-2140.

Nikulina E, Tidwell JL, Dai HN, Bregman BS, Filbin MT (2004) The phosphodiesterase inhibitor rolipram delivered after a spinal cord lesion promotes axonal regeneration and functional recovery. Proc Natl Acad Sci U S A 101:8786-8790.

NINDS (2013) Amyotrophic Lateral Sclerosis (ALS) Fact Sheet. NIH Publication No 13-916.

Nishitoh H, Kadowaki H, Nagai A, Maruyama T, Yokota T, Fukutomi H, Noguchi T, Matsuzawa A, Takeda K, Ichijo H (2008) ALS-linked mutant SOD1 induces ER stress- and ASK1-dependent motor neuron death by targeting Derlin-1. Genes Dev 22:1451-1464.

Ohuchida K, Mizumoto K, Ishikawa N, Fujii K, Konomi H, Nagai E, Yamaguchi K, Tsuneyoshi M, Tanaka M (2005) The role of S100A6 in pancreatic cancer development and its clinical implication as a diagnostic marker and therapeutic target. Clin Cancer Res 11:7785-7793.

Olive PL, Banath JP (2006) The comet assay: a method to measure DNA damage in individual cells. Nat Protoc 1:23-29.

Ong DS, Kelly JW (2011) Chemical and/or biological therapeutic strategies to ameliorate protein misfolding diseases. Curr Opin Cell Biol 23:231-238.

Orozco D, Tahirovic S, Rentzsch K, Schwenk BM, Haass C, Edbauer D (2012) Loss of fused in sarcoma (FUS) promotes pathological Tau splicing. EMBO Rep 13:759-764.

Ortega-Cubero S, Lorenzo-Betancor O, Lorenzo E, Alonso E, Coria F, Pastor MA, Fernandez-Santiago R, Marti MJ, Ezquerra M, Valldeoriola F, Compta Y, Tolosa E, Agundez JA, Jimenez-Jimenez FJ, Gironell A, Clarimon J, de Castro P, Garcia-Martin E, Alonso-Navarro H, Pastor P (2013) Fused in Sarcoma (FUS) gene mutations are not a frequent cause of essential tremor in Europeans. Neurobiol Aging.

Panagopoulos I, Aman P, Fioretos T, Hoglund M, Johansson B, Mandahl N, Heim S, Behrendtz M, Mitelman F (1994) Fusion of the FUS gene with ERG in acute myeloid leukemia with t(16;21)(p11;q22). Genes Chromosomes Cancer 11:256-262.

Parmalee N, Mirzozoda K, Kisselev S, Merner N, Dion P, Rouleau G, Clark L, Louis ED (2012) Genetic analysis of the FUS/TLS gene in essential tremor. Eur J Neurol 20:534-539.

Pasinelli P, Brown RH (2006) Molecular biology of amyotrophic lateral sclerosis: insights from genetics. Nat Rev Neurosci 7:710-723.

Polymenidou M, Lagier-Tourenne C, Hutt KR, Bennett CF, Cleveland DW, Yeo GW (2012) Misregulated RNA processing in amyotrophic lateral sclerosis. Brain Res 1462:3-15.

Provenzano PP, Keely PJ (2011) Mechanical signaling through the cytoskeleton regulates cell proliferation by coordinated focal adhesion and Rho GTPase signaling. J Cell Sci 124:1195-1205.

Qiu H, Lee S, Shang Y, Wang WY, Au KF, Kamiya S, Barmada SJ, Finkbeiner S, Lui H, Carlton CE, Tang AA, Oldham MC, Wang H, Shorter J, Filiano AJ, Roberson ED, Tourtellotte WG, Chen B, Tsai LH, Huang EJ (2014) ALS-associated mutation FUS-R521C causes DNA damage and RNA splicing defects. J Clin Invest.

Rabbitts TH, Forster A, Larson R, Nathan P (1993) Fusion of the dominant negative transcription regulator CHOP with a novel gene FUS by translocation t(12;16) in malignant liposarcoma. Nat Genet 4:175-180.

Raddaoui E, Donner LR, Panagopoulos I (2002) Fusion of the FUS and ATF1 genes in a large, deep-seated angiomatoid fibrous histiocytoma. Diagn Mol Pathol 11:157-162.

Rademakers R, Neumann M, Mackenzie IR (2012) Advances in understanding the molecular basis of frontotemporal dementia. Nat Rev Neurol 8:423-434.

Rajput A, Rajput AH, Rajput ML, Encarnacion M, Bernales CQ, Ross JP, Farrer MJ, Vilarino-Guell C (2013) Identification of FUS p.R377W in essential tremor. Eur J Neurol 21:361-363.

Rakhit R, Crow JP, Lepock JR, Kondejewski LH, Cashman NR, Chakrabartty A (2004) Monomeric Cu,Zn-superoxide dismutase is a common misfolding intermediate in the oxidation models of sporadic and familial amyotrophic lateral sclerosis. J Biol Chem 279:15499-15504.

Ranganathan S, Bowser R (2003) Alterations in G(1) to S phase cell-cycle regulators during amyotrophic lateral sclerosis. Am J Pathol 162:823-835.

Rao KS (2007) DNA repair in aging rat neurons. Neuroscience 145:1330-1340.

Rapp TB, Yang L, Conrad EU, 3rd, Mandahl N, Chansky HA (2002) RNA splicing mediated by YB-1 is inhibited by TLS/CHOP in human myxoid liposarcoma cells. J Orthop Res 20:723-729.

Reaume AG, Elliott JL, Hoffman EK, Kowall NW, Ferrante RJ, Siwek DF, Wilcox HM, Flood DG, Beal MF, Brown RH, Jr., Scott RW, Snider WD (1996) Motor neurons in Cu/Zn superoxide dismutase-deficient mice develop normally but exhibit enhanced cell death after axonal injury. Nat Genet 13:43-47.

Reddy K, Zamiri B, Stanley SY, Macgregor RB, Jr., Pearson CE (2013) The disease-associated r(GGGGCC)n repeat from the C9orf72 gene forms tract length-dependent uni- and multimolecular RNA G-quadruplex structures. J Biol Chem 288:9860-9866.

Reixach N, Deechongkit S, Jiang X, Kelly JW, Buxbaum JN (2004) Tissue damage in the amyloidoses: Transthyretin monomers and nonnative oligomers are the major cytotoxic species in tissue culture. Proc Natl Acad Sci U S A 101:2817-2822.

Renton AE, Chio A, Traynor BJ (2014) State of play in amyotrophic lateral sclerosis genetics. Nat Neurosci 17:17-23.

Renton AE et al. (2011) A hexanucleotide repeat expansion in C9ORF72 is the cause of chromosome 9p21-linked ALS-FTD. Neuron 72:257-268.

Riggi N, Cironi L, Suva ML, Stamenkovic I (2007) Sarcomas: genetics, signalling, and cellular origins. Part 1: The fellowship of TET. J Pathol 213:4-20.

Ringholz GM, Appel SH, Bradshaw M, Cooke NA, Mosnik DM, Schulz PE (2005) Prevalence and patterns of cognitive impairment in sporadic ALS. Neurology 65:586-590.

Robberecht W, Philips T (2013) The changing scene of amyotrophic lateral sclerosis. Nat Rev Neurosci 14:248-264.

Rogakou EP, Nieves-Neira W, Boon C, Pommier Y, Bonner WM (2000) Initiation of DNA fragmentation during apoptosis induces phosphorylation of H2AX histone at serine 139. J Biol Chem 275:9390-9395.

Rogelj B, Easton LE, Bogu GK, Stanton LW, Rot G, Curk T, Zupan B, Sugimoto Y, Modic M, Haberman N, Tollervey J, Fujii R, Takumi T, Shaw CE, Ule J (2012) Widespread binding of FUS along nascent RNA regulates alternative splicing in the brain. Sci Rep 2:603.

Rosen DR, Siddique T, Patterson D, Figlewicz DA, Sapp P, Hentati A, Donaldson D, Goto J, O'Regan JP, Deng HX, et al. (1993) Mutations in Cu/Zn

superoxide dismutase gene are associated with familial amyotrophic lateral sclerosis. Nature 362:59-62.
Rotunno MS, Bosco DA (2013) An emerging role for misfolded wild-type SOD1 in sporadic ALS pathogenesis. Frontiers in cellular neuroscience 7:253.
Rulten SL, Rotheray A, Green RL, Grundy GJ, Moore DA, Gomez-Herreros F, Hafezparast M, Caldecott KW (2013) PARP-1 dependent recruitment of the amyotrophic lateral sclerosis-associated protein FUS/TLS to sites of oxidative DNA damage. Nucleic Acids Res.
Sama RR, Ward CL, Bosco DA (2014) Functions of FUS/TLS from DNA repair to stress response: implications for ALS. ASN Neuro.
Sama RR, Ward CL, Kaushansky LJ, Lemay N, Ishigaki S, Urano F, Bosco DA (2013) FUS/TLS assembles into stress granules and is a prosurvival factor during hyperosmolar stress. J Cell Physiol 228:2222-2231.
Sanchez-Ramos C, Tierrez A, Fabregat-Andres O, Wild B, Sanchez-Cabo F, Arduini A, Dopazo A, Monsalve M (2011) PGC-1alpha regulates translocated in liposarcoma activity: role in oxidative stress gene expression. Antioxid Redox Signal 15:325-337.
Sareen D, O'Rourke JG, Meera P, Muhammad AK, Grant S, Simpkinson M, Bell S, Carmona S, Ornelas L, Sahabian A, Gendron T, Petrucelli L, Baughn M, Ravits J, Harms MB, Rigo F, Bennett CF, Otis TS, Svendsen CN, Baloh RH (2013) Targeting RNA foci in iPSC-derived motor neurons from ALS patients with a C9ORF72 repeat expansion. Sci Transl Med 5:208ra149.
Sasayama H, Shimamura M, Tokuda T, Azuma Y, Yoshida T, Mizuno T, Nakagawa M, Fujikake N, Nagai Y, Yamaguchi M (2012) Knockdown of the Drosophila fused in sarcoma (FUS) homologue causes deficient locomotive behavior and shortening of motoneuron terminal branches. PLoS One 7:e39483.
Sato S, Idogawa M, Honda K, Fujii G, Kawashima H, Takekuma K, Hoshika A, Hirohashi S, Yamada T (2005) Beta-catenin interacts with the FUS proto-oncogene product and regulates pre-mRNA splicing. Gastroenterology 129:1225-1236.
Scarmeas N, Shih T, Stern Y, Ottman R, Rowland LP (2002) Premorbid weight, body mass, and varsity athletics in ALS. Neurology 59:773-775.
Schwartz JC, Ebmeier CC, Podell ER, Heimiller J, Taatjes DJ, Cech TR (2012) FUS binds the CTD of RNA polymerase II and regulates its phosphorylation at Ser2. Genes Dev 26:2690-2695.
Scigelova M, Hornshaw M, Giannakopulos A, Makarov A (2011) Fourier transform mass spectrometry. Mol Cell Proteomics 10:M111 009431.
Sharma S (2007) Age-related nonhomologous end joining activity in rat neurons. Brain Res Bull 73:48-54.
Sherr CJ (1994) G1 phase progression: cycling on cue. Cell 79:551-555.

Shing DC, McMullan DJ, Roberts P, Smith K, Chin SF, Nicholson J, Tillman RM, Ramani P, Cullinane C, Coleman N (2003) FUS/ERG gene fusions in Ewing's tumors. Cancer Res 63:4568-4576.

Smith DL, Pozueta J, Gong B, Arancio O, Shelanski M (2009) Reversal of long-term dendritic spine alterations in Alzheimer disease models. Proc Natl Acad Sci U S A 106:16877-16882.

Sreedharan J, Brown RH, Jr. (2013) Amyotrophic lateral sclerosis: Problems and prospects. Ann Neurol 74:309-316.

Sreedharan J, Blair IP, Tripathi VB, Hu X, Vance C, Rogelj B, Ackerley S, Durnall JC, Williams KL, Buratti E, Baralle F, de Belleroche J, Mitchell JD, Leigh PN, Al-Chalabi A, Miller CC, Nicholson G, Shaw CE (2008) TDP-43 mutations in familial and sporadic amyotrophic lateral sclerosis. Science 319:1668-1672.

Sribenja S, Li M, Wongkham S, Wongkham C, Yao Q, Chen C (2009) Advances in thymosin beta10 research: differential expression, molecular mechanisms, and clinical implications in cancer and other conditions. Cancer Invest 27:1016-1022.

Stevanin G et al. (2007) Mutations in SPG11, encoding spatacsin, are a major cause of spastic paraplegia with thin corpus callosum. Nat Genet 39:366-372.

Stolow DT, Haynes SR (1995) Cabeza, a Drosophila gene encoding a novel RNA binding protein, shares homology with EWS and TLS, two genes involved in human sarcoma formation. Nucleic Acids Res 23:835-843.

Storlazzi CT, Mertens F, Nascimento A, Isaksson M, Wejde J, Brosjo O, Mandahl N, Panagopoulos I (2003) Fusion of the FUS and BBF2H7 genes in low grade fibromyxoid sarcoma. Hum Mol Genet 12:2349-2358.

Suzuki N, Kato S, Kato M, Warita H, Mizuno H, Shimakura N, Akiyama H, Kobayashi Z, Konno H, Aoki M (2012) FUS/TLS-immunoreactive neuronal and glial cell inclusions increase with disease duration in familial amyotrophic lateral sclerosis with an R521C FUS/TLS mutation. J Neuropathol Exp Neurol 71:779-788.

Takahama K, Oyoshi T (2013) Specific Binding of Modified RGG Domain in TLS/FUS to G-Quadruplex RNA: Tyrosines in RGG Domain Recognize 2'-OH of the Riboses of Loops in G-Quadruplex. J Am Chem Soc 135:18016-18019.

Takahama K, Arai S, Kurokawa R, Oyoshi T (2009) Identification of DNA binding specificity for TLS. Nucleic Acids Symp Ser (Oxf):247-248.

Takahama K, Sugimoto C, Arai S, Kurokawa R, Oyoshi T (2011a) Loop lengths of G-quadruplex structures affect the G-quadruplex DNA binding selectivity of the RGG motif in Ewing's sarcoma. Biochemistry 50:5369-5378.

Takahama K, Kino K, Arai S, Kurokawa R, Oyoshi T (2011b) Identification of Ewing's sarcoma protein as a G-quadruplex DNA- and RNA-binding protein. FEBS J 278:988-998.

Takahama K, Takada A, Tada S, Shimizu M, Sayama K, Kurokawa R, Oyoshi T (2013) Regulation of telomere length by G-quadruplex telomere DNA- and TERRA-binding protein TLS/FUS. Chem Biol 20:341-350.

Tan AY, Manley JL (2009a) The TET family of proteins: functions and roles in disease. J Mol Cell Biol 1:82-92.

Tan AY, Manley JL (2009b) TLS inhibits RNA polymerase III transcription. Mol Cell Biol 30:186-196.

Tan AY, Riley TR, Coady T, Bussemaker HJ, Manley JL (2012) TLS/FUS (translocated in liposarcoma/fused in sarcoma) regulates target gene transcription via single-stranded DNA response elements. Proceedings of the National Academy of Sciences of the United States of America 109:6030-6035.

Taylor JP (2014) Neurodegenerative diseases: G-quadruplex poses quadruple threat. Nature 507:175-177.

Thompson A, Schafer J, Kuhn K, Kienle S, Schwarz J, Schmidt G, Neumann T, Johnstone R, Mohammed AK, Hamon C (2003) Tandem mass tags: a novel quantification strategy for comparative analysis of complex protein mixtures by MS/MS. Anal Chem 75:1895-1904.

Tortarolo M, Veglianese P, Calvaresi N, Botturi A, Rossi C, Giorgini A, Migheli A, Bendotti C (2003) Persistent activation of p38 mitogen-activated protein kinase in a mouse model of familial amyotrophic lateral sclerosis correlates with disease progression. Mol Cell Neurosci 23:180-192.

Uetake Y SG (2012) Practical Methodology for Long-Term Recordings of Live Human Cells. In: Biomedical Optical Phase Microscopy and Nanoscopy (Shaked NT ZZ, Satterwhite L, ed), pp 43-52: Academic Press.

Uranishi H, Tetsuka T, Yamashita M, Asamitsu K, Shimizu M, Itoh M, Okamoto T (2001) Involvement of the pro-oncoprotein TLS (translocated in liposarcoma) in nuclear factor-kappa B p65-mediated transcription as a coactivator. J Biol Chem 276:13395-13401.

Urwin H et al. (2010) FUS pathology defines the majority of tau- and TDP-43-negative frontotemporal lobar degeneration. Acta Neuropathol 120:33-41.

van Blitterswijk M, Wang ET, Friedman BA, Keagle PJ, Lowe P, Leclerc AL, van den Berg LH, Housman DE, Veldink JH, Landers JE (2013) Characterization of FUS mutations in amyotrophic lateral sclerosis using RNA-Seq. PloS one 8:e60788.

Van Langenhove T, van der Zee J, Sleegers K, Engelborghs S, Vandenberghe R, Gijselinck I, Van den Broeck M, Mattheijssens M, Peeters K, De Deyn PP, Cruts M, Van Broeckhoven C (2010) Genetic contribution of FUS to frontotemporal lobar degeneration. Neurology 74:366-371.

Vance C et al. (2009) Mutations in FUS, an RNA processing protein, cause familial amyotrophic lateral sclerosis type 6. Science 323:1208-1211.

Vasak M, Meloni G (2011) Chemistry and biology of mammalian metallothioneins. J Biol Inorg Chem 16:1067-1078.

Vermeulen K, Van Bockstaele DR, Berneman ZN (2003) The cell cycle: a review of regulation, deregulation and therapeutic targets in cancer. Cell Prolif 36:131-149.

Walker AK, Soo KY, Sundaramoorthy V, Parakh S, Ma Y, Farg MA, Wallace RH, Crouch PJ, Turner BJ, Horne MK, Atkin JD (2013) ALS-associated TDP-43 induces endoplasmic reticulum stress, which drives cytoplasmic TDP-43 accumulation and stress granule formation. PLoS One 8:e81170.

Wang H, O'Reilly EJ, Weisskopf MG, Logroscino G, McCullough ML, Thun MJ, Schatzkin A, Kolonel LN, Ascherio A (2011a) Smoking and risk of amyotrophic lateral sclerosis: a pooled analysis of 5 prospective cohorts. Arch Neurol 68:207-213.

Wang JW, Brent JR, Tomlinson A, Shneider NA, McCabe BD (2011b) The ALS-associated proteins FUS and TDP-43 function together to affect Drosophila locomotion and life span. J Clin Invest 121:4118-4126.

Wang WY, Pan L, Su SC, Quinn EJ, Sasaki M, Jimenez JC, Mackenzie IR, Huang EJ, Tsai LH (2013) Interaction of FUS and HDAC1 regulates DNA damage response and repair in neurons. Nat Neurosci 16:1383-1391.

Wang X, Arai S, Song X, Reichart D, Du K, Pascual G, Tempst P, Rosenfeld MG, Glass CK, Kurokawa R (2008) Induced ncRNAs allosterically modify RNA-binding proteins in cis to inhibit transcription. Nature 454:126-130.

Wang Z, Harkins PC, Ulevitch RJ, Han J, Cobb MH, Goldsmith EJ (1997) The structure of mitogen-activated protein kinase p38 at 2.1-A resolution. Proc Natl Acad Sci U S A 94:2327-2332.

Waters BL, Panagopoulos I, Allen EF (2000) Genetic characterization of angiomatoid fibrous histiocytoma identifies fusion of the FUS and ATF-1 genes induced by a chromosomal translocation involving bands 12q13 and 16p11. Cancer Genet Cytogenet 121:109-116.

Wolozin B (2012) Regulated protein aggregation: stress granules and neurodegeneration. Molecular neurodegeneration 7:56.

Wood DK, Weingeist DM, Bhatia SN, Engelward BP (2010) Single cell trapping and DNA damage analysis using microwell arrays. Proc Natl Acad Sci U S A 107:10008-10013.

Woulfe J, Gray DA, Mackenzie IR (2009) FUS-immunoreactive intranuclear inclusions in neurodegenerative disease. Brain Pathol 20:589-597.

Wu CH et al. (2012) Mutations in the profilin 1 gene cause familial amyotrophic lateral sclerosis. Nature 488:499-503.

Wu YR, Foo JN, Tan LC, Chen CM, Prakash KM, Chen YC, Bei JX, Au WL, Chang CW, Wong TY, Liu JJ, Zhao Y, Tan EK (2013) Identification of a novel risk variant in the FUS gene in essential tremor. Neurology 81:541-544.

Xia R, Liu Y, Yang L, Gal J, Zhu H, Jia J (2012) Motor neuron apoptosis and neuromuscular junction perturbation are prominent features in a Drosophila model of Fus-mediated ALS. Mol Neurodegener 7:10.

Xiao L, O'Callaghan JP, O'Donnell JM (2011) Effects of repeated treatment with phosphodiesterase-4 inhibitors on cAMP signaling, hippocampal cell proliferation, and behavior in the forced-swim test. J Pharmacol Exp Ther 338:641-647.

Xu Z, Poidevin M, Li X, Li Y, Shu L, Nelson DL, Li H, Hales CM, Gearing M, Wingo TS, Jin P (2013) Expanded GGGGCC repeat RNA associated with amyotrophic lateral sclerosis and frontotemporal dementia causes neurodegeneration. Proc Natl Acad Sci U S A 110:7778-7783.

Yamagishi S, Yamada M, Ishikawa Y, Matsumoto T, Ikeuchi T, Hatanaka H (2001) p38 mitogen-activated protein kinase regulates low potassium-induced c-Jun phosphorylation and apoptosis in cultured cerebellar granule neurons. J Biol Chem 276:5129-5133.

Yamazaki T, Chen S, Yu Y, Yan B, Haertlein TC, Carrasco MA, Tapia JC, Zhai B, Das R, Lalancette-Hebert M, Sharma A, Chandran S, Sullivan G, Nishimura AL, Shaw CE, Gygi SP, Shneider NA, Maniatis T, Reed R (2012) FUS-SMN protein interactions link the motor neuron diseases ALS and SMA. Cell Rep 2:799-806.

Yang L, Liu ZR (2004) Bacterially expressed recombinant p68 RNA helicase is phosphorylated on serine, threonine, and tyrosine residues. Protein Expr Purif 35:327-333.

Yang L, Calingasan NY, Lorenzo BJ, Beal MF (2008) Attenuation of MPTP neurotoxicity by rolipram, a specific inhibitor of phosphodiesterase IV. Exp Neurol 211:311-314.

Yasuda K, Zhang H, Loiselle D, Haystead T, Macara IG, Mili S (2013) The RNA-binding protein Fus directs translation of localized mRNAs in APC-RNP granules. J Cell Biol 203:737-746.

Yoshimura A, Fujii R, Watanabe Y, Okabe S, Fukui K, Takumi T (2006) Myosin-Va facilitates the accumulation of mRNA/protein complex in dendritic spines. Curr Biol 16:2345-2351.

Zarubin T, Han J (2005) Activation and signaling of the p38 MAP kinase pathway. Cell Res 15:11-18.

Zhang YY, Mei ZQ, Wu JW, Wang ZX (2008) Enzymatic activity and substrate specificity of mitogen-activated protein kinase p38alpha in different phosphorylation states. J Biol Chem 283:26591-26601.

Zheng W, Deng X, Liang H, Song Z, Gao K, Yang Y, Deng H (2013) Genetic analysis of the fused in sarcoma gene in Chinese Han patients with essential tremor. Neurobiol Aging 34:2078 e2073-2074.

Zhou BB, Elledge SJ (2000) The DNA damage response: putting checkpoints in perspective. Nature 408:433-439.

Zhu J, Mix E, Winblad B (2001) The antidepressant and antiinflammatory effects of rolipram in the central nervous system. CNS Drug Rev 7:387-398.

Zinszner H, Sok J, Immanuel D, Yin Y, Ron D (1997) TLS (FUS) binds RNA in vivo and engages in nucleo-cytoplasmic shuttling. J Cell Sci 110 (Pt 15):1741-1750.